

## IV. APPLIED BATTERY RESEARCH FOR TRANSPORTATION

Introduction

Materials Development

Calendar and Cycle Life Studies

Abuse Tolerance Studies



---

## IV. APPLIED BATTERY RESEARCH FOR TRANSPORTATION

### IV.A Introduction

The Applied Battery Research (ABR) for transportation program is being conducted in support of the US Drive Partnership, which is targeting more fuel-efficient light duty vehicles that can reduce U.S. dependence on petroleum without sacrificing performance. There is an emphasis on developing and improving critical component technologies; and energy storage technologies are one of the most critical components needed to enable the wide-spread commercialization of electric drive vehicles. In PHEVs, energy storage devices provide the primary power source for a number of “all-electric” miles, after which the vehicles operate in the HEV mode. They enhance the efficiency of the prime power source (currently, an internal combustion engine) in HEVs by leveling the load and capturing regenerative braking energy. Better energy storage systems are needed to help expand the commercial markets for HEVs and to help make PHEVs and EVs commercially viable. The energy storage requirements for various vehicular applications were presented in Section III.

The ABR program is focused on materials and cell couples for high energy batteries for use in PHEV40 (PHEVs with a 40 mile all electric range) light-duty vehicles. The key barriers associated with PHEV batteries are:

- High cost
- Insufficient energy density to meet 40-mile all-electric range,
- Limited calendar and cycle life,
- Insufficient tolerance to abusive conditions, and
- Operation between -30°C and +52°C.

The program is seeking to develop higher energy materials, higher voltage electrolytes, combined into more optimal cell chemistries that are more stable and long-lived in the cell environment; as well as possessing cost advantages over current materials. The program is also focused on understanding and enhancing the abuse tolerance of the individual materials, components, and cell chemistries, which will help reduce the level of sophistication of the electronic control system and thereby realize cost savings.

Six DOE national laboratories and two external laboratories are collaborating in the program. Argonne National Laboratory (ANL) provides coordination of the program activities for DOE. The other five participating DOE laboratories are Brookhaven National Laboratory (BNL), Idaho National Laboratory (INL), Lawrence Berkeley National Laboratory (LBNL), Oak Ridge National Laboratory (ORNL), and Sandia National Laboratories (SNL). The two additional laboratories contributing to the program are the Army Research Laboratory and the Jet Propulsion Laboratory. As part of this program, ANL researchers maintain close communications and collaborations with a large number of international material supply companies, through which they gain access to the latest advanced electrode and electrolyte materials for evaluation.

The Applied Battery Research for transportation program is organized into three main tasks to address the issues associated with PHEV and HEV energy storage technologies:

**Advanced Battery Materials Development**—focuses on research, development, and engineering of higher energy materials and cell chemistries that simultaneously address the life, performance, abuse tolerance, and cost issues needed for a 40 mile all electric mile range PHEV.

**Calendar & Cycle Life Studies**—deals with understanding the factors that limit life in different Li-ion cell chemistries, which are used as feedback to the materials development task. This task also deals with the establishment of in-program material and cell fabrication capabilities for use in these life studies.

**Abuse Tolerance Studies**—deals with understanding the factors that limit the inherent thermal and overcharge abuse tolerance of different Li-ion cell materials, components, and cell chemistries, as well as developing approaches for enhancing their inherent abuse tolerance.

A high level overview of the program is shown in Figure IV - 1.

## High Level ABR Program Overview

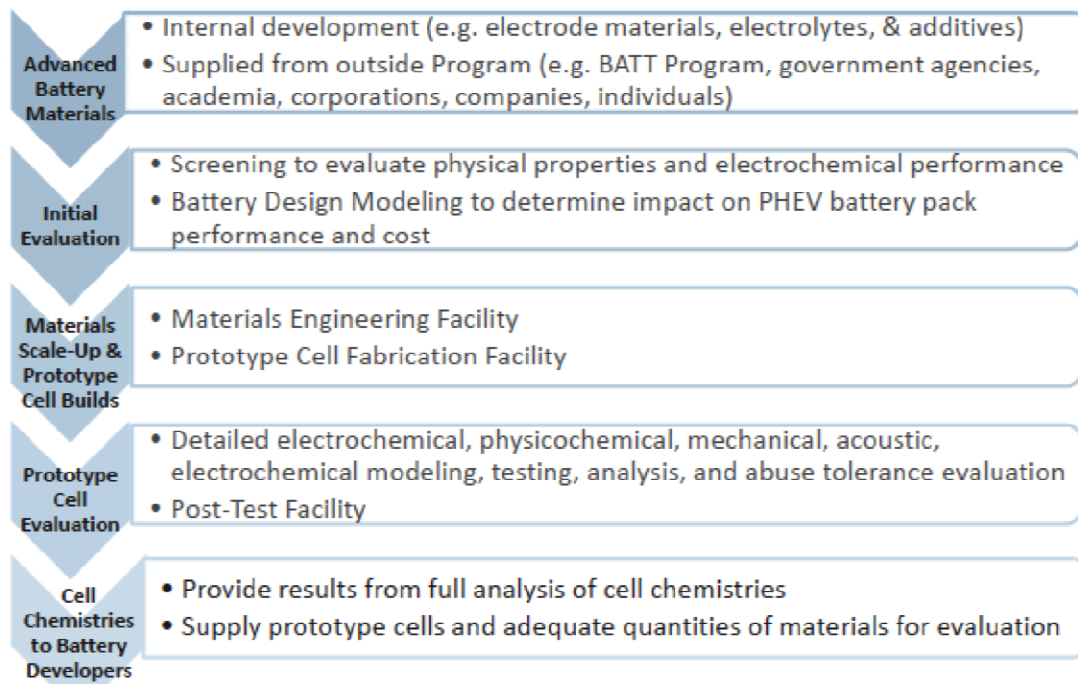


**Figure IV - 1:** An overview of the major activities in the Advanced Battery Development program.

2011 was a transitional year for the program, with major supporting facilities becoming operational. ANL has installed and is bringing into full operation three new facilities: a materials scale up facility, a cell fabrication facility, and a cell tear down and diagnostics facility. These three operations will be critical to the future success of this program as they will enable full investigation and characterization of new material and cell variations in commercially relevant cells (18650s and 1Ahr pouch cells).

Thus, ABR will quickly begin testing and diagnosing the most promising new cell materials using a full design of experiments approach, permitting it to access much of the huge experimental space in Li ion batteries, including such factors as active material particle shape and size, electrode loading, binder type and amount, conductive additive type and amount, electrolyte additive type and amount, etc. This capability should permit the program to quickly identify and mitigate the multiple failure modes that arise when advanced energy storage materials are used in cells. In addition, it is hoped that the facilities will be available to aid industry in understanding and diagnosing issues with their cell chemistries. The procedure that these facilities will enable to be followed is shown in Figure IV-2.

The remainder of this section provides technical highlights and progress on the Applied Battery Research program for FY 2011. The information provided is representative only and detailed information is available from publications cited in each project overview.

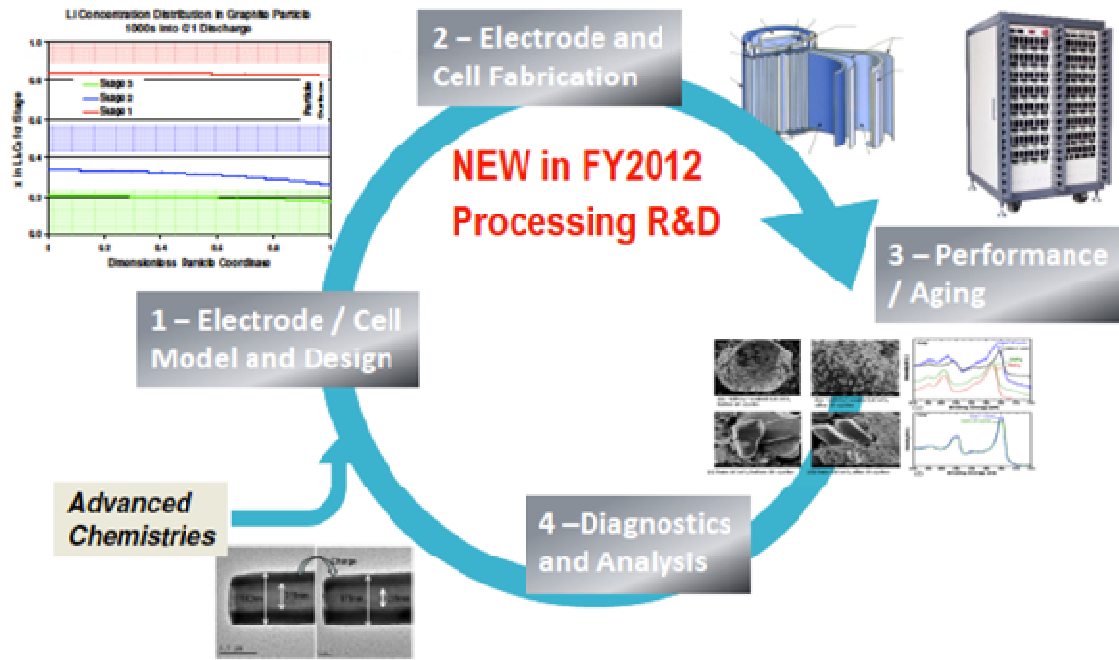


Figure IV - 2: ABR process flow, showing introduction of new materials, electrode and cell modeling and design, cell building, testing and diagnostics.

---

## IV.B Materials Research

### IV.B.1 Cell Components and Composition

#### IV.B.1.1 Screen Electrode Materials and Cell Chemistries (ANL)

Wenquan Lu

Argonne National Laboratory  
9700 South Cass Avenue  
Argonne, IL 60439-4837  
Phone: (630) 252-3704; Fax: (630) 972-4414  
E-mail: [luw@anl.gov](mailto:luw@anl.gov)

##### Collaborators:

Miguel Miranda (ANL)  
Nathan Liu (ANL)  
Bryant Polzin (ANL)  
Andrew Jansen (ANL)  
Huiming Wu (ANL)  
Dennis Dees (ANL)  
Khalil Amine (ANL)  
Gary Henriksen (ANL)  
Cell Fabrication Facility (CFF-ANL)  
Material Engineering Facility (MEF-ANL)  
Toda Kogyo (Japan)  
ConocoPhillips (USA)  
Enerdel (USA)  
Saft (France)

##### Subcontractor:

Illinois Institute of Technology, Chicago, IL

Start Date: October, 2008

Projected End Date: September, 2012

### Objectives

The primary objective is to identify and evaluate low-cost materials and cell chemistries that can simultaneously meet the life, performance, and abuse tolerance goals for batteries used in PHEV applications.

A secondary objective is to enhance the understanding of the impact of advanced cell components on the electrochemical performance and safety of lithium-ion batteries.

### Technical Barriers

There are no commercially available high energy materials that can produce a battery capable of meeting the 40-mile all-electric-range (AER) within the weight and volume constraints established for PHEVs by DOE and the USABC. Identification of new high-energy electrode materials is the primary goal for this project.

An overwhelming number of materials are being marketed by vendors for lithium-ion batteries. It is a challenge for developers to screen all of these materials and claims.

Establishing the impact of formulation and processing on electrode performance for materials with a broad variation in chemical and physical properties is another major challenge.

### Technical Targets

- Higher energy density materials identification and evaluation.
- Low cost cell components identification and characterization.

### Accomplishments

- Several **composite structure cathode materials** from various material suppliers, Toda Kogyo, BASF, H. Wu (ANL) Material Engineering Facility (MEF), etc. were received and characterized. Different electrochemical properties were observed for the different composite materials with various compositions. The screening results were transferred to the **Cell Fabrication Facility** (CFF). Two of the materials (HE5050 from Toda Kogyo and H. Wu's from ANL) were selected for evaluation in the larger format cells (pouch cells or 18650 cylindrical cells). The electrodes made by the CFF group were tested to validate the screening results.
- **Graphite** from ConocoPhillips (A12) was received and screened at Argonne. This surface modified graphite showed high energy density and low irreversible capacity loss. This material was selected

for use as the standard anode electrode material for the ABR program.

- Multiple electrode materials ( $\text{LiNi}_{0.5}\text{Mn}_{1.5}\text{O}_4$ , HE5050,  $\text{LiNi}_{0.8}\text{Co}_{0.15}\text{Al}_{0.05}\text{O}_2$ , A12,  $\text{Li}_4\text{Ti}_5\text{O}_{12}$ ) made by Enerdel and Saft, for use in **high voltage electrolyte** investigations, were characterized. The obtained information was shared with ABR participants (ANL, ARL, BNL, LBNL, and SNL).
- An overcharge protection **redox shuttle** (RS2), made by the **Materials Engineering Facility** (MEF), was investigated in terms of its electrochemical and thermal properties. Its performance was validated versus that of the smaller batch lab-scale samples. In addition, the material screening group worked closely with MEF on the scale-up of the **composite-structure cathode materials**, which is under development.
- Other cell components, such as binders, separators, carbon blacks, and current collectors, were also

characterized. The test results have been shared with the suppliers.

◇ ◇ ◇ ◇ ◇

## Introduction

The curves in Figure IV - 3 were calculated using Argonne's battery design model. The model indicates that one needs higher energy electrode materials than those that are commercially available in order to achieve the 40-mile AER within the weight and volume constraints established by DOE and the USABC. For example, if one uses a 20% margin for energy fade over the life of the battery, one would need a combination of anode and cathode materials that provide 420mAh/g and 220mAh/g respectively, at the beginning of life, assuming an average cell voltage of 3.6 volts. The search for new high energy density materials is the focus of this project.

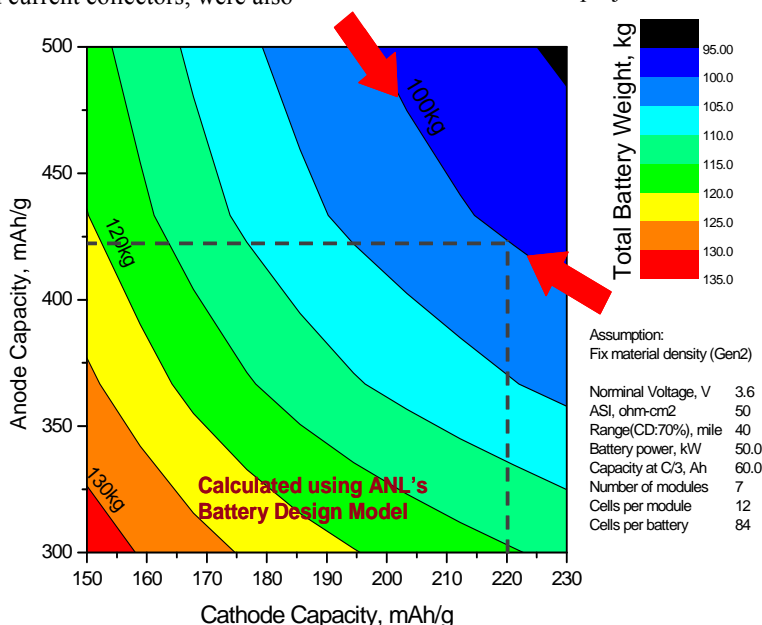


Figure IV - 3: Specific capacity requirements for anode and cathode materials in high-energy lithium ion batteries

In addition to high energy density electrode materials, other cell components continue to be evaluated to address performance, safety, and cost issues.

## Approach

The search for new high-energy materials includes new commercially available materials, as well as new high energy density materials under development. During the search and evaluation process, the cost issue is always considered, e.g. avoiding the rare elements, expensive precursors, and/or elaborate processing.

Once the electrode materials are identified and received, their chemical and physical properties are checked, including XRD, SEM, BET, particle size, density, etc. This type of information is generally provided by the material supplier. Internal tests are conducted if the desired information is not available. This information is useful to determine the electrode formulation.

The selected electrode materials are evaluated in controlled conditions following established protocols. The commonly used parameters, such as pulse power and charge depleting (CD) capacity tests are derived from the "Battery Test Manual for Plug In Hybrid Electric Vehicle" (Mar. 2008) issued by INL. Depending on the portion of total cell energy that is available for use during the CD

discharge, the CD rate can vary from C/2 to C/3. Similarly, the pulse power rate could change from about 2C to 1.5C.

Coin cells (2032 size) are used for the initial screening studies. If promising results are obtained with coin cells, then larger laboratory cells such as the 32 cm<sup>2</sup> stainless steel planar test cell fixtures or simple single-stack pouch cells, are used. Preliminary accelerated aging studies are performed at 55°C for promising materials to give a preliminary indication of life. Where appropriate, the thermal abuse response is studied using differential scanning calorimetry (DSC). Materials that show characteristics favorable to PHEV batteries are then recommended for more extensive life evaluation under Task IV.C.2 (cell fabrication and testing). The flow chart of material screening is illustrated in Figure IV - 4.

In addition to electrode materials, other cell components, such as separators, binders, current collectors, etc., are secured and evaluated to establish their impact on electrochemical performance, thermal abuse, and cost. The test methods for different materials are separately defined.

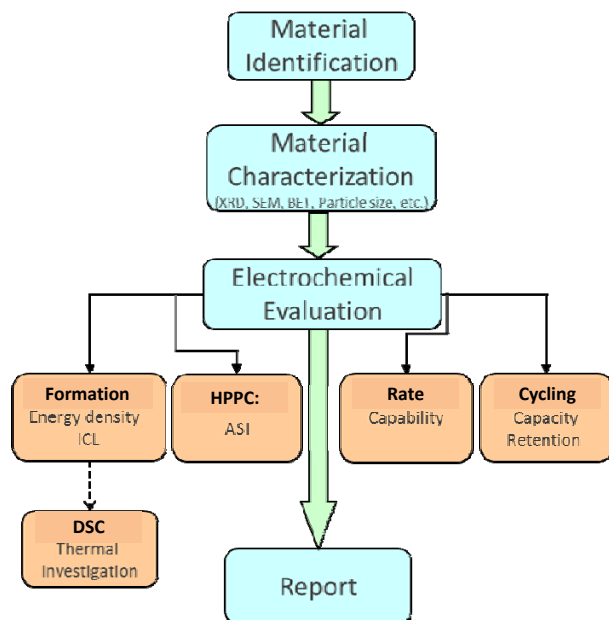


Figure IV - 4: Material screening procedure

## Results

**Composite-structure cathode materials.** Recently, composite-structure cathode materials developed at Argonne National Laboratory have drawn great attention for their application as next generation cathode materials due to their high energy density. Several composite-structure cathode materials were received and investigated. All of them showed the activation of the Li<sub>2</sub>MnO<sub>3</sub> component during the first formation cycle and high energy density at low rate compared to conventional cathode materials. However, they also showed varying types of electrochemical performance in terms of

irreversible capacity loss, rate capability, and cycle life with changes of Li<sub>2</sub>MnO<sub>3</sub> component. One of composite-structure materials, HE5050 from Toda Kogyo, will be discussed below as an example.

The HE5050 electrode material was initially tested against lithium metal in the half cell configuration between 4.6V and 2.0V. In Figure IV - 5, we see an activation plateau at about 4.5V during the 1<sup>st</sup> formation cycle, which is the characteristic feature of composite-structure cathode materials. The voltage plateau disappears after the first cycle. The specific capacity was determined to be ~250mAh/g at the C/10 rate. The irreversible capacity loss (ICL) during the 1<sup>st</sup> cycle is about 17%. The ICL was found to change from one composite-structure material to another.

Hybrid pulse power characterization (HPPC) was then conducted on graphite/HE5050 full cells. In this study, the anode is surfaced modified graphite from ConocoPhillips. In Figure IV - 6, it can be seen that the area specific impedance (ASI) calculated from the HPPC is not flat. The minimum appeared from 30% to 50% depth of discharge (DOD). The impedance after 60% of DOD increases rapidly. The high impedance at lower DOD will limit its application in automotive applications.

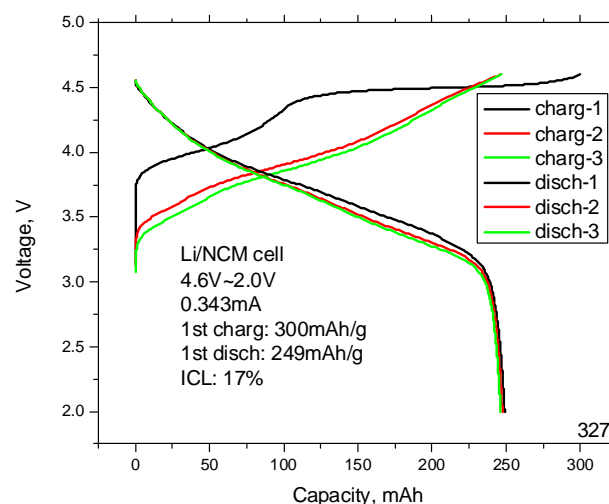


Figure IV - 5: Voltage profile of HE5050 during formation in the half cell configuration

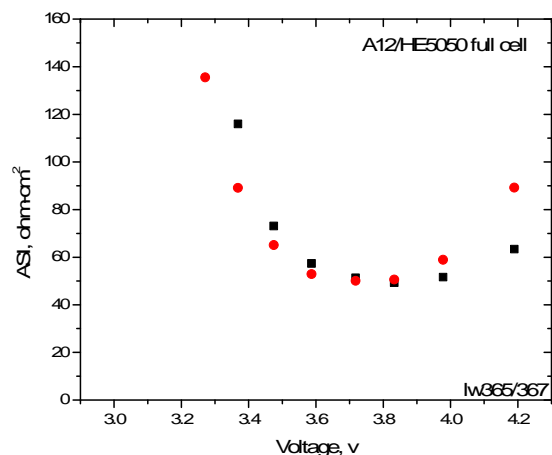


Figure IV - 6: Area specific impedance of graphite/HE5050 cell

The cycle performance of a full cell is shown in Figure IV - 7. The applied voltage window for the graphite/HE5050 full cell is between 4.5V and 2.5V. The capacity retention was close to 90% over 50 cycles at the C/3 charge and discharge rate and room temperature. In addition to capacity fade, voltage depression was also noticed for the HE5050 composite-structure cathode. This issue together with the capacity fade of this material is under investigation.

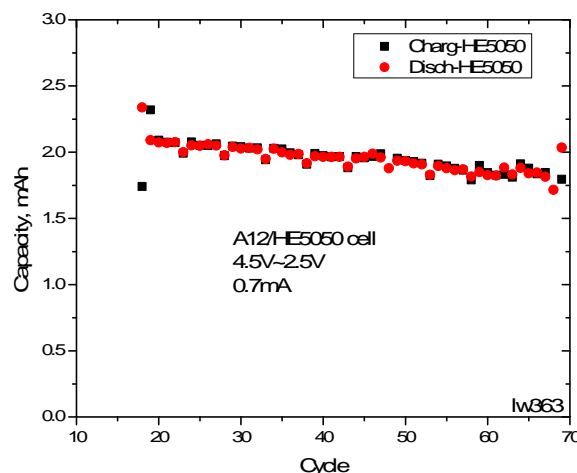


Figure IV - 7: Cycle performance of HE5050 full cell

**Surface modified graphite.** Surface modified graphite (A12) from ConocoPhillips was received and characterized as an anode material. Very high capacity (361mAh/g) was observed during formation cycles (Figure IV - 8). This number is close to the theoretical value for graphite. The coulombic efficiency was around 90% during the very first cycle.

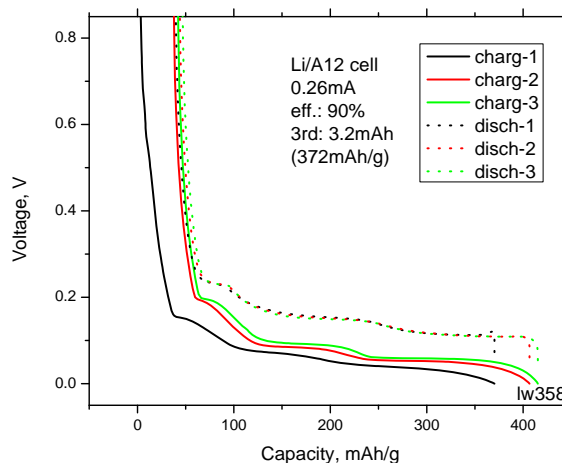


Figure IV - 8: Voltage profile of A12 graphite from ConocoPhillips

The rate performance of A12 graphite half-cell is shown in Figure IV - 9. In this test, the charge rate was fixed at C/5. The discharge rate varied from C/5 to 1C. Almost 100% capacity was obtained during the discharge process up to 1C rate, which demonstrates its excellent rate capability.

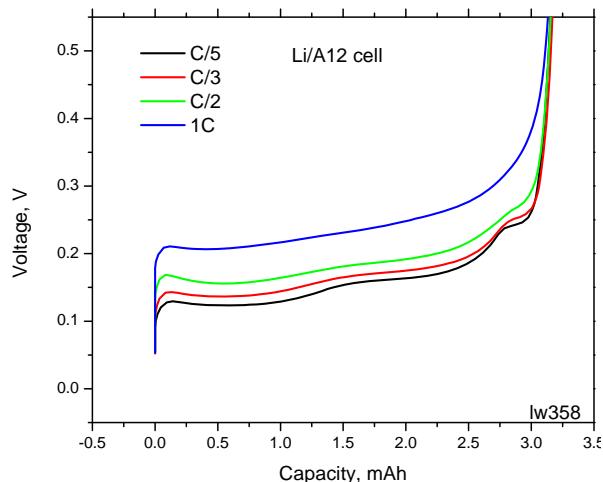


Figure IV - 9: Rate performance of A12 graphite from ConocoPhillips

Due to space limitations, other activities under material screening area, such as electrode evaluations for high voltage electrode materials and CFF, electrolyte additives, and electrode materials from MEF are not detailed in this report.

## Conclusions and Future Directions

As example, HE5050 was characterized in terms of its energy density, rate capability, HPPC, cycle performance, and thermal stability. This composite-structure material demonstrated high energy density, as high as 800mWh/g, almost 200mWh/g more than  $\text{LiNi}_{0.8}\text{Co}_{0.15}\text{Al}_{0.05}\text{O}_2$  (NCA). This composite cathode material also shows reasonable cycle performance at room temperature, about 90%

capacity retention after 50 cycles. The material has been selected as cathode material by CFF for large format cell fabrication and testing.

Surface modified graphite from ConocoPhillips was investigated as an anode material. The material demonstrates high capacity and good rate performance. This material was selected as the standard anode material by CFF for use in building large format cells to study various cathode materials, such as composite-structure cathode materials and high voltage spinel cathode materials.

In the future, the focus of this project will remain on the identification and characterization of new high energy density cathode and anode materials. As for cathode materials, the composite-structure materials will be intensively studied in terms of their rate capability, capacity fade rates, thermal stability and cycle life. In order to balance the high energy density cathode, high energy density anodes, such as silicon and silicon composites, will be searched for and investigated.

9. Electrochemical and Thermal Characterization of Graphite Anode for Li-ion Batteries, W. Lu, C. M. López, N. Liu, A. Jansen, and D. Dees, 35th International Conference and Exposition on Advanced Ceramics and Composites (ICACC'11) Jan. 23rd-28th, 2011.

### FY 2011 Publications/Presentations

1. Screen Electrode Materials & Cell Chemistries, W. Lu, 2011 DOE Annual Peer Review Meeting Presentation, May 9<sup>th</sup>-13<sup>th</sup> 2011, Washington DC.
2. Multi-scale Study of Thermal Stability of Lithiated Graphite, Z. Chen, Y. Qin, Y. Ren, W. Lu, C. Orendorff, E. P. Roth and K. Amine, *Energy Environ. Sci.*, 2011, 4, 4023-4030
3. Study of  $\text{Li}_{1+x}(\text{Mn}_{4/9}\text{Co}_{1/9}\text{Ni}_{4/9})_{1-x}\text{O}_2$  cathode materials for vehicle battery applications, S.-H. Kang, W. Lu, K. G. Gallagher, S.-H. Park, and V. G. Pol, *J. Electrochem. Soc.* 158 A936 (2011).
4. High-Energy Electrode Investigation for Plug-in Hybrid Electric Vehicles, W. Lu, A. Jansen, D. Dees, P. Nelson, N. R. Veselka, and G. Henriksen, *J. Power Sources*, 196, 2011, 1537-1540.
5. Electrolyte additive to improve performance of MCMC/LiNi<sub>1/3</sub>Co<sub>1/3</sub>Mn<sub>1/3</sub>O<sub>2</sub> Li-ion cell, Y. Qin, Z. Chen, W. Lu, and K. Amine, *J. Power sources*, 195, 2010, 6888-6892.
6. Electrochemical and Thermal Studies of Fluorinated Electrolytes in Li-Ion Cell, A. Benmayza, V. Ramani, J. Prakash, and W. Lu, 220th ECS Meeting & Electrochemical Energy Summit in Boston, Massachusetts (October 9-14, 2011).
7. Evaluation of Overcharge Protection Redox Shuttle Electrolyte Additive for Lithium Ion Batteries, W. Lu, N. Liu, L. Zhang, J. Zhang, T. Dzwiniel, K. Pupek, K. Amine, G. Krumdick, and D. Dees, PBFC-5, Argonne National Laboratory, Chicago IL Sep. 2011
8. A. Ben Mayza, V. Ramani, J. Prakash, and W. Lu, Electrochemical and Thermal Studies of Fluorinated Electrolytes in Li-Ion Cells"219th ECS Meeting in Montreal, Canada (May 1 - 6, 2011).

## IV.B.1.2 Streamlining the Optimization of Li-Ion Battery Electrodes (ANL)

Wenquan Lu and Sun-Ho Kang

Argonne National Laboratory  
9700 South Cass Avenue  
Argonne, IL 60439-4837  
Phone: (630) 252-3704; Fax: (630) 972-4414  
E-mail: [luw@anl.gov](mailto:luw@anl.gov)

Collaborators:

Miguel Miranda (ANL)  
Nathan Liu (ANL)  
Dennis Dees (ANL)  
Gary Henriksen (ANL)  
Electron Microscopy Center (ANL)

Subcontractor:

Illinois Institute of Technology, Chicago, IL

Start Date: October, 2008

Projected End Date: September, 2012

### Objectives

To establish the scientific basis needed to streamline the optimization of lithium-ion electrode processing.

- To identify and characterize the physical properties relevant to the electrode performance at the particle level.
- To quantify the impact of fundamental phenomena associated with electrode formulation and fabrication (process) on lithium ion electrode performance.

### Technical Barriers

Develop a cost-effective and abuse tolerant lithium-ion battery for a PHEV with a 40 mile all electric range that meets or exceeds all performance goals.

- Establish the interdependence of lithium-ion electrode performance and the specifics of the electrode fabrication process.
- Reduce the complexity of the optimization process caused by the broad range of active materials, additives, and binders.
- Quantify the impact of fundamental phenomena on electrode performance.

### Technical Targets

- Correlate the electronic conductivity with the electrochemical performance of the electrode.
- Develop a model to quantify the impact of electronic conductivity on cell performance.

### Accomplishments

- Single particle conductivity was measured using nano probe SEM. The higher conductivity of  $\text{LiNi}_{0.8}\text{Co}_{0.15}\text{Al}_{0.05}\text{O}_2$  measured by this technique indicates that the lower conductivity obtained using the conventional method was due to interfacial resistance.
- The physical properties of carbon coated  $\text{LiNi}_{1/3}\text{Co}_{1/3}\text{Mn}_{1/3}\text{O}_2$  samples were characterized. The electrode conductivity was investigated using 4 point probe modeling.
- The electrodes and the cells made of NCM powder with and without carbon coating were also studied in terms of their electrochemical and physical properties.
- $\text{LiFePO}_4$  was used as media to investigate the effect of carbon black additive and binder on the electrode and cell performance.

◇ ◇ ◇ ◇ ◇

### Introduction

In general, the performance of a lithium-ion electrode is highly dependent on the specifics of the fabrication process. Furthermore, the broad range of active materials for both positive and negative electrodes (e.g. oxides, phosphates, graphites, carbons, and alloys), as well as polymer binders and conductive additives, compounds the complexity of the optimization process. The literally hundreds of variables associated with the fabrication of new active material electrodes generally require lengthy development efforts to be fully optimized. This sometimes causes promising materials to be discarded prematurely. Quantifying the impact on performance of the fundamental phenomena involved in electrode formulation and fabrication should greatly shorten the optimization process for new electrode active materials. The goal of this work is to establish the scientific basis needed to streamline the lithium-ion electrode optimization process for new materials.

## Approach

The conventional approach is to optimize the electrode by varying the amounts of conductive additive and binder to reach the percolation threshold at the laminate level. New electrode materials are generally judged on their electrochemical properties. This method, generally adopted by industry, requires lengthy development efforts to fully optimize a single material and sometimes causes promising materials to be discarded. Our new approach in this project attempts to establish the scientific basis at the particle level. The focus is on the chemical and physical properties (e.g. primary particle size, secondary particle size and extent of agglomeration, as well as the surface characteristics, see Figure IV - 10), which, in most cases, can dictate the overall performance of the electrode.

Based on modeling work by Dennis Dees, it was established that the electronic conductivity does not impact on electrode impedance when the electronic conductivity is much larger than the ionic conductivity ( $>0.01$  S/cm). Therefore, it will be very helpful to optimize the electronic conductivity of the electrode to meet the energy and power requirements. The factors affecting the distribution of binder and conductive additives throughout the composite matrix is being systematically investigated at the particle level, as well as their effect on overall electrode performance. Modeling work is being conducted to help quantify the impact of fundamental phenomena on electrode performance.

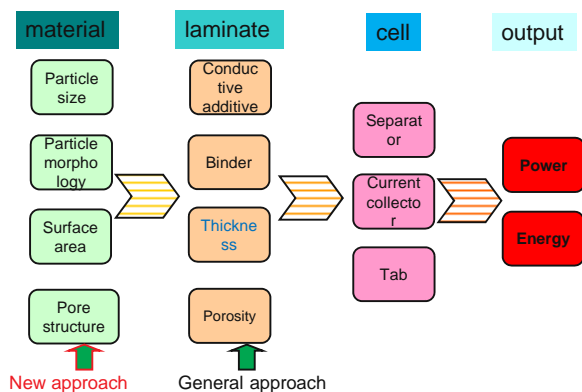


Figure IV - 10: Schematic diagram of streamlining the optimization of electrode

## Results

**Carbon coated  $\text{LiNi}_{1/3}\text{Co}_{1/3}\text{Mn}_{1/3}\text{O}_2$**  The single particle investigation demonstrated that the interfacial resistance of electrode particles is a significant contributor to electrode resistance. It is rational to expect that the conductive carbon coating can improve the electrode conductivity. The carbon coating of NCM particles was engineered by Hosaka, using a novel carbon coating technology.

Two different carbon coated NCM samples (1wt.% and 3wt.%) were prepared by Hosokawa. SEM and TGA results confirmed the desired amount of carbon was coated on the surface of particles (see Annual Report 2010). The conductivity of electrodes made with both uncoated and coated NCM particles were also investigated using the 4-point probe method. The coated carbon on the particle was taken into consideration when preparing the electrode slurry. For instance, only 1wt% additional carbon was added into composite when 4wt% carbon additive is the target for 3wt% carbon coated NCM particles. The substrates for the electrodes are either conductive aluminum foil or insulating polyester. The four point probe results indicate that the electrode sheet resistance is higher when polyester was used as substrate, and lower when aluminum foil was used as substrate. The phenomena will be further discussed in the modeling study.

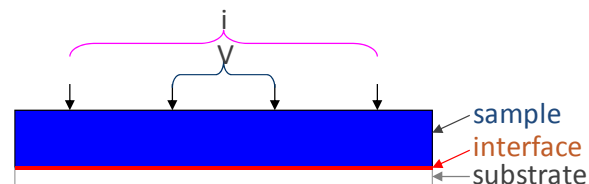


Figure IV - 11: Four point probe electrode conductivity geometry

Figure IV - 11, shown above, is the four point probe electrode conductivity geometry used in the modeling effort. The model adopted a three-layer geometry. The top layer is the coating of electrode materials including active material, carbon additive, and PVDF binder. The bottom layer is the substrate (either metal foil or insulating substrate). Finally, the middle layer is the interface between coating and substrate. The conductivity of coating was assumed isotropic. In the model, the substrate was considered either very conductive or very insulating, which will not be calculated. The interface resistance was set to  $10000 \text{ ohm-cm}^2$  to ensure the current would go through the coating when the polyester was used as substrate. The resistance of substrate was set to zero when the aluminum foil was used as the substrate. The error limit was set to 0.00001. By using the model, the contact resistance and interface resistance can be obtained.

Figure IV - 12 illustrates the voltage profile of schematic diagram of four point probe measurement of electrode when polyester was used as substrate. The current was applied to the electrode through outer two probes, the voltage was monitored through two inner probes. The current distribution around the two probes from cross section of electrode could be seen clearer from upper portion of Figure IV - 13. As seen from both Figure IV - 12 and lower portion of Figure IV - 13, the voltage distribution around the inner two probes is evenly distributed, which makes the measurement more accurate.

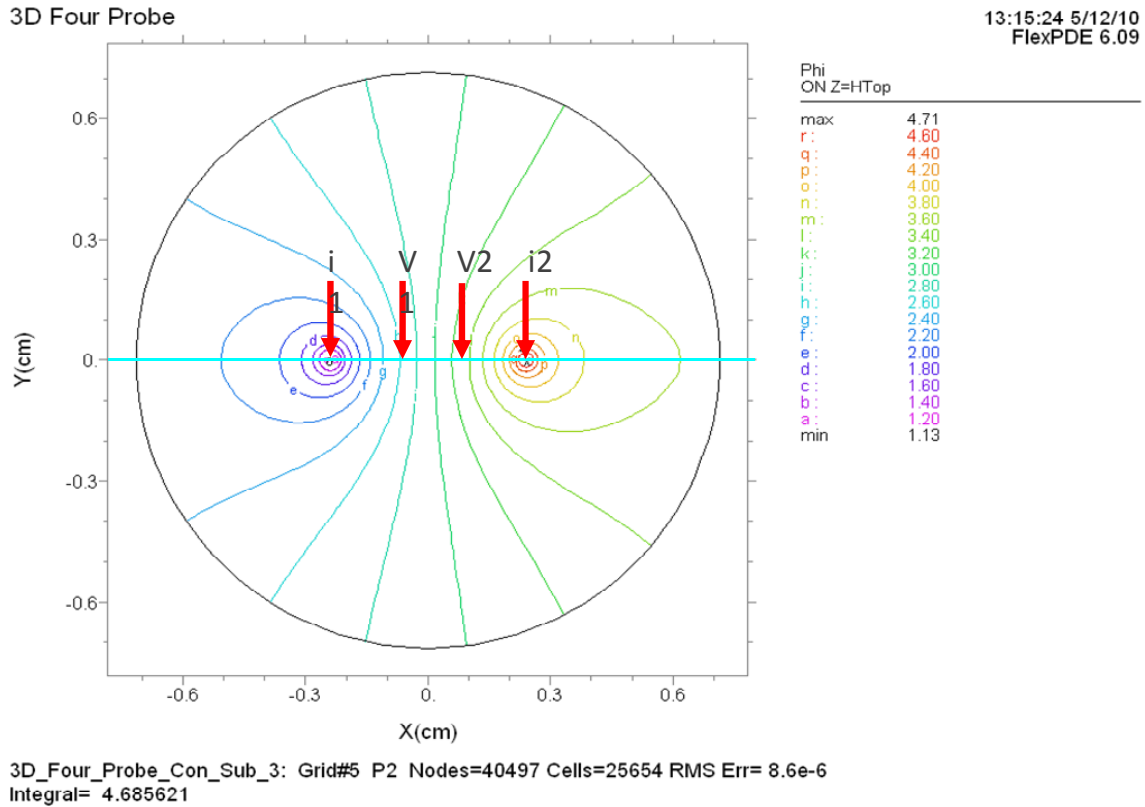


Figure IV - 12: Voltage profile of electrode at surface of electrode

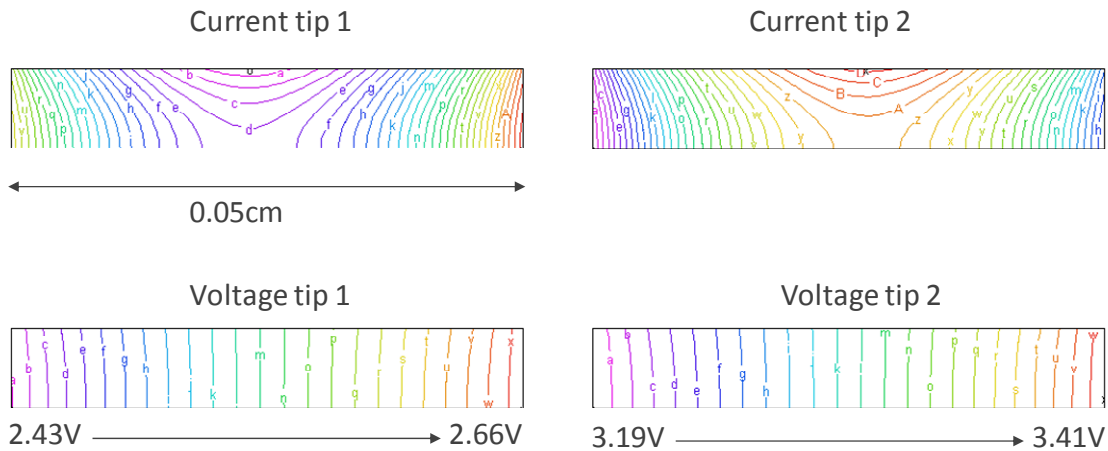


Figure IV - 13: Current and voltage distribution around four probes

The electrode conductivity was calculated using the model by varying the probe contact resistance and interfacial resistance for electrode coating on either aluminum or polyester. The calculated conductivity is shown in Figure IV - 14. The calculated conductivity from modeling fits very well with the 4 probe measurement. The

probe contact resistance was also obtained from this model, which was used, along with the conductivity, to calculate the interfacial resistance between electrode coating and aluminum substrate. It was determined that the interfacial resistance was 0.2 ohm-cm<sup>2</sup>, which is much higher than the electrode resistance. The modeling results

confirmed the previous finding reported in 2010. The interfacial resistance between the coating and substrate significantly contributes to the total electrode resistance, which can in turn affect the cell power performance.

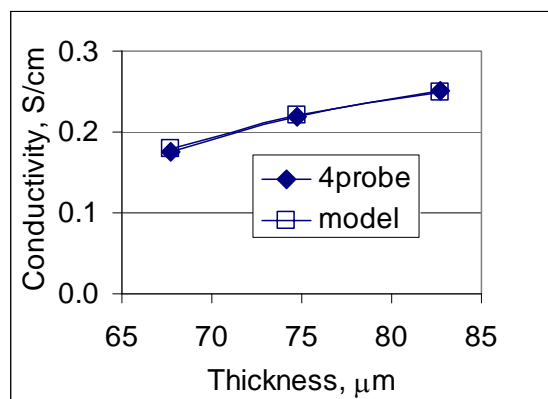


Figure IV - 14: Electrode conductivity of coating using polyester as substrate

The hybrid pulse power characterization (HPPC) was carried out on the half cells containing NCM powders with and without carbon coating. The calculated area specific impedances (ASI) at the same depth of discharge (DOD) are shown in Figure IV - 15. The impedance of both electrodes is relatively constant with porosity. The left plot of the ASI results for the electrode without carbon coating as a function of electrode porosity is less constant with the impedance decreasing with more calendaring. As for electrode with 3% carbon coating, the overall impedance is reduced from around 40 ohm-cm<sup>2</sup> to 30 ohm-cm<sup>2</sup>. The test results demonstrated that the carbon coating on NCM powder did significantly improve the power performance at the cell level.

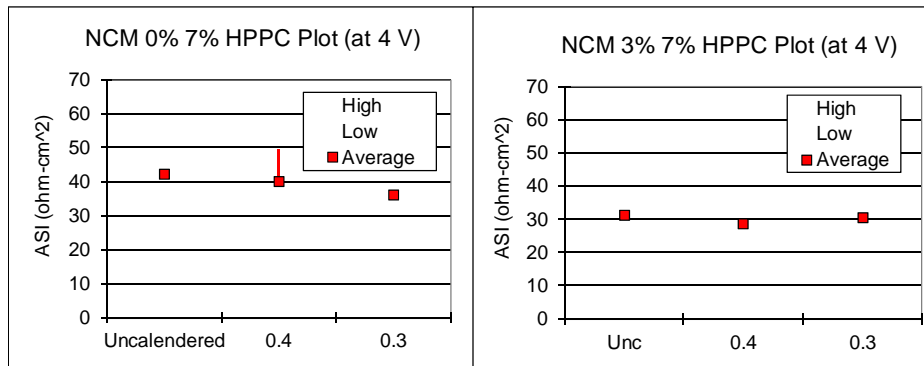


Figure IV - 15: ASI of NCM electrode with and without carbon coating

**The carbon and binder effect on LiFePO<sub>4</sub>** electrodes was studied by varying the carbon black and binder content and measuring its impact on the cell energy and power performance. The ratios examined between active material/carbon/PVDF were 86/7/7, 82/9/9, 70/20/10, 70/15/15, and 70/10/20. The voltage profile was fitted, shown in Figure IV - 16, using a model from the literature (Prosini, *J Solid State Electrochem* (2009) 13:1859–1865). In the equation, the ohmic resistance and mass transport resistances as a function of carbon/PVDF ratio were analyzed. It was found that the optimized

electrode composition was a function of carbon/PVDF ratio.

The overpotential as a function of test rate is shown in Figure IV - 17 for electrodes with various electrode compositions at 40% and 60% DOD. It can be seen that the overpotential difference is hard to differentiate at lower rates. However, the overpotential becomes larger when less conductive additive was used in the electrode. The results indicate that the higher active material composition is suitable for energy cells.

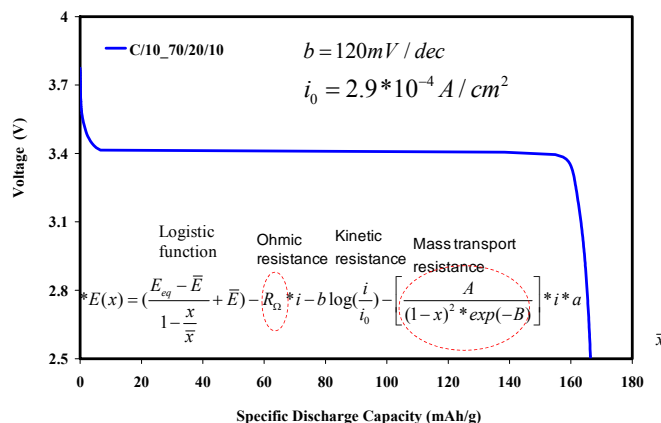


Figure IV - 16: Analytical modeling of the Experimental data

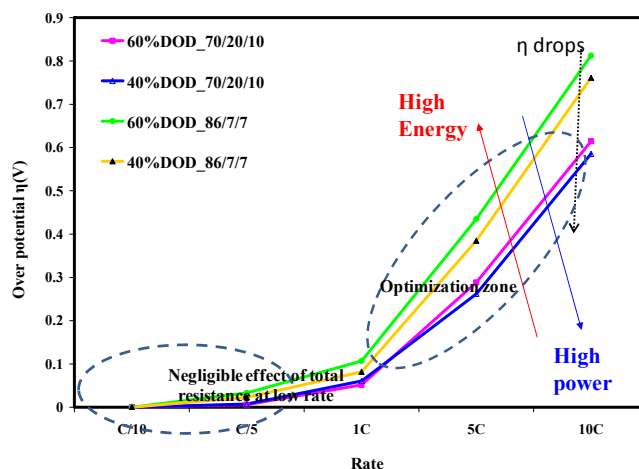


Figure IV - 17: Electrode composition vs. overpotential at different discharge rates

## Conclusions and Future Directions

Four probe modeling was used to investigate the electrode resistance. The modeling results confirmed that the interfacial resistance is at least one of major contributor for the electrode impedance. The information should lead to better understanding of electrode optimization. The impedance results from the hybrid pulse power characterization also confirmed that the electrode with carbon coated power show better power-capability; even less addition carbon black was added into formulation.

Carbon and binder effect on cell energy and power was investigated using  $\text{LiFePO}_4$  as test media. The model indicated that carbon/PVDF ratio dramatically affected both ohmic resistance and mass transfer resistance. Modeling also suggested that ohmic is a key factor in determining the high-rate performance at different compositions.

In the future, the interactions between components of composite electrodes and the interfacial resistance between the particles and particle/substrate will be further

investigated using BCF thin film electrodes. The modeling work will be continued to better understand the interfacial phenomenon.

## FY 2011 Publications/Presentations

1. Streamlining the Optimization of Li-Ion Battery Electrodes, W. Lu, 2011 DOE Annual Peer Review Meeting Presentation, May 9<sup>th</sup>-13<sup>th</sup> 2011, Washington DC.
2. Electronic Conductivity Optimization of Lithium-Ion Battery Electrode, W. Lu, N. Liu, and D. Dees, 220th ECS Meeting & Electrochemical Energy Summit in Boston, Massachusetts (October 9-14, 2011).
3. Electrode Optimization for High Performance Li-Ion Cells, A. Benmayza, V. Ramani, J. Prakash, and W. Lu, 220th ECS Meeting & Electrochemical Energy Summit in Boston, Massachusetts (October 9-14, 2011)

## IV.B.1.3 Scale-Up of BATT Program Materials for Cell-Level Evaluation (LBNL)

Vincent Battaglia (Principal Investigator)  
Lawrence Berkeley National Laboratory  
1 Cyclotron Road  
M.S.70R0108B  
Berkeley, CA 94720  
Phone: (510) 486-7172; Fax: (510) 486-4260  
E-mail: vsbattaglia@lbl.gov

Start Date: October 1, 2009  
Projected End Date: September 31, 2013

### Objectives

- Evaluate advanced materials from the BATT Program in half and full coin-cells.
- Establish a baseline  $\text{LiNi}_{1/2}\text{Mn}_{3/2}\text{O}_4$  (LNMO) material.

### Technical Barriers

Principal investigators (PIs) in the BATT program are focused on developing new anode and cathode active materials and electrolytes. Minimal effort is focused on electrode fabrication and most testing is performed on half cells. Thus, full-cell performance with cycling beyond 100 cycles is rarely obtained.

At the beginning of this fiscal year, there were no commercial suppliers of  $\text{LiNi}_{1/2}\text{Mn}_{3/2}\text{O}_4$  identified that were willing to provide a large number of independent National Laboratory and university researchers with materials to study and publish relevant results.

### Technical Targets

- Evaluate chemistries that push Li-ion technology toward the 40-mile PHEV or pure EV goals.
- Obtain a  $\text{LiNi}_{1/2}\text{Mn}_{3/2}\text{O}_4$  material that can be produced in 1 kg quantities and distributed to other investigators in the ABR and BATT Programs.

### Accomplishments

- Demonstration at 30°C of 1,000 full-cycles with 80% capacity retention in 1-mAh Graphite/LMNO coin cells.
- Evaluated materials from four suppliers.
- Procured and distributed baseline material to PIs

- In the process of making matching cathode and anode laminates with Hydro Quebec (HQ) for distribution to ABR and BATT PIs.



### Introduction

LBNL has been developing a robust electrode fabrication process for the past seven years. The culmination of this effort resulted in the online publication of a cell fabrication manual. Notwithstanding, many researchers in the BATT program do not have the facilities to make quality electrodes and cells. With the resources offered by this task, LBNL can fabricate and test any material developed in the program.

If the challenging energy density targets of EVs and PHEVs are to be realized, materials capable of cycling larger quantities of lithium and at higher voltages are required. To begin developing high-voltage electrolytes, high-voltage cathodes are required.  $\text{LiNi}_{1/2}\text{Mn}_{3/2}\text{O}_4$  intercalates lithium with a flat potential at 4.7 V. Developing a baseline system with this cathode and a graphitic anode will allow investigators to develop and study the interactions of high-voltage materials in a full cell.

### Approach

LBNL, working with Argonne, is identifying entities capable of supplying 1 kg quantities of high-voltage NiMn-spinel. The sources are contacted and materials sent to LBNL. The materials are physically characterized using SEM, BET, PSA, and XRD. They are then electrochemically characterized in half cells and full cells with graphite-based electrodes. Materials that demonstrate good performance are cycle life tested. The best, accessible material will be scaled-up to a 6' long laminate by HQ.

### Results

**$\text{LiNi}_{1/2}\text{Mn}_{3/2}\text{O}_4$ .** During the first quarter, a Visiting Scholar joined the group and went to work learning our electrode and cell fabrication processes. By the end of the second quarter he was able to fabricate well-cycling cells. Cycling was performed against Li titanate (electrodes provided by ANL), and two types of graphite: MCMB (Osaka Gas) and CGP-G8 (Conoco Phillips). The majority of the cycling was performed at C/1 charge and discharge.

Through other research, we found that this cathode cycles against lithium up to 4.88 V at C/10 before electrolyte instabilities become dramatically evident. The cycling against lithium was performed with an upper cut-off voltage of 4.85 V and was actually the poorest among all of the anodes. We believe this was a result of a combination of high charge rates, a low upper-cut-off voltage, and excessive impedance rise in the lithium electrode. This cell also displayed the largest rate of overall side reactions of 2% of the capacity per cycle. The cycling against the other electrodes was much more stable with the best coming from the cell with CGP-G8, shown in Figure IV - 18.

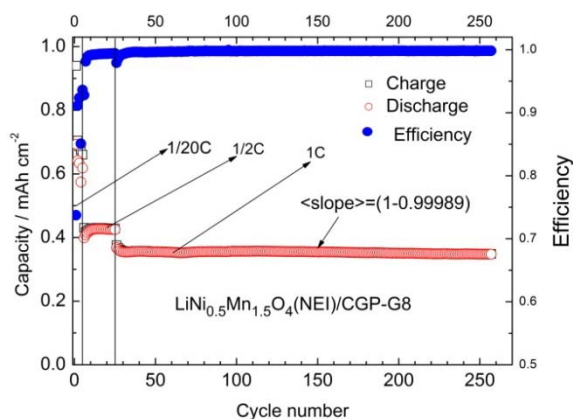


Figure IV - 18: Cycling results of a Graphite/LiNi<sub>1/2</sub>Mn<sub>3/2</sub>O<sub>4</sub> cell.

From our knowledge, this is the best cycling data ever published of a high-voltage, LiNi<sub>1/2</sub>Mn<sub>3/2</sub>O<sub>4</sub> material vs. a graphite electrode with an ordinary electrolyte: the cathode material has no doping, the electrolyte (1M LiPF<sub>6</sub> in EC:DEC 1:2) has no additives.

In the third quarter, we received four LiNi<sub>1/2</sub>Mn<sub>3/2</sub>O<sub>4</sub> materials from HydroQuebec. We evaluated their physical properties and then their electrochemical properties, specifically, their capacity and rate performance. Figure IV - 19 a,b,c show the results of the performance.

Figure IV - 19a, is of the normalized capacity at C/10 for electrodes of different loadings of HQ-1. As expected, the rate capability as a function of C-rate drops as the loading increases. From this graph one can extract capacity as a function of C-rate where 90% of the capacity is still accessible and replotted as in Figure IV - 19b. This was repeated for HQ-2 and the material from NEI. Here we see that the HQ-1 material has superior rate capability. To determine if this capability is a result of particle size, we divided the rate capability of Figure IV - 19b by the loading in g/cm<sup>2</sup> and by the BET surface area of each material and plotted it in Figure IV - 19c. As it turns out, the HQ-1 material had the largest particle size and the smallest surface area and thus this normalization of the data could not explain the superior rate performance.

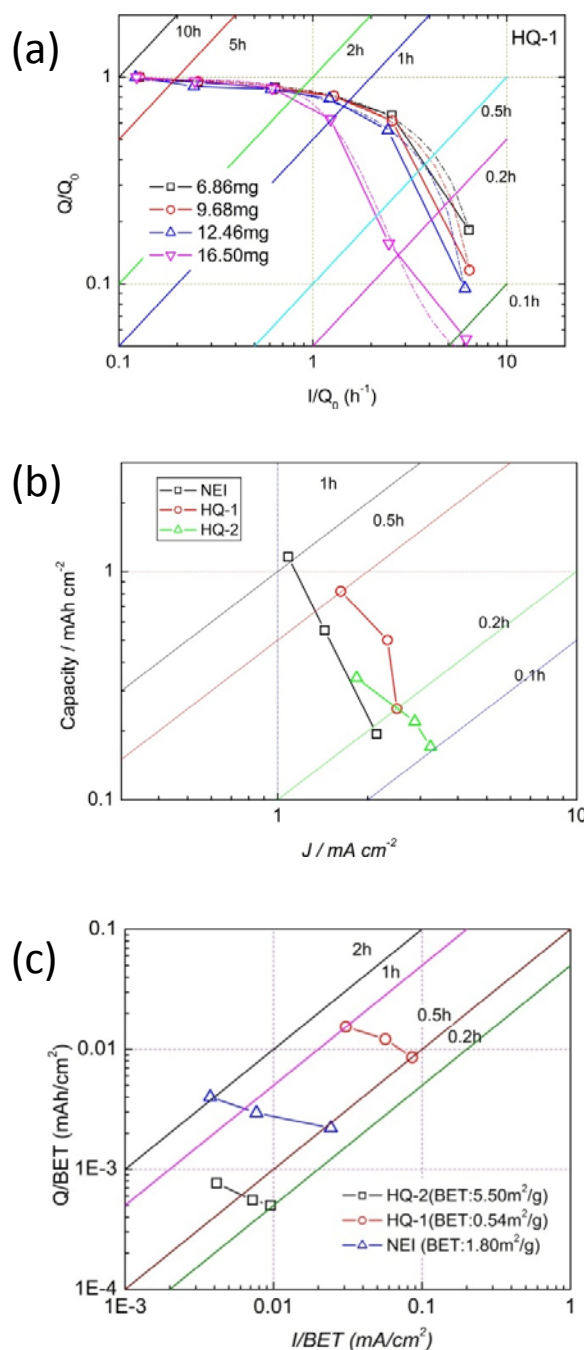


Figure IV - 19: (a). Rate capability of HQ-1 at different loadings, (b). Comparison of rate capabilities of different materials, (c). rate capability of different materials normalized with their specific surface area.

During the fourth quarter we received a second batch of spinel material from NEI. This batch is intended to go to HQ for making laminates and then distributed to interested investigators. HQ received 1 kg of anode material from Conoco Phillips and casted laminates. Our group will now use half-cell and full-cell data to determine the optimum loading of the cathode in order to optimize

the matching of electrodes when paired in a coin cell. The relevant equation that pertains to this matching is given here:

$$\frac{l_c}{l_a} = \frac{q_{r,a} + q_{i,a} \frac{A_a}{A_c}}{1.1(q_{r,c} + q_{i,c})}$$

where  $l_c/l_a$  is the ratio of the mass loadings per unit area,  $q_r$  is the specific reversible capacity,  $q_i$  is the specific irreversible capacity, and  $A$  is the superficial area of the electrode. Subscripts a and c refer to the anode and cathode, respectively. One can measure the reversible capacities from half-cell data and the irreversible capacities from full-cell data. Table IV - 1 gives the irreversible capacities we measured for 4 different electrode loadings. The average of the four measurements is 2.43. Thus, the cathode should have an active material mass per  $\text{cm}^2$  of 2.43 times the mass per  $\text{cm}^2$  of the anode.

Table IV - 1: 1<sup>st</sup> Cycle (10% excess anode)

$l_c/l_a$ (actual)	$q_{i,c}$ (mAh/g)	$q_{i,a}$ (mAh/g)	$l_c/l_a$ (calc.)
<b>2.35</b>	<b>19.95</b>	<b>61.98</b>	<b>2.35</b>
<b>2.52</b>	<b>14.16</b>	<b>62.82</b>	<b>2.46</b>
<b>2.62</b>	<b>13.24</b>	<b>64.06</b>	<b>2.48</b>
<b>2.83</b>	<b>22.89</b>	<b>76.86</b>	<b>2.42</b>
<b>Average</b>			<b>2.43</b>

## Conclusions and Future Directions

LBNL has evaluated a number of materials both physically and electrochemically, some of the results are presented here. We have measured both cycling and rate capability and have found that the material from NEI cycles very well against all electrodes it was cycled against. NEI has been a good working partner and we have ordered 1 kg of LNMO from them for making baseline electrodes. Through half-cell and full-cell measurements, we have determined an optimum loading of cathode vs. CGP-G8.

Through Brett Lucht (U. Rhode Island) we have established a contact with BASF and are working with them toward acquiring a high-voltage spinel material and their high-energy NCM material.

Beyond the high-voltage spinel effort, we have also acquired a few other samples of advanced materials from BATT PIs including an anode material from P. Kumta and an electrolyte additive from D. Scherson. We look forward to working with them in developing test protocols.

## FY 2011 Publications/Presentations

1. 2011 DOE Annual Peer Review Meeting Presentation.

## IV.B.2 Applied Battery Research on Anodes

### IV.B.2.1 Developing a New High Capacity Anode with Long Life (ANL)

Ali Abouimrane & Khalil Amine

Argonne National Laboratory  
9700 South Cass Avenue  
Argonne, IL 60439-4837  
Phone: (630) 252-3729 or 3838; Fax: (630) 972-4520  
E-mail: [abouimrane@anl.gov](mailto:abouimrane@anl.gov); [amine@anl.gov](mailto:amine@anl.gov)

Collaborators:

B. Liu, D. Dambournet (CSE/ANL).  
P. Chupas, K. Chapman, Y. Ren (APS/ANL).  
Z. Fang (University of Utah).  
FMC, Northwestern University.

Start Date: October, 2008

Projected End Date: September, 2014

#### Accomplishments

We have prepared and explored the  $M_aO_b-Sn_xCo_yC_z$  anode system (where  $M=Si, Sn, Mo, Ge$ ) in terms of electrochemistry and material characteristics. We identified  $SiO-Sn_xCo_yC_z$  as the best material in terms of cost, voltage output, cycling performance, and deliverable capacity. Accomplishments include the following:

- A scalable amount of anode material (~ 250 grams) was prepared, and achieved 900 mAh/g capacity for 100 cycles.
- Battery performance was studied at room and high temperature and shows good performance.
- In the full cell configuration, the anode exhibited high capacity with good cyclability.



#### Objectives

Develop new high-capacity anode materials based on a mixture of  $M_aO_b$  oxides ( $M = Si, Sn, Mo, Ge$ ) and  $Sn_xCo_yC_z$  alloy. Characterize, and test the cycling performance of these new anodes for potential use in transportation applications such as PHEVs and EVs.

#### Technical Barriers

The primary technical barrier is the development of a safe and cost-effective PHEV battery (40 mile electric range) that meets or exceeds all DOE performance goals. The actual technical barriers are:

- Cell energy density (by volume and/or by weight) limitations and
- Battery cycle life and high temperature performance.

#### Technical Targets

When this new anode chemistry is combined with lithium nickel manganese cobalt (NMC) oxide cathodes, the following results can be achieved:

- Cell with nominal voltage of 3.5 V,
- Cell with energy density approaching 400 Wh/kg, and
- Cell with higher energy density per volume.

#### Introduction

State-of-the-art lithium-ion battery technology is being developed for large-scale applications such as EVs and HEVs. For this purpose, lithium-ion batteries must have long-term cycling performance with high capacity. The graphite that is currently used as an anode material has a capacity of about 372 mAh/g, where lithium forms graphite intercalation compounds ( $LiC_6$ ) with excellent reversibility. Ongoing research efforts have focused on utilizing various materials (oxides, alloys, tin, and silicon) to increase battery capacity, cycle life, and charge-discharge rates. Attention has been recently given to the potential of metal oxide anodes for lithium-ion batteries because of their low price and high theoretical capacities (more than 600 mAh/g). However, these anode materials suffer from poor cyclability due to the volume expansion of the lithiated material. Other interesting anode materials are tin-based alloys, which have been investigated for use in electronic devices and introduced into the market by Sony. For these anodes a practical capacity of about 400-500 mAh/g can be achieved, and the capacity per volume of the full cell is increased by 30% compared with that of the graphite anode.

#### Approach

Finding new anode materials with higher capacity has been one of the most important research focuses in efforts

to develop batteries for new applications such as electric and hybrid vehicles. Tin-based alloys have been investigated for use in electronic devices with the introduction of Nexelion by Sony. The tin-based alloys contain a huge amount of inactive, expensive, and toxic cobalt, which prevents volume expansion during cycling. Our objective for new anodes is to reduce the cobalt amount, increase the capacity to 600-800 mAh/g, and increase the tap density to above 1.9 g/cc, which is 65% higher than that of graphite (1.1~1.2 g/cc). New materials based on the  $M_aO_b$  oxides ( $M = Si, Sn, Mo, Ge$ ) and  $Sn_xCo_yC_z$  alloys were prepared and tested as anodes for lithium batteries. In the  $M_aO_b-Sn_xCo_yC_z$  composite,  $Sn_xCo_yC_z$  plays the role of a buffer for the  $M_aO_b$  anode and improves its cyclability, while  $M_aO_b$  provides more capacity.

## Results

We have studied various compositions of the oxide-alloy composite  $M_aO_b-Sn_xCo_yC_z$  (where  $M = Si, Sn, Mo, Ge$ ). These materials deliver a capacity between 400 and 900 mAh/g. This material was prepared by ball milling. For example, we investigated lithium insertion and deinsertion in 50 wt% SiO-50 wt%  $Sn_{30}Co_{30}C_{40}$  anode material. As shown in Figure IV - 20, a quasi-plateau located below 0.6 V appears in the first discharge curve, and the capacity is about 1430 mAh/g. During this discharge process a capacity of 90 mAh/g was delivered before reaching a voltage of 0.75 V. This capacity can be attributed to the formation of a solid-electrolyte interphase (SEI) layer, which consists of ethylene oxide-based oligomers, LiF,  $Li_2CO_3$ , and lithium alkyl carbonate ( $ROCO_2Li$ ). As the anode material contains both an oxide and alloy, the electrochemical process involves two major reactions:  $MO + 2Li \rightarrow M + Li_2O$  and  $M + xLi \rightarrow MLi_x$ . The charge-discharge reversibility of this material is poor, about 79%, for the 1<sup>st</sup> cycle. After the 1<sup>st</sup> cycle, the charge-discharge curves of each cycle are similar in shape, indicating that the electrode reactions become more reversible.

The rate capability is shown in Figure IV - 21 for the 50 wt%  $MoO_3$ -50 wt%  $Sn_{30}Co_{30}C_{40}$  anode material. The anode was tested between 0.005 and 2.5 V at various current densities from 50 to 2400 mA/g. This anode exhibits superior rate capability; even at the 7~8-C current rate, a capacity about 325 mAh/g was delivered with outstanding charge-discharge efficiency.

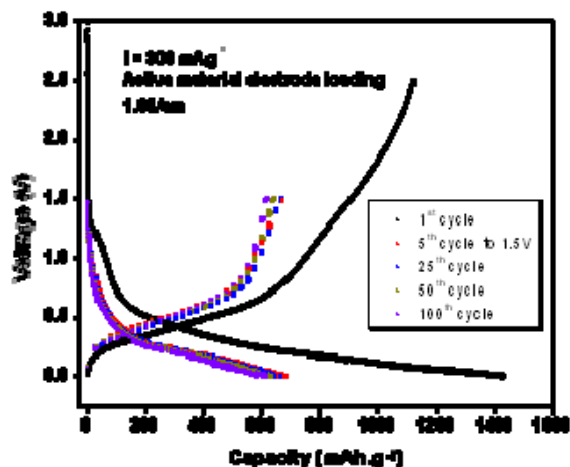


Figure IV - 20: Voltage profile of Li/50 wt% SiO-50 wt%  $Sn_{30}Co_{30}C_{40}$  half-cell at the 1<sup>st</sup>, 5<sup>th</sup>, 25<sup>th</sup>, 50<sup>th</sup>, and 100<sup>th</sup> cycles.

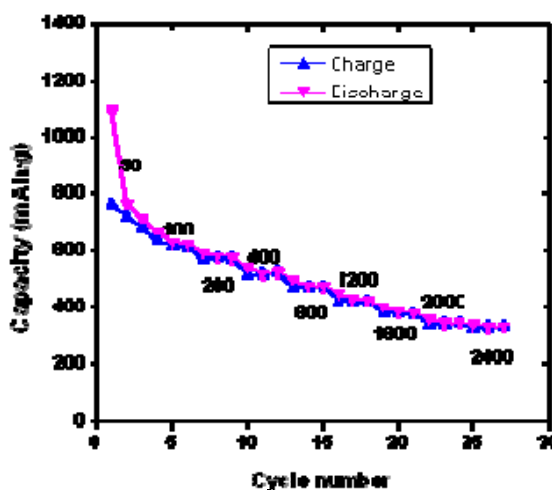


Figure IV - 21: Rate capability of Li/50 wt%  $MoO_3$ -50 wt%  $Sn_{30}Co_{30}C_{40}$  half-cell.

In order to demonstrate scale-up of the 50 wt.% SiO-50 wt.%  $Sn_{30}Co_{30}C_{40}$  anode material, we employed ultra-high-energy ball milling to prepare a single batch of 250 grams. With Spex ball milling, we were able to prepare only 16 grams in one batch. Particle sizes are less than 70  $\mu m$  and less than 30  $\mu m$  for materials prepared by Spex and high-energy ball milling, respectively. Half-cell cycling tests (Figure IV - 22) show that the ultra-high-energy ball milling sample yielded a specific capacity of 930 mAh/g under a current rate of 300 mA/g, which is much higher than the specific capacity attained for the Spex milling material (only 650 mAh/g at 300 mA/g). This considerable difference is attributed to the smaller particle size in the case of the high-energy ball milling preparation, which facilitates lithium insertion and enhances the rate capability. The anodes prepared by both milling techniques exhibit good cycling performance. Indeed, no capacity fade was observed after 50 cycles.

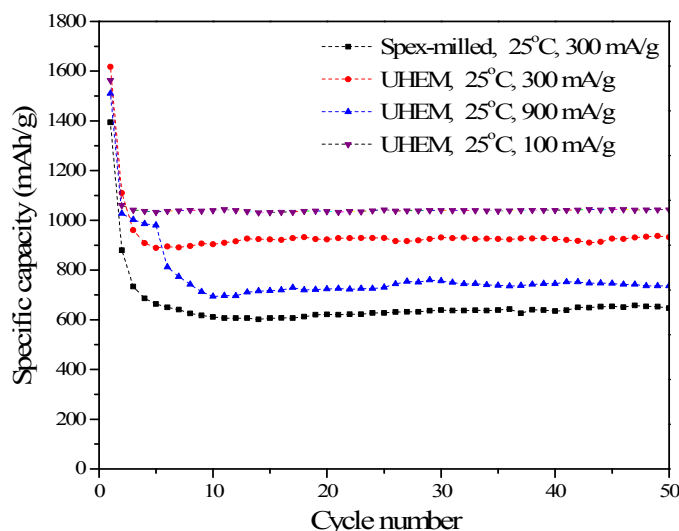


Figure IV - 22: Cycle performance of 50wt.% SiO-50wt.% Sn<sub>30</sub>Co<sub>30</sub>C<sub>40</sub> prepared by Spex-milling and ultrahigh energy milling.

## Conclusions and Future Directions

Our results demonstrate that the SiO-Sn<sub>x</sub>Co<sub>y</sub>C<sub>z</sub> anode material delivers a capacity near 900 mAh/g at room temperature. No capacity fade with cycling was observed even under a high rate of 1C. We envisage testing this anode material at high temperature (55°C) and in the full cell configuration using 5-V LiNi<sub>0.5</sub>Mn<sub>1.5</sub>O<sub>4</sub> spinel, NMC, and ANL-developed NMC materials. As this material shows ~25% first-cycle irreversibility, further work using a mixture of this anode material with a small amount of carbon-coated lithium from FMC Corp. is also envisaged.

## FY 2011 Publications/Presentations

1. 2011 DOE Annual Peer Review Meeting Presentation, May 9-13, 2011, Washington DC.

## IV.B.2.2 Develop Improved Methods of Making Inter-metallic Anodes (ANL)

Andrew N. Jansen

Argonne National Laboratory  
9700 South Cass Avenue  
Argonne, IL 60439-4837  
Phone: (630) 252-4956; Fax: (630) 972-4461  
E-mail: [jansen@anl.gov](mailto:jansen@anl.gov)

Collaborators:

Jack Vaughney, Argonne  
Dileep Singh, Argonne  
Kristen Pappacena, Argonne  
Dennis Dees, Argonne  
Paul Nelson, Argonne  
Joseph Kubal, Argonne

Start Date: October, 2008

Projected End Date: September, 2011

### Accomplishments

- Tested tailor made intermetallic alloys of 0.5 micron particle size with several different metal dopants.
- Developed blending and coating process to make electrodes with varying thickness of  $\text{Cu}_6\text{Sn}_5$ .
- Evaluated the influence of binders and inert additives to electrode powder mix.
- Expanded Argonne's Battery Design Model to assess the benefit of using intermetallic alloys in PHEV batteries.
- Measured mechanical properties of several intermetallic alloys to predict optimum particle size.



### Objectives

The objective of this work in FY2011 is to produce an intermetallic electrode that can achieve over 200 cycles while retaining 80% of its initial capacity. Likely solutions to these problems will involve the proper choice of binders and methods of controlling the particle size and morphology during production, and during repeated cycling.

### Technical Barriers

PHEVs need a high energy density battery to meet the 40 mile range target in 120 kg (80 L) battery size. Intermetallic alloys have the potential to be high capacity anode materials, but the following issues must be addressed

- Low cycle life
- Large volume expansion upon lithiation.

### Technical Targets

- Determine the influence of binder on  $\text{Cu}_6\text{Sn}_5$  cycle life.
- Explore methods of controlling particle size and morphology.
- Produce an intermetallic electrode capable of 200 cycles and 80% capacity retention.

### Introduction

Previous work from the BATT program has shown that doped- $\text{Cu}_6\text{Sn}_5$  materials have reversible capacities similar to graphite. Their voltage profile (Figure IV - 23) is approximately 100 mV above graphite potential, which should enhance safety but not significantly affect energy. When their high material density is taken into account the volumetric capacities are nearly 3X that of an optimized graphite based electrode as can be seen in Figure IV - 24. This will enable the use of much thinner negative electrodes; smaller batteries for same energy.

Work on the  $\text{Li}_x\text{Si}$  system has shown that using binders more appropriate for the volume expansion of the  $\text{Li}_x\text{Si}$  system can greatly enhance cycle life. It is hoped that with proper binder selection and particle size and morphology  $\text{Cu}_6\text{Sn}_5$ -based materials will find success as lithium-ion anodes.

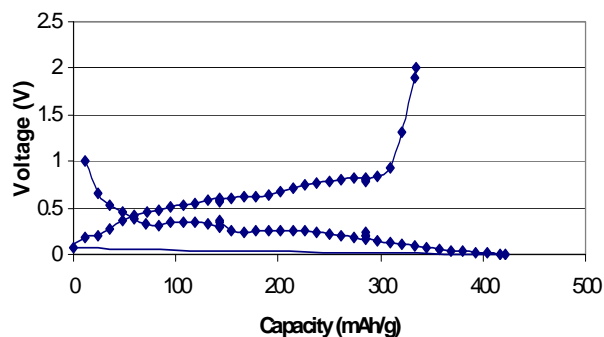


Figure IV - 23: Charge and discharge voltage profile of  $\text{Cu}_6\text{Sn}_5$  versus lithium.

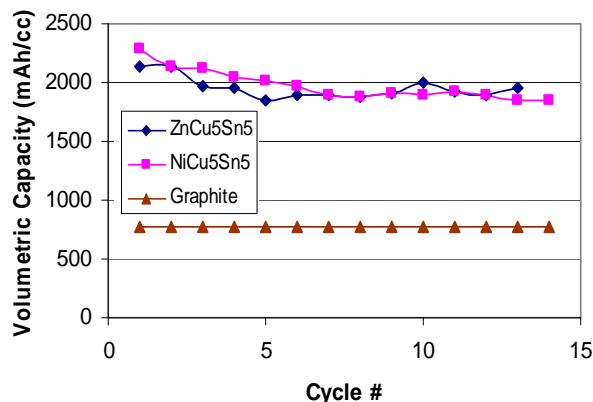


Figure IV - 24: Volumetric capacity density of  $\text{Cu}_6\text{Sn}_5$ -based intermetallic alloys compared against graphite.

## Approach

The general approach is to explore alternative methods of making electrodes based on intermetallic alloys, such as  $\text{Cu}_6\text{Sn}_5$ , which suffer from severe volume expansion upon lithiation. Earlier work in this task showed that the choice of binders and additives in the electrode did not improve the poor cycle life. This work was done for a relatively large particle of 10  $\mu\text{m}$ .

Efforts were then directed to determine the ideal particle size to minimize particle cracking during cycling. This work indicated that the alloy particle must be submicron in size. A contract was established with Wildcat Discovery Technologies to make  $\text{MCu}_5\text{Sn}_5$  alloy powders that are near 400 nm. These powders were received in the summer of 2010. This year's effort (FY11) was devoted to characterizing the performance of these smaller particles in new electrode studies.

Success will be achieved upon development of an electrode that can accommodate the large volume expansion and contraction during deep discharge cycling, and can prevent the excluded metal (such as copper) from agglomerating into an inert mass during cycling.

## Results

In FY09, several classes of commercial binders were evaluated with a commercially prepared sample of  $\text{Cu}_6\text{Sn}_5$  powder. The binders include PVDF-based polymers with functional groups tailored for anodes and cathodes over a range of molecular weights, and a few aqueous-based binders. Several methods of making electrode slurry were explored including an initial step of dry blending the  $\text{Cu}_6\text{Sn}_5$  powder with acetylene black carbon and SFG-6 graphite on a roller mill.

The cycle life of each electrode was determined from coin cells, and was found to be only around 20 cycles. The choice of binder did not significantly affect the capacity loss rate of these electrodes. This result was not expected

and a search was begun to determine the cause of this excessive capacity loss.

Electrodes were also made with  $\text{Cu}_6\text{Sn}_5$  and acetylene black as the baseline mix, into which graphite, MgO or alumina powder was added. It was hoped that this would help prevent the metal diffusion (Cu and its substitutes) away from the active tin. Unfortunately, the addition of metal oxide additives to the bulk electrode did not appear to prevent capacity fade in these thick electrode designs.

Cells were also made with the large (10  $\mu\text{m}$ ) particles of  $\text{Cu}_6\text{Sn}_5$  and cycled with baseline electrolyte and electrolyte with 10% FEC. At the end of life the cells were opened and the electrodes washed with DMC/DEC. A relatively large film was observed covering the electrode particles and large cracks were observed on its surface and the particles underneath. These film sheets are over twice as large as the original particle. FEC had a strong influence on surface morphology but did not appear to prevent particle/film cracking. Copper color was also observed on both electrodes after cycling, which indicates that copper displacement is a problem. The copper foil underneath appeared to be unaffected.

It became clear that the commercially obtained  $\text{Cu}_6\text{Sn}_5$  baseline material was not ideal for use in a lithium-ion battery. No binder or inert additive was found that could compensate for the large volume expansion that occurs upon lithiation. Repeated cycling caused the particle to crack and split into smaller particles that are no longer connected to the conductive electrode matrix. Modeling work in literature suggests that the particle cracking problem can be avoided by starting with a particle that is less than a critical size.

In FY10, efforts were directed to determine the optimum particle size for  $\text{Cu}_6\text{Sn}_5$  based on the model of Huggins and Nix<sup>16</sup>. They developed a simplified model based on the modulus and fracture toughness of the bulk Sn material. The results of this model can be represented by the following equation:

$$h_c \approx \frac{23}{\pi} \left( \frac{3K_{Ic}}{Be_\tau} \right)^2$$

where

$h_c$  is critical size in  $\mu\text{m}$   
 $K_{Ic}$  is fracture toughness in  $\text{MPa}\cdot\text{m}^{1/2}$   
 $B$  is elastic modulus in GPa  
 $e_\tau$  is strain dilation ( $\Delta V/V$ )

<sup>16</sup> R.A. Huggins and W.D. Nix, "Decrepitation For Capacity Loss During Cycling of Alloys in Rechargeable Electrochemical Systems", *Ionics* 6 (2000) p. 57-63.

This opens up a new approach to searching for optimum intermetallic anode materials: Find metallic and intermetallic alloys that are capable of being lithiated and then determine their bulk mechanical properties to determine a critical particle size. If the particle size is too small then try to increase the fracture toughness and decrease the elastic modulus of the metal anode material through alloying with additional metals and phases.

The mechanical properties of  $\text{Li}_x\text{M}_y\text{Cu}_5\text{Sn}_5$  electrode materials are not known in literature. Efforts were undertaken to determine these properties for  $\text{Cu}_6\text{Sn}_5$  and its alloys. The mechanical properties of several intermetallic alloys were determined at Argonne. The elastic modulus was obtained using a Universal Materials Testing Machine (Instron). Measurements were made from stress strain plots obtained during four-point-bend tests using rectangular bars of the test material (Figure IV - 25). Outer fiber stress and associated strain were obtained from standard elastic beam theory. Slope of the stress vs. strain plot gave the elastic modulus of each alloy.

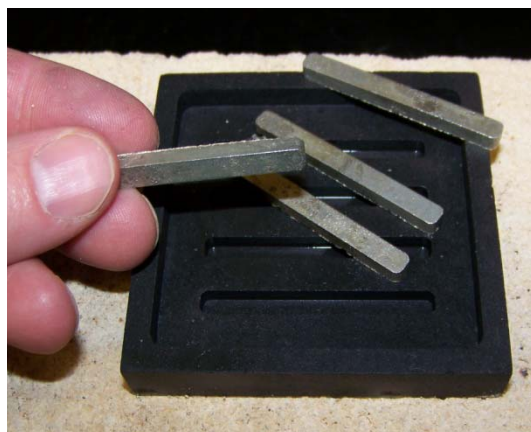


Figure IV - 25: Photo of rectangular bars cast from various intermetallic alloys used for mechanical property studies.

The fracture toughness was obtained via a Single Edged Notched Bend (SENB) test. A thin wafering blade was used to notch the samples such that the notch depth to sample thickness was  $\sim 0.5$ . Samples were tested in three-point bend loading configuration at a constant displacement rate. Fracture toughness was determined from the peak load at failure, sample dimensions, and a standard fracture mechanics relationship.

In this year's effort, the mechanical properties of a lithiated copper tin alloy were measured using cast bars of the alloy. These results are tabulated here (Table IV - 2) with comparison to unlithiated alloys.

Table IV - 2: Mechanical Properties of Lithiated Copper Tin alloys

Alloy	Strength (MPa)	Biaxial Modulus (GPa)	Fracture Toughness ( $\text{MPa m}^{0.5}$ )
$\text{Cu}_6\text{Sn}_5$	$71 \pm 18$	$54 \pm 12$	$2.19 \pm 0.54$
$\text{NiCu}_5\text{Sn}_5$	$44.4 \pm 2.7$	$79.1 \pm 4.1$	$1.32 \pm 0.13$
$\text{ZnCu}_5\text{Sn}_5$	$104.2 \pm 3.1$	$55.3 \pm 4.4$	$2.56 \pm 0.23$
$\text{FeCu}_5\text{Sn}_5$	$88.0 \pm 6.5$	$74.3 \pm 2.8$	$2.38 \pm 0.15$
$\text{Cu}_5\text{Sn}_6$	$73.9 \pm 2.7$	$54.0 \pm 7.8$	$2.56 \pm 0.40$
$\text{Li}_5\text{Cu}_6\text{Sn}_5$	$23.7 \pm 9.3$	$54 \pm 19$	$0.95 \pm 0.39$

From this table it can be seen that lithiation lowers the fracture toughness and strength, but does not affect the modulus. The critical particle size can now be estimated based on Huggins' decrepitation model. This result is compared against unlithiated alloys in the table below. If the results of these data and the model are correct, it predicts an unfortunate response of the particle to lithiation. Namely, as the alloy becomes lithiated, it becomes more brittle. This indicates that even smaller particle sizes are required to prevent particle cracking upon lithiation.

The measured mechanical properties were then used in the equation above from Huggins' model and the optimum particle size was calculated. Two optimum particle sizes were calculated – one for lithiation halfway (to  $\text{Li}_2\text{CuSn}$ ) and one for full lithiation (to  $\text{Li}_{17}\text{Sn}_4$ ). These results are shown in Table IV - 3. In general, the optimum particle size is near 0.5 microns for half lithiation, and near 50 nanometers for full lithiation for all of the alloys studied, except for the nickel based alloy, which required even smaller particles. It is no surprise that the efforts based on the commercial sample with 10 micron particle size met with little success as this is nearly two orders of magnitude larger than the 0.5 micron predicted particle size.

A search was performed to find a new source for smaller particle size  $\text{Cu}_6\text{Sn}_5$  based intermetallic alloys that led to Wildcat Discovery Technologies. They are a high throughput materials discovery company with specialty synthesis capabilities. Wildcat performed a high throughput screen to identify reaction conditions for the target particle size that Argonne provided. A variety of morphologies were induced, and a final selection was made for one synthesis method based on its resulting primary particle size and separation. Five 100-g alloys were then synthesized by Wildcat Discovery Technologies with the composition of  $\text{MCu}_5\text{Sn}_5$ , where M was Cu, Sn, Ni, Zn, and Fe with a controlled particle size near 0.5 microns.

Table IV - 3: Optimum Particle Sizes Calculated for Halfway and Full Lithiation

Intermetallic Alloy	10Li + MCu <sub>5</sub> Sn <sub>5</sub> ↔ 5Li <sub>2</sub> CuSn + M		85Li + 4MCu <sub>5</sub> Sn <sub>5</sub> ↔ 5Li <sub>17</sub> Sn <sub>4</sub> + 20Cu + 4M	
	Critical Particle Size, μm (eT = 0.63)	Theoretical Capacity, mAh/g	Critical Particle Size, μm (eT = 1.8)	Theoretical Capacity, mAh/g
Cu <sub>6</sub> Sn <sub>5</sub>	0.27	257	0.033	507
NiCu <sub>5</sub> Sn <sub>5</sub>	0.046	258	0.0057	510
ZnCu <sub>5</sub> Sn <sub>5</sub>	0.36	256	0.044	507
FeCu <sub>5</sub> Sn <sub>5</sub>	0.17	259	0.021	511
Cu <sub>5</sub> Sn <sub>6</sub>	0.37	~244	0.046	566
Li <sub>5</sub> Cu <sub>6</sub> Sn <sub>5</sub>	0.051	-	0.0063	-

Table IV - 4: Estimated Electrode Capacity Density for Five Electrodes

Anode	Tap Density g/mL	2 <sup>nd</sup> Delithiation Capacity of Alloy, mAh/g	Electrode Capacity Density mAh/cm <sup>3</sup>
Cu <sub>6</sub> Sn <sub>5</sub>	2.05	472	544
NiCu <sub>5</sub> Sn <sub>5</sub>	2.90	434	513
ZnCu <sub>5</sub> Sn <sub>5</sub>	2.48	488	704
FeCu <sub>5</sub> Sn <sub>5</sub>	2.46	514	757
Cu <sub>5</sub> Sn <sub>6</sub>	2.51	557	816
Graphite	0.8 - 1.1	340	440

Half cells were made with electrodes based on the new smaller alloys from Wildcat Discovery Technologies. While the primary particle size is near 400 nm, many of these particles are agglomerated into secondary particles. Energetic milling and mixing techniques are needed to break up these particles during the slurry making process. Differences were seen in the voltage profiles for these five alloys (Figure IV - 26).

In particular, the 0.4 volt plateau corresponding to Li<sub>2</sub>CuSn was not seen for the Ni and Zn substituted alloys. These metals may interfere with this phase formation. The capacity of these five alloys was near, or slightly over, the theoretical capacity. An estimate of the electrode capacity density was also made based on these electrodes and is shown in the Table IV - 4. All of the MCu<sub>5</sub>Sn<sub>5</sub> electrodes have an electrode capacity density greater than graphite electrodes, and continues to warrant further consideration.

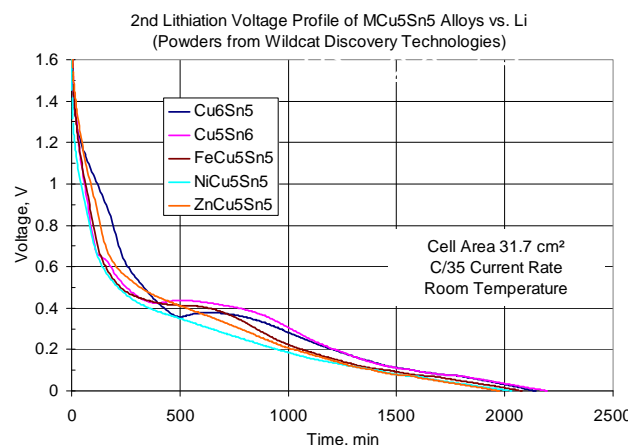


Figure IV - 26: SEM photo of optimum Cu<sub>6</sub>Sn<sub>5</sub> powder based on mechanical properties for discharge to Li<sub>2</sub>CuSn.

Electrodes made with these smaller sized particles did not improve the cycle life problem. Variations in the amount of carbon black and PVDF binder were studied. The influence of a lower cutoff voltage was also assessed. To date, no effective means of extending the cycle life to 200 cycles has been achieved. It is hoped that improved slurry processing and electrode composition and processing will improve the cycle life. But, it is possible that the poor cycle life could be due to the larger surface area (higher activity) of the smaller particles, or the primary particles are still too large, or copper displacement is preventing re-alloying. Effort should also be directed to other classes of binders (cellulose and polyimide).

### Conclusions and Future Directions

It became clear in this effort that engineering efforts alone cannot solve the problem of expansion and contraction during cycling. It was hoped that success would be achieved if an intermetallic alloy could be made with an ideal composition and optimum particle size in an electrode configuration that can accommodate large volume changes of its active material.

FY11 efforts were centered on electrochemically testing MCu<sub>5</sub>Sn<sub>5</sub> alloys with 0.5 micron particle size from Wildcat Discovery Technologies. The mass specific capacity of these materials is up to 60 % more than a typical graphite material. When the capacity density of the actual complete electrode is measured, the volumetric capacity density is up to 85 % more than a typical graphite electrode. This increase in capacity density proves the desire to have intermetallic electrodes is justified. Unfortunately, the cycle life problem for MCu<sub>5</sub>Sn<sub>5</sub> based materials has not been solved. It is likely that the copper displaced during lithiation cannot re-alloy during delithiation to the original starting material.

**FY 2011 Publications/Presentations**

1. Poster presentation at the DOE Vehicles Technology Program 2009 Annual Merit Review Meeting.
2. Oral presentation at the DOE Vehicles Technology Program 2010 Annual Merit Review Meeting.
3. Poster presentation at the DOE Vehicles Technology Program 2011 Annual Merit Review Meeting.
4. A. N. Jansen, J. A. Clevenger, A. M. Baebler, J. T. Vaughey, “Variable temperature performance of intermetallic lithium-ion battery anode materials”, *J. Alloys and Compounds*, 509(13), 4457 – 4461 (2011).

## IV.B.2.3 Spherical Carbon Anodes Fabricated by Autogenic Reactions (ANL)

Vilas G. Pol

Argonne National Laboratory  
9700 South Cass Avenue  
Argonne, IL 60439-4837  
Phone: (630) 252-8127; Fax: (630) 972-4176  
E-mail: [pol@anl.gov](mailto:pol@anl.gov)

### Collaborators:

Michael Thackeray, Argonne National Laboratory  
Dennis Dees, Argonne National Laboratory  
Francois Henry, Superior Graphite  
Jorge Ayala, Superior Graphite  
Zhenhua Mao, ConocoPhillips  
Mark Ewen, ConocoPhillips

Start Date: October, 2010

Projected End Date: September, 2014

### Objectives

- The objective of this project is to synthesize novel spherical carbon materials and evaluate their physical, chemical and electrochemical properties for lithium-ion battery applications.
- Collaborate with industry to access high-temperature furnaces to increase the graphitic component in the as-prepared carbon spheres.
- Study electrochemical, thermal and physical properties such as BET surface area, tap density, true density, composition, structural and morphological properties of as-prepared and heat-treated carbon spheres.

### Technical Barriers

Graphitic carbon, although widely used as the predominant anode in lithium-ion batteries, accommodates lithium close to the potential of metallic lithium which makes it an intrinsically unsafe material - particularly when used in conjunction with flammable electrolyte solvents and metal oxide cathodes at high potentials. The safety concerns of graphite can be somewhat mitigated by using meso-carbon micro beads (MCMB) with rounded edges. However, MCMB products are synthesized at or above 2800°C, making it an expensive form of graphite.

### Technical Targets

- Synthesize novel carbon materials, notably with rounded shapes such as spheres and improve the safety characteristics of the carbon materials over existing graphite products.
- Evaluate thermal stability/reactivity of lithiated carbon electrodes in electrolyte.
- Evaluate the physical, chemical and electrochemical properties of the carbon-based electrodes for lithium-ion battery applications.
- Model current distribution around carbon spheres and further increase the electrochemical properties of the carbon spheres by combining it with a lithium-alloying component (Si, Sn and Sb).

### Accomplishments

- Numerous batches of carbon sphere samples were autogenically synthesized at 700°C and dispatched to industrial collaborators, Superior Graphite, and ConocoPhillips for high temperature heat treatment.
- After receiving heat-treated samples (2400°C and 2800°C for 1 hour), the morphology, structure and compositional properties were studied and compared with autogenically as-prepared hard carbon spheres.
- Evaluated the electrochemical properties of autogenically as-prepared carbon spheres and compared with heat-treated samples. The chemical and thermal stability in the electrolyte over the operating voltage range of lithium-ion cells was studied.



### Introduction

Carbon is an extremely versatile material that exists in numerous forms with diverse physical, chemical, electrical and electrochemical properties. From an electrochemical standpoint, graphite negative electrodes and carbonaceous current collecting agents are workhorse materials in the lithium battery industry. Graphite is an intercalation electrode; it accommodates one lithium atom per C<sub>6</sub> unit a few tens of millivolts above the potential of metallic lithium, generating a theoretical electrochemical capacity of 372 mAh/g. MCMB with rounded edges are a synthetic, but expensive, form of graphite used by the lithium battery industry, can minimize heat-generating side reactions during overcharge. Furthermore, hard carbons, comprised

of disordered graphitic planes, can yield a higher electrochemical capacity than graphite but at higher potentials (vs. metallic lithium) thereby offering enhanced safety. Therefore, we have developed a novel autogenic process to synthesize hard carbon spheres first and further heat treat to higher temperatures to study the thermal effects on morphological, structural and electrochemical behavior.

### Approach

Highly spherical carbon particles are fabricated by self-generated, high pressure (autogenic) reactions from carbon precursors, including plastic waste containing hydrocarbons and are then explored and studied. The initial basic science research on the as-prepared carbon spheres was funded by the EFRC, the Center for Electrical Energy Storage – *Tailored Interfaces*. Industrial collaborations and studies with Superior Graphite and ConocoPhillips were initiated and funded by ABR. The carbon sphere materials offer the possibility of providing a uniform current distribution at the particle surface, thus having the potential for providing superior safety characteristics relative to natural graphite electrodes.

This project includes not only an optimization of the synthesis conditions and electrochemical properties of the as-prepared and heated carbon products, but also a study of their chemical and thermal stability in the electrolyte over the operating voltage range of lithium-ion cells, either on their own or, in a new project initiative, in new architectures with lithium-alloying components to increase the intrinsic capacity of spherical carbon-composite anode materials. To increase the graphitic order in the carbon spheres (CS), the particles were heated to 2400°C (CS-24) by Superior Graphite and to 2800°C by ConocoPhillips (CS-28) in an inert atmosphere.

### Results

Scanning electron microscope images of the as-prepared and CS-24 shows almost perfectly spherical shape, smooth surfaces and 2 – 5 μm diameters (Figure IV - 27a). Though the CS are remarkably stable up to 2400°C, the spherical carbon particles tend to fuse or sinter (indicated by arrows) during heat treatment to 2800°C (Figure IV - 27b) for 1h in inert conditions.

The physical properties of untreated CS, CS-24 and CS-28 samples in terms of morphology, composition, density and structure were determined. The carbon spheres prepared at 700°C are extremely hard and dense, having a true density equivalent to that of graphite (2.2 g/cm<sup>3</sup>). The true density of CS-24 is 2.1 g/cm<sup>3</sup> and CS-28 is slightly lower, 2.04 g/cm<sup>3</sup>. By contrast, the tap density of all the carbon samples is less than 1 g/cm<sup>3</sup>, due to the difficulty of compacting the powders because of an apparent electrostatic charge between the particles. EDS analysis

showed that the spheres consisted of >99% carbon; no other impurities were detected.

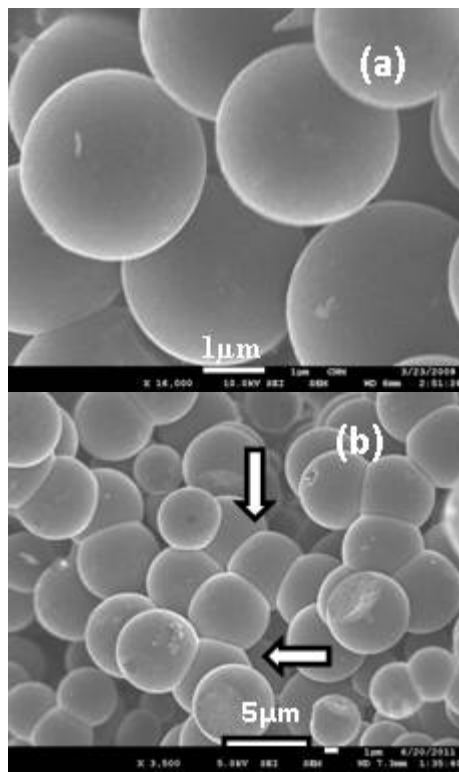


Figure IV - 27: (a) Scanning electron micrographs of autogenically as-prepared carbon spheres, and (b) as-prepared carbon spheres heated to 2800°C.

The BET surface area of the as-prepared CS product was measured to be 4.4 m<sup>2</sup>/g, the particles having a total pore volume of 0.0078 cc/g. Heating the spheres to 2400°C for 1h (CS-24) in an inert atmosphere reduced the surface area to 1.1 m<sup>2</sup>/g and the total pore volume to 0.0043 cc/g. Further heating the carbon spheres to 2800°C for 1h (CS-28) in an inert atmosphere reduced the surface area to 1 m<sup>2</sup>/g and the total pore volume to 0.0032 cc/g. We attributed the decrease in surface area and total pore volume in the heated carbon spheres to the removal of pores or voids during the high temperature treatment.

The structural evolution of the carbon spheres, as a function of temperature was monitored by Raman spectroscopy, Figure IV - 28. The most noticeable features in the Raman spectra of CS (top) are the G (graphitic) band appearing at 1582 cm<sup>-1</sup> and the second-order G' band at about 2670 cm<sup>-1</sup> as an indication of sp<sup>2</sup> carbon networks. In the as-prepared carbon spheres, the ID/IG ratio is 1.1, while in the CS-24 is 0.46 and in the CS-28 is 0.35, indicating increases in the graphitic order in the carbon particles due to heat treatment. The slight increase in the graphitic character of the CS-24 and CS-28 samples was also corroborated by powder X-ray diffraction.

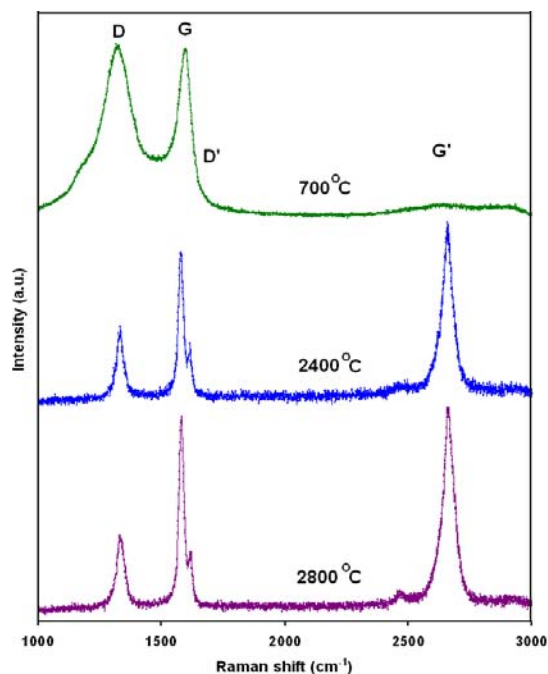


Figure IV - 28: Raman spectra of (a) as prepared CS (top), CS-24 (middle) and CS-28 (bottom).

An evaluation of the thermal stability and reactivity of lithiated CS-24 was carried out and compared with lithiated natural graphite. Between 100 and 200°C, approximately 380 J/g heat was generated due to breakdown of the SEI layer on the carbon spheres. This heat generation value was less than that observed for the lithiated natural graphite electrode (409 J/g), emphasizing the slight advantage that the carbon spheres may have with respect to safety.

The lithium insertion/extraction properties of spherical carbon particle electrodes (CS/Li, CS-24/Li and CS-28/Li) are shown in Figure IV - 29a-c. The 1<sup>st</sup> and 2<sup>nd</sup> discharge/charge cycles of a Li/CS cell are shown in Figure IV - 29a (inset). The voltage profile of the autogenically prepared carbon spheres are different (sloping behavior) to the graphitic materials such as SFG 6. The sloping discharge profile on the second and subsequent cycles is characteristic for a hard carbon containing turbostratically-disordered graphene (or graphitic) sheets on both sides of which lithium can bond to carbon during the electrochemical charge of a lithium-ion cell.

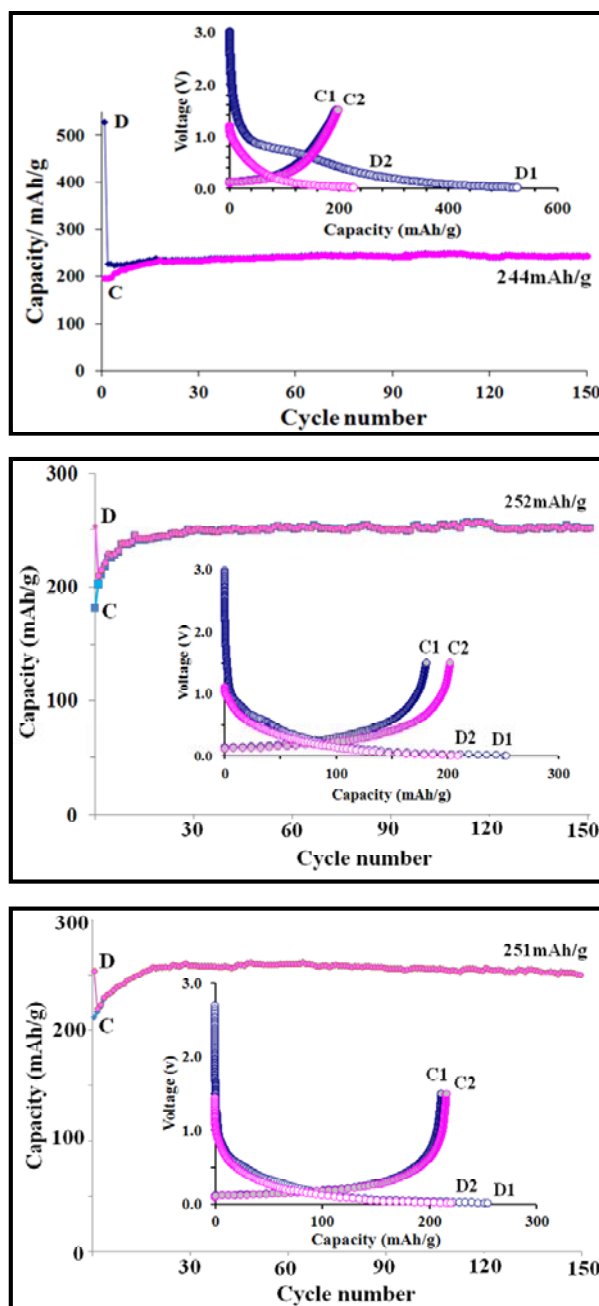


Figure IV - 29: (a) Capacity vs. cycle number of Li/CS cells (0.24 A/g (~1C) rate); 1.5 V – 10 mV); (b) Capacity vs. cycle number of Li/CSP-24 cells (0.24 A/g (~1C) rate); (c) Capacity vs. cycle number of Li/CS-28 cells (0.24 A/g (~1C) rate) and corresponding discharge-charge profiles for the 1<sup>st</sup> and 2<sup>nd</sup> cycles.

The 1<sup>st</sup> and 2<sup>nd</sup> discharge/charge cycles and capacity vs. cycle number plots of Li/CS-24 and Li/CS-28 cells are shown in Figure IV - 29. The heat-treated spherical carbon particle electrodes with higher graphitic character were cycled (Figure IV - 29b and Figure IV - 29c, and insets) and compared with the parent CS (Figure IV - 29a) under the similar conditions. For the CS-24 and CS-28 electrodes,

the capacity increased steadily on cycling at a 1C rate to reach ~250 mAh/g after 25 cycles, i.e., marginally greater than the capacity of the CS electrodes (~240mAh/g) after the same number of cycles. Most of the electrodes needed several break-in cycles to reach a stable cycling capacity. Overall, the capacity delivered by all the electrodes, their cycling profiles, and cycling stability was similar. The coulombic efficiency of all the half cells during subsequent cycles was >99%.

A noticeable advantage of the CS-24 and CS-28 electrodes was that the heat-treatment process slightly increased the graphitic order (as shown in Raman spectra) within the carbon spheres, significantly reducing the first-cycle capacity loss relative to as-prepared CS electrodes. This improvement in the first-cycle coulombic efficiency is attributed to the removal of entrapped pores and voids during high temperature heat treatment of the carbon spheres. However, the overall specific capacity of the carbon spheres was not dramatically improved, indicating the difficulty to achieve higher efficiency from such amorphous glassy carbon products, even after heat treatment. Moreover, spherical carbon particles offer the possibility of smoothing the current distribution on the surface of the spheres, minimizing the possibility of dendrite formation and short circuits.

### Conclusions and Future Directions

Autogenic reactions offer a relatively simple and facile method to fabricate carbon spheres from polyethylene products, including plastic waste. When used as electrodes, the as-prepared carbon spheres electrodes deliver a stable capacity of ~250 mAh/g for hundreds of cycles in lithium half cells. A perceptible advantage of the CS-24 and CS-28 electrodes was the significant reduction in the first-cycle capacity loss. Spherical carbon particles are likely to offer the possibility of providing a uniform current distribution at the particle surface, and for providing enhanced safety relative to natural graphite electrodes. In his respect, a decrease in heat generation was observed for the lithiated carbon spheres compared to natural graphite electrodes, emphasizing this safety advantage. Analogous results were obtained when mesitylene was used as the precursor to prepare spherical carbon and heat-treated products.

In future, we plan to evaluate electrochemical properties of carbon sphere anodes in a full lithium-ion configuration, for example, against Argonne's standard high capacity cathodes of nominal formula  $0.5\text{Li}_2\text{MnO}_3 \bullet 0.5\text{LiNi}_{0.44}\text{Co}_{0.25}\text{Mn}_{0.31}\text{O}_2$  to monitor, in particular, cycle life and rate performance. Diagnostic studies will be performed to gain a detailed understanding of structural and morphological changes to the carbon sphere materials.

In order to achieve capacities higher than 250 mAh/g (i.e., higher than the theoretical value of graphite (372 mAh/g), we have initiated experiments to prepare high capacity composite electrodes, for example, carbon-Si, carbon- Sb and carbon-Sn using the novel anode architectures obtained with autogenic or sonochemical reactions. Preliminary results are encouraging; indications are that capacities >400 mAh/g can be obtained with a small amount of a Li-alloying element in the electrode. Physical, chemical and electrochemical properties of these composite electrodes will be evaluated. The investigations will be complemented by modeling the current distribution to determine the benefit of using carbon spheres vs. other forms of carbon with respect to suppressing lithium dendrite formation and enhancing the safety of lithium-ion cells; the modeling studies will be conducted in collaboration with Dennis Dees at Argonne.

### FY 2011 Publications/Presentations/Patents

1. V. G. Pol and M. M. Thackeray, 2011 DOE Annual Peer Review Meeting Presentation, Washington DC, 9-13 May 2011.
2. V. G. Pol and M. M. Thackeray, *Autogenic reactions for fabricating lithium battery electrode materials*, Ceramic Materials for Energy Applications: Ceramic Engineering and Science Proceedings, Proceedings of the 35<sup>th</sup> International Conference on Advanced Ceramics & Composites (ICACC), Volume 32, Issue 9 (2011).
3. V. G. Pol and M. M. Thackeray, *Spherical carbon particles and carbon nanotubes prepared by autogenic reactions: Evaluation as anodes in lithium electrochemical cells*, Energy & Environ. Sci., 4, 1904–1912 (2011). (Front cover).
4. V. G. Pol and M. M. Thackeray, *Autogenic reactions for the fabrication of lithium battery electrode materials*, Int. Conference on Advanced Ceramics and Composites (ICACC11), Daytona Beach, Florida, USA, 23-28 January (2011).
5. V.G. Pol (Invited), *Making carbon spheres and carbon nanotubes from scrap plastics*, 2011 Plastic recycling conference, New Orleans, LA, 1-2 March (2011).

## IV.B.2.4 Functionalized Surface Modification Agents to Suppress Gassing Issue of $\text{Li}_4\text{Ti}_5\text{O}_{12}$ -Based Lithium-Ion Chemistry (ANL)

Yan Qin, Zonghai Chen, and Khalil Amine

Argonne National Laboratory  
9700 South Cass Avenue  
Argonne, IL 60439-4837  
Phone: (630) 252-3838; Fax: (630) 972-4451  
E-mail: [amine@anl.gov](mailto:amine@anl.gov)

Collaborators:  
EnerDel  
University of Colorado

Start Date: October, 2009  
Projected End Date: September, 2014

- The source of the gassing was identified, and a mechanism was proposed.
- A solution was proposed according to the proposed mechanism.
- A surface modification additive was proposed and tested and shown to be promising.



### Introduction

$\text{Li}_4\text{Ti}_5\text{O}_{12}$  (LTO) is a promising alternative anode material, which exhibits extremely long life, high power, low cost, and unmatched safety characteristics for HEV applications. The long cycle life arises from the structural stability of LTO, which is able to accommodate up to three lithium ions in the spinel structure without volume expansion. By contrast, the conventional carbon anode expands up to 16 vol% during charging.<sup>17</sup> The high operation voltage of LTO prevents the growth of lithium dendrites, which results in good safety. Recent research progress indicates that it might be possible to achieve high tap density and excellent rate capability with “micron secondary nano primary” structure LTO.<sup>18</sup>

Coupling LTO with high-voltage, high-energy cathode materials like  $\text{LiNi}_{0.5}\text{Mn}_{1.5}\text{O}_4$  (LMNO) or  $\text{LiMn}_2\text{O}_4$  (LMO) provides an opportunity to meet both the energy and power requirements for PHEV applications. So far the LNMO/LTO system using conventional electrolyte has achieved 5000 cycles at 25°C.

Despite all the advantages of the LMO/LTO and LNMO/LTO chemistry, one obstacle prevents it from commercialization. The LTO continuously releases gas when aging or operating at elevated temperature. This gas deteriorates the cycling and power performance. Furthermore, the majority of the gas is hydrogen, which poses a serious safety problem.

### Objectives

The objective of this work is to explore methods and to develop functionalized surface modification agents to address the gassing issue of lithiated  $\text{Li}_4\text{Ti}_5\text{O}_{12}$  (LTO) during high-temperature aging or operation. This can be the enabling technology for  $\text{Li}_4\text{Ti}_5\text{O}_{12}$  anodes to achieve long-life, high-power batteries with unmatched safety for use in PHEVs.

### Technical Barrier

The primary barrier is continuous gas generation, which damages the cycle and calendar life of lithium-ion batteries with LTO-based chemistry.

### Technical Targets

The objective of this work is to investigate the gassing mechanism of  $\text{Li}_4\text{Ti}_5\text{O}_{12}$  and to develop advanced processes to solve this problem.

- Identify gassing mechanism.
- Identify and develop advanced processes to eliminate the gassing issue.

### Accomplishments

- The condition that leads to severe gassing was identified.
- The major component of the gas was identified.
- The salt effect on the gassing was investigated and identified.

<sup>17</sup>T. Ohzuku, A. Ueda, N. Yamamoto, J. Electrochem. Soc., **142**, (1995) 1431.

<sup>18</sup> K. Amine, I. Belharouak, Z. Chen, etc. Advanced Materials, **22** (2010) 3052.

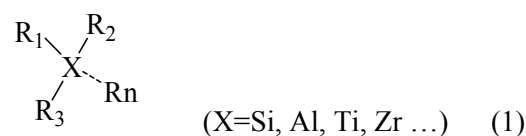
## Approach

To overcome the above technical barrier, we sought to identify the LTO gassing mechanism and to propose possible solutions to mitigate this problem. The study shows that the following key factors contribute to the gassing phenomena:

- Lithiated LTO;
- Lithium salt, such as LiPF<sub>6</sub> or LiBF<sub>4</sub>; and
- Carbonate solvents.

Since such reactions always occur on the surface of the electrode, surface modification is the key to control such a reaction.

Here we propose to develop functionalized surface modification (see Formula 1) agents for PHEV battery applications.



In the above formula, R<sub>1-n</sub> are functional groups, at least one of which is an adhesion group that can selectively remove the acidic function groups like –OH on the material surface.

A surface modification method other than additives has also been investigated to protect the electrode surface from undesired reaction.

## Results

Figure IV - 30 shows a pouch cell with LTO/LMO chemistry before and after 80 days of high temperature aging. The presence of a gas was noticed during the 80 days.

To identify the source of the gas, we studied a whole battery, LTO anode, and LiMnO<sub>4</sub> cathode separately at different charge states with different salt and solvent. The results showed that only the LTO in the charged state (Li<sub>4+x</sub>Ti<sub>5</sub>O<sub>12</sub>) will release gas at elevated temperature when coexisting with electrolyte (LiPF<sub>6</sub> and carbonate solvents). No gassing was observed at the fully discharged state, or at room temperature (25°C). Similar phenomena were not observed for cells using carbon anodes.

As shown in Figure IV - 31, gas chromatography/ mass spectrometry (GC/MS) indicates that the major component of the gas is hydrogen, about 70~90%. Other observed gas components are CO<sub>2</sub>, CO, and CH<sub>4</sub>, etc., which are commonly released during the formation cycle of the lithium-ion battery.



Figure IV - 30: LTO/LMO pouch cells before (right) and after (left) 80 days of aging at 63°C. The electrolyte is 1.2 M LiPF<sub>6</sub> in ethylene carbonate (EC)/ethyl methyl carbonate (EMC) at ratio of 3:7.

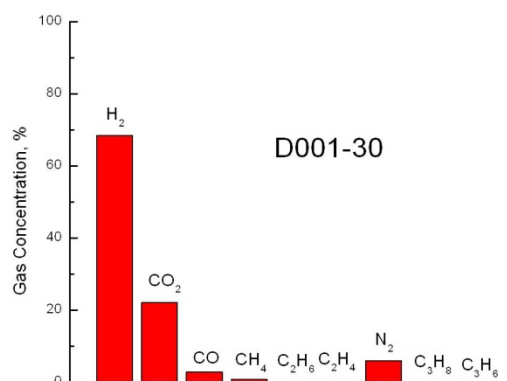
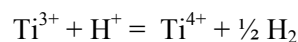


Figure IV - 31: Results of GC-MS analysis showing majority of the gas is H<sub>2</sub>.

To further correlate the gas with the lithiated LTO, *in situ* GC-MS analysis was carried out with the experimental set-up shown in Figure IV - 32. The lithiated LTO was immersed in the electrolyte with and without the lithium salt LiPF<sub>6</sub>. With the temperature at 80°C, the generated gas was collected and analyzed by GC. The result indicates that the charged LTO (Li<sub>4+x</sub>Ti<sub>5</sub>O<sub>12</sub>) directly participates in the reaction and produces the hydrogen following the reaction:



Due to the large amount of hydrogen observed, the hydrogen source should involve the carbonate solvents besides the trace amount of water in the cell.

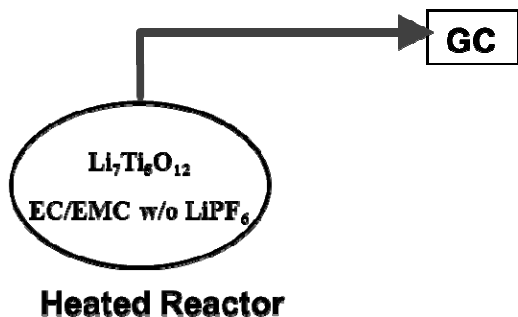
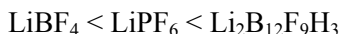


Figure IV - 32: Experimental set-up to measure the generated gas by reaction of lithiated LTO with electrolyte.

This reaction will be significantly suppressed in the absence of LiPF<sub>6</sub>. Only a trace amount of H<sub>2</sub> was observed without LiPF<sub>6</sub> in the electrolyte. We speculate that the salt might act as the bridge between the reaction site, lithiated LTO surface, and the H<sub>2</sub> source (carbonate solvent).

The salt effect has been further investigated. Figure IV - 33 shows that the generated gas amount increases in the following order:



LiBF<sub>4</sub> salt produces less gas than LiPF<sub>6</sub>. The salts LiTFSI and LiBETI will not produce any gas; however, because they have a severe corrosion problem, they might not be the solution.

The detailed reaction pathway involving the three key factors is still not clear, requiring further investigation.

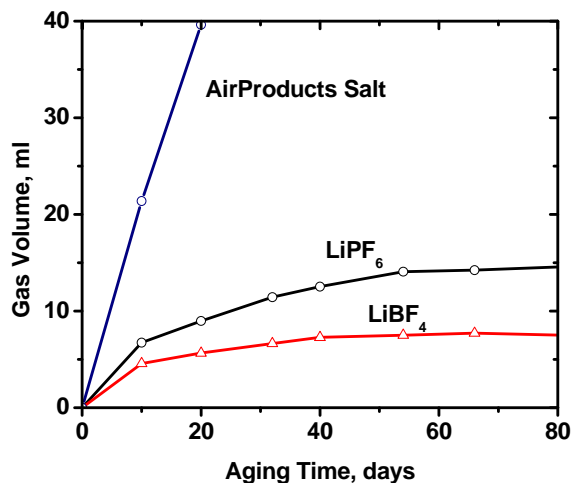


Figure IV - 33: Gas evolution progress for different lithium salts in propylene carbonate: ethyl methyl carbonate: diethyl carbonate: dimethyl carbonate (1:1:1:1). LiBF<sub>4</sub> produce less gas than LiPF<sub>6</sub> and Air Products salt (Li<sub>2</sub>B<sub>12</sub>F<sub>9</sub>H<sub>3</sub>).

A hypothesis was proposed and is represented in Figure IV - 34, which illustrates the process by which the carbonate solvent reacts on the surface of LTO to produce H<sub>2</sub>. Although this hypothesis successfully correlates the LTO with the hydrogen source, carbonates, it needs to be further

improved to accommodate the salt effect, which is still under investigation.

Since the reaction involves the electron transferring from LTO to solvent, if we could cut off the electron transfer pathway, we might be able to control gassing.

Surface modification of LTO either by additives or by atomic layer deposition could be the possible solution.

Since the charged LTO surface is where the reaction takes place, a type of additives is proposed to passivate the surface of the LTO through interaction with the surface group of -OH to shut off the reaction pathway.

Figure IV - 35 shows that with the addition of chlorosilane additive in the electrolyte of LiPF<sub>6</sub> in EC/EMC, the gas is significantly reduced and stabilized after 10 days of aging.

We will explore more efficient additives and other surface modification methods to further reduce gassing.

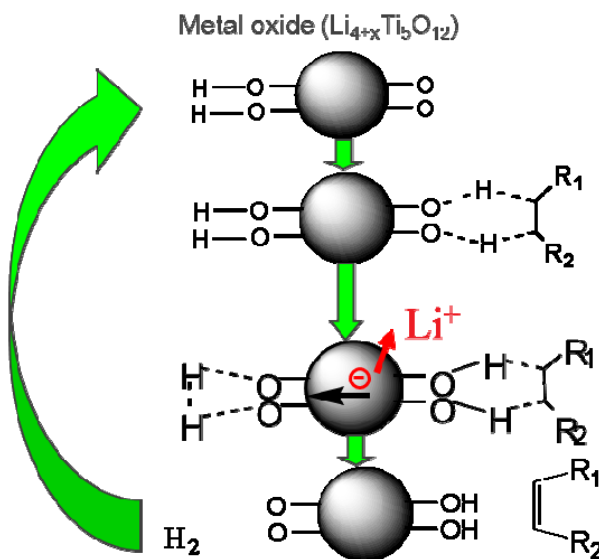


Figure IV - 34: Proposed reaction mechanism. However, more work needs to be done to address salt effect.

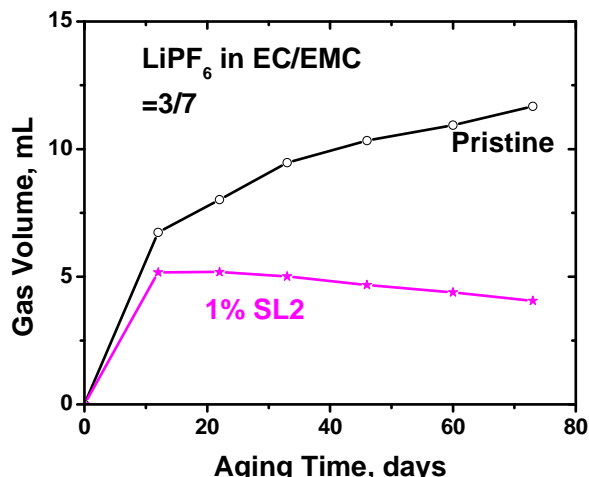


Figure IV - 35: The positive impact of our approach to significantly reduce the gas evolution in LTO/LiMn<sub>2</sub>O<sub>4</sub> cells aged at 55°C using chlorosilane treatment on Li<sub>4</sub>Ti<sub>5</sub>O<sub>12</sub>.

## Conclusions and Future Directions

Nano-structured Li<sub>4</sub>Ti<sub>5</sub>O<sub>12</sub> is a promising anode material for high power lithium-ion batteries with extremely long life and unmatched tolerance to overcharge and thermal abuses.

Gassing of Li<sub>4+x</sub>Ti<sub>5</sub>O<sub>12</sub> at elevated temperature is the remaining issue that hinders the deployment of this chemistry.

Three key factors contributing to the gassing have been identified: lithiated LTO, lithium salt, and carbonate solvents.

A hypothesis on the gassing reaction was proposed. However, the salts' effect needs to be addressed.

Surface modification of LTO by an additive has a positive effect on reducing and stabilizing gas.

More fundamental research is needed to reveal the true mechanism and to completely resolve the problem. The following items are key components for future work:

1. Investigate the reaction kinetics using *in situ* XANES (X-ray Absorption Near-Edge Structure).
2. Use kinetics data obtained from XANES to quantify the effectiveness of surface modification agents.
3. Explore additives and “poisoning” agents to suppress the catalytic activity of LTO.
4. Explore coating LTO to eliminate the catalytic reactivity at the surface of LTO.

## FY 2011 Publications/Presentations

1. 2011 DOE Annual Peer Review Meeting Poster, May 9-13, 2011, Washington DC.

## IV.B.3 Applied Battery Research on Cathodes

### IV.B.3.1 Engineering of High Energy Cathode Material (ANL)

Huiming Wu and Khalil Amine

Argonne National Laboratory  
9700 South Cass Avenue  
Argonne, IL 60439-4837  
Phone: (630) 252-3838; Fax: (630) 972-4520  
E-mail: [amine@anl.gov](mailto:amine@anl.gov)

Collaborators:

Ilias Belharouak, Argonne National Laboratory  
Ali Abouimrane, Argonne National Laboratory  
Y.K. Sun, Hanyang University  
Alan W. Weimer group, University of Colorado Boulder

Start Date: October 1, 2008

Projected End Date: September 30, 2014

#### Accomplishments

- Developed a carbonate-based co-precipitation process that provides spherical particle morphology.
- Proposed a new composition based on the Argonne high-energy composite layered cathode with good reproducibility and scale-up ability.
- Optimized suitable composition and engineered the material to improve electrochemical performance for PHEV applications.
- Explored surface modification to enable high rate and long cycle life at high voltage (4.6 V).
- Transferred the knowhow to ANL's ES division for further scale up of the material to 10kg batches.



#### Objectives

- Enable the use of the Argonne high-energy composite layered cathode,  $x\text{Li}_2\text{MnO}_3 \cdot (1-x)\text{LiNiO}_2$ , in a PHEV with electric drive range of 40 miles.
- Optimize cathode composition and engineer this material to improve its packing density and rate capability for PHEV applications.
- Explore surface protection to enable high capacity and long cycle life at high voltage (4.6 V).

#### Technical Barriers

- Poor continuous charge and discharge rate capability
- High electrode impedance
- Low pulse power
- Low packing density, which translates to low volumetric energy density
- Reactivity with the electrolyte at high voltage

#### Technical Targets

- Improve the rate capability from C/10 to 1C ~ 2C.
- Improve the packing density to 2~2.4 g/cc.
- Stabilize the surface of the particles to improve significantly the calendar and cycle life.

#### Introduction

The 40-mile electric-drive PHEV requires development of a very high-energy cathode and anode that offers 5,000 charge-depleting cycles, 15 year calendar life, and excellent abuse tolerance. These challenging requirements make it difficult for conventional cathode materials to be adopted in PHEVs. Here, we report on a very high-energy material based on a lithium-rich nickel manganese oxide composite electrode as a potential cathode for PHEV and all-electric vehicle applications. This material exhibits over 200 mAh/g of capacity, relatively good stability, and improved safety characteristics.

#### Approach

Develop a process that leads to very dense material to increase the electrode loading density and, therefore, the electrode capacity per unit volume.

Optimize suitable composition and engineer the material to improve the electrochemical performance for PHEV applications.

Investigate nano-coating of the material with metal oxides by atomic layer deposition (ALD) to reduce the initial interfacial impedance and stabilize the cathode interface in order to improve the cycle life at elevated temperature.

## Results

In the past year, our focus was on developing high-energy cathodes based on the layered lithium-rich nickel manganese oxide composite with a Co-free composition of  $\text{Li}_{1.2}\text{Ni}_{0.3}\text{Mn}_{0.6}\text{O}_{2.1}$  (Ni/Mn ratio = 1:2). This material shows a high capacity of 200 mAh/g at 1 C rate with good cycle performance. Furthermore, this composition is easy to reproduce and scale up. We have already produced the material at the kg scale in our bench Laboratory. The kg-level material has been used for pouch cell builds at Argonne's cell building facility and will be distributed to all parties within the ABR program for testing and diagnostics.

The material was prepared from a spherical nickel manganese carbonate precursor. Figure IV - 36 shows scanning electron microscopy (SEM) images of  $\text{Li}_{1.2}\text{Ni}_{0.3}\text{Mn}_{0.6}\text{O}_{2.1}$  high-energy cathode material. It shows uniform spherical secondary particles (10 $\mu\text{m}$ ) made from dense 80 nm primary particles, resulting in high tap density. The small nano-primary particles will allow for a reduction of the lithium diffusion pathway and thus improve the rate capability. The X-ray diffraction (XRD) profile shows the typical characteristics for this class of materials.

**Electrochemical performance of the kg-level material ( $\text{Li}_{1.2}\text{Ni}_{0.3}\text{Mn}_{0.6}\text{O}_{2.1}$ ).** Figure IV - 37 shows the charge and discharge capacities as a function of the lithium amount for the composition of  $\text{Li}_x\text{Ni}_{0.3}\text{Mn}_{0.6}\text{O}_{2.1}$ . When lithium amount  $x$  was fixed in the window of 0.94 to 1.03, the materials always

delivered a high capacity of about 250 mAh/g, which means the lithium amount for the  $\text{Li}_x\text{Ni}_{0.3}\text{Mn}_{0.6}\text{O}_{2.1}$  composition is not so sensitive as the case of  $\text{Li}_x\text{Ni}_{0.2}\text{Mn}_{0.6}\text{O}_2$  (Ni/Mn ratio=1:3) we reported before. As a result, the high-energy cathode composition  $\text{Li}_{1.2}\text{Ni}_{0.3}\text{Mn}_{0.6}\text{O}_{2.1}$  is able to be reproduced easily.

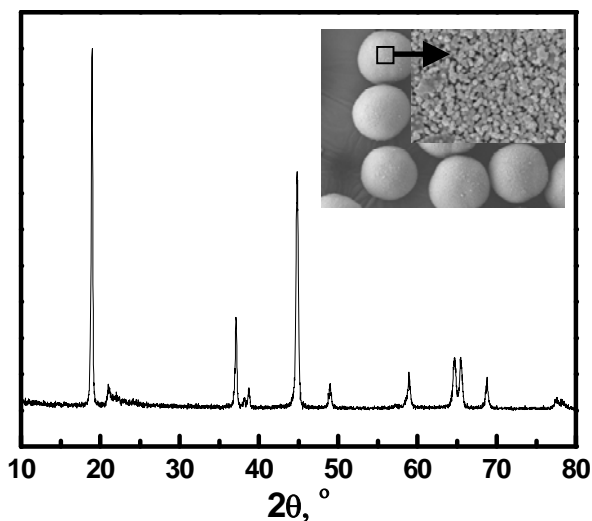


Figure IV - 36: XRD profile and SEM images of  $\text{Li}_{1.2}\text{Ni}_{0.3}\text{Mn}_{0.6}\text{O}_{2.1}$

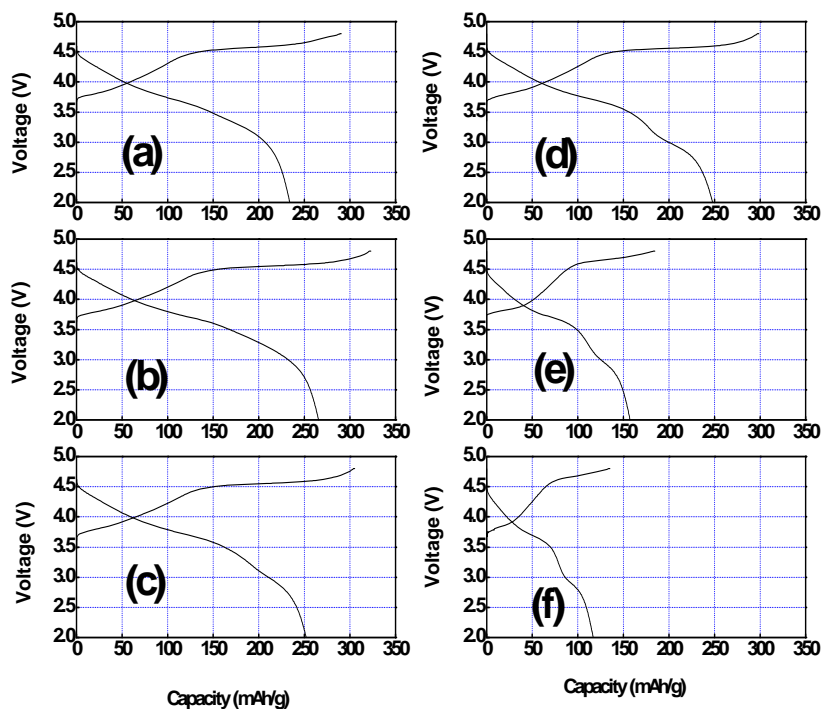


Figure IV - 37: Charge and discharge capacity of  $\text{Li}_x\text{Ni}_{0.3}\text{Mn}_{0.6}\text{O}_{2.1}$  (a:  $x=1.03$ , b:  $x=1.0$ , c:  $x=0.97$ , d:  $x=0.94$ , e:  $x=0.91$ , f:  $x=0.88$ )

Figure IV - 38 shows the results of a rate capability study of  $\text{Li}/\text{Li}_{1.2}\text{Ni}_{0.3}\text{Mn}_{0.6}\text{O}_{2.1}$  cells at different charge and discharge currents between 2.0 to 4.6 V. The  $\text{Li}_{1.2}\text{Ni}_{0.3}\text{Mn}_{0.6}\text{O}_{2.1}$  electrode showed excellent capability, delivering over 200 mAh/g at about the 1-C rate. We also found good results for the area specific impedance (ASI) of the electrode. The lowest ASI value observed is only 20  $\text{ohm}\cdot\text{cm}^2$ . At the end of the discharge, the ASI value increased and more work need to be done to lower the value near the end of the discharge to meet the PHEV regenerative charging requirement.

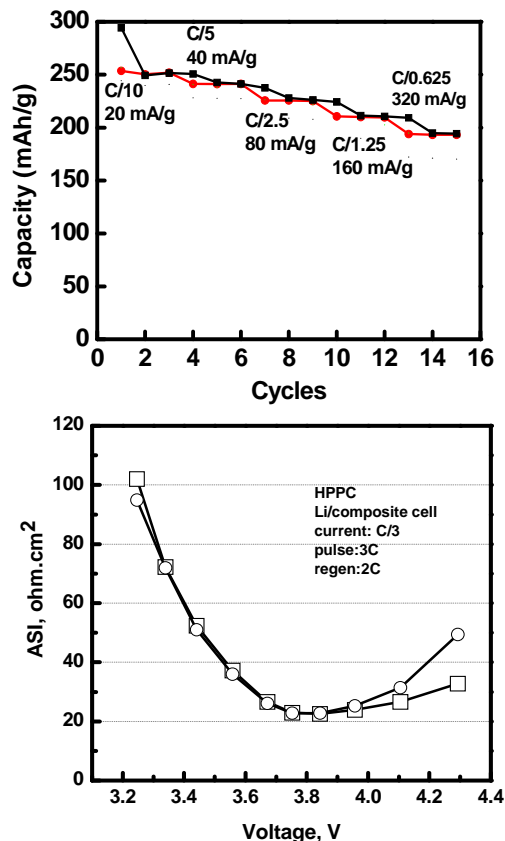


Figure IV - 38: Rate performance and ASI value of  $\text{Li}_{1.2}\text{Ni}_{0.3}\text{Mn}_{0.6}\text{O}_{2.1}$

Figure IV - 39 shows the performance of  $\text{Li}_{1.2}\text{Ni}_{0.3}\text{Mn}_{0.6}\text{O}_{2.1}$  with different anodes. At room temperature, more than 200 mAh/g capacity was reached for all three different anode materials (Li metal,  $\text{Li}_4\text{Ti}_5\text{O}_{12}$ , and graphite) at the C/3 rate. Also, for this cathode, the cycle stability was excellent. After 100 cycles, there was no obvious capacity fade with respect to the different anodes. Even after 400 cycles, the cells with the  $\text{Li}_4\text{Ti}_5\text{O}_{12}$  anode shows stable cycling performance.

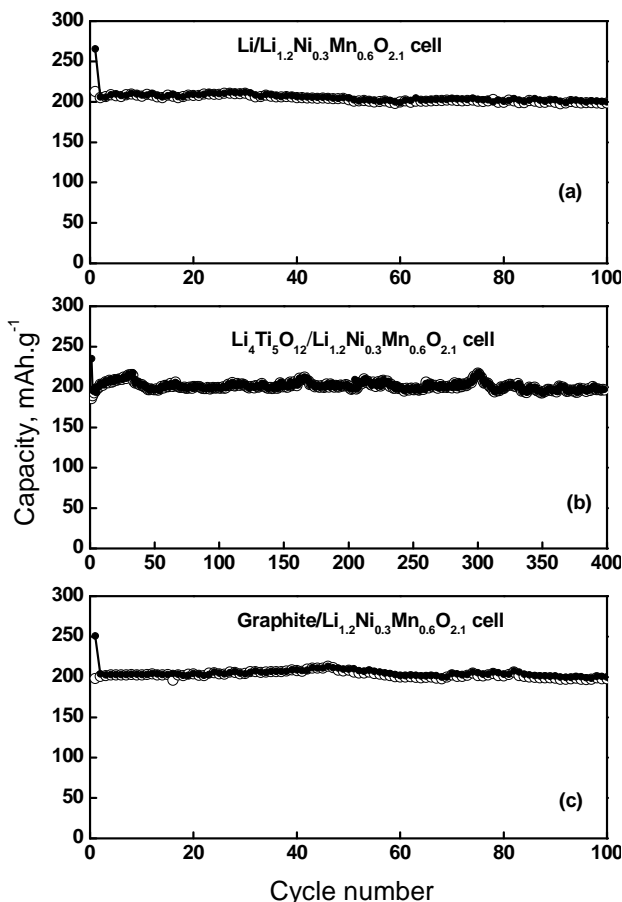


Figure IV - 39: Cycle performance of  $\text{Li}_{1.2}\text{Ni}_{0.3}\text{Mn}_{0.6}\text{O}_{2.1}$  at C/3 rate and room temperature

**Effect of  $\text{Al}_2\text{O}_3$ -ALD coating on cycling performance of  $\text{Li}_{1.2}\text{Ni}_{0.3}\text{Mn}_{0.6}\text{O}_{2.1}$  at high temperature.** As will be discussed shortly, the discharge capacity of a pure  $\text{Li}_{1.2}\text{Ni}_{0.3}\text{Mn}_{0.6}\text{O}_{2.1}$  full cell at high temperature ( $55^\circ\text{C}$ ) faded gradually with cycling (to be shown later in Fig.7). The high-energy cathode  $\text{Li}_{1.2}\text{Ni}_{0.3}\text{Mn}_{0.6}\text{O}_{2.1}$  is a manganese-rich material. When using a graphite anode in the cell, the manganese easily dissolves in the electrolyte solution at high temperature, reduces at the anode and compromises the SEI leading poor cycle life. Another issue is that at high temperature and high voltage (4.6 V), the reaction between charged electrodes and electrolyte is very active. We investigated protecting each particle with a very stable thin coating as a barrier against any interfacial reaction between charged cathode and electrolyte. Also, the coating can either eliminate or significantly reduce the dissolution of the manganese. Figure IV - 40 and Figure IV - 41 show scanning transmission electron microscopy (STEM) with compositional mapping via energy dispersive X-ray spectroscopy (EDX) for the bare and  $\text{Al}_2\text{O}_3$ -ALD coated  $\text{Li}_{1.2}\text{Ni}_{0.3}\text{Mn}_{0.6}\text{O}_{2.1}$  samples. As expected, EDX maps of Mn and Ni (Figure IV - 41c and Figure IV - 41d, respectively) illustrate the presence of these elements throughout the cathode material. A map of Al also reveals

even coverage, suggesting that the  $\text{Al}_2\text{O}_3$  coating is uniform on the particle surface (Figure IV - 41e). Most notably, a composite image combining the maps of Mn, Ni, and Al (Figure IV - 41f) shows a distinct particle edge where only Al is present, which corresponds to an  $\text{Al}_2\text{O}_3$  coating with a thickness of 5-10 nm. In stark contrast to the strong Al signal in the EDX spectrum of the coated sample (Figure IV - 41b), the spectrum of the uncoated sample only contains signals for Ni and Mn (Figure IV - 40b). As such, it is clear that our treatment produces an evenly distributed coating of  $\text{Al}_2\text{O}_3$  across the particle surface, while an untreated sample contains no such coating.

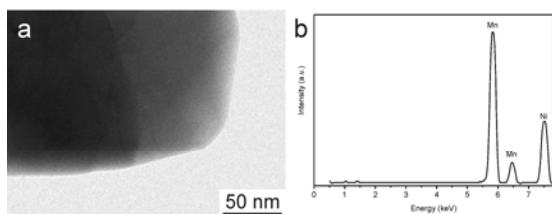


Figure IV - 40: a) STEM image of an uncoated  $\text{Li}_{1.2}\text{Ni}_{0.3}\text{Mn}_{0.6}\text{O}_{2.1}$  particle in bright field mode. b) EDX spectrum with metal signals labeled.

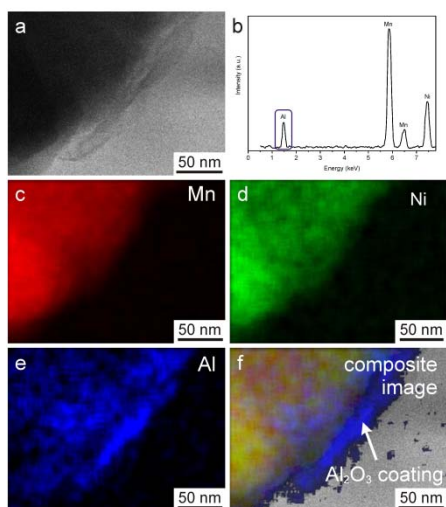


Figure IV - 41: a) STEM image of a  $\text{Li}_{1.2}\text{Ni}_{0.3}\text{Mn}_{0.6}\text{O}_{2.1}$  particle coated with  $\text{Al}_2\text{O}_3$  in bright field mode. b) EDX spectrum with metal signals labeled. Signal corresponding to Al is circled. Compositional EDX maps of the particle surface for individual elements: c) Mn, d) Ni, and e) Al. f) A composite image of a, c, d, and e illustrating the distinct  $\text{Al}_2\text{O}_3$  coating along the edge of the particle.

Figure IV - 42 shows the cycling performance of the  $\text{Al}_2\text{O}_3$ -ALD-coated  $\text{Li}_{1.2}\text{Ni}_{0.3}\text{Mn}_{0.6}\text{O}_{2.1}$  and uncoated samples. This test was carried out at  $55^\circ\text{C}$  at C/3. The coated material achieved 250 mAh/g and showed excellent cycling performance at high temperature. For the  $\text{Al}_2\text{O}_3$ -coated samples we used particles with one ALD coating cycle and ten ALD coating cycles. We found that for 10-cycle ALD coating, the capacity of the samples was low initially, and then as the cycling increased, high capacity was achieved. We believe that the thick coating requires a few cycles to allow

for electrolyte to wet the electrode. This result indicates that protecting the surface of the composite active material by ALD coating can improve the electrochemical performance.

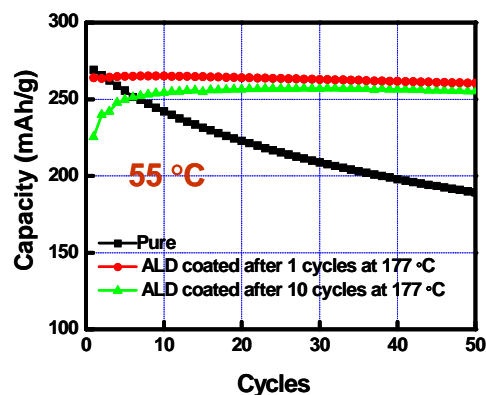


Figure IV - 42: Cycle performance of  $\text{Li}_{1.2}\text{Ni}_{0.3}\text{Mn}_{0.6}\text{O}_{2.1}$  with and without  $\text{Al}_2\text{O}_3$  ALD coating

Figure IV - 43 shows differential scanning calorimetry (DSC) profiles of bare  $\text{Li}_{1.2}\text{Ni}_{0.3}\text{Mn}_{0.6}\text{O}_{2.1}$ ,  $\text{Li}_{1.2}\text{Ni}_{0.3}\text{Mn}_{0.6}\text{O}_{2.1}$  coated with one  $\text{Al}_2\text{O}_3$  ALD cycle, and  $\text{Li}_{1.2}\text{Ni}_{0.3}\text{Mn}_{0.6}\text{O}_{2.1}$  coated with ten  $\text{Al}_2\text{O}_3$  ALD cycles, which had been cycled 3 times and charged to 4.6 V in half cells. Compared with the pristine material, the  $\text{Al}_2\text{O}_3$ -coated  $\text{Li}_{1.2}\text{Ni}_{0.3}\text{Mn}_{0.6}\text{O}_{2.1}$  material showed significant improvement in safety performance with a slight increase in the onset temperature of reaction with the electrolyte, which is probably due to the decrease of the reactivity because of protection by a highly dense  $\text{Al}_2\text{O}_3$  coating. Therefore, the coated samples showed improved thermal stability.

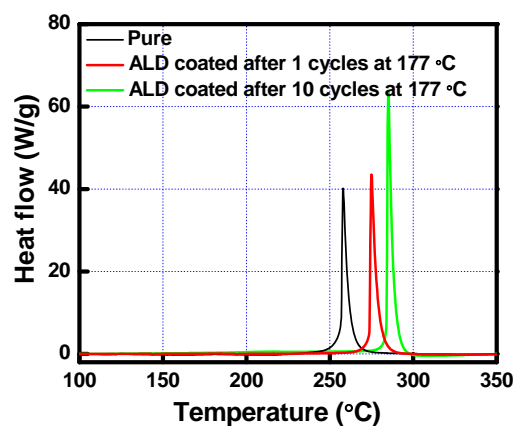


Figure IV - 43: DSC result of  $\text{Li}_{1.2}\text{Ni}_{0.3}\text{Mn}_{0.6}\text{O}_{2.1}$  by  $\text{Al}_2\text{O}_3$  ALD coating

## Conclusions and Future Directions

A new  $\text{Li}_{1.2}\text{Ni}_{0.3}\text{Mn}_{0.6}\text{O}_{2.1}$  composition was found to provide good reproducibility during scale up. This material shows:

- Spherical particle morphology

- Sharp particle distribution for uniform performance
- Pure structure with no impurities

The performance of the Co-free  $\text{Li}_{1.2}\text{Ni}_{0.3}\text{Mn}_{0.6}\text{O}_{2.1}$  cathode is excellent compared with Co-doped high energy material (HEM), showing good rate capability, good cycling performance, and better safety.

Surface modification of the HEM cathode with  $\text{Al}_2\text{O}_3$  using ALD shows good cycle life at  $55^\circ\text{C}$  and improved safety characteristics.

For the PHEV application of the high energy cathode, we still need to:

- Further engineer the composite cathode to increase the rate by optimizing the secondary and primary particles
- Further optimize the co-precipitation process to increase packing density to 2.4 g/cc
- Further optimize the composition by varying the lithium and Ni/Mn ratio to improve the capacity and performance
- Explore further the surface modification of the high energy cathode to further improve the power capability
- Investigate the nano-coating of the material with metal fluoride, phosphate, and oxide to reduce the initial interfacial impedance and stabilize the cathode interface in order to improve the cycle life at elevated temperature.

$\text{Ni}_{0.3}\text{Mn}_{0.7}\text{CO}_3$  precursor for high capacity Li-ion battery cathodes,” *J. Mater. Chem.*, **21** (25): 9290.

8. H. Deng, I. Belharouak, C. S. Yoon, Y. K. Sun, K. Amine, “High temperature performance of surface-treated  $\text{Li}_{1.1}\text{Ni}_{0.15}\text{Co}_{0.1}\text{Mn}_{0.55}\text{O}_{1.95}$  layered oxide,” *J. Electrochem. Soc.*, **157** (10) A1035.

### FY 2011 Publications/Presentations

1. K. Amine and H/ Wu, 2011 DOE Annual Peer Review Meeting Presentation, May 9-13, 2011, Washington DC.
2. Wu and K. Amine, 5th International Conference Polymer Batteries and Fuel Cells (PBFC-5), Argonne, IL, August 1-5, 2011.
3. K. Amine, USDrive Electrochemical Energy Storage Tech Team Applied Battery Research for Transportation (ABR) Program Informational Meeting, Argonne National Laboratory, October 5-6, 2011.
4. K. Amine, H. Wu, 4th International Conference on Advanced Lithium Batteries for Automobile Application, Beijing, China, Sept. 21-23, 2011.
5. Abouimrane, O.C. Compton, H.X.Deng, I. Belharouak, D.A. Dikin, S. T. Nguyen, K. Amine, “Improved Rate Capability in a High-Capacity Layered Cathode Material via Thermal Reduction,” *Electrochem. Solid. State Lett.*, **14** (9) A126.
6. I. Belharouak, G.M. Koenig, J. W. Ma, D. P. Wang, K. Amine, “Identification of  $\text{LiNi}_{0.5}\text{Mn}_{1.5}\text{O}_4$  spinel in layered manganese enriched electrode materials,” *Electrochem.Comm.* **13** (3) 232.
7. D. P. Wang, I. Belharouak, G. M. Koenig, G.W. Zhou, K. Amine, “Growth mechanism of

## IV.B.3.2 Developing New High Energy Gradient Concentration Cathode Material (ANL)

Gary Koenig and Khalil Amine

Argonne National Laboratory  
9700 South Cass Avenue  
Argonne, IL 60439-4837  
Phone: (630) 252-3838; Fax: (630) 972-4451  
E-mail: [amine@anl.gov](mailto:amine@anl.gov)

Collaborators:  
Ilias Belharouak, Argonne National Laboratory  
Yang-Kook Sun, Hanyang University

Start Date: October 1, 2008  
Projected End Date: September 30, 2014

- Demonstrate that a tailored relative transition metal composition at the surfaces of gradient particles influences safety and cycle life.

### Accomplishments

- Developed a co-precipitation process with a predetermined relative transition metal compositional profile for synthesis of high energy gradient concentration precursors and cathode materials.
- Characterized the material and demonstrated that both the precursor and lithiated final material had a gradient in relative transition metal concentration at the individual particle level.
- Demonstrated that gradient concentration cathode materials' safety and cycle life were dependent on the detailed compositional profile.



### Objectives

- The objective of this work is to develop a high energy cathode material for PHEV applications. The material is being developed to provide:
- Over 200 mAh/g reversible capacity
- Good rate capability
- Excellent cycle and calendar life
- Good abuse tolerance

### Technical Barriers

The technical barrier is to develop a cathode material for PHEV batteries that meets or exceeds DOE technical objectives, including outperforming the NMC baseline material.

### Technical Targets

- Develop a model to predetermine the gradient in concentration in particles produced in a coprecipitation process.
- Develop a process for precursors with a gradient in transition metal composition that have enriched manganese compositions.
- Demonstrate in a proof-of-principle experiment that precursors could be synthesized with predetermined compositional profiles.
- Demonstrate high capacity (>200 mAh/g) in final materials produced using the gradient precursors.

### Introduction

Lithium transition metal oxides containing a variety of compositions have been investigated for lithium-ion battery cathode materials. Common transition metals incorporated in these materials include cobalt, nickel, and manganese. Materials with relatively high nickel compositions have reported large capacities (>200 mAh/g) and excellent rate capability but often experience significant loss of capacity on extended cycling and have safety performance challenges. Materials with relatively high manganese compositions have reported excellent safety and cycle life, but have also reported lower capacities and rate capabilities relative to the materials enriched in nickel. Recently, cathode materials have been designed that attempt to control the transition metal composition at the individual particle level (~10  $\mu\text{m}$ ). Initially, particles were designed with a constant composition core that was enriched in nickel to take advantage of nickel-enriched materials high capacity and rate capability. Surrounding this core was a constant composition shell that was enriched in manganese to take advantage of the desirable safety and cycle life properties of Mn-enriched materials (presuming that the stability arises from increased stability of the material in contact with the electrolyte). While these cathode materials showed good performance, inspection of the interiors of these particles revealed that there was an interface that

developed between the Ni-enriched core and Mn-enriched shell, which led to concerns over the stability of this material during extended cycling and the Li-diffusion in this new interfacial region.

One strategy proposed to mitigate the formation of a discontinuous core and shell region within cathode particles was to use a shell that had a gradient in composition from Ni-enriched near the core to Mn-enriched near the surface. These core-gradient shell materials also have shown impressive cycling and safety performance as lithium-ion battery cathode materials, however, there still are a number of challenges with regards to predetermining the compositional profile within particles and with synthesizing materials that have large changes in relative transition metal composition from the core to the surface. The work below describes efforts to develop the gradient process for predetermined relative transition metal compositional profiles.

## Approach

The approach for developing high energy concentration gradient cathode materials has been to develop a general synthetic method to tailor the internal compositional gradient within individual cathode particles. We have developed a model used to deposit a gradual compositional gradient throughout the precursor particles from the interior to the surface to suppress stresses inside the particle during lithium intercalation and diffusion. Some of the first materials that we have synthesized have been enriched in Mn (> 50% relative composition) in efforts to further improve safety and cycling performance, as well as to take advantage of overall material compositions previously developed at Argonne with lithium and manganese enrichment that have shown promise as high energy cathode materials.

## Results

Synthesis of gradient transition metal cathode materials starts with the synthesis of transition metal precursor particles. The experimental setup for synthesizing gradient concentration precursor particles is shown in Figure IV - 44. Typical synthesis conditions include a 2 L/hr flow of material out of the reactor with ~100 grams particles/hr and ~350 grams of particles collected from the reactor at the end of the process. Two solutions with dissolved metal salts were prepared, one enriched in Mn (“Mn solution”) and the other enriched in Ni (“Ni solution”). The Ni solution is fed to the reactor, where it is precipitated by a co-precipitating agent (e.g. sodium carbonate). The gradient is initiated by feeding the Mn solution into the Ni solution, which results in a gradual increase in the relative amount of the Mn in the solution fed to the reactor and concurrently a gradual increase in

the Mn composition of the material deposited on the particles collected from the reactor.

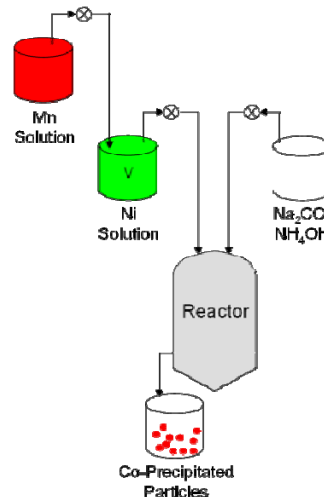


Figure IV - 44: Schematic of synthesis of co-precipitated transition metal precursors.

By using an input-output analysis of the process in Figure IV - 44 and controlling the volume, concentration, and flow rates used in the process, we can predetermine the composition of the transition metal fed to the reactor. An example of a predetermined concentration of the relative Mn composition fed to the reactor compared to the relative Mn composition as determined from EDXS can be seen in Figure IV - 45. The EDXS data shows excellent agreement with the predetermined concentration profile later in the process and also has a gradual increase in Mn concentration. The measured Mn composition from EDXS is lower than projected for early times in the process, which is in part due to contributions from the Ni-enriched core in the measurement. The results above indicate that we were successful in depositing a predetermined gradual increase in Mn composition onto the surfaces of the precursor particles.

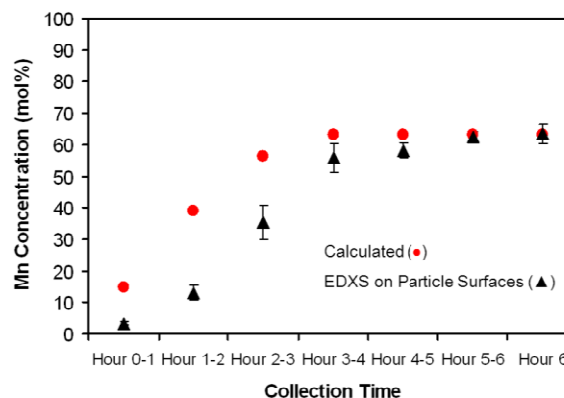


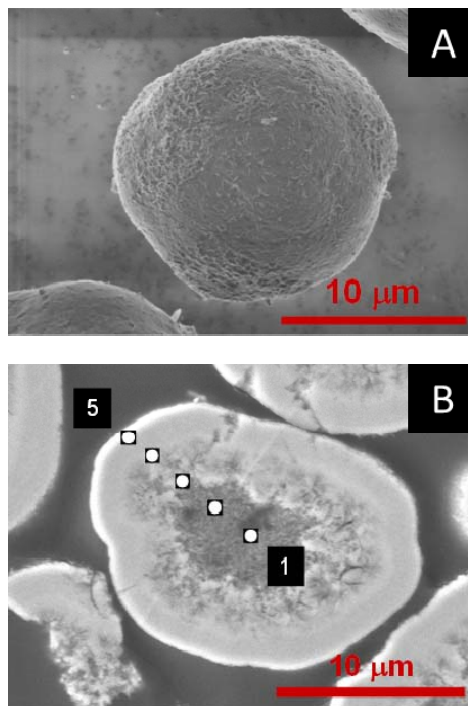
Figure IV - 45: Relative Mn concentration at the surfaces of precursors collected from the reactor at different times as determined by calculation using predetermined process conditions and measured using EDXS.

After confirming the increase in relative Mn composition on the surfaces of the particles, we next confirmed an internal gradient within our precursor materials. The surface morphology of a representative particle collected from the reactor between hours 4-5 can be found in Figure IV - 46A. These particles were embedded in a resin and microtomed to reveal the morphology of their interior cross-sections (Figure IV - 46B). The interior cross-sections revealed a gradient in the particle morphology. The particles have a porous core that becomes denser near the surface of the particle. We did not anticipate the core of the particles being porous, and the porous cores will decrease the tap density of our materials and may have a negative impact on the mechanical integrity of the particles. Future efforts will be directed at producing particles with uniform densities throughout the particle interiors. EDXS was also performed at various locations on the particle interior, and confirmed that the relative Mn composition increased from the particle interior to the particle surface. Similar analysis was done after lithiation of the particles, and confirmed that the gradient was maintained after calcination at elevated temperatures (900°C).

The lithiated gradient final materials that have gravimetric capacities of ~200 mAh/g at rates of 20 mA/g. In addition, we have also found evidence that Mn enrichment at the surface of the materials improves the final material cycle life and safety. Figure IV - 47 shows the relative discharge capacity during the first 40 cycles of Li half cells paired with final materials prepared using precursors collected from the reactor during hours 3-4, hours 4-5, hours 5-6 and at the end of 6 hours. The lithium to transition metal ratio of the final materials were all 1:1. The material made from the precursor collected during hours 3-4 lost almost 40% of its capacity, while the other 3 materials showed ~10% capacity fade during the first 40 cycles. This result indicates that a Mn-enrichment at the surface helps to increase the cycle life, however, there were not gains seen during the final 2 hours, indicating that it may be possible to use less overall Mn enrichment and still have good cycle life performance.

## Conclusions and Future Directions

We have developed a process model that allows us to predetermine the internal relative transition metal composition profile within precursor particles. These precursors were then used to make lithium-ion battery cathodes with gradients in internal transition metal composition. The gradient particles with Mn-enriched surfaces had advantages with regards to cycle life and safety.



Point	%Mn
1	21.2
2	25.7
3	34.5
4	56.6
5	54.7

Figure IV - 46: SEMs of the exterior (A) and interior (B) of a precursor particle collected from the reactor between hours 4-5. The table contains relative transition metal composition of Mn as determined from EDXS at points indicated on (B).

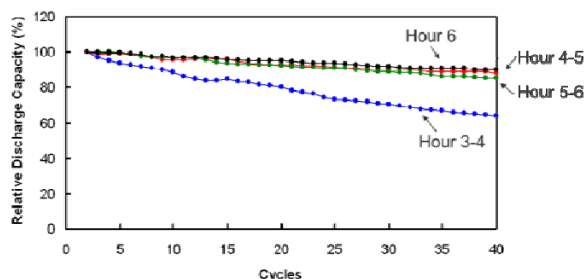


Figure IV - 47: Relative discharge capacities after 40 charge discharge cycles of Li half cells with cathodes comprised of lithiated final materials synthesized using precursors collected from the indicated times.

Future work on these gradient materials will focus on engineering the particles to not have hollow interiors, and

moving to increased Ni compositions in the core. We want to achieve higher capacities and rate capability, and further enriching the core in Ni should help to achieve this goal. We will then be able to predetermine and test different Mn-enriched gradients to achieve the necessary cycle life and safety performance for our materials. We hypothesize that the hollow interiors were the result of the process not reaching steady state. We will give the particles more time to grow before initiating the gradient, and run the process for longer times, in an effort to avoid having porous cores.

### FY 2011 Publications/Presentations

1. 2011 DOE Annual Peer Review Meeting Presentation, May 9th-13th 2011, Washington DC.
2. 2010 American Institute of Chemical Engineers Annual Meeting Presentation, November 7th-12th 2010, Salt Lake City, UT.
3. 2010 Electrochemical Society Annual Meeting, October 10-15 2010, Las Vegas, NV.
4. G. M. Koenig, I. Belharouak, H. Deng, Y.-K. Sun, and K. Amine, *Chem. Mater.*, **23** (7) (2011) 1954.
5. G. M. Koenig, I. Belharouak, H. M. Wu, and K. Amine, *Electrochim. Acta*, **56** (3) (2011) 1426.

## IV.B.3.3 Design and Evaluation of Novel High Capacity Cathode Materials (ANL)

Christopher S. Johnson

Argonne National Laboratory  
9700 South Cass Avenue  
Argonne, IL 60439-4837  
Phone: (630) 252-4787; Fax: (630) 252-4176  
E-mail: [cjohnson@anl.gov](mailto:cjohnson@anl.gov)

### Collaborators:

Vic Maroni, Argonne National Laboratory  
Dean Bass, Argonne National Laboratory  
Shawn Rood, Argonne National Laboratory  
A. Jeremy Kropf Argonne National Laboratory

Start Date: October, 2008

Projected End Date: September, 2012

### Objectives

The project objective is to design, evaluate and screen high-capacity cathodes that will provide high-energy for transportation batteries. Novel electrode materials are needed in order to advance the field and push the limits of state-of-art technology into new cathode systems. To satisfy the energy requirements of batteries for 40 mile all-electric mode in PHEVs, we are focusing on novel systems that can maximize the available energy density, but also try to utilize inexpensive materials, such as inherently safe oxides of Fe, V, and Mn that possess high-capacities.

### Technical Barriers

- Low energy density
- High cost
- Low abuse tolerance

### Technical Targets

- 96 Wh/kg, 316 W/kg (PHEV 40 mile requirement)
- Cycle life: 3000 cycles
- Calendar life: 15 years
- Improved abuse tolerance

### Accomplishments

- We finalized the synthesis of  $\text{Li}_5\text{FeO}_4$  (termed LFO) as a lithium-rich cathode precursor. The optimal

synthesis yields a phase pure material that can be produced in 24 hours. The original synthesis procedure published in the literature took 72 hours.

- Discovered that Raman spectroscopy can be used to determine the purity and stability of synthetic products of  $\text{Li}_5\text{FeO}_4$ . A number of experiments were done to measure the air stability. Air stability is critical if one plans to process this material into electrodes in a dry room facility.
- Raman spectroscopy can be used to evaluate the surface-coated electrode materials and their coverage.
- We have discovered other non-lithium containing transition metal vanadium oxide cathodes that feature high capacities greater than 500 mAh/g.
- Used AC impedance technique to measure the difference between delithiated or activated LFO versus as-prepared LFO. The activated LFO is approximately one order of magnitude lower cell resistance.
- Determined that faster current rates can be used to remove Li from LFO, particularly if the LFO is made from lithium hydroxide hydrate ( $\text{LiOH}\cdot\text{H}_2\text{O}$ ) and iron oxide ( $\text{Fe}_2\text{O}_3$ ).

✧ ✧ ✧ ✧ ✧

### Introduction

High-energy Li-ion cells and batteries are needed for advanced transportation technologies, such as PHEVs and, in the long-run, EVs. Cathode materials in Li-ion batteries contain a variety of 4 V cathode oxides such as  $\text{LiCoO}_2$  (LCO),  $\text{LiNi}_{0.8}\text{Co}_{0.15}\text{Al}_{0.05}\text{O}_2$  (NCA),  $\text{LiNi}_{1/3}\text{Mn}_{1/3}\text{Co}_{1/3}\text{O}_2$  (NMC) with layered structures, and  $\text{LiMn}_2\text{O}_4$  (LMO) spinel or substituted spinels. 5 V spinels,  $\text{LiNi}_{0.5}\text{Mn}_{1.5}\text{O}_4$  also have received much attention. Blends of 4 V cathode oxide materials such as NCA and LMO can be used in order to capture performance characteristics of both electrodes. In order to achieve an extended range all electric mode PHEV, new cathodes and anodes are required which possess higher energies than what is commercially available. Higher energy cells can be achieved when 'layered-layered' or 'layered-spinel' composite oxides with capacities above 220 mAh/g are used. These electrodes consist of Li-rich layered oxides that in the presence of Ni and Mn form  $\text{LiM}_6$  units resulting in ordered or disordered monoclinic  $\text{Li}_2\text{MnO}_3$

components as nanosized domains in the electrode. To achieve the high-capacity, high voltages are needed to activate the  $\text{Li}_2\text{MnO}_3$  component, which releases net  $\text{Li}_2\text{O}$ , leaving a reversible cycling  $\text{MnO}_2$  component, but the oxygen loss negatively affects the rate capability.

Electrode materials such as layered  $\text{Li}_2\text{MnO}_3$  (LMO;  $\text{Li}_2\text{O}\cdot\text{MnO}_2$ ; 459 mAh/g) are good, but higher intrinsic capacities are needed. The defect-antifluorite  $\text{Li}_5\text{FeO}_4$  (LFO;  $5\text{Li}_2\text{O}\cdot\text{Fe}_2\text{O}_3$ ; 867 mAh/g) oxide have compositions that possess high lithium content (highly lithiated). Due to the large amount of electrochemically active lithium (2Li/Mn & 5 Li/Fe), they have very promising high-energy density if they can cycle reversibly. The first charge reaction is expected to release  $\text{O}_2$  with concomitant Li removal, but the discharge reaction is irreversible, being generally accepted that it is not possible to reintroduce oxygen as oxide anions (with Li insertion) into the resultant lattice of the  $\text{MnO}_2$  and  $\text{Fe}_2\text{O}_3$  matrices in the cell to reform LMO and LFO.

## Approach

Our approach is to couple high-capacity cathodes with high-capacity anodes, such as Si composite materials, that can result in a cell with high-energy.  $\text{MnO}_2$ ,  $\text{V}_2\text{O}_5$  and  $\text{LiV}_3\text{O}_8$  are the commonly known materials that feature high-capacity, stability, and potentially low cost in volume production. These materials operate at lower-voltage than 4V, but feature practical capacities above 250 mAh/g, which translate to high-energy densities. To implement such materials in Li-ion cells, however, a source of lithium is needed in the cell. Pre-lithiation components are necessary in order to load the anode with lithium during

the first charge, then discharge or insert lithium into the charged cathode (i.e. making  $\text{LiMnO}_2$ ,  $\text{Li}_3\text{V}_2\text{O}_5$  and  $\text{Li}_3\text{V}_3\text{O}_8$  on full discharge). One method of introducing lithium to a cell is the application of stabilized lithium metal powder materials such as SLMP<sup>®</sup> (FMC Lithium) loaded in the Si or carbon anode. Through pre-SEI formation, this extra lithium counteracts irreversible capacity loss in the cell for high capacity anodes. SLMP<sup>®</sup> can also be used in conjunction with charged cathodes.

We have focused on the lithiating materials LFO and Co-substituted LFO to introduce Li into our cells. These high lithium containing materials (867 mAh/g) together with the ‘charged cathodes’ can be used with high-capacity anode materials such as Si or Si-composites, or other high-capacity anode materials to make novel high-energy density Li batteries.

## Results

In the last few annual reports, we introduced LFO, discussed its structure, and demonstrated the release of 4 lithium cations below about 4.3 V during the first charge in a Li half cell. In this year we measured the AC impedance of the LFO in Li half cells to interrogate the impedance changes. AC impedance Nyquist plots are shown in Figure IV - 48 for a newly build Li/LFO half-cell and a charged Li/LFO electrode. The results demonstrate that LFO does not add impedance to the cell, and, in fact, dramatically lower cell impedance is observed for LFO in the charged state. We are still trying to discern the cause of this effect through careful diagnostic studies such as *in situ* XAS.

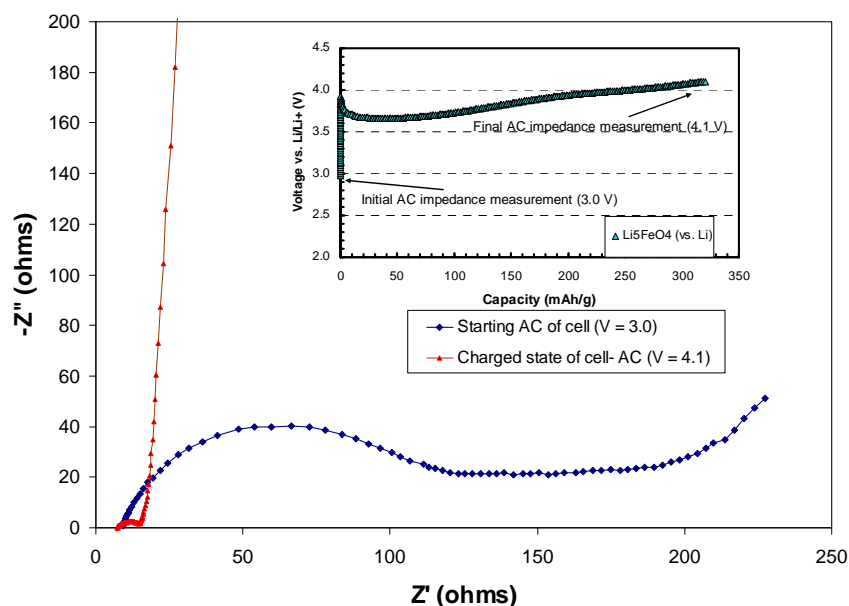


Figure IV - 48: AC impedance Nyquist plots of Li/Li<sub>5</sub>FeO<sub>4</sub> cells.

**C<sub>6</sub>/Li<sub>5</sub>FeO<sub>4</sub>-LiV<sub>3</sub>O<sub>8</sub> (LFO-LVO) Cells.** C<sub>6</sub>/Li<sub>5</sub>FeO<sub>4</sub>-LiV<sub>3</sub>O<sub>8</sub> full cells were constructed to evaluate the electrochemical performance of the individual blended

cathode components. The voltage profiles during charge/discharge cycling of such a cell are shown in Figure IV - 49.

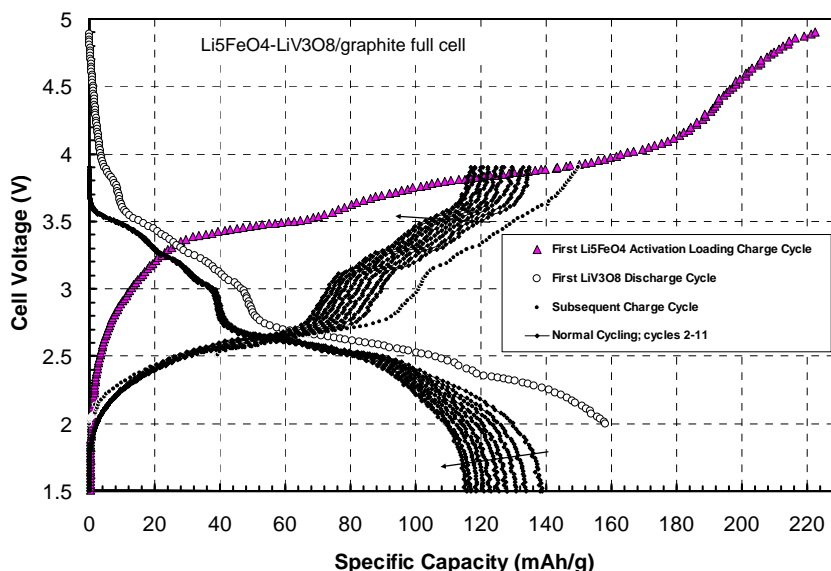


Figure IV - 49: Voltage profiles of C<sub>6</sub>/Li<sub>5</sub>FeO<sub>4</sub>-LiV<sub>3</sub>O<sub>8</sub> full cells

While there is noticeable capacity fade, it is clear that such a cell is operational. We have produced and demonstrated cycling of a vanadium oxide carbon full cell using LFO material to provide Li to the cell. About 120 mAh/g was realized. However, the irreversible capacity is too large and needs to be corrected.

**Li/LFO Cells.** It is important to be able to activate the LFO (remove lithium) as quickly as possible from the material. Therefore a test was done to charge Li/LFO cells at different rates. Rates were varied between 10 to 100 mA/g (Figure IV - 50). Note that the capacity drawn out of the LFO is still above 700 mAh/g, thereby demonstrating the ability to electrochemically drive lithium quickly out of the structure. This capability is important for forming or faster activation of cells. The mechanism of oxidation of LFO and release of Li is still under investigation.

Cathodes made with LFO from preparations based on the Li<sub>2</sub>CO<sub>3</sub> + Fe<sub>2</sub>O<sub>3</sub> reaction showed diminished capacity (data not shown). XRD of the LFO used in these preparations revealed an appreciable carbonate presence (by XRD). LFO cathodes made from LFO produced by the LiOH-H<sub>2</sub>O + Fe<sub>2</sub>O<sub>3</sub> reaction showed capacities on charging that exceeded 700 mAh/g for charging currents up to 100 mA/g. The LFO in these latter cathodes was carbonate free (per XRD; data not shown).

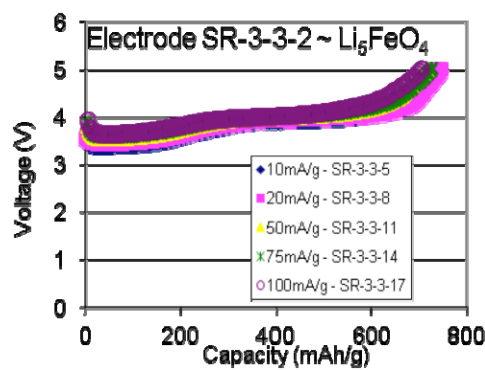


Figure IV - 50: Initial charge voltage profiles for Li/LFO cells at different rates from 10 to 100 mA/g. 100 mA/g is about C/6 rate.

**Li/Si-Carbon Composite Electrode.** To enable the LFO for use in a high energy Li-ion cell, it must be paired not only with a 'charged' electrode, but also with a high-capacity Si anode. A Si-carbon composite anode was obtained from a BATT researcher for this study. Figure IV - 51 shows the cycling performance of the Li/Si-carbon composite half cell. The irreversible capacity loss is somewhat low, but the capacity degrades with cycling, the cell loses about 20% over 23 cycles. Clearly an improved Si anode will need to be procured or obtained in order to make the LFO-based high-energy cell.

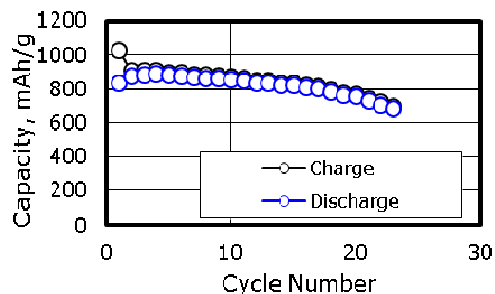


Figure IV - 51: Cycle performance of Li/Si-carbon composite cell over a voltage window of 0 to 2.0 V.; current = 150 mA<sub>g</sub><sup>-1</sup> (C/6)

**Stability of LFO.** The stability of LFO is critical if the electrode coating and production is to be done in a dry room environment. It is a concern since the material contains a very large amount of active Li (5 Li/Fe), and could be full of nascent Li<sub>2</sub>CO<sub>3</sub> impurities. Raman spectroscopy was used to measure the purity of LFO in air.

Powdered samples were examined using two types of containers. In one case the powders were placed between rectangular glass microscope cover slides and the boundaries of the slides were sealed with Scotch Tape to minimize air contact and to present a flat surface to the microscope objective. We also used a sealable metal cell with a CaF<sub>2</sub> window: this type of cell was much easier to load in a glove box.

The LFO Raman spectrum (Figure IV - 52) exhibits over a dozen distinct features with a signature peak at ca. 656 cm<sup>-1</sup>. Group theory predicts dozens of Raman active modes for the LFO crystal lattice. The as-prepared LFO samples tend to contain traces of CO<sub>3</sub><sup>2-</sup>.

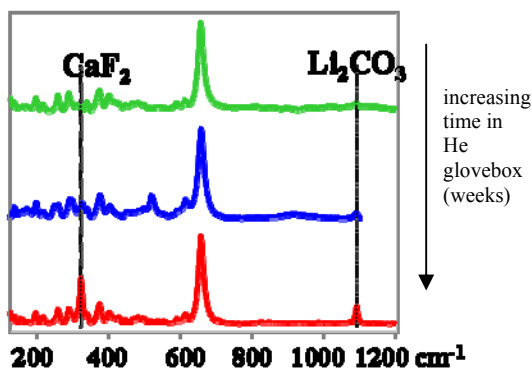


Figure IV - 52: Raman spectra with 633 nm laser excitation within a sealed CaF<sub>2</sub> sample holder under He.

When LFO is exposed to ambient laboratory air (presumably containing normal amounts of CO<sub>2</sub> and H<sub>2</sub>O), it rapidly reacts. The light gray colored LFO turns rust red (Figure IV - 53). Raman spectroscopy shows clear evidence for formation of Li<sub>2</sub>CO<sub>3</sub>, as well as Fe-containing phases we have not clearly identified. We note that LiFeO<sub>2</sub> does

not exhibit a first order Raman spectrum, but most other iron oxide phases of interest do (e.g., FeO, Fe<sub>2</sub>O<sub>3</sub>, Fe<sub>3</sub>O<sub>4</sub>, FeOOH). The adsorption of water in the material is also clearly evident by the strong hydroxyl OH<sup>-</sup> vibration stretch (Figure IV - 54).



Figure IV - 53: LFO powders – left side (rust brown colored) is LFO exposed for 5 days in ambient laboratory air, and right side powder (gray colored) is the LFO stored in a vial in the dry room for 5 days.

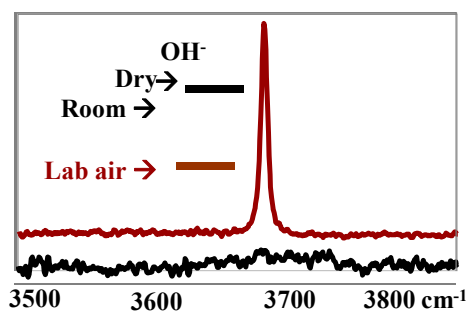


Figure IV - 54: Raman spectra of LFO powders -top is LFO exposed for 5 days in ambient laboratory air, and bottom is the LFO stored in a vial in the dry room for 5 days.

Through use of analytical Raman spectroscopy it was determined that LFO can be handled in the dry room for multiple days, which makes it possible to coat and process electrodes in an industrial setting.

## Conclusions and Future Directions

This year a number of experiments on Li<sub>5</sub>FeO<sub>4</sub> (LFO) were completed. Due to the large amount of available lithium (5 Li/Fe), this material has promising features and characteristics as a very high-capacity (867 mAh/g), low cost, pre-lithiation precursor cathode material for lithium battery applications. However, cell chemistry improvements will be necessary to make these materials viable in Li-ion batteries. The LFO material is intended to provide a different option and approach to use low-cost, safe materials consisting of Fe, V, and Mn elements in the electrode. The dry room stability is adequate for electrode processing. A good Si electrode needs to be obtained to couple the LFO and the ‘charged’ material in a Li-ion cell. The rate of LFO activation; that is, the removal of 4 lithiums from the material can be achieved in 6 hours. Finally it was found that LFO can be synthesized in 24 h in Ar using LiOH-H<sub>2</sub>O + Fe<sub>2</sub>O<sub>3</sub>. Experiments on very high-

capacity (>500 mAh/g) substituted vanadium oxide cathodes were started, and these encouraging experiments are ongoing, and will be reported in due course.

For the future directions, we plan to synthesize additional samples of LFO, doped or substituted with a focus on improving the electrochemical properties by optimizing morphology, particle size, surface area, and coatings. We will have completed cell-testing with blended charged cathodes using these new formulations in both lithium half cells and Li-ion full cells, including Si cells. Finally we will improve the properties of charged cathodes such as LVO, MnO<sub>2</sub>, and high capacity V<sub>2</sub>O<sub>5</sub> (442 mAh/g) coating processes, powder optimization and dopants. Using diagnostic methods, we hope to understand the rate-determining step for the LFO bond breakage and formation of oxygen gas from the structure collapse. From the Raman studies, we know that iron-containing phase is formed from LFO upon removal of lithium, but this condensation reaction mechanism is unknown. Once the mechanism is discerned, we will apply this knowledge to choose the right combination of particle morphology, particle size, surface area of the powder, and electrochemical conditions, in order to optimize the LFO for the Li<sub>2</sub>O removal reaction, and to improve its reversibility on charge-discharge cycling in combination with an optimized charged cathode.

### **FY 2011 Publications/Presentations**

1. 2011 DOE Annual Peer Review Meeting Presentation, May 9<sup>th</sup>-13<sup>th</sup> 2011, Washington DC.

## IV.B.3.4 Novel Composite Cathode Structures (ANL)

Christopher S. Johnson

Argonne National Laboratory  
9700 South Cass Avenue  
Argonne, IL 60439-4837  
Phone: (630) 252-4787; Fax: (630) 252-4176  
E-mail: [cjohnson@anl.gov](mailto:cjohnson@anl.gov)

Collaborators:

Mike Slater, Argonne National Laboratory  
Eungje Lee, Argonne National Laboratory  
Mahalingam Balasubramanian, Argonne National Laboratory  
Zhengcheng Zhang, Argonne National Laboratory  
Donghan Kim, Argonne National Laboratory  
Prof. Stephen Hackney, Michigan Technological University

Start Date: October, 2010

Projected End Date: September, 2016

### Objectives

The project objective is to conduct ion-exchange reactions to make new cathode materials with high-energy and high-rate. We will produce an optimized material that shows an improvement over the drawbacks of standard high-energy cathodes. These ion-exchange cathodes should thus demonstrate <10% irreversible capacity in the first cycle, > 200 mAh/g at a C rate, no alteration in voltage profile during cycling, lower cost, and improved safety.

### Technical Barriers

- Low energy density
- High cost
- Low abuse tolerance

### Technical Targets

- 96 Wh/kg, 316 W/kg (PHEV 40 mile requirement)
- Cycle life: 3000 cycles
- Calendar life: 15 years
- Improved abuse tolerance

### Accomplishments

- $\text{Na}_x\text{Li}_y(\text{Ni}_{0.25}\text{Mn}_{0.75})\text{O}_z$  cathode precursors synthesized;  $x=1.0, 1.1, \text{ and } 1.2, y=0.2, 0.1, \text{ and } 0.$  Li ion-exchange reactions of the above Na-Li materials successfully conducted. The typical content of the

product material is  $\text{Li}_{1.06}\text{Na}_{0.02}\text{Ni}_{0.21}\text{Mn}_{0.63}\text{O}_2$  with compositions measured by ICP-AES. Ni and Mn ratio is maintained and most Na is effectively removed in these ion-exchange reactions.

- The capacity measured at a C/15 rate was 230 mAh/g between 4.8 to 2.0 V in Li-half cells. Over 40 cycles were completed with no loss in capacity. The C rate capacity is above 200 mAh/g. 15C rate capacity is 150 mAh/g.
- HRTEM suggests that the ion-exchanged material consists of a repeating two-layer two-phase laminate structure that displays a natural super-lattice. Further, the data suggests a non-homogenous Ni-Mn distribution in the a/b plane. Ramifications of these findings will be considered. Finally, results of many electron diffraction patterns taken, surprisingly show no spinel domains in the fresh as-prepared materials. Next we will interrogate cycled samples.
- Initial DSC data (charged electrode thermal properties) shows the ion-exchange sample has 10% less heat evolved (4.6 V charged cathode) than a typical composite 'layered-layered' ANL-NMC material:  $0.5\text{Li}_2\text{MnO}_3 \bullet 0.5\text{LiNi}_{0.44}\text{Co}_{0.25}\text{Mn}_{0.31}\text{O}_2$ . The onset temperature is also shifted about 30°C higher.

◇ ◇ ◇ ◇ ◇

### Introduction

Li-ion batteries are used for energy storage in a number of applications, including PHEVs and EVs. Maximizing energy density and power of the cathode material will improve these vehicles. A number of materials with composition  $\text{LiMO}_2$  (M=Mn, Ni, Co) have been reviewed [1].  $\text{LiMO}_2$  classes of cathodes are layered oxides having 2-dimensional layers which supports reversible lithium insertion/extraction.  $\text{LiMO}_2$  ( $\alpha$ - $\text{NaFeO}_2$ ; S.G. R-3m) hexagonal structure consists of alternating Li and M layers formed by the stacking of close-packed oxygen atoms. To some degree, site disorder occurs between Li and M, which negatively affects the electrochemical performance due to M partially blocking lithium diffusion [1]. For example  $\text{Li}(\text{Ni}_{0.5}\text{Mn}_{0.5})\text{O}_2$  has 8-11% disorder due in part to  $\text{Ni}^{2+}$  (0.69Å) and  $\text{Li}^+$  (0.76 Å) having similar ionic radii [2, 3]. However, if some Mn and Ni cations are substituted by lithium, then Li-excess  $\text{Li}_{1+z}(\text{Ni}_{0.5}\text{Mn}_{0.5})_{1-z}\text{O}_2$  materials are formed resulting in less site disorder, and improved electrochemistry [4, 5]. Since the Li content is greater than the Ni+Mn content, the additional Li moves to Ni and Mn sites, preferentially

forming  $\text{LiM}_6$  domains containing Mn [6]. In this respect, these  $\text{LiM}_6$  domains associate to form ordered or disordered monoclinic  $\text{Li}_2\text{MnO}_3$  component in 'layered-layered'  $x\text{Li}_2\text{MnO}_3 \cdot (1-x)\text{LiMO}_2$  ( $M=\text{Mn, Ni, Co}$ ) composite oxides [7].

Another synthesis route to minimize site disorder in  $\text{LiMO}_2$  is lithium ion-exchange of the isostructural layered Na phases ( $\text{Na}[\text{M}]\text{O}_2$ ) [8,9]. In this case, the large cation radii of  $\text{Na}^+$  (1.02 Å) causes an increase in the interlayer slab space for  $\text{Na}[\text{M}]\text{O}_2$ , and the separation of layers and cation sites are conserved in the  $\text{LiMO}_2$  product. For example, Robertson et al. [10] exploited the good cation ordering in  $\text{Li}(\text{Mn,Ni})\text{O}_2$  samples derived from the sodium analogues to hinder the nucleation of spinel domains within electrodes on cycling. Paulsen and Dahn used this precursor method to synthesize materials with increased Ni contents to make  $\text{Li}_{2/3}[\text{Ni}_{1/3}\text{Mn}_{2/3}]\text{O}_2$  [11] and other variants [12] that are not easily accessible directly.

In this work, a Li-exchanged material was synthesized from the corresponding sodium layered precursor  $\text{Na}_x\text{MO}_2$ . The M in  $\text{Na}_x\text{MO}_2$  contains a combination of Li with Ni and Mn, and the sum of Na+Li in the precursor is greater than Ni+Mn. Not only is this combination expected to minimize site disorder in the layered structure, but with additional lithium, the formation of  $\text{LiM}_6$  ( $M=\text{Mn}$  and/or  $\text{Mn/Ni}$ ) domains in the layer will also add a stabilizing component to the material. The literature has not discussed systems where the sum of Na+Li is greater than M, derived from ion-exchange reactions of sodium-lithium analogs. Therefore, the electrochemical-structural property gap between  $\text{Li}_{1+z}(\text{M})_{1-z}\text{O}_8$  and lithium-exchanged  $\text{Na}_x\text{M}_{1-y}\text{Li}_y\text{O}_8$  cathodes is bridged and reported in this communication.

## Approach

We will synthesize, characterize, and develop new cathode materials that exploit the difference in sodium versus lithium cation radii and their respective coordination properties. Cathodes will be derived from layered sodium transition metal oxide precursors that contain modest amounts of lithium in the transition metal (TM) layer. The sodium in the precursor materials is then ion-exchanged with lithium to form layered composite oxide cathodes for lithium batteries. We will focus on electrode materials that contain redox active Ni, and low cost Mn and Fe transition metals.

## Results

The experimentally determined stoichiometry of the product synthesized from lithium ion-exchange from the layered precursor  $\text{Na}_{0.9}\text{Li}_{0.3}\text{Ni}_{0.25}\text{Mn}_{0.75}\text{O}_8$  was  $\text{Li}_{1.32}\text{Na}_{0.02}\text{Ni}_{0.25}\text{Mn}_{0.75}\text{O}_y$  (IE-LNMO). X-ray absorption near-edge spectroscopy (XANES) results fit a model where Ni is divalent and Mn is nearly tetravalent [13], the

normalized composition for  $y=2$  thus is

$\text{Li}_{1.09}\text{Na}_{0.02}\text{Ni}_{0.21}\text{Mn}_{0.62}\text{O}_2$ : the number of cations is slightly less than the number of oxygen anions ( $1.94/2=0.97$ ) implying that a spinel component may be present in the ion-exchanged product. The XRD pattern of the precursor (Fig. 1a) can be indexed to the JCPDS card 27-0751 ( $\text{Na}_{0.7}\text{MnO}_{2.05}$  match). Note some unidentified impurities marked by arrows in Fig. 1a are present. Nevertheless, the major XRD peaks in the pattern match that of similarly synthesized  $\text{Na}_{2/3}(\text{Ni}_{1/3}\text{Mn}_{2/3})\text{O}_2$  composition whose structure (hexagonal; S. G.:  $\text{P6}_3\text{mmc}$ ) was solved by Paulsen and Dahn [11]. It is not known where the Li in  $\text{Na}_{0.9}\text{Li}_{0.3}\text{Ni}_{0.25}\text{Mn}_{0.75}\text{O}_8$  resides, although it is reasonable to predict that it is located in the Ni-Mn layer, because Li prefers octahedral coordination, while Na is larger, and instead, can adopt prismatic coordination in the adjacent layer. The XRD of IE-LNMO product is shown in Figure IV - 55b. The pattern contains combinations of broad and narrow peaks, and Rietveld refinement of the structure was not possible. However, there is a strong (003) layering peak that is shifted to higher angles relative to  $\text{Na}_{0.9}\text{Li}_{0.3}\text{Ni}_{0.25}\text{Mn}_{0.75}\text{O}_8$  with d-spacing (5.656 Å). The IE-LNMO has smaller d-spacing (4.989 Å) confirming shrinkage of the c-axis consistent with removal of most large Na cations for smaller Li cations. There are also small peaks at  $\sim 20\text{-}23^\circ 2\theta$  (Figure IV - 55a inset) indicating Ni-Mn ordering in the TM layer likely due to the presence of some Li. These types of small peaks at  $\sim 20\text{-}23^\circ 2\theta$  are also present in high-temperature synthesized highly crystalline composite 'layered-layered' or 'layered-spinel' which is an identification marker for lithium in the transition metal layer or  $\text{LiMn}_6$  unit/ $\text{Li}_2\text{MnO}_3$  component, particularly when Mn is combined with Ni [14-16]. The overall XRD pattern of IE-LNMO suggests a defect-laden layered material, perhaps with stacking faults in the c-direction while still possessing Ni-Mn ordering. It is unknown what role the presence of Na may play during the ion-exchange reaction, and if the residual Na in the IE-LNMO plays an active role in structure stabilization and electrochemical performance. More work is necessary to accurately determine the precise structure of

$\text{Li}_{1.32}\text{Na}_{0.02}\text{Ni}_{0.25}\text{Mn}_{0.75}\text{O}_y$  and the mechanism of formation.

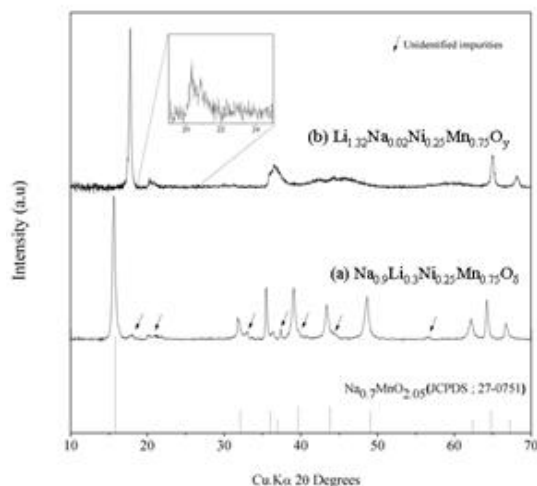


Figure IV - 55: (a) X-ray powder diffraction patterns of  $\text{Na}_{0.9}\text{Li}_{0.3}\text{Ni}_{0.25}\text{Mn}_{0.75}\text{O}_8$  precursor (arrows mark minor impurities) and (b) ion-exchanged  $\text{Li}/\text{Li}_{1.32}\text{Na}_{0.02}\text{Ni}_{0.25}\text{Mn}_{0.75}\text{O}_y$  (IE-LNMO) product (inset is enlarged  $20\text{-}24.5^\circ 2\theta$  section).

The galvanostatic first, second and 40<sup>th</sup> cycle voltage profiles for the Li/IE-LNMO cell are shown in Figure IV - 56a. The first charge voltage profile is characterized by an initial sloping region up to 4.5 V, followed by a voltage plateau which slowly progresses to the 4.8 V cut-off. The subsequent discharge profile consists of three distinct regions (marked as 1, 2, and 3), where the slope of the curve changes: 4.5 - 3.75 V, 3.75 - 3.25 V, and 3.25 to 2.0 V cut-off. In the second cycle, the charge voltage profile is characterized by an initial low voltage plateau at approximately 2.8 to 3.0 V, followed by a long sloping shape up to 4.8 V: the 4.5 V plateau on the first cycle is not observed. The 40<sup>th</sup> voltage profile shows distinctly two regions with an inflection at  $\sim 3.75$  V during charge, and again three regions during discharge. There is no discernible change in the voltage profile of the material after 40 cycles. The first charge capacity is 252 mAh/g, and the first discharge capacity is 234 mAh/g, which is an irreversible capacity loss of only 7%. Figure IV - 56b provides the capacity versus cycle number to 40 cycles. The discharge capacity values range between 220 mAh/g - 225 mAh/g and are steady with excellent coulombic efficiency. Calculations show that the average oxidation state of Mn at the end of the first discharge cycle is 3.56, and slightly higher with continuous cycling. Since the Mn in the material remains above the Jahn-Teller distortion critical threshold of 3.5 Mn average oxidation state, it is hypothesized that good electrochemical reversibility is maintained [17]. Rate study results are shown as specific discharge capacity versus current rate in Figure IV - 56b inset. The curve is fairly flat above 220 mAh/g at a 75 mA/g current, and is above 200 mAh/g at 300 mA/g. Notably, this cathode yielded  $\sim 150$  mAh/g at very high 1500 mA/g, which corresponds to about a 8C rate.

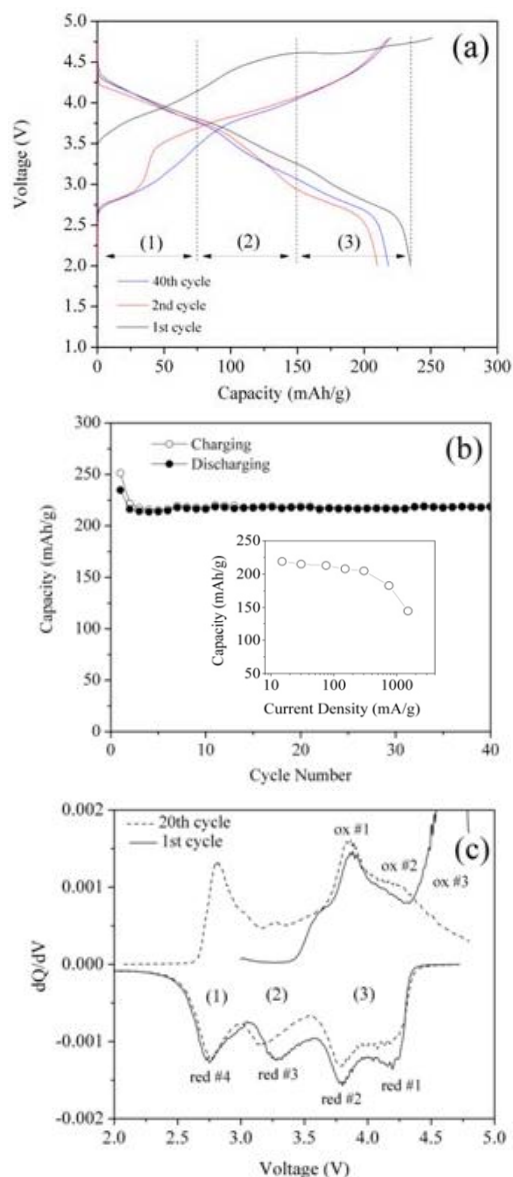


Figure IV - 56: (a) 1<sup>st</sup>, 2<sup>nd</sup>, and 40<sup>th</sup> voltage profiles of Li/IE-LNMO cell between 4.8 V and 2.0 V (15 mA/g), (b) capacity versus cycle number, and inset is the capacity versus current rate, (c) derivative plot ( $dQ/dV$ ) of the Li/IE-LNMO cell.

A first discharge curve from an uncycled fresh cell was conducted to evaluate whether a spinel component is present in the material. Indeed, a flat voltage plateau was observed at  $\sim 2.7$  to 2.8 V with a discharge capacity of 40 mAh/g. The  $dQ/dV$  plot showed one symmetrical peak confirming the presence of a '3 V' cubic spinel component, such as  $\text{Li}_4\text{Mn}_5\text{O}_{12}$  (Mn(IV)), or slightly Ni-substituted version with the formulation  $\text{Li}_{1.33-y}\text{Ni}_{3y/2}\text{Mn}_{1.67-y/2}\text{O}_4$ ;  $0 \leq y \leq 0.33$ ;  $y$  is close to 0. Note a spinel component in the material would help to minimize the first cycle irreversible capacity loss in this electrode. This is because Li cannot be extracted from  $\text{Li}_4\text{Mn}_5\text{O}_{12}$  spinel component

on the first charge step, but on the subsequent first discharge step, lithium can insert in the spinel to form the end member  $\text{Li}_7\text{Mn}_5\text{O}_{12}$ , thereby contributing capacity at voltages below about 3 V.

Since the voltage profiles (Figure IV - 56a) for Li/IE-LNMO cell are complex, derivative capacity-voltage  $dQ/dV$  plots for 1<sup>st</sup> and 20<sup>th</sup> cycles were calculated and graphed to accentuate redox features occurring in the electrode (Figure IV - 56c). First charge process in increasing voltage for cycle 1 shows one shoulder, one peak, a second shoulder and one large off-scale peak at highest potential. Since the material likely contains divalent nickel, it is possible that one peak and the higher-voltage shoulder centered at  $\sim 3.8 - 3.9$  V are due to Ni(II/IV) in a layered component [18]. The pre-peak shoulder at  $\sim 3.65-3.7$  V could involve some minor  $\text{Mn}^{3+}$  oxidation, perhaps from a spinel or layered component. The 4<sup>th</sup> oxidation peak above  $\sim 4.5$  V is irreversible and indicative of lithium removal accompanied with oxygen loss from the material [19]. Note that this voltage plateau is consistent with the electrochemical activation of  $\text{Li}_2\text{MnO}_3$  component in 'layered-layered' and 'layered-spinel' composites [14-16]. On discharge, the layered Ni(IV) component is reduced to Ni(II) (red1 & red 2). Next, the  $dQ/dV$  plot shows reduction peak (red3) at  $\sim 3.2$  V, perhaps due to Mn reduction in the layered component derived from  $\text{Li}_2\text{O}$  removal [14]. Continuing to lower potentials gives a 4<sup>th</sup> reduction peak (red4) at  $\sim 2.7$  V: this peak is from a spinel component in the cathode. As can be seen in 20<sup>th</sup>  $dQ/dV$  curve, all three redox regions (labeled 1, 2, 3) are reversible in a 4.8 to 2.0 V window.

Figure IV - 57 shows the field-emission scanning electron microscope (FESEM) and HRTEM of the ion-exchanged sample. The process causes shearing of the layers as can be identified by the particles that have been 'sliced' along the c-axis. The morphologies resemble a 'stack-of-cards' after the exchange, indicating that Na is pulled out of the layer and replaced concomitantly with Li. These thin plates demonstrate how flexible and easily gliding the layers are relative to one another. Careful HRTEM work has been able to distinguish the layering of this material as a two-layer-two phase laminate structure with a natural super-lattice repeat layer stacking pattern Figure IV - 57 (b).

In Figure IV - 58, two representative DSC patterns are taken from an ion-exchanged cathode material charged to 4.6V versus an ANL-NMC cathode charged to the same voltage. Total heat released from the ion-exchanged

cathode is slightly lower and the onset temperature is approximately the same.

In summary, the presence of a Ni-containing layered component, a Mn layered component, and a '3 V' Mn spinel component are all observed (redox regions 1, 2, & 3; Figure IV - 56c) suggesting that a new, novel 'layered-spinel' composite oxide was synthesized from ion-exchange. Further studies are in progress to evaluate a number of different Li+Na/M ratios, their structures, and the source of the very high-rates. Different solvents and salts for the ion-exchange reaction are also being studied.

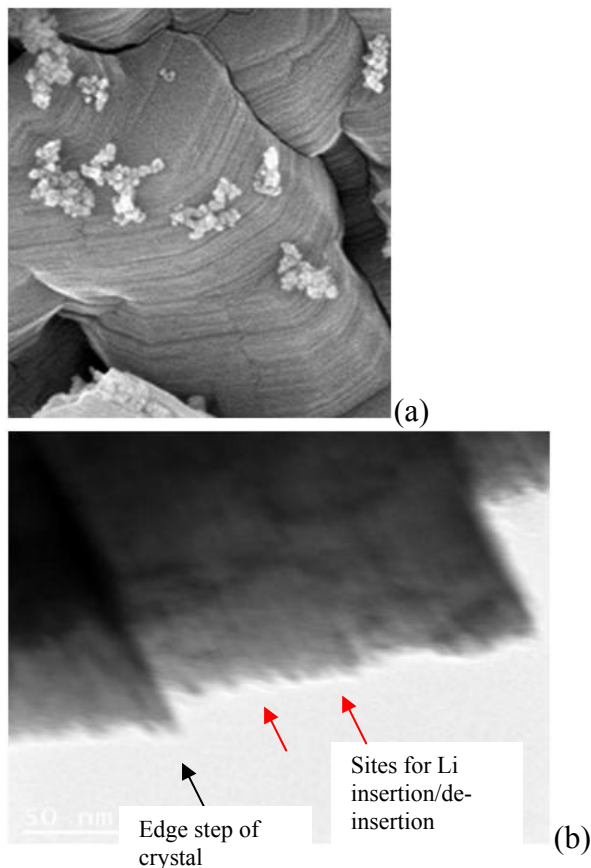


Figure IV - 57: (a) FESEM of  $\text{Li}_{1.06}\text{Na}_{0.02}\text{Ni}_{0.21}\text{Mn}_{0.63}\text{O}_2$  (layered compound with a number of c-direction stacking faults), and (b) HRTEM of Li ion-exchanged material perpendicular to the c-axis showing points of entry for fast Li cation insertion/de-insertion.

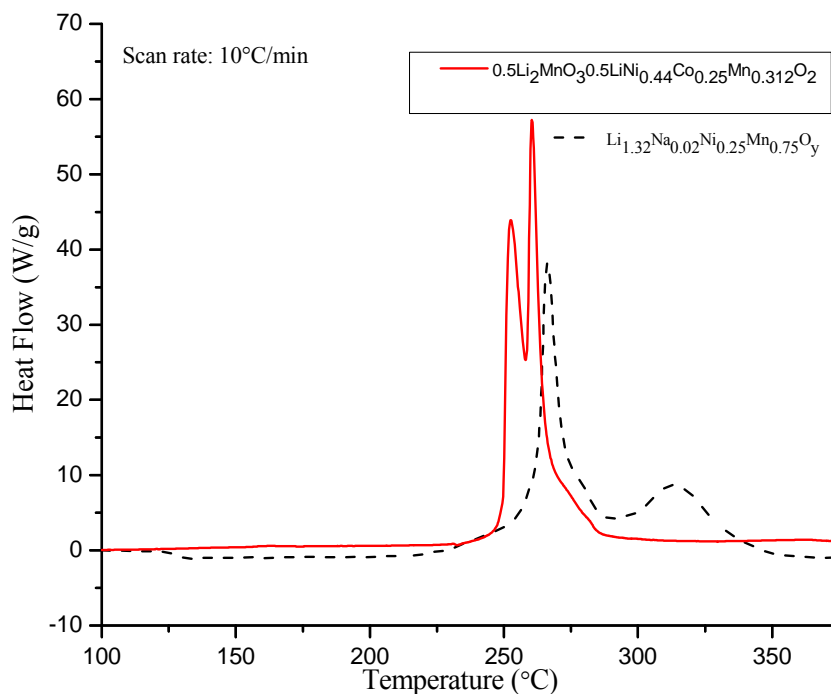


Figure IV - 58: DSC output of 4.6 V charged ion-exchanged cathode versus an Argonne composite 'layered-layered' ANL-NMC cathode:  $0.5\text{Li}_2\text{MnO}_3 \bullet 0.5\text{LiNi}_{0.44}\text{Co}_{0.25}\text{Mn}_{0.312}\text{O}_2$

## Conclusions and Future Directions

Novel and new Li-rich nickel-manganese oxide cathode material with the compositions such as  $\text{Li}_{1.32}\text{Na}_{0.02}\text{Ni}_{0.25}\text{Mn}_{0.75}\text{O}_y$  are synthesized by ion-exchange reactions from layered  $\text{Na}_x\text{Li}_y\text{Ni}_{0.25}\text{Mn}_{0.75}\text{O}_\delta$  ( $x+y=1.2$ ) precursors. Because of the radii size mismatch of Na and Li cations, the Li in the precursor likely favors sites in the Ni-Mn layer. After Li ion-exchange, the XRD pattern shows a high intensity layered (003) peak, other broad peaks, and ordering peaks at  $\sim 20\text{-}23^\circ 2\theta$ . These ordering peaks, and the quantity of lithium content present strongly suggests that some Li is within the Ni-Mn layer. In addition, the voltage profile shows a plateau at 4.5 V indicative of  $\text{Li}_2\text{O}$  electrochemical loss from a  $\text{Li}_2\text{MnO}_3$  component. The  $dQ/dV$  curves show three reversible redox peaks with a spinel component signature. From the electrochemical results, combination of redox Ni(II) in the layered component and Mn(III/IV) in both the layered and spinel components suggest that a type of 'layered-spinel' composite was formed, perhaps with defect-laden features and layered stacking faults. The stacking faults and the presence of a spinel component may contribute to the cycling stability and very high-rate capability observed. However, more work is needed to discern the precise structure of this new material. In conclusion this electrode material exhibits high discharge rates ( $\sim 150 \text{ mAh/g @}$

$1500 \text{ mA/g}$ ) and a stable high capacity during cycling ( $\sim 220 \text{ mAh/g @ 40 cycles}$ ): thus demonstrating dual function electrochemical behavior in one cathode material potentially useful for PHEV and EV applications. Ion exchange reactions where the sodium in mixed Na/Li layered phases is replaced with excess lithium may facilitate the formation of new composite phases with superior electrochemical performances.

Future work will examine the effect that the ion-exchange media has on the structure and electrochemical performance. For low cost processing, we will focus on water based ion-exchange methods with low-temperature vacuum drying.

## References

1. M. S. Whittingham, *Chem Rev.*, 104 (2004) 4271.
2. Y. Hinuma, Y. S. Meng, K. Kang, G. Ceder, *Chem. Mater.*, 19 (2007) 1790.
3. A. Van der Ven, G. Ceder, *Electrochem. Commun.*, 6 (2004) 1045.
4. S. T. Myung, S. Komaba, S. Kurihara, K. Hosoya, N. Kumagai, Y. K. Sun, I. Nakai, M. Yonemura, T. Kamiyama, *Chem. Mater.* 18 (2006) 1658.
5. S.-H. Park, S.-H. Kang, C. S. Johnson, K. Amine, M. M. Thackeray, *Electrochem. Commun.*, 9 (2007) 262.

6. Y.S. Meng, G. Ceder, C. P. Grey, W.-S. Yoon, M. Jiang, J. Bréger, Y. Shao-Horn, *Chem. Mater.* 17 (2005) 2386.
7. M. M. Thackeray, S.-H. Kang, C. S. Johnson, J. T. Vaughey, R. Benedek, S. A. Hackney, *J. Mater. Chem.*, 17 (2007) 3112.
8. A. R. Armstrong, P. G. Bruce, *Nature*, 381 (1996) 499.
9. F. Capitaine, P. Gravereau, C. Delmas, *Solid State Ionics*, 89 (1996) 197.
10. A.D. Robertson, A. R. Armstrong, A. J. Paterson, M. J. Duncan, P. G. Bruce, *J. Mater. Chem.*, 13 (2003) 2367.
11. J. M. Paulsen, and J. R. Dahn, *J. Electrochem. Soc.*, 147 (2000) 2478.
12. J. Paulsen, R. A. Donaberger, J. R. Dahn, *Chem. Mater.*, 12 (2000) 2257.
13. M. Balasubramanian ; unpublished data.
14. M. M. Thackeray, C. S. Johnson, J. T. Vaughey, N. Li, S. A. Hackney, *J. Mater. Chem.* 15 (2005) 2257.
15. C. S. Johnson, N. Li, J. T. Vaughey, S. A. Hackney, M. M. Thackeray, *Electrochem. Commun.* 7 (2005) 528.
16. J. Cabana, S.-H. Kang, C. S. Johnson, M. M. Thackeray, C. P. Grey, *J. Electrochem. Soc.* 156 (2009) A730.
17. M. M. Thackeray , *Prog. In Solid State Chem.*, 25 (1997) 1.
18. W. Yoon, C. P. Grey, M. Balasubramanian, X. Q. Yang, J. McBreen, *Chem. Mater.*, 15 (2003) 3161.
19. C. S. Johnson, J.-S. Kim, C. Lefief, N. Li, J. T. Vaughey, M. M. Thackeray, *Electrochem. Commun.* 6, (2004), 1085.
- (Japan)-Argonne Battery Workshop, Argonne, October 2010 (Invited).
6. C. S. Johnson et al., “High-Power and High-Energy Li-Ni-Mn Oxides for Lithium Batteries”, 1st NEDO (Japan)-Argonne Battery Workshop, Argonne, October 2010 (Invited).
7. C. S. Johnson et al., “High-Performance Oxide Cathodes for Li-ion Batteries”, The 220th Electrochemical Society Meeting, Boston, MA, October 2011 (Oral).

## Publications

1. D. Kim, S.-H. Kang, M. Balasubramanian, C. S. Johnson, “High-Energy and High-Power Li-rich Nickel Manganese Oxide Electrode Materials”, *Electrochem. Commun.*, 12 (2010) 1618.

## FY 2011 Publications/Presentations

### Presentations

1. 2011 DOE Annual Peer Review Meeting Presentation, May 9th-13th 2011, Washington DC.
2. S. Johnson et al., “Synthesis of a Series of High Energy Cathodes via an Ion-Exchange Method”, The 218th Electrochemical Society Meeting, Las Vegas, Nevada, October 2010 (Oral).
3. S. Johnson et al., “High-Energy and High-Power Composite Li-Battery Cathodes Synthesized from Ion-exchange Reaction”, Materials Research Society Spring Meeting, San Francisco, April/May 2010 (Invited).
4. C. S. Johnson et al., “High-Energy and High-Power Li-rich Nickel Manganese Oxide Electrode Materials”, 1st Argonne-PNNL Battery Workshop, Argonne, November 2010 (Invited).
5. C. S. Johnson et al., “High-Power and High-Energy Li-Ni-Mn Oxides for Lithium Batteries”, 1st NEDO

## IV.B.3.5 Development of High-Capacity Cathode Materials with Integrated Structures (ANL)

Michael Thackeray

Argonne National Laboratory

9700 South Cass Avenue

Argonne, IL 60439

Phone : (630) 252-9184 ; Fax : (630) 252-4176

E-mail: [thackeray@anl.gov](mailto:thackeray@anl.gov)

Collaborators:

ANL: S.-H. Kang, K. G. Gallagher, D. Kim

M. Balasubramanian (APS)

MIT: Y. Shao-Horn, C. Carlton (MIT)

Start Date: October 1, 2009

Projected End Date: September 30, 2014

### Accomplishments

- Chemical compositions of lithium-nickel-manganese-oxide composite electrode structures in a three-component ‘layered-layered-spinel’ system were examined; an optimum composition on the  $\text{Li}_2\text{MnO}_3 \cdot \text{LiMn}_{0.5}\text{Ni}_{0.5}\text{O}_2$  -  $\text{LiMn}_{1.5}\text{Ni}_{0.5}\text{O}_4$  tie-line was identified.
- Studies of the voltage decay phenomenon and solubility effects in  $\text{Li}/x\text{Li}_2\text{MnO}_3 \cdot (1-x)\text{LiMO}_2$  cells were undertaken.
- The effects of blending ‘layered-layered’ electrode materials with a high-power olivine ( $\text{LiFePO}_4$ ) component on cell impedance, particularly at low states-of-charge (SOC) were investigated.



### Objectives

The major objective of this work is to develop Li- and Mn-rich cathode materials with integrated structures that promise low cost, good thermal stability and an improved first-cycle efficiency while maintaining high capacity at an acceptable rate (e.g.,  $\geq 200$  mAh/g at 1C). Cathode performance goals are a reversible 230 mAh/g capacity with  $>85\%$  first cycle efficiency. Specific objectives of this study are to:

1. design and synthesize stabilized Li- and Mn-rich metal oxide electrodes with integrated structures that contain layered and spinel components
2. identify and overcome degradation phenomena associated with high-capacity ‘composite’ cathode materials, and
3. supply promising high-capacity cathode materials for a PHEV cell build.

### Technical Barriers

- Low energy density
- Poor low temperature operation
- Abuse tolerance limitations

### Technical Targets (USABC - End of life)

- 142 Wh/kg, 317 W/kg (PHEV 40 mile requirement)
- Cycle life: 5000 cycles
- Calendar life: 15 years

### Introduction

Li- and Mn-rich oxide electrodes with integrated or composite ‘layered-layered’ structures such as  $x\text{Li}_2\text{MnO}_3 \cdot (1-x)\text{LiMO}_2$  ( $M=\text{Mn, Ni, Co}$ ), are known deliver a high capacity ( $\sim 250$  mAh/g) when charged to high potentials ( $>4.4$  V vs.  $\text{Li}^+/\text{Li}$ ). Present limitations of these cathode materials are 1) a relatively poor rate capability, 2) high impedance, particularly at low SOC, and 3) poor cycling performance with respect to carbon-based anodes especially at high temperatures. These performance limitations are attributed to poor electronic/ionic conductivity in the oxide bulk, surface damage from repeated high-voltage cycling, and Mn dissolution in the electrolyte. In addition to the above-mentioned limitations, ‘layered-layered’ electrode materials exhibit significant voltage decay on extended cycling, which creates issues not only in terms of a decrease in cell energy but also in battery management (voltage monitoring). This project addresses the above-mentioned limitations in an attempt to meet the targeted electrode and cell performance goals using integrated electrode structures.

### Approach

To address the limitations associated with ‘layered-layered’  $x\text{Li}_2\text{MnO}_3 \cdot (1-x)\text{LiMO}_2$  electrodes, multiple parallel efforts are adopted:

1. embedding a spinel component in the 'layered-layered' matrix by chemical composition design to stabilize the electrode to electrochemical cycling,
2. elucidating the root causes of voltage decay on cycling, and
3. blending a high-capacity  $x\text{Li}_2\text{MnO}_3 \cdot (1-x)\text{LiMO}_2$  component with a high-power component, such as carbon-coated  $\text{LiFePO}_4$ , to improve the overall performance of the composite electrode.

## Results

### 'Layered-Layered-Spinel' Electrodes.

Based on previous reports that integrated 'layered-spinel' composite structures can be formed between layered  $\text{Li}_2\text{MnO}_3$  and spinel structures within the system  $\text{Li}_{1+x}\text{Mn}_{2-x}\text{O}_4$ , the strategy in this study was to embed the high potential spinel  $\text{LiMn}_{1.5}\text{Ni}_{0.5}\text{O}_4$  into a 'layered-layered'  $\text{Li}_2\text{MnO}_3 \cdot \text{LiMn}_{0.5}\text{Ni}_{0.5}\text{O}_2$  component to evaluate if the spinel component had any stabilizing influence on the 'layered-layered' electrode. Electrode compositions were therefore selected that fell on the  $\text{Li}_2\text{MnO}_3 \cdot \text{LiMn}_{0.5}\text{Ni}_{0.5}\text{O}_2$  -  $\text{LiMn}_{1.5}\text{Ni}_{0.5}\text{O}_4$  tie line of the  $\text{Li}_2\text{MnO}_3$ - $\text{LiMn}_{0.5}\text{Ni}_{0.5}\text{O}_2$ - $\text{LiMn}_{1.5}\text{Ni}_{0.5}\text{O}_4$  phase diagram as indicated in Figure IV - 59. The composition of these electrodes can be more simply represented as having the general formula  $\text{Li}_x\text{Ni}_{0.25}\text{Mn}_{0.75}\text{O}_y$  for  $0.5 \leq x \leq 1.5$ ;  $2.0 \leq y \leq 2.5$ . The values  $x=0.5$  and  $y=2.0$  correspond to the spinel end-member  $\text{LiMn}_{1.5}\text{Ni}_{0.5}\text{O}_4$ , whereas the values 1.5 and  $y=2.5$  correspond to the 'layered-layered' end-member  $\text{Li}_2\text{MnO}_3 \cdot \text{LiMn}_{0.5}\text{Ni}_{0.5}\text{O}_2$ . Because the oxygen content can vary slightly within each sample, the  $y$  parameter is not defined for simplicity.

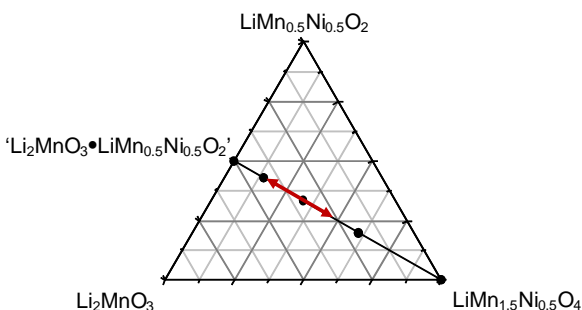


Figure IV - 59: A compositional phase diagram of the 'layered-layered-spinel'  $\text{Li}_2\text{MnO}_3$ - $\text{LiMn}_{0.5}\text{Ni}_{0.5}\text{O}_2$ - $\text{LiMn}_{1.5}\text{Ni}_{0.5}\text{O}_4$  system showing the region (red arrow) on the  $\text{Li}_2\text{MnO}_3 \cdot \text{LiMn}_{0.5}\text{Ni}_{0.5}\text{O}_2$  -  $\text{LiMn}_{1.5}\text{Ni}_{0.5}\text{O}_4$  tie line that produced the best electrode performance.

The rate capability of various  $\text{Li}_x\text{Ni}_{0.25}\text{Mn}_{0.75}\text{O}_y$  electrodes was determined as a function of  $x$  (the extent of layered or spinel character). Figure IV - 60 shows for the range  $1.2 \leq x \leq 1.5$ , a maximum in the rate capability was obtained for  $x=1.2$ , indicating a benefit of using a three-component electrode. Using lower values of  $x$ , i.e., a

higher spinel concentration compromised the capacity of the cell because the capacity of the spinel component, delivered at high potentials ( $\sim 4.7$  V), was not accessed during cell operation (4.6 to 2.0 V).

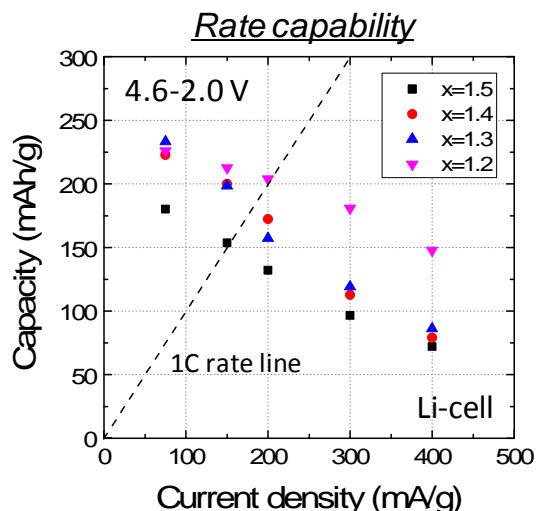


Figure IV - 60: Rate capability of 'layered-layered-spinel' electrodes,  $\text{Li}_x\text{Ni}_{0.25}\text{Mn}_{0.75}\text{O}_y$ , for  $1.2 \leq x \leq 1.5$ ;  $2.0 \leq y \leq 2.5$ .

### Limitations of Layered-Layered Electrodes.

#### Voltage Decay

It is well known that 'layered-layered'  $x\text{Li}_2\text{MnO}_3 \cdot (1-x)\text{LiMO}_2$  electrodes suffer from a voltage decay phenomenon on cycling that compromises the energy and energy efficiency of the cell. This phenomenon was therefore studied by means of  $dQ/dV$  plots in cells containing 'layered-layered-spinel' cathodes to determine if the presence of a spinel component might arrest the voltage decay. The  $dQ/dV$  plots of 4 cells with various  $\text{Li}_x\text{Ni}_{0.25}\text{Mn}_{0.75}\text{O}_y$  electrodes are shown in Figure IV - 61.

The  $dQ/dV$  plot of a lithium cell with a spinel-free cathode composition  $\text{Li}_{1.5}\text{Ni}_{0.25}\text{Mn}_{0.75}\text{O}_y$  (i.e.,  $0.5\text{Li}_2\text{MnO}_3 \cdot 0.5\text{LiMn}_{0.5}\text{Ni}_{0.5}\text{O}_2$ ), shows a significant shift to lower potentials on successive cycles (dotted box regions), which corresponds to the continuous voltage decay of these cells. By contrast, with decreasing Li content (or increasing spinel content), smaller shifts in the  $dQ/dV$  plots are observed, indicating that the spinel component appears to enhance the structural stability of the 'layered-layered' component to electrochemical cycling.

#### Manganese Dissolution

The electrochemical cycling data, obtained at  $55^\circ\text{C}$ , of a standard Argonne 'layered-layered' electrode with composition  $0.5\text{Li}_2\text{MnO}_3 \cdot 0.5\text{LiMn}_{0.31}\text{Co}_{0.25}\text{Ni}_{0.44}\text{O}_2$ , (ANL-NMC) in a lithium half-cell (blue) and a full Li-ion cell with a MCMB graphite anode (red), are shown in Figure IV - 62. The significant capacity loss of the Li-ion cell is

reminiscent of the behavior of Li-ion cells with spinel ( $\text{LiMn}_2\text{O}_4$ ) cathodes that results from the solubility of manganese from the spinel cathode and consequent poisoning of the graphitic anode.

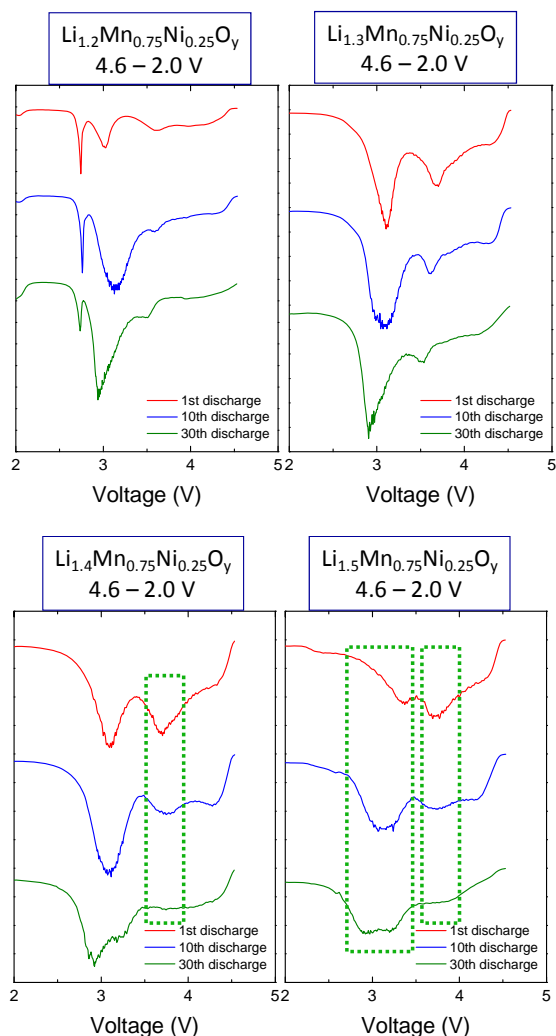


Figure IV - 61: Differential capacity plots of lithium cells with  $\text{Li}_x\text{Ni}_{0.25}\text{Mn}_{0.75}\text{O}_y$  electrodes ( $0.5 \leq x \leq 1.5$ ;  $2.0 \leq y \leq 2.5$ ). Top left,  $x=1.2$ ; Top right,  $x=1.3$ ; Bottom left,  $x=1.4$ ; Bottom right,  $x=1.5$ .

Cycled cells were disassembled after cycling, and solubility tests on the transition metal conducted, the results of which are provided in Table IV - 5. It is clear from this Table that lithium- and manganese-rich ‘layered-layered’ electrodes appear to suffer from the same solubility problems as manganese-rich spinel electrodes. It is well known that blended electrodes and surface coatings help to reduce solubility effects. Studies, using these approaches were therefore initiated in this project.

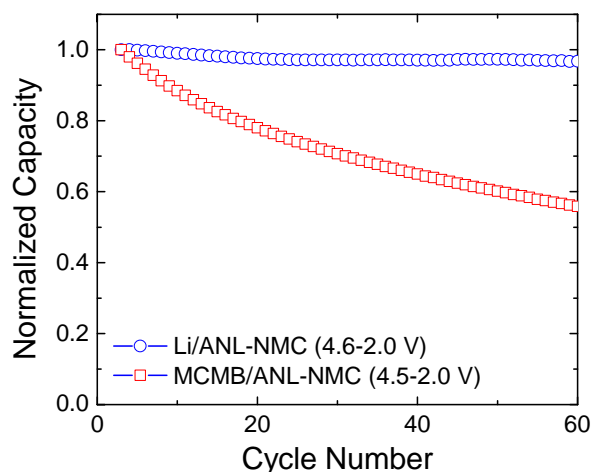


Figure IV - 62: Cycling data of a ‘layered-layered’ electrode  $0.5\text{Li}_2\text{MnO}_3 \cdot 0.5\text{LiMn}_{0.31}\text{Co}_{0.25}\text{Ni}_{0.44}\text{O}_2$  in a half-cell (blue) and in a full Li-ion cell (MCMB graphite anode) (red).

Table IV - 5: Concentration of transition metal ions after cycling at  $55^\circ\text{C}$  ( $\mu\text{g}$  metal detected on MCMB surface /g cathode)

Mn	Co	Ni
804	65	241

#### Pulse Power

As stated above, it has been established previously by the lithium battery community that the performance of a manganese-rich spinel electrode can be improved by blending it with other metal oxide or phosphate components. A study was therefore conducted to evaluate whether similar beneficial effects could be obtained for blended ‘layered-layered’ electrodes. A blended electrode, consisting of Argonne’s standard ‘layered-layered’ ANL-NMC material and an industrial  $\text{LiFePO}_4$  product, was selected for this purpose.

Cycling data of lithium half cells with standard ‘layered-layered’ ANL-NMC and  $\text{LiFePO}_4$  electrodes, and with a blended ANL-NMC/ $\text{LiFePO}_4$  electrode are shown in Figure IV - 63. All cells showed stable cycling behavior, the cell with the blended electrode showing slightly lower capacity than the standard  $0.5\text{Li}_2\text{MnO}_3 \cdot 0.5\text{LiMn}_{0.31}\text{Co}_{0.25}\text{Ni}_{0.44}\text{O}_2$  electrode, as expected (Fig. 5, top). Rate studies indicated that the blended electrode showed superior performance at higher rates, typically greater than  $200 \text{ mA/g}$  (Fig. 5, bottom). These studies are still in progress.

#### Conclusions and Future Directions

- The performance limitations of layered-layered  $x\text{Li}_2\text{MnO}_3 \cdot (1-x)\text{LiMO}_2$  electrodes ( $M=\text{Mn}, \text{Ni}, \text{Co}$ ), such as voltage decay, Mn dissolution and power capability have been studied.

- Progress was made in identifying and developing ‘layered-layered-spinel’ composite electrode structures that showed slightly enhanced stability to electrochemical cycling than conventional ‘layered-layered’ systems; the results are consistent with data emanating from the BATT program that demonstrate that ‘layered-layered’ composite electrodes transform, at least in localized regions, to spinel-like configurations that appear to enhance the cycling stability of the electrode if the transition to spinel is controlled. Three component ‘layered-layered-spinel’ electrodes therefore hold considerable promise for further improvement and development. The exploitation and optimization of these three-component composite electrodes will remain be a major focus of the R&D project in FY2012.

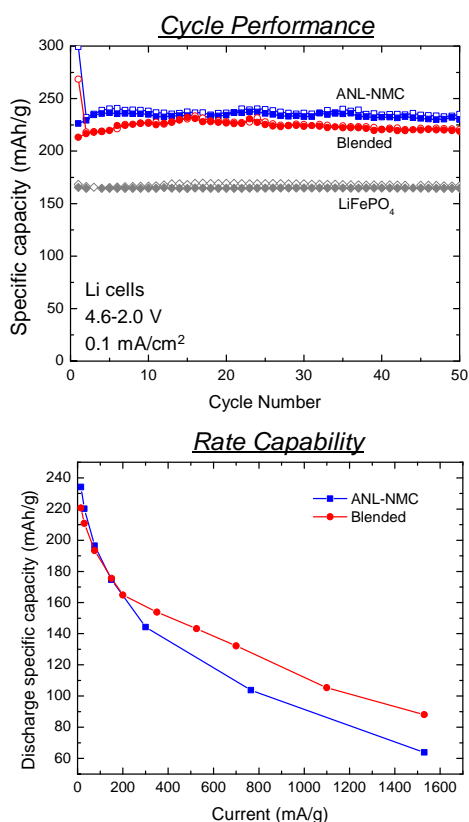


Figure IV - 63: Top: Cycling data of lithium half cells with layered-layered NMC-ANL, LiFePO<sub>4</sub> and blended cathodes. Bottom: Rate capability of lithium cells containing a ‘layered-layered’ ANL-NMC cathode, with and without a LiFePO<sub>4</sub> component.

- The rate capability of the electrode was enhanced by the incorporation a high power, LiFePO<sub>4</sub> component. The initial results auger well for further improvement and, accordingly, will receive further attention in FY2012.
- Manganese dissolution remains a problem for these high capacity electrodes, which likely also affects the

rate capability of the electrode. Efforts will be made in FY2012 to examine the effects of surface coatings in an attempt to lower these damaging effects.

- Strong collaborations with materials manufacturers and the lithium battery industry have been established at Argonne over the past several years. These contacts will be exploited to aid the future development of high capacity, integrated electrode structures, which are currently receiving prominent attention by the battery community worldwide.

## FY 2011 Publications/Patents/Presentations

### Publications

- K. G. Gallagher and S.-H. Kang, *xLi<sub>2</sub>MnO<sub>3</sub>•(1-x)LiMO<sub>2</sub> Blended with LiFePO<sub>4</sub> to Achieve High Energy Density and Pulse Power Capability*, J. Power Sources **196**, 9702-9707 (2011).

### Patents

No patents were filed.

### Presentations

- D. Kim, K. G. Gallagher, and S.-H. Kang, *Synthesis and Electrochemistry of Li<sub>x</sub>(Ni<sub>0.25-y</sub>Co<sub>2y</sub>Mn<sub>0.75-y</sub>)O<sub>2</sub> Electrode Materials with an Integrated ‘Layered-Spinel’ Structure*, 218th Electrochemical Society Meeting, Las Vegas, USA, 10-15 October, 2010.
- K. G. Gallagher, D. Kim and S.-H. Kang, *Capacity and Power Fade of Graphite/xLi<sub>2</sub>MnO<sub>3</sub>•(1-x)LiMO<sub>2</sub> (M=Ni, Co, Mn) Li-ion Cells*, 218<sup>th</sup> Electrochem. Soc. Meeting, Las Vegas, 10-15 October, 2010.
- S.-H. Kang, *Development of High-Capacity, Cathode Materials with Integrated Structures*, Presentation at the Annual Merit Review Meeting, DOE Vehicle Technologies Program, Washington DC, 9-13 May, 2011.
- D. Kim, S.-H. Kang, C. S. Johnson, M. M. Thackeray, *Synthesis and Electrochemical Characterization of Integrated Composite Electrodes for Lithium and Sodium Energy Storage*, Post-doctoral Seminar, Argonne National Laboratory, USA, 12 September 2011.

## IV.B.3.6 Cathode Processing Comparison Study (ANL)

Ilias Belharouak

Argonne National Laboratory  
9700 South Cass Avenue  
Argonne, IL 60439-4837  
Phone: (630) 252-4450; Fax: (630) 972-4544  
E-mail: [belharouak@anl.gov](mailto:belharouak@anl.gov)

Collaborators:

Gary Koenig, Dapeng Wang, Huiming Wu, Khalil Amine, Greg Krumdick, Argonne National Laboratory  
Rich Axelbaum, Washington University in Saint Louis

Start Date: January, 2011

Projected End Date: September, 2014

### Objectives

- The objective of this work is to develop a better correlation between the electrochemical properties of a high capacity NMC material and its structural, morphological, and physical properties:
- Develop a comparative study at the level of the NMC precursors.
- Compare the electrochemical performance of NMC type cathodes made through different synthetic routes.
- Assist the materials screening and cell fabrication efforts through the sampling of NMC cathodes.
- Assist the material scale up effort.

### Technical Barriers

The primary technical barrier is the development of a safe cost-effective PHEV battery with a 40 mile all electric range that meets or exceeds all performance goals.

- Develop cost effective synthetic methods for the scale up of transition metal precursors.
- Synthesize high capacity materials with high packing density, spherical morphology, and suitable porosity.
- Comprehend the inconsistencies and fluctuations of the electrochemical results in NMC type cathodes.

### Technical Targets

- Establish a comparative study at the NMC precursor using three synthetic routes: hydroxide, carbonate, and oxalate processes.

- Establish a comparative study at the level of the NCM materials and link the results to the precursors study.

### Accomplishments

- Prepared  $(\text{Ni}_x\text{Mn}_y\text{CO}_3)$  ( $x=0.2, 0.25, \text{ and } 0.3; x+y=1$ ) carbonate precursor using a continuous stirred tank reactor (CSTR) at the pilot scale level.
- Investigated the nucleation and growth of precursor particles during the CSTR process by monitoring particle size distributions, particle morphologies, chemical compositions, and structures with time.
- Investigated the electrochemical performance of the final lithiated cathode materials.
- Initiated the hydroxide co-precipitation process
- Transferred the carbonate process technology for the purpose of materials scale up.



### Introduction

Composite lithium- and manganese-rich  $\text{Li}_{1+x}\text{M}_{1-x}\text{O}_2$  compounds ( $M = \text{Mn, Ni, Co}$ ) have become attractive cathode materials because of their high capacity ( $>200$  mAh/g) and enhanced structural stability. The electrochemical performance of these materials strongly depends upon the physical properties of the precursor materials that serve as sources for lithiation. In current Li-ion battery materials, hydroxide co-precipitation is largely used to produce transition metal hydroxide precursors. Carbonate co-precipitation has also emerged as an alternative method to produce transition metal (Mn, Ni, Co) precursors. The main advantage is that in the carbonate matrix, the oxidation state of the cations is kept as  $2+$  for all transition metals. Also, the experimental conditions under which carbonates are usually made are less harsh than those of the hydroxide process, namely, the pH value is usually close to 8. Co-precipitation in the continuous stirred tank reactor (CSTR) is used here for the synthesis of small quantities of carbonate precursors due to its advantages such as homogeneous composition, narrow particle size distribution, high tap density, and facile scale-up to a few hundreds of grams collected over a short time. The present research gives insights into the nucleation and growth mechanism of carbonate precursors prepared by the CSTR co-precipitation process. Our goal was to determine the CSTR experimental conditions that influence the chemical homogeneity, morphology, and physical properties of carbonate precursors (and, subsequently, the

electrochemical characteristics of the final materials) during production.

## Approach

Three synthetic routes, hydroxide, carbonate, and oxalate processes, will be developed to prepare the precursors that will serve to produce high capacity cathode materials  $\text{Li}_{1+t}(\text{Ni}_x\text{Co}_y\text{Mn}_z)_{1-t}\text{O}_2$  ( $t>0$ ,  $x+y+z=1$ ). A comparative study using the three routes will be made using materials morphology, physical characteristics, and electrochemical properties. Blending between materials made through the carbonate or hydroxide precursors and the same compositions made through the oxalate will be done to get the most use of the high packing density for

high energy density and high porosity for high rate capability.

## Results

Nickel sulfate, manganese sulfate, sodium carbonate, and ammonium hydroxide were used as the starting materials to prepare  $\text{Ni}_{0.3}\text{Mn}_{0.7}\text{CO}_3$  precursor. A schematic of the water-jacketed CSTR (4L capacity reactor) system is shown in Figure IV - 64. Product overflow was periodically collected during the experiment, and the particle size distribution was measured with a particle size analyzer. The precursor material, which was used to prepare the cathode materials, was collected from hour 5 to hour 8 of the process.

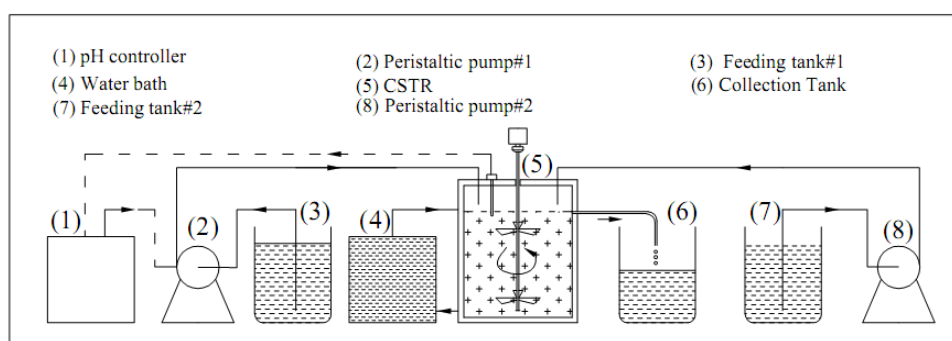


Figure IV - 64: Schematic drawing of CSTR system used for this experiment

Figure IV - 65 shows the particle size distribution of particles collected during the 8 hours of CSTR co-precipitation. At the very beginning, the particle distribution was unexpectedly broad, with particle sizes ranging from 1 to 80  $\mu\text{m}$ . We speculated the large particles were formed by agglomeration of very small seeds which is likely due to the electrostatic force or surface tension between the seed particles. As time elapses, the particle

size distribution narrowed slightly, and the distribution maximum shifted to a center around 20  $\mu\text{m}$ . In addition, a small peak appeared below 1  $\mu\text{m}$ , possibly due to the disintegration of the large agglomerates. After 15 min, the curve became a single distribution peak, with the maximum increasing to 8  $\mu\text{m}$  (35 min), 14  $\mu\text{m}$  (100 min), 16  $\mu\text{m}$  (160 min), and up to 36  $\mu\text{m}$  at the end of the CSTR experiment.

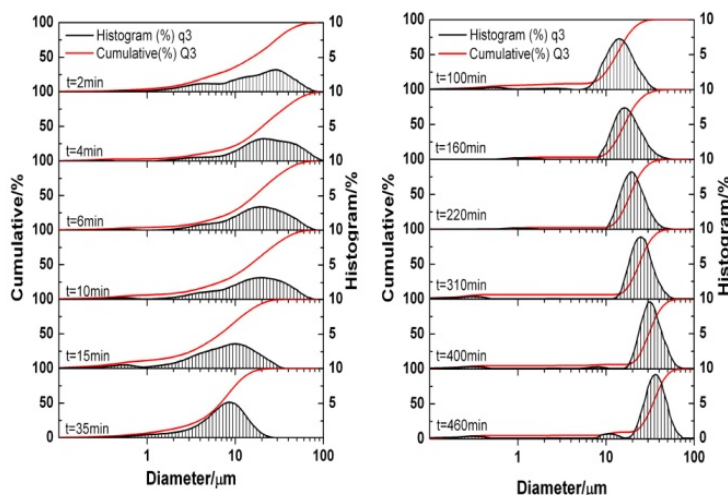


Figure IV - 65: Particle size distribution of samples collected at different reaction times.

Figure IV - 66 shows SEM images of the precursors collected during the CSTR experiment. The SEM images were chosen to reflect the trend of particle nucleation and growth during the co-precipitation process. During the first minutes (2 min) of the experiment, the precursor particles

were composed of large loose agglomerates with no defined shape.

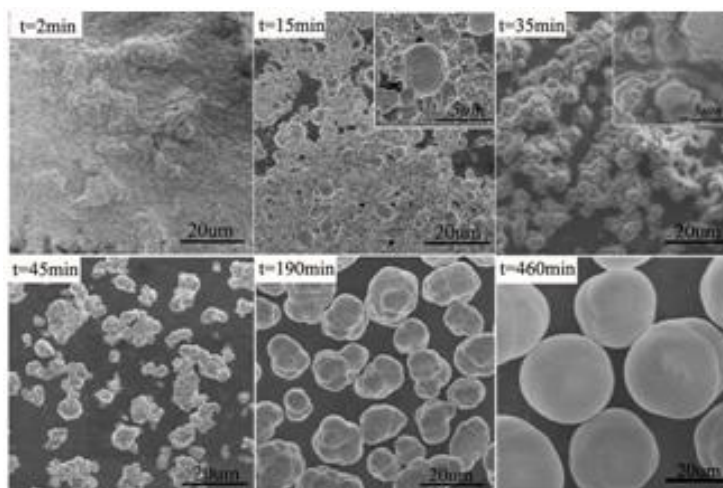


Figure IV - 66: SEM images of samples collected at different reaction times

Thereafter, some spherical agglomerates were formed with different sizes. After 35 min, more segregation was observed within the agglomerations, and particles continued to grow with a round shape. These SEM observations were in accordance with the particle size distribution results detailed in Figure IV - 65. The surface of the final collected particle was apparently smooth and dense; however, a surface analysis performed by the BET method showed that these particles had a large surface area of  $152 \text{ m}^2/\text{g}$  with an average pore size of 1.7 nm. Therefore, we concluded that these spherical precursor particles were actually secondary particles composed of nano-size primary particles of the same chemical composition.

Figure IV - 67 shows the evolution of the average particle size (D50) with time. During the first 35 min of the reaction, D50 decreased from 20 to 8  $\mu\text{m}$ . Thereafter, D50 increased almost linearly during the rest of the experiment. The calculated growth rate was 3.4  $\mu\text{m}$  per hour. During the collection time, the average size of the particles increased from 24  $\mu\text{m}$  (300 min) to 34  $\mu\text{m}$  (460 min). As a result, the individual particles grew in mass, even though the feeding rate was kept constant during the co-precipitation. The possible explanation is that some additional nucleation sites were available at the surface of the freshly formed particles for further growth.

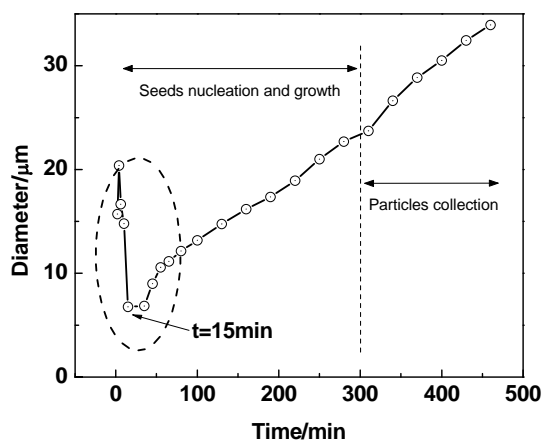


Figure IV - 67: Average particle size (D50) evolution as a function of time

Figure IV - 68 shows the compositions measured using EDXS obtained on particles collected during the co-precipitation reaction. Our qualitative analysis of the transition metals showed that the Mn/Ni atomic ratio fluctuated with time early in the process and then became more stable after 5 hours of reaction. The horizontal dotted line in Figure IV - 68 shows the nominal Mn/Ni atomic ratio expected under our experimental conditions. A huge deviation of the nominal and measured Mn/Ni atomic ratio was apparent at the beginning of the co-precipitation reaction. As time increased, the Mn/Ni atomic ratio increased and then approached the desired ratio after 5 hours of co-precipitation. For this reason, the precursor particles that were selected for the electrochemical study

were collected after 5 hours of co-precipitation. Quantitatively, ICP analysis was used to determine the chemical composition of the precursor collected after 5 hours. In this case, the Mn/Ni ratio was 2.37 which is very close to 7:3 nominal ratio.

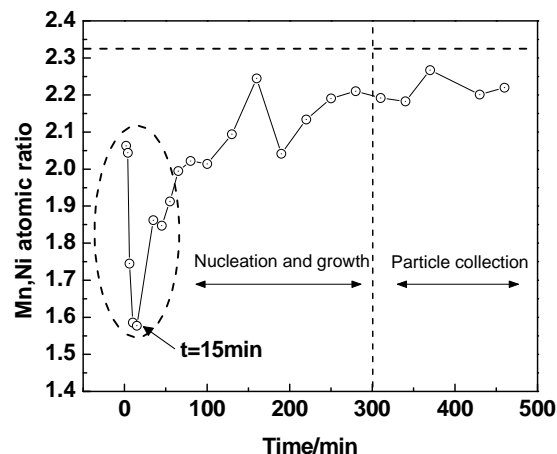


Figure IV - 68: EDXS of collected samples

X-ray diffraction provided further structure and phase information of the samples collected during the nucleation and growth processes (Figure IV - 69). It can be seen that the main component of the precipitates was carbonates; however, at an early stage, the small broad peak at  $2\theta = 11.6^\circ$  was consistent with the formation of nickel oxyhydroxide impurity. This peak became less important for the subsequent sample and finally disappeared after 15 min. At the beginning of the co-precipitation, NiOOH formed because it is thermodynamically much more stable than  $\text{NiCO}_3$  and also because the possibly localized high pH value within the reactor favors the formation of the hydroxide. At the early stage of the reaction a competition between the hydroxide and carbonate co-precipitation may have occurred because of the likelihood of fluctuations in pH and transition metal concentration inside the reactor. The peak signature of the observed nickel oxyhydroxide was very broad possibly due to the nano-character of the crystallites of the co-precipitated phase. Thereafter, as the solution became more homogeneous, the pH in the CSTR reactor stabilized, and therefore, the carbonate co-precipitation process dominated the reaction and gave rise to the production of spherical carbonate precursor particles. Since the particles formed before 5 hours were less homogeneous in chemical composition and morphology, they were not used as the precursor for the preparation of the cathode material.

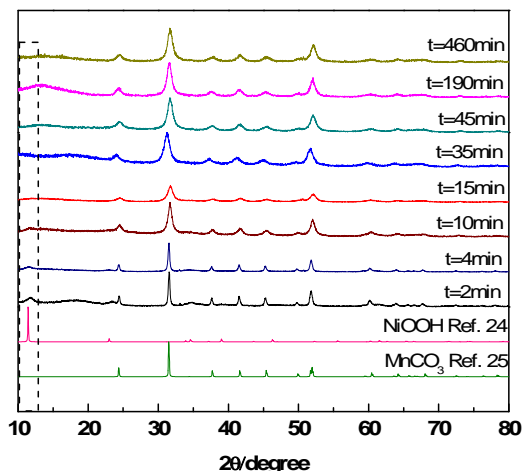


Figure IV - 69: X-ray diffraction patterns of samples from different collection times

The precursor particles, which were collected during hours 5-8 of the co-precipitation process and used to prepare the cathode material, had XRD patterns consistent with manganese carbonate, although the peaks were relatively broad, which is likely due to the small grain size of the precursor particles. After lithiation, the cathode material  $\text{Li}_{1.5}(\text{Ni}_{0.3}\text{Mn}_{0.7})\text{O}_{2+\gamma}$  had a surface area of only  $1 \text{ m}^2/\text{g}$  because during the high temperature calcination with lithium carbonate, the nano-primary particles fused to one another, resulting in larger primary particles without change in the morphology of the secondary particles (Figure IV - 70). The structure of  $\text{Li}_{1.5}(\text{Ni}_{0.3}\text{Mn}_{0.7})\text{O}_{2+\gamma}$  was primarily indexed based on the R-3m space group, which is the structure of the major layered component in similar materials, with the existence of a secondary component belonging to the  $\text{Li}_2\text{MnO}_3$ -like phase.

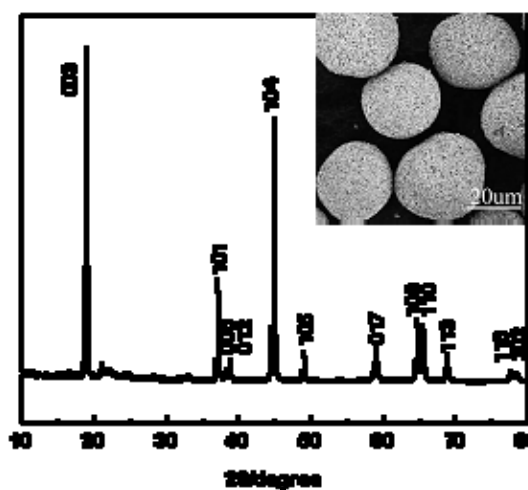


Figure IV - 70: X-ray diffraction patterns of  $\text{Li}_{1.5}(\text{Ni}_{0.3}\text{Mn}_{0.7})\text{O}_{2+\gamma}$ . Inset is SEM image.

Figure IV - 71 shows the cycling behavior of the  $\text{Li}_{1.5}(\text{Ni}_{0.3}\text{Mn}_{0.7})\text{O}_{2+\gamma}$  in a lithium cell at C/10 rate. As can be seen, starting from the second cycle, the discharge capacity of 200 mAh/g was retained for over 100 cycles. The large particles ( $\sim 30 \mu\text{m}$ ) possibly limited the lithium diffusion and led to electrochemically inactivated core. Further processing and optimization of the co-precipitation parameters to produce precursor particles less than  $20 \mu\text{m}$  can improve the capacity of the  $\text{Li}_{1.5}(\text{Ni}_{0.3}\text{Mn}_{0.7})\text{O}_{2+\gamma}$  material.

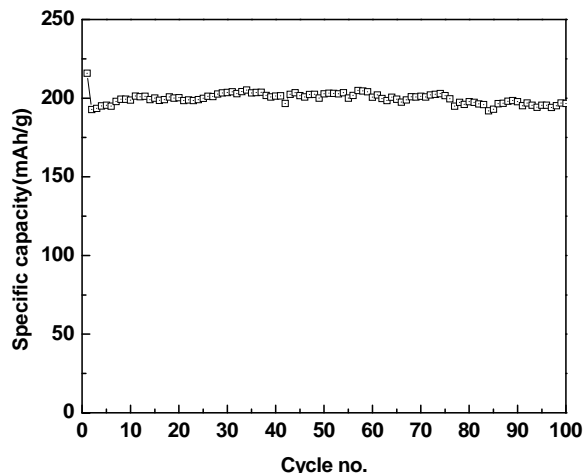


Figure IV - 71: Cycling performance of  $\text{Li}_{1.5}(\text{Ni}_{0.3}\text{Mn}_{0.7})\text{O}_{2+\gamma}$  between 2-4.6 V

## Conclusions and Future Directions

A CSTR was used to synthesize  $\text{Ni}_{0.3}\text{Mn}_{0.7}\text{CO}_3$ , and the nucleation and growth of the precursor particles were monitored as a function of time. The pH zone that favors carbonate co-precipitation reaction was calculated based on the thermodynamic equilibrium between the chemical species existing in the reaction medium. Particle size analysis combined with SEM, EDX, and XRD results confirmed that the nucleation and growth process began with the formation of a mixture composed of a carbonate-type dominating phase and a nickel oxyhydroxide-type impurity phase, which disappeared with time. The co-precipitation reaction started with the formation of seed particles having irregular shape and fluctuating chemical stoichiometry, and ended with the production of spherical, homogeneous particles of carbonate precursor with a chemical composition close to the nominal one. These precursor particles continued their growth during the 8 hours of CSTR reaction and reached a final average diameter of  $35 \mu\text{m}$ . This trend was also observed for different experimental conditions, indicating that the continued particle growth is typical for producing transition metal carbonates. Future work will focus on addressing this phenomenon so that the spherical precursor particles could be mass produced with smaller average size

(around  $15\text{-}20 \mu\text{m}$ ). These properties along with better chemical homogeneity would help in the acceptance of this carbonate co-precipitation process as an alternative route to the well-established hydroxide process by industries working in the production of precursors for cathode materials in lithium-ion batteries.

## FY 2011 Publications/Presentations

1. Growth mechanism of  $\text{Ni}_{0.3}\text{Mn}_{0.7}\text{CO}_3$  precursor for high capacity Li-ion battery cathodes. Dapeng Wang, Ilias Belharouak, Gary M. Koenig, Jr, Guangwen Zhou and Khalil Amine. *J. Mater. Chem.*, 2011, 21, 9290–9295

## IV.B.4 Applied Battery Research on Electrolytes

### IV.B.4.1 Novel Electrolytes and Electrolyte Additives for PHEV Applications

(ANL)

Daniel P. Abraham

Argonne National Laboratory  
9700 South Cass Avenue  
Argonne, IL 60439-4837  
Phone: (630) 252-4332; Fax: (630) 972-4406  
E-mail: [abraham@anl.gov](mailto:abraham@anl.gov)

Collaborators:

Gang Cheng, Argonne National Laboratory  
Brett Lucht, University of Rhode Island  
Alex Wei, Purdue University

Start Date: October, 2008

Projected End Date: September, 2012

#### Objectives

The performance, calendar-life, and safety characteristics of Li-ion cells are dictated by the nature and stability of the electrolyte and the electrode-electrolyte interfaces. Desirable characteristics for these electrolytes include stability in the 0 to 5V vs. Li range, excellent lithium ion conductivity, wide temperature stability range, non-reactivity with the other cell components, non-toxicity and low cost. Our goal is to develop novel electrolytes and electrolyte additives to meet the cost, calendar life and safety requirements of batteries for PHEV applications.

#### Technical Barriers

This project addresses the following technical barriers to the development of a PHEV battery with a 40 mile all electric range that meets or exceeds all performance goals.

- Cell Performance
- Cell Calendar and Cycle Life
- Cell Safety/Abuse Tolerance

#### Technical Targets

- Develop novel electrolytes with electrochemical stability in the 0 to 5V vs. Li voltage range.
- Develop additives to conventional electrolytes that improve cell shelf and cycle life by 50%. Cell

performance and thermal abuse characteristics should stay the same or be enhanced by these additives.

#### Accomplishments

- Identified new family of heteroaromatic substituted carboxylic ester-based compounds as electrolyte additives
  - Determined effects on cell performance and calendar life
  - Argonne filed a USA Patent Application based on these compounds (ANL-376, Cheng, G.; Abraham, D.P., 2010, September 23)
  - Recommended list of electrolyte additive compounds for scale-up
- Investigating the relationship of additive structure to characteristics of surface films at both positive and negative electrodes
  - Currently examining the effect of SEI composition/morphology on interactions with Li-ion cell performance
- Designed and synthesized various GC-derivative compounds including alkyl ethers, carboxylic esters, and alkyl carbonates
  - Examined performance/cycling behavior of these compounds, both as co-solvents and as electrolyte additives
  - Argonne filed a USA Patent Application (ANL-368, Serial No. 12/910,549) and is in the process of filing another non-provisional patent application (ANL-382, Argonne Invention No. ANL-10-093) based on data from these compounds.

✧ ✧ ✧ ✧ ✧

#### Introduction

Recent advances in cathode and anode materials have refocused attention on electrolytes as the technological bottleneck limiting the operation and performance of lithium-battery systems. Whereas, attributes such as cell potential and energy density are related to the intrinsic property of the positive and negative electrode materials,

cell power density, calendar-life and safety are dictated by the nature and stability of the electrolyte and the electrode-electrolyte interfaces. A wide electrochemical window, wide temperature stability range, non-reactivity with the other cell components, non-toxicity, low cost, and a lithium-ion transference number approaching unity are, in general, desirable characteristics for lithium battery electrolytes. In addition, the electrolyte should have excellent ionic conductivity to enable rapid ion transport between the electrodes, and be an electronic insulator to minimize self-discharge and prevent short-circuits within the cell. Research on electrolytes and on functional electrolyte additives to improve cell life, thermal abuse behavior and low-temperature (<math>0^{\circ}\text{C}</math>) performance of high-power lithium-ion cells is being conducted at ANL as part of DOE's ABR program. The research is intended to spur commercialization of lithium-ion batteries for a wide range of vehicle applications, including HEVs, PHEVs and EVs.

### Approach

Our approach is to (i) develop novel electrolytes that include glycerol carbonate (GC), and modifications thereof, (ii) examine electrolyte additives that can enhance cell life by protecting the electrode surfaces, (iii) investigate the use of ionic liquids, and mixtures of ionic

liquids and carbonate solvents, to enable high-safety batteries. GC can be a potential low-cost substitute for currently used lithium-battery solvents. Our approach is to dry/purify GC obtained from a commercial manufacturer and examine its performance in lithium-ion cells.

Furthermore, we've developed techniques to replace the H (in the OH) group of GC with other alkyl species to form methyl ethers, ethyl ethers, and oligoethylene oxide ethers that will be examined as potential solvents. The electrolyte additives to generate passivation films at the positive and negative electrode surfaces are being determined by theoretical (molecular orbital) calculations on the electrolyte component to examine oxidation and reduction voltages. Some of the ionic liquids under consideration are ones reported to show promise in the lithium-battery literature.

### Results

The methyl ester derivative of GC was synthesized as shown in Figure IV - 72. The methyl carbonate derivative of GC (aka GCMC) was synthesized as shown in Figure IV - 73; the compound was provided by Dr. Kang Xu, ARL.

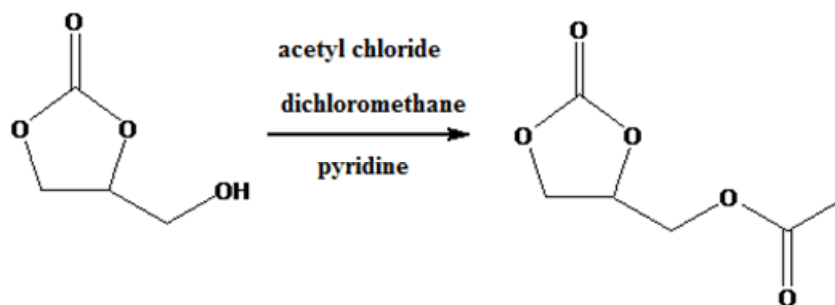


Figure IV - 72: Synthesis of the methyl ester derivative of GC

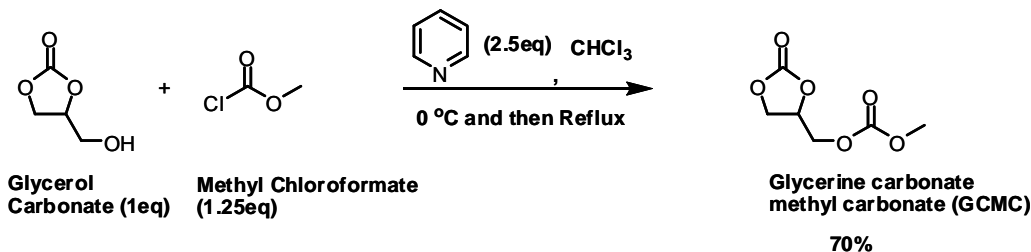


Figure IV - 73: Synthesis of the GCMC compound

Figure IV - 74 shows cycling and AC impedance data from NCA//Graphite cells comparing the effects of 5wt% GCMC additive in the baseline electrolyte. It is evident that GCMC addition can improve cycling performance of Gen2 electrolyte; 5wt% addition of GCMC to Gen2

electrolyte provides better capacity retention (98%) than that of 2wt% addition (94%). EIS data reveal that the impedance of coin cells containing 5wt% GCMC additive is almost identical to that of the Gen2 electrolyte.

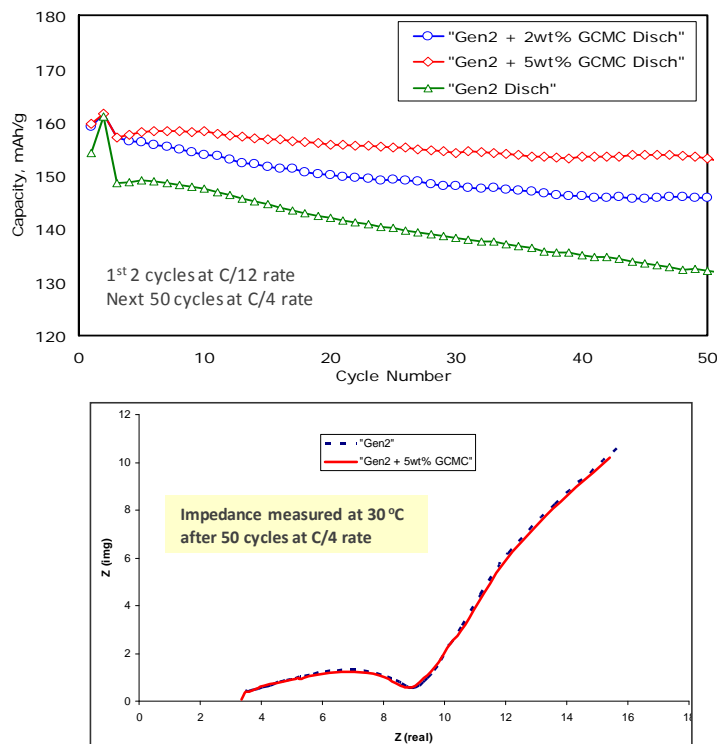


Figure IV - 74: Cycling and EIS data from NCA/Graphite cells comparing the effects of 5wt% GCMC additive in the baseline electrolyte.

Figure IV - 75 shows cycling data from NCA/Graphite coin cells containing 1.2M LiPF<sub>6</sub> in GCMC:EMC=1:6 (by wt%). The data indicate that cells with the GCMC-based

electrolyte showed improved capacity retention compared to cells with the Gen2 electrolyte.

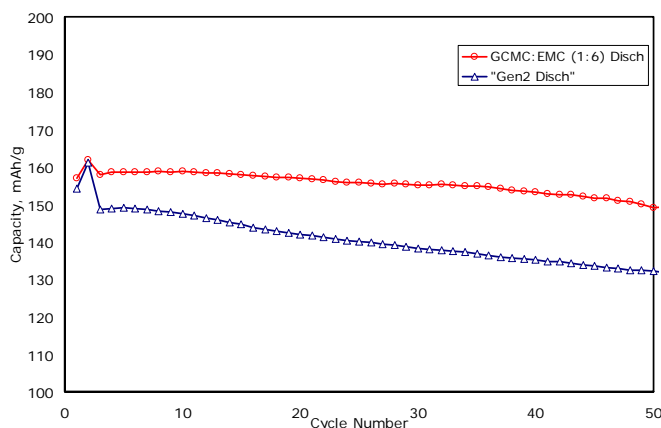


Figure IV - 75: Cycling data from NCA/Graphite coin cells containing 1.2M LiPF<sub>6</sub> in GCMC:EMC=1:6 (by wt%).

We successfully prepared several derivatives of GC, including methyl ester, alkyl ethers etc. We demonstrated that both the oxide-positive and graphite-negative electrodes can be cycled in methyl ester derivative of GC. We also identified the next generation of GC derivatives that show promise either as electrolyte solvents or as additives, and established collaboration with Prof.

Alexander Wei at Purdue University, to synthesize these compounds.

Furthermore, we discovered a new family of heteroaromatics substituted carboxylic ester-based compounds that have been identified as electrolyte additives. (see examples in Figure IV - 76).

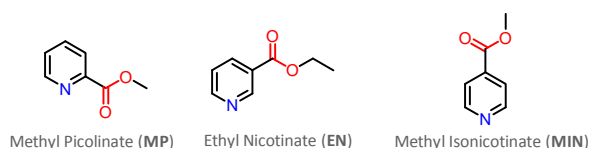


Figure IV - 76: Substituted carboxylic ester-based compounds that have been identified as electrolyte additives.

Our experiments showed that even small amounts of these additives can significantly improve capacity retention without causing impedance rise, a common problem associated with many electrolyte additives (Figure IV - 77). Small amounts (0.3 wt%) of MP, EN and MIN addition to baseline electrolyte improve capacity retention. MIN appears to be the best performer based on initial capacity loss. It is evident that small structural changes cause significant impact on initial cycling behavior – further studies are planned to obtain information on the effect of molecular structure on SEI characteristics. Note that the additives do not significantly alter cell impedance. The graphite SEI generated by MP may have the strongest interaction with the Li-ion, which may explain why the compound displays the widest mid-frequency arc.

Some examples of N-containing heteroaromatic-substituted carboxylic esters are shown below.

The effect of the compounds in Figure IV - 78, as additives to the baseline electrolyte, is shown in Figure IV - 79. Small amounts (0.3 wt%) of 3,4-DEPC, 2,3-PzDCA, 3,4-PyDCA, 2-MPzC and MMPC addition to Gen2 electrolyte improves capacity retention. 3,4-PyDCA seems to be the best candidate in the group in terms of minimal initial capacity loss. Surprisingly, the cell with 0.3wt% 2,3-PyDCA showed an abnormal first cycle and died during the second cycle; this effect was reproducible and was observed in three different cells. It is evident that small structural changes cause significant impact on initial cycling behavior. The SEI generated by the various additives is expected to bear signatures of the corresponding lithium-additive complexes. Stronger

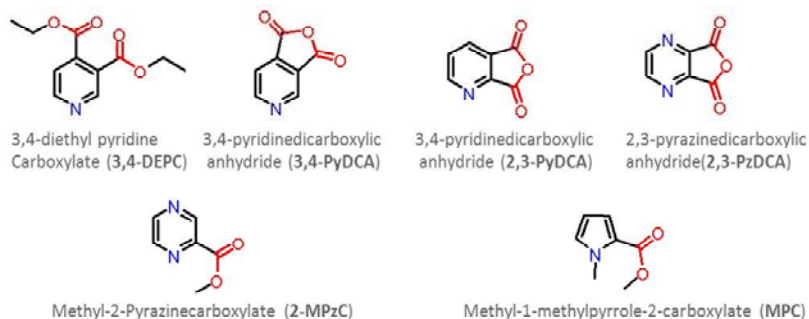


Figure IV - 78: Nitrogen -containing heteroaromatic-substituted carboxylic esters

SEI/Li<sup>+</sup> interaction may cause higher impedance. The “initial induction period” reflects changes in SEI characteristics during cycling.

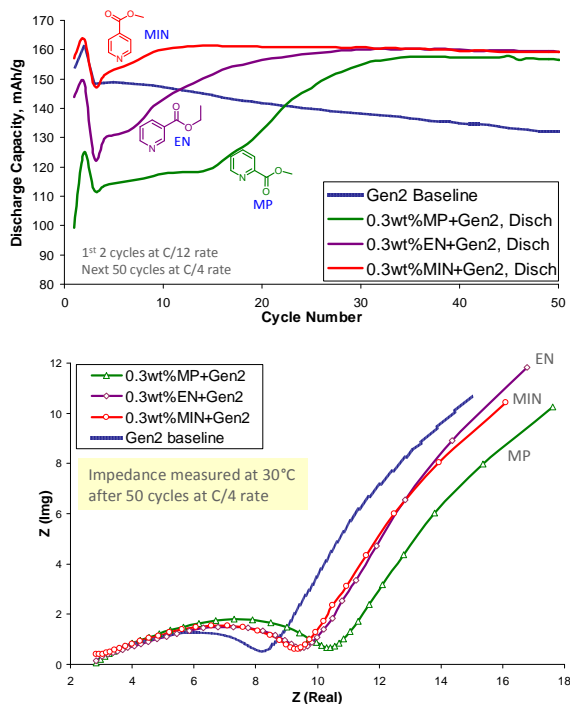


Figure IV - 77: Cycling and EIS data from NCA//Graphite cells comparing the effects of various additives with that of the baseline electrolyte.

## Conclusions and Future Directions

We have identified a new family of heteroaromatics-substituted carboxylic ester-based electrolyte additives/co-solvents. Small additions (~0.3 wt%) of these compounds, which include methyl picolinate (MP), methyl isonicotinate (MIN), 3,4-diethyl pyridinecarboxylate (3,4-DEPC), 2,3-pyrazinedicarboxylic anhydride (2,3-PzDCA), etc. to the baseline electrolyte (1.2M LiPF<sub>6</sub> in 3EC:7EMC) improves capacity retention of NCA(+)//graphite(-) cells.

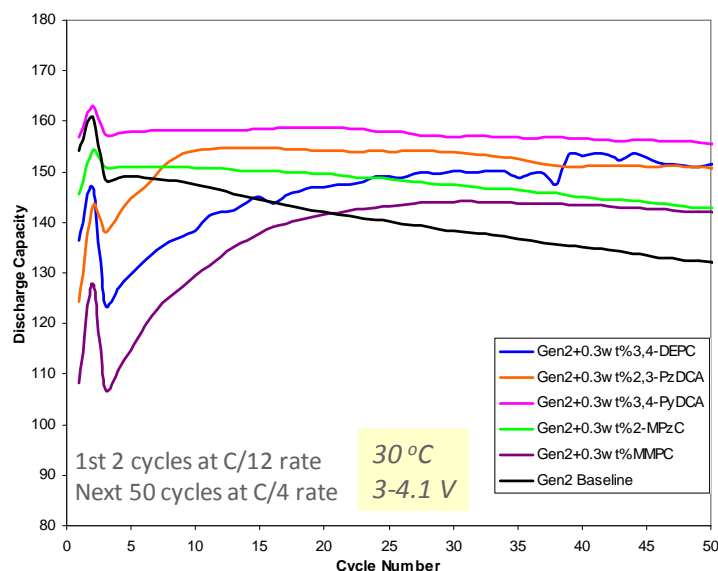


Figure IV - 79: Cycling data from NCA//Graphite cells with and without the electrolyte additives shown in Figure IV - 78.

We have conducted extensive investigations on compounds derived from GC. Our data show that cells with 5wt% GCMC (Glycerol Carbonate Methyl Carbonate) as an additive to the baseline electrolyte exhibit improved long-term cycling performance. Note that GCMC can be used as a replacement for Ethylene Carbonate (EC) in the electrolyte. Alkyl ether derivatives of GC have also been evaluated as electrolyte solvents or co-solvents. Noted that the secondary functional group on the molecules has a significant effect on electrochemical performance.

We will continue exploring novel electrolyte additives based on our approach: screening, testing, analyzing and optimizing. Our next experiments will be on electrodes identified for the next set of ABR PHEV cells. These experiments will include electrolyte stability studies at voltages >4.5V using high-energy NMC layered electrodes, and electrolyte stability studies at voltages >4.8V using  $\text{LiNi}_{1/2}\text{Mn}_{3/2}\text{O}_4$  spinel electrodes. We also plan to conduct surface characterization of formed and cycled electrodes to (i) understand composition/constitution of “stable” electrode passivation layers; (ii) determine oxidation/reduction pathways that lead to “stable” passivation layers; and (iii) optimize and design better candidates to meet cost, calendar life and safety requirements of batteries for PHEV applications. We also plan to continue investigations of GC derivatives, such as systematically changing functional group on GC to effect changes in electrochemical behavior. Charting the structure – activity relationships will yield the mechanistic understanding required to design better electrolyte systems

#### FY 2011 Publications/Presentations

1. 2011 DOE Annual Peer Review Meeting Presentation, May 9<sup>th</sup>-13<sup>th</sup> 2011, Washington DC.
2. “Heteroaromatics-Based Electrolytes for Lithium and Lithium-Ion Batteries” USA Patent Application, ANL-376, Cheng, G.; Abraham, D.P., inventors; 2010, September 23.
3. “Advanced Electrolyte for Lithium and Lithium-Ion Batteries” Argonne National Laboratory Invention Report ANL-10-093, Cheng, G.; Abraham, D.P., inventors; 2010, November 05.
4. Cheng, G.; Abraham, D.P.; “Advanced Electrolyte for Lithium and Lithium-ion Batteries”, Intellectual Property Decision Meeting of ANL-10-093, Argonne, IL, Jan 19th, 2011.

## IV.B.4.2 Develop Electrolyte Additives (ANL)

Zhengcheng Zhang

Argonne National Laboratory  
9700 South Cass Avenue  
Argonne, IL 60439-4837  
Phone: (630) 252-7868; Fax: (630) 972-4440  
E-mail: [zzhang@anl.gov](mailto:zzhang@anl.gov)

Collaborators:

Khalil Amine, Argonne National Laboratory  
Lu Zhang, Argonne National Laboratory  
Yan Qin, Argonne National Laboratory  
Zonghai Chen, Argonne National Laboratory  
Peng Du, Argonne National Laboratory

Start Date: FY09

Projected End Date: September, 2014

### Accomplishments

- A screening rule for SEI additives was established based on a literature survey and experimental results, which successfully led to several novel additives with improved cell performance.
- 3-Oxabicyclo[3.1.0]hexane-2,4-dione (OBD) was evaluated and studied as an SEI additive, and interphase characterization was conducted by various techniques; with optimal concentration of OBD, improved capacity retention can be achieved, and impedance increase can be controlled.
- Ethylene phosphate-based compounds have been proposed as novel SEI additives, and organic synthesis is ongoing with promising progress.



### Objectives

The objective of this work is to develop novel electrolyte additives that can improve the state-of-the-art lithium-ion battery electrolyte, especially with regard to cycle and calendar life, safety, and the electrochemical window, to meet the requirements of EV and PHEV applications.

### Technical Barriers

The general technical barrier is the development of novel functional electrolytes for lithium-ion batteries tailored to EV and PHEV applications that meet or exceed all performance goals. Specific barriers of electrolyte development include:

- Insufficient voltage stability,
- High flammability and low safety,
- Poor cycle and calendar life, and
- Surface reactivity with electrodes.

### Technical Targets

- Screening and evaluation of novel electrolyte additives to improve the cycle and calendar life of lithium-ion cells,
- Establishment of connections between chemical structures and cell performance, and
- Synthesis of novel solid-electrolyte interface (SEI) additives tailored to improvements of cell performance and safety.

### Introduction

The electrolyte is an indispensable component of lithium-ion batteries. Due to its physical position of being sandwiched between the cathode and anode, the electrolyte is in close interaction with both electrodes and thus significantly affects cell performance. When new electrode materials emerge, the need for compatible electrolytes usually arises. Conventional carbonate-based electrolytes have been used by the state-of-art lithium-ion battery industry; however, the flammability and anodic instability at high potential make it unsuitable for high-voltage cathodes. With numerous high-energy cathode materials emerging, the electrolyte must become more safe and stable without diminishing the cell electrochemical performance.

Among the efforts to develop novel electrolytes, utilization of additives is an efficient method to improve the cell performance and safety properties without significantly changing the electrolyte composition. Additives tend to work on the interphases, where most electrochemical reactions take place in the cell system. Whether or not these reactions proceed properly determines the cell performance and safety properties. By strengthening the SEI, major improvements could be achieved in terms of cycle life, calendar life, and safety. Development of novel additives tailored to prolonged cell cycle life and improved safety is one of the most important goals of lithium-ion battery research. In particular, additives that work on the interface between the anode and electrolyte are extremely important. During the formation process of lithium-ion cells, a thin passivation film, called

the SEI layer, forms on the anode surface, preventing further reactions of electrolyte. The SEI acts both as an ionic conductor and as an electronic insulator, and by creating this kinetic barrier, the whole cell system can be kept very stable even under the fully charged state when a lithiated carbonaceous anode reaches 0.1 V vs.  $\text{Li}^+/\text{Li}$ . For full cells utilizing carbon anodes, the formation process is potential dependent and stepwise, and is determined by the reactive components of the electrolyte that participate in the formation reactions. Therefore, the SEI layer can be tuned to yield better cell performance through the use of advanced additives.

## Approach

The approach for development of novel electrolytes and additives consists of three phases. The first phase is the screening of commercially available compounds by use of density functional theory (DFT) and quick test procedures. DFT calculation can assess whether the candidates have appropriate potential ranges (usually  $> 0.8$  V vs.  $\text{Li}^+/\text{Li}$ ), which is one important criterion of SEI additives. Due to a lack of understanding regarding the connections between chemical structures and cell performance, the screening process is based on trial and error. Empirical knowledge combined with such understanding can be used to generate screening candidates for quick evaluation. In this phase, some candidates will stand out with superior features. In the second phase, the promising candidates undergo thorough study and mechanism analysis to gain insights into their superior performance. Various techniques, including electrochemical analysis, spectroscopy, and computation and simulation, are utilized to gather as much information as possible about the connections between the chemical

structures and the cell performance. In this phase, better understanding should be obtained in terms of how the chemical compounds work in the cell system. In the third phase, based on the knowledge gained, promising electrolytes and additives are proposed, and organic synthesis is conducted to make these compounds. Evaluations of the novel compounds gives feedback regarding our electrolyte designs, thus leading to modifications and even more new designs.

## Results

**Screening rule for SEI additives.** We developed a general screening rule solely based on chemical structures, as shown in Figure IV - 80. Some representative examples of good SEI additives have been reported in the literature, including vinylene carbonate (VC), vinyl ethylene carbonate (VEC), 3,9-divinyl-2,4,8,10-tetraoxaspiro[5,5]undecane (TOS), lithium bis(oxalato)borate (LiBOB), and lithium difluoro(oxalato)borate (LiDFOB). These additives share one common feature—they are all unsaturated compounds. As the degree of unsaturation (DU) increases, there is a better chance for an additive to provide improvements to the lithium-ion cell system by forming a sturdy SEI layer. Increased DU usually means that more functional groups, such as cyclic and double bond structures, are available in the additive, and these functional groups can be readily activated during the SEI formation process and form into a more crosslinked or a stronger polymer SEI layer. By using this simple rule, we generated and evaluated a list of more than 30 compounds, which resulted in identification of several promising new SEI additives.

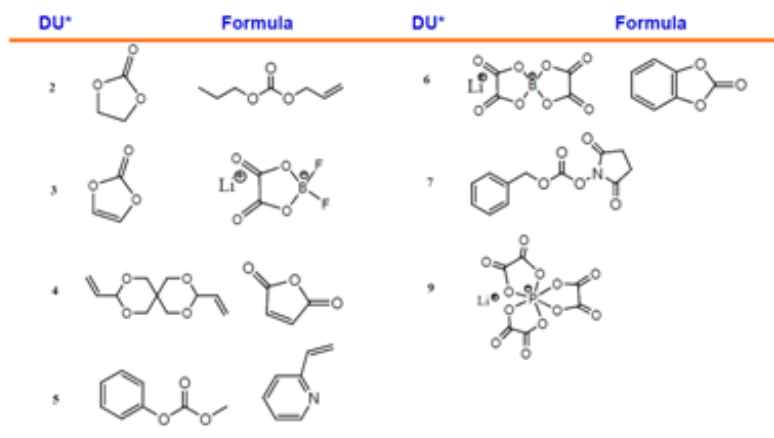


Figure IV - 80: Degree of unsaturation (DU) of representative SEI additives.

**Novel SEI Additive: 3-Oxabicyclo[3.1.0]hexane-2,4-dione (OBD).** OBD was evaluated as a novel SEI additive with attractive features, such as improved cycle life and controlled impedance increase when tested in

cells. The OBD was selected on the basis of our screening rule and quick test results, and serves as an example of our screening strategy. The structure of OBD is composed of two cyclic structures and two double bonds, yielding  $\text{DU} =$

4, double the DU of ethylene carbonate (EC). The high DU for OBD indicates its promise as an SEI additive.

As shown in Figure IV - 81, MCMB/Li<sub>1.1</sub>(Mn<sub>1/3</sub>Ni<sub>1/3</sub>Co<sub>1/3</sub>)<sub>0.9</sub>O<sub>2</sub> cells containing none or various amounts of OBD were tested in terms of capacity retention. Clearly, addition of OBD to the cell system produced a dramatic change in cell performance. With 0.1 wt% OBD, the capacity retention was improved from 60% to 72% after 200 cycles, and as the amount of OBD increased to 0.2 wt%, the capacity retention was further improved to 82%. However, when the amount of OBD was increased to 1.0 wt%, the capacity retention dropped to 50%, even lower than that of the cell with no additive. Therefore, in the case of OBD, an appropriate concentration of additive did improve the cell performance, but when the concentration was too high, it degraded the performance. The different effects derive from the SEI layers formed with OBD.

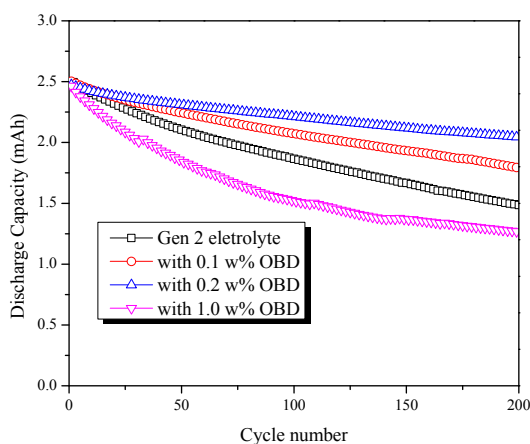


Figure IV - 81: Capacity retention profiles of MCMB/Li<sub>1.1</sub>(Mn<sub>1/3</sub>Ni<sub>1/3</sub>Co<sub>1/3</sub>)<sub>0.9</sub>O<sub>2</sub> coin cells showing the impact of OBD additive on capacity retention. The cells were cycled at 55 °C, and cut-off voltages were 2.7 and 4.2 V.

The SEI formation process is irreversible and mainly occurs during the first cycle; therefore, the electrochemical reaction within the first cycle is of great importance to the SEI layer properties. Figure IV - 82 shows differential capacity profiles of coin cells tested with MCMB anodes, nickel cobalt manganese (NCM) cathodes, and Gen 2 electrolytes composed on 1.2 M LiPF<sub>6</sub> in EC/EMC (3:7 by weight) with none or various amounts of OBD. The initial charging process was performed at the C/10 rate (~0.2 mA). For the Gen 2 electrolyte with no additive, two major peaks were evident around 2.83 and 2.89 V, mainly assigned to the EC decomposing process. When OBD was added, the EC peaks were depressed, and a new peak appeared at around 2.25 V. For instance, at 0.1 wt%, the EC peak at the higher voltage was greatly decreased, and

the peak at the lower voltage was depressed even further. As the amount of OBD was increased to 0.2 wt%, the EC peak at higher voltage disappeared, and the lower peak was further depressed. However, the new peak at 2.25 V shifted to higher voltage, with no significant change in intensity. The shift was probably due to a potential shift in the electrodes. Upon further OBD increase to 0.4 wt% and 1.0 wt%, both EC peaks were gone, and the peak at 2.25 V remained the same with no intensity increase. The profiles in Figure IV - 82 suggest that the concentration of additive did affect the SEI layer compositions. At 0.2 wt%, EC-derived species, reflected by the 2.8V peaks, were relatively depressed and co-located with the OBD decomposing product (2.2V peaks). When the amount of OBD was increased to 0.4 wt%, the OBD component became the predominant one and did not change with further increase of OBD.

Impedance control is another desirable feature for SEI additives. Adding SEI additive usually results in a thicker SEI layer, which means higher impedance during normal cycling. Only a few additives have been reported in the literature to benefit both cycle life and impedance. The impedance control derives from the polymerization process, which determines the morphology and composition of the SEI layer. OBD, however, was able to provide low impedance due to the low amount required to improve the cycle life. As shown in Figure IV - 83, with no more than 0.2 wt% OBD, the impedance increase was controlled both before and after 200 cycles at 55 °C.

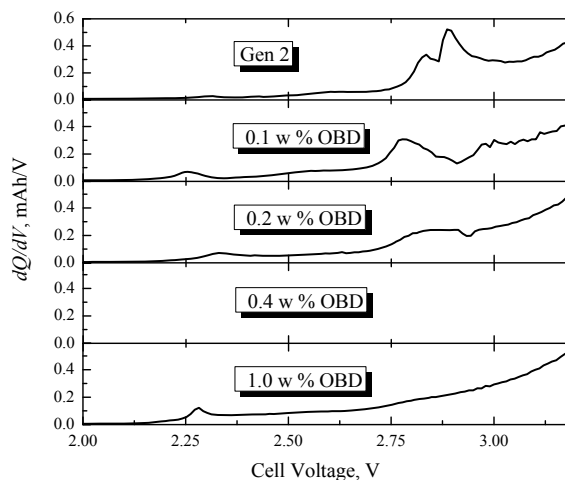


Figure IV - 82: Differential capacity profiles of MCMB/NCM cells in Gen 2 electrolyte with 0 to 1 wt% OBD. The cells were cycled at 55 °C. The charge rate was C/10 with cut-off voltage 3 ~ 4 V.

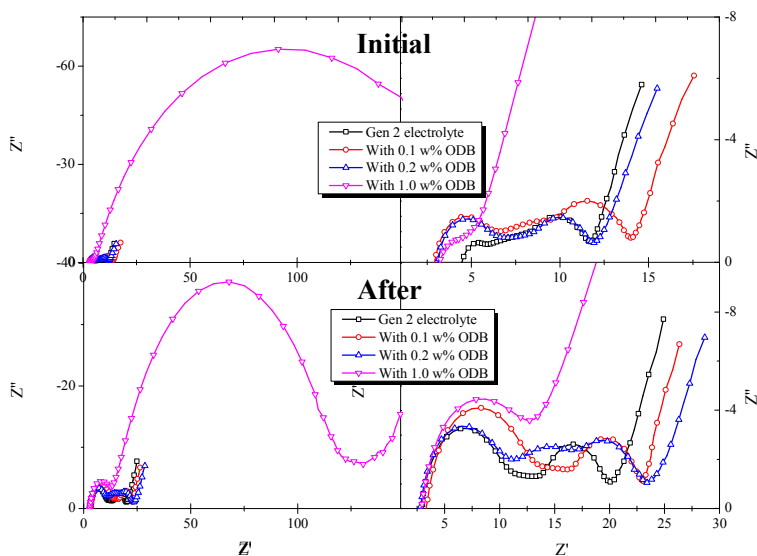


Figure IV - 83: Nyquist plots for MCMB/NCM cells containing different amounts of ODB in electrolyte of 1.2M LiPF<sub>6</sub> with ethylene carbonate/diethyl carbonate (3:7 weight ratio).

Fourier transform infrared (FTIR) spectroscopy was employed to further explore the mechanism of ODB as an SEI additive. MCMB/NCM coin cells with various amounts of ODB were charged with two formation cycles, and then the MCMB electrodes were taken out and studied through FTIR analysis. As shown in Figure IV - 84, very similar results were observed with and without ODB; however, subtle differences can be found, such as an additional peak at 1723 cm<sup>-1</sup> from the 1.0 wt% ODB sample, and a peak at 1150 cm<sup>-1</sup> for the 0.2 wt% ODB sample. The first peak may indicate an additional carboxylic group present in the SEI layer when a relative large amount of ODB is used. The later one was evidence of a different C-O stretching mode resulting from ODB in the SEI layer.

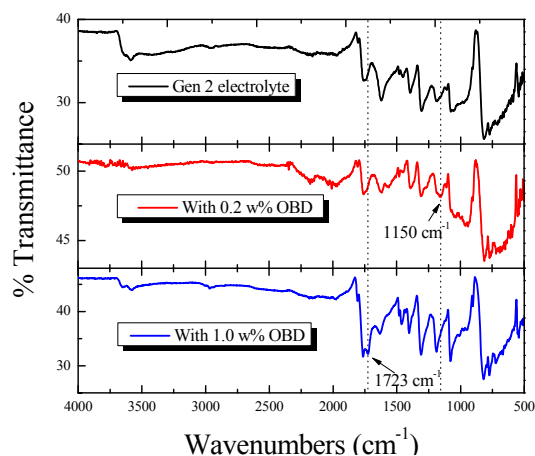


Figure IV - 84: FTIR spectra of MCMB electrodes obtained from MCMB/NCM coin cells containing different amounts of ODB in electrolyte of 1.2M LiPF<sub>6</sub> with EC/DEC (3:7 weight ratio) after formation cycles.

**Ethylene phosphate-based compounds.** Based on our screening results, we identified novel compounds that have potential to be excellent SEI additives. One example presented here is ethylene phosphate-based compounds, shown in Figure IV - 85. As we discussed above, cyclic and double bond structures are very promising when determining good SEI candidates. Cyclic ethylene phosphate with a DU of 2 was chosen as the base to build novel SEI additives. In addition, phosphorus is known to be flame retardant, which brings an additional feature to SEI additives. Functional groups with higher DU, such as ester, ring, double bond structures, were also proposed in building novel additives, which could increase the activities and add extra benefits to the electrolyte system. Other groups include heteroatoms, such as silicon, and ether chain, allowing us to tune the SEI properties.

## Conclusions and Future Directions

We have established a screening rule based on the degree of unsaturation of chemical structures. This rule has proved to be useful for finding promising candidates to form a stable SEI layer.

Currently, ethylene methyl phosphate is being synthesized. Some difficulties in separation and purification were met and are being addressed. Figure IV - 86 is the nuclear magnetic resonance (NMR) spectrum for this compound. A small amount of impurities were observed. Further effort is needed to obtain a higher purity of this compound.

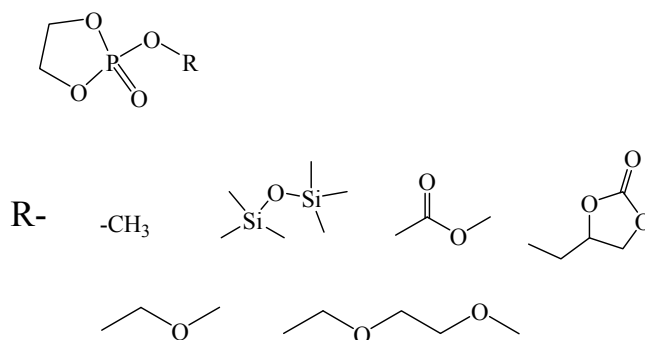


Figure IV - 85: Proposed ethylene phosphate-based compounds as potential SEI additives.

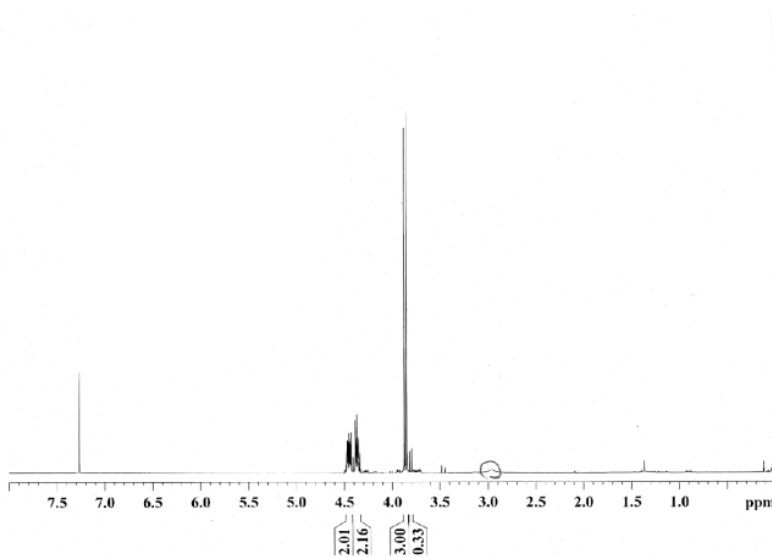


Figure IV - 86: <sup>1</sup>H NMR of ethylene methyl phosphate.

The novel SEI additive OBD was developed and evaluated. By controlling the amount used in the cell system, not only was the cycle life significantly improved but also the impedance control. Differential capacity profiles and FTIR were used to explore the mechanism of the OBD effect.

Ethylene phosphate-based compounds were proposed to construct novel SEI additives. Ethylene methyl phosphate is the first example and is currently being synthesized. Further effort is needed to purify this material to meet the requirements of cell tests.

The future direction of this project is twofold. The mechanism behind promising SEI additives that have been developed is one major topic. Characterization, computation, and mechanism analysis are planned. The other future work is the development of novel SEI additives by using organic synthesis. One example is the ongoing development of ethylene phosphate-based additives. More efforts are needed on additive synthesis to generate novel compounds.

### FY 2011 Publications/Presentations

1. Lu Zhang, Zhengcheng Zhang, Jun Lu, Kirlous H. A Henin, Khalil Amine, "Novel SEI additive to improve the cycle life of lithium-ion battery," in preparation.
2. Lu Zhang, Zhengcheng Zhang, Khalil Amine, "Novel redox shuttle additive for high voltage cathode materials: Tetraethyl 2,5-di-tert-butyl-1,4-phenylene diphosphate," *Energy & Environmental Science*, 4, 2858, 2011.
3. "Lithium tetrafluoro oxalato phosphate as electrolyte additive for lithium-ion cells," *Electrochemical and Solid-State Letters*, 13 (2) A11-A14, 2010.
4. "New electrolyte additive for lithium ion battery," US patent application with internal # ANL-IN-09-108.
5. "Non-aqueous electrolyte for lithium ion battery," US patent application with internal # ANL-IN-10-082.

## IV.B.4.3 High Voltage Electrolyte for Lithium-ion Battery (ANL)

Zhengcheng Zhang, Khalil Amine

Argonne National Laboratory  
9700 South Cass Avenue  
Argonne, IL 60439-4837  
Phone: (630) 252-7868; Fax: (630) 972-4440  
E-mail: [zzhang@anl.gov](mailto:zzhang@anl.gov)

### Collaborators:

Huiming Wu, Argonne National Laboratory  
Ali Abouimrane, Argonne National Laboratory  
Larry Curtiss, Argonne National Laboratory  
Kevin Gering, Idaho National Laboratory  
Richard Jow, US Army Research Laboratory  
Daikin Industries, Ltd.  
EnerDel, LLC

Start Date: October, 2010 (New Project)

Projected End Date: September, 2014

### Objectives

The objective of this work is to develop an electrolyte with wide electrochemical window that can provide stable cycling performance for cathode materials that can be charged above 4.5 V vs Li<sup>+</sup>/Li.

FY11's objective is to identify, synthesize and evaluate new solvent systems as possible electrolyte candidates for high voltage application.

### Technical Barriers

The primary technical barrier is the development of a safe and cost-effective PHEV battery with a 40 mile all electric range that meets or exceeds all performance goals. The energy density of the battery can be increased by using high voltage and high capacity cathode materials. However, the conventional electrolyte does not meet the requirement for normal operation of these batteries especially under harsh conditions. Poor electrochemical stability is one of the drawbacks of the conventional electrolyte which tends to decompose on the surface of the charged electrode, especially by oxidative decomposition on the cathode surface above 4.5V.

### Technical Targets

The technical target of this project is to develop an electrolyte system which can meet the operation requirement for the high energy density lithium ion battery system for

PHEV/HEV applications. The new electrolyte will meet the following requirements:

- Wide electrochemical window (>5V Li<sup>+</sup>/Li)
- High ionic conductivity (>10<sup>-3</sup>S/cm, high power)
- High thermal stability (abuse tolerance)
- Non-flammability (improved safety)
- Solid electrolyte interphase formation capability

### Accomplishments

- Sulfone-based electrolytes were examined as high voltage electrolyte using LiNi<sub>0.5</sub>Mn<sub>1.5</sub>O<sub>4</sub> (LNMO) as cathode. Significant improvements were achieved including enlarged electrochemical window, reduced flammability and comparable cycle life.
- Silane/Sulfone and Sulfone/Carbonate hybrid electrolytes were investigated to further improve the conductivity and electrode/seperator wettability. The performance of these hybrid electrolytes was evaluated in LNMO/Li<sub>4</sub>Ti<sub>5</sub>O<sub>12</sub> chemistry and LNMO/Graphite chemistry.
- New additives were tailored to enable the application of Silane/Sulfone hybrid electrolytes in graphite (MCMB) anode cell chemistry.
- Fluorinated ether and fluorinated ester compounds were designed, synthesized and evaluated as high voltage electrolyte in LMO/LTO chemistry.



### Introduction

New cathode and anode materials have been the focus of the development for high power and high energy lithium-ion batteries for HEVs and PHEVs. To enable many high energy electrodes, new electrolytes are needed and those with high voltage stability are far less developed than the electrode materials. Very few efforts have been dedicated to the development of improved performance electrolytes including the high voltage solvents. The state-of-the-art electrolyte is a non-aqueous solution of a lithium salt (LiPF<sub>6</sub>) dissolved in a carbonate solvent mixture such as ethylene carbonate and diethyl carbonate. However, these carbonate solvents are organic chemicals, which are very flammable and can be oxidatively cleaved into gaseous products at a potential between 4.5 ~ 5.0V vs Li<sup>+</sup>/Li. A high voltage electrolyte is urgently needed to meet the requirement for the high energy density lithium-ion battery for PHEV application.

## Approach

The approach for the high voltage electrolyte activity is to develop an electrolyte system suitable for cathode materials that can be charged to higher potentials ( $>4.5V$  vs  $Li^+/Li$ ) based on the previous experiences of electrolyte development. At the first stage of the research is to choose an LTO anode coupled with 5V spinel LTO cathode to demonstrate the anti-oxidation capability of the solvents.

The final stage of the research will be focused on the graphite anode coupled with the high voltage cathode to gain the practical energy density. This stage is a continuation for the discovered solvents in the first stage in LMO/LTO cell and further explores the applicability in LMO/Graphite or LMO/Si or Sn chemistry. Tailored electrolyte additive is proposed to address the graphite anode surface reaction with the electrolyte to form solid electrolyte interphase film. Efforts this year have focused on the first stage research.

## Results

**Sulfone Containing Hybrid Electrolytes.** Sulfone based electrolyte has been proposed and studied for lithium ion battery. However, both symmetrical and asymmetrical sulfones are solid or viscous liquids at room temperature. The high viscosity leads to low conductivity

and poor wetting of the electrode and separator. To improve the performance of sulfone electrolytes, hybrid electrolytes based on silane and sulfones were proposed and investigated at the beginning of FY2011.

Figure IV - 87 shows the conductivities of tetramethylene sulfone (TMS)/tri(ethylene glycol) trimethylsilane (1NM3) electrolyte with 1.0M  $LiPF_6$  salt concentration at various temperatures. Interestingly, the hybrid electrolyte exhibited higher conductivity than the component electrolyte alone, indicating a certain extent of molecular level synergetic effect. The TMS/1NM3 mixed electrolytes showed much higher conductivity at ratios of 9:1 and 5:5 than those of 8:2 and 7:3. It is known that high polar and low viscosity molecules will facilitate the ion dissociation and thus ion transfer in the solution. TMS has much higher dipole moment (4.35D), therefore it dominates the ion dissociation of the mixed solvent at high concentration. However, the lower viscosity of 1NM3 (1.4cP for 1NM3, 10.1cP for TMS at 30°C) will facilitate the ion transfer in the mixed solvent with low TMS concentration at ratio of 5:5. The TMS/1NM3 mixed electrolyte showed the optimal ambient conductivity of  $2.0 \times 10^{-3}$  S/cm, which is comparable with the conventional carbonate based electrolyte.

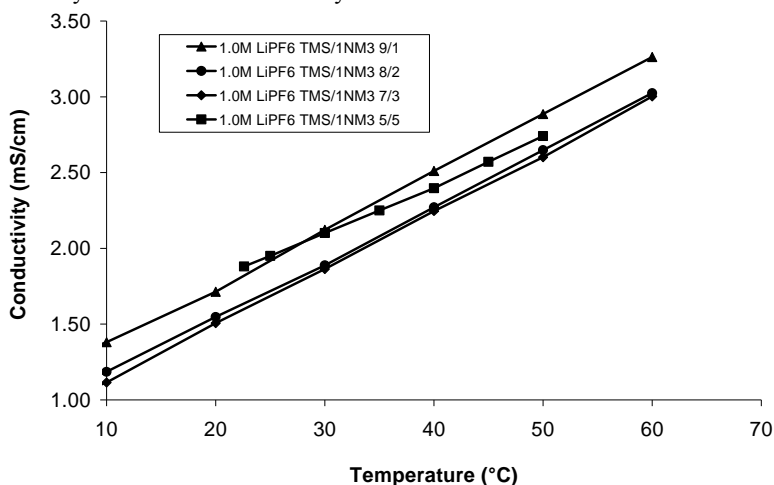


Figure IV - 87: Ionic conductivity vs. temperature relationship of 1.0M  $LiPF_6$  TMS/1NM3 electrolyte.

Sulfone/carbonate hybrid electrolyte was also studied. Figure IV - 88A is the typical LMO/LTO cell charge and discharge profiles using TMS/ethyl methyl carbonate

(EMC) electrolyte in a ratio of 5/5 in weight. Due to the diluting effect and high polarity of EMC, the hybrid electrolyte exhibited excellent power capability as shown in Figure IV - 88B.

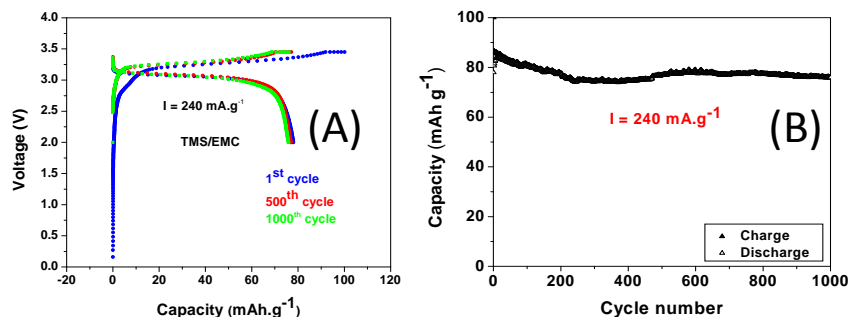


Figure IV - 88: (A) Typical LMO/LTO cell charge and discharge profiles using TMS/ethyl methyl carbonate (EMS) electrolyte in a ratio of 5/5 in weight; (B) Cycling performance with high current rate using of TMS/EMS electrolyte in LMO/LTO cell.

Some preliminary research was conducted on graphite based cell using TMS/1NM3 electrolyte. As anticipated from our previous experience, the bare electrolyte showed incompatibility with graphite based electrode (no cycling performance at all in Figure IV - 89A) though it performed well in LTO based cell. Low concentration of LiDfOB was added into the TMS/1NM3 electrolyte to stabilize the lithiated graphite surface. Figure IV - 90 illustrates the differential capacity profiles of the  $\text{LiNi}_{1/3}\text{Co}_{1/3}\text{Mn}_{1/3}\text{O}_2$  (NMC)/MCMB lithium-ion cells with various additive concentrations. The initial data below 3.0 V during the first charge are shown to demonstrate the SEI formation process. The additive effect on the SEI formation was clearly observed by the peaks at 2.2V. Different from the peaks at about 2.7-3.0V which is independent of the additive and its concentration, the peak at 2.2V depends on the additive type and its concentration. Not observed for the cell without additives, the peak at 2.2 V is believed to

result from the SEI layer formed by the decomposition of additives, which is evidenced by the increases of peak intensity with the increasing additives from 2% to 4% for both LiDfOB and VC. The best cycling performance was obtained with 4% LiDfOB additive as shown in Figure IV - 89D, suggesting that the passivation film was optimized at this concentration. More additive will lead to the significant increase the thickness of SEI film causing high impedance.

The electrolyte with additive LiDfOB or VC can significantly improve the cycling performance of the graphite based cells as shown in Figure IV - 89B, Figure IV - 89C and Figure IV - 89D. When additive is added, the capacity retention of the cell is improved with 4% LiBOB shown the best results.

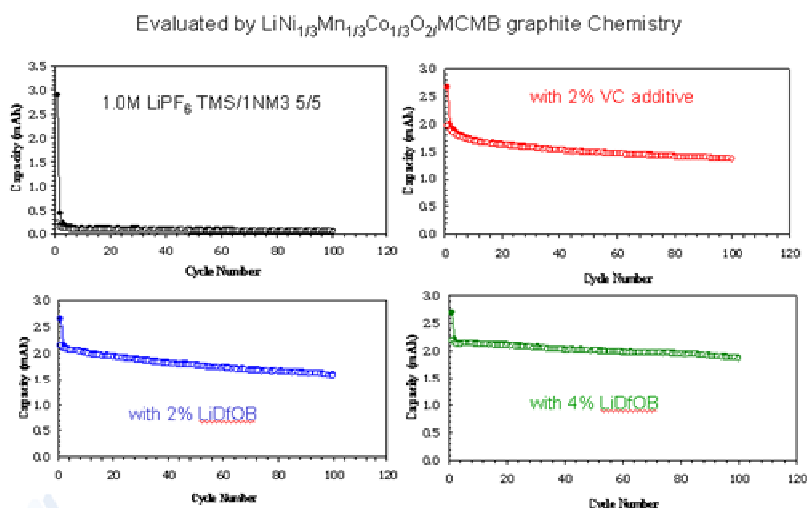


Figure IV - 89: NMC/MCMB cell cycling performance using 1.0M LiPF<sub>6</sub> TMS/1NM3 (A) without additive, (B) with 2% VC, (C) with 2% LiDfOB, and (D) with 4% LiDfOB.

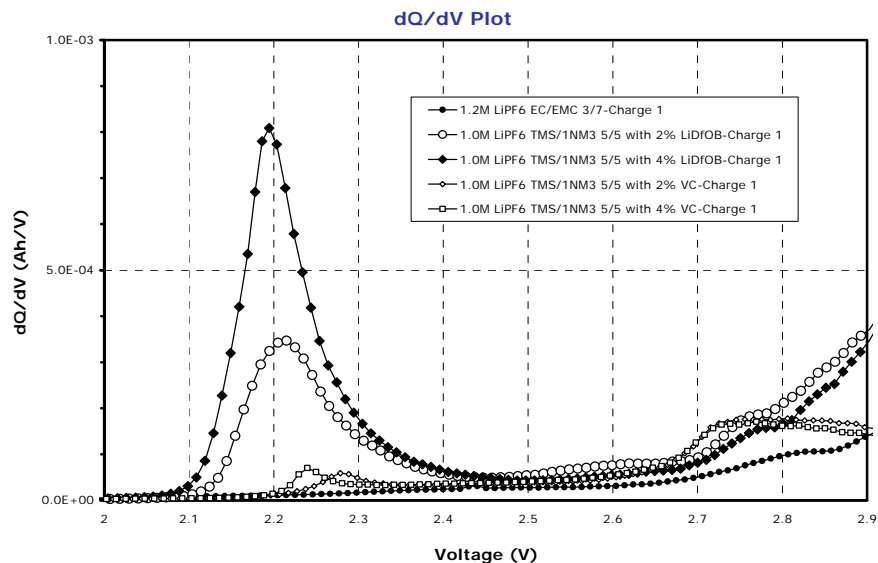


Figure IV - 90: Differential capacity profiles LiNi<sub>1/3</sub>Co<sub>1/3</sub>Mn<sub>1/3</sub>O<sub>2</sub> (NMC)/MCMB cells with different concentrations of LiDFOB as additive in 1.0M LiPF<sub>6</sub> TMS/1NM3 5/5 electrolyte.

Fluorinated Compounds as High Voltage Electrolytes. Fluorinated ethylene carbonate (FEC) is widely studied as an SEI additive (Figure IV - 91). FEC decomposes at high reduction potential forming a new SEI on the surface of graphite. However, our recent study has shown that FEC tends to thermally decompose at elevated temperature especially in the presence of the lithium salt. An ether-based fluorinated compound (D2) was selected and formulated into the conventional electrolyte of 1.2M LiPF<sub>6</sub> EC/EMC and investigated using a 5V-spinel LNMO cathode coupled with a 1.5V-LTO anode. The voltage stability of the fluorinated electrolytes was determined by cyclic voltammetry. LNMO/Li half cell was scanned from 3.0V to 5.0 V with a scan rate of 0.1mV/s for two cycles and the results are shown in Figure IV - 92.

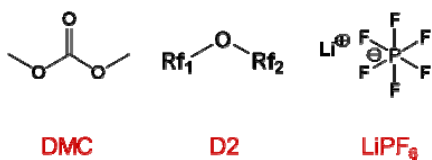


Figure IV - 91: Fluorinated Compounds as High Voltage Electrolytes

Two fluorinated electrolytes 1.2 M LiPF<sub>6</sub> in EC/EMC/D2 2:6:2 and 1.2 M LiPF<sub>6</sub> in EC/DMC/D2 2:5:3 showed the same CV profiles as the conventional

electrolyte 1.2M LiPF<sub>6</sub> EC/EMC 3:7. The peaks at high potential around 4.7V is related to Ni<sup>2+</sup>/Ni<sup>3+</sup> and Ni<sup>3+</sup>/Ni<sup>4+</sup> redox couples of LNMO. A small peak at the low potential around 4V is due to the redox of low concentration of Mn<sup>3+</sup> in the LNMO. Both peaks are reversible indicating the electrolytes are stable with high voltage LNMO cathode.

Cell performance was evaluated at room temperature and elevated temperature at the 2C rate. Figure IV - 93 shows the cycling performance of LNMO/LTO cell between 2.0~3.45 V. At room temperature, all cells showed good stability with a capacity loss less than 4% at 200 cycles. However, at high temperature (55°C), the cycling performance of the conventional electrolyte degraded quickly and after 200 cycles, it only delivered 78% of its initial capacity and lost all capacity at 400 cycles. In contrast, the D2 based fluorinated electrolytes are stable at this testing condition with over 80% capacity retention at 200 cycles and 70% at 400 cycles. These preliminary data indicate that the fluorinated electrolytes have potential use for high voltage cathode materials especially at harsh conditions.

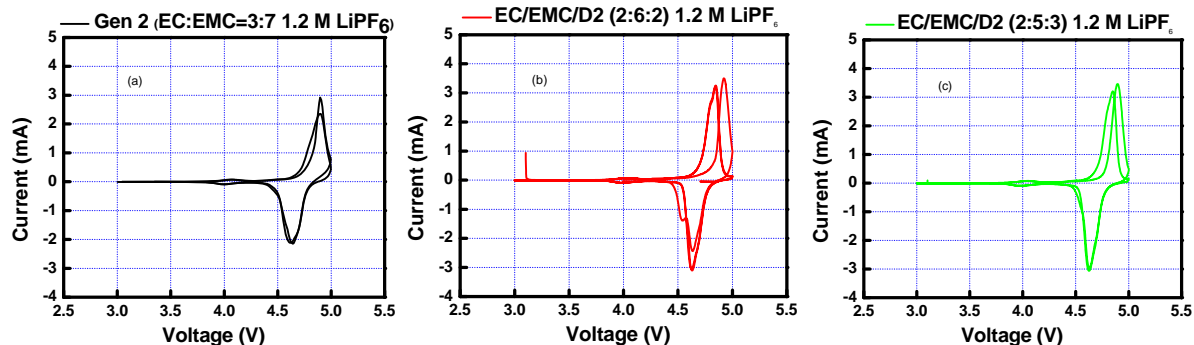


Figure IV - 92: CV profiles of LNMO/Li half cell with different electrolytes (A, top, 1.2 M LiPF<sub>6</sub> in EC/EMC 3:7) (b, lower left, 1.2 M LiPF<sub>6</sub> in EC/EMC/D2 2:6:2) and (c, lower right, 1.2 M LiPF<sub>6</sub> in EC/DMC/D2 2:6:2).

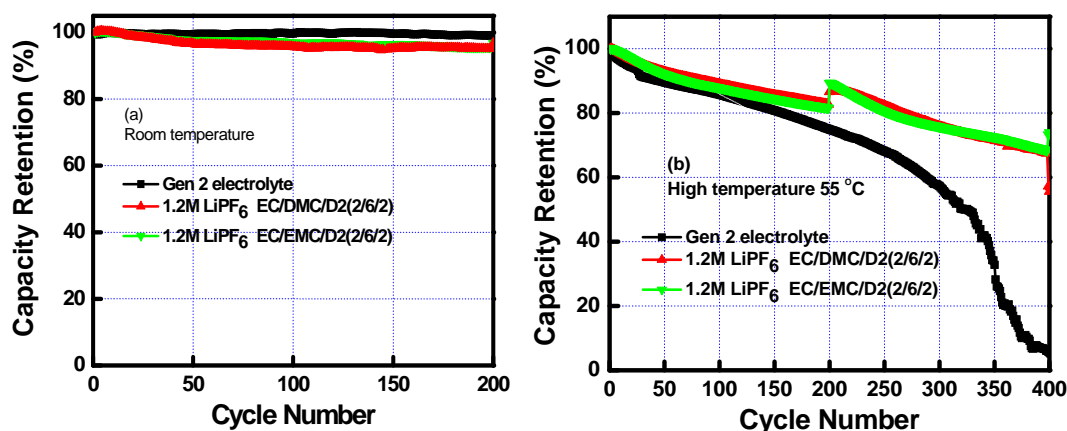


Figure IV - 93: Cycle performance of LNMO/LTO cell with fluorinated electrolytes 1.2 M LiPF<sub>6</sub> in EC/EMC/D2 2:6:2 and 1.2 M LiPF<sub>6</sub> in EC/EMC/D2 2:5:3 at room temperature and high temperature (55°C).

## Conclusions and Future Directions

Hybrid electrolytes were developed by incorporating silane and carbonate electrolyte into sulfone electrolyte. The synergetic effect was observed for sulfone/silane combination in terms of conductivity and the electrochemical window. Sulfone/carbonate hybrid electrolyte exhibited excellent power capability due to the improved conductivity.

The electrolyte with additive LiDfOB or VC significantly improves the cycling performance of the graphite based cells. The best results were obtained with 4% LiBOB indicating an integrated SEI formation on the surface of the graphite.

Fluorinated carbonate and ether compounds were developed as high voltage electrolytes. These new electrolyte showed excellent voltage stability and good cycling performance at elevated temperature. When cycled between 2.0~3.45 V, the LNMO/LTO showed good cycle stability at room temperature and at 55°C with a capacity loss less than 4% at 200 cycles. These preliminary data indicated that the fluorinated electrolytes have potential

use for high voltage cathode materials especially under harsh conditions.

Future direction will be focused on the new fluorinated electrolyte to further improve the cell performance both in LTO and graphite based high voltage cathode cells. The characterization of the enabling mechanism will also be initiated in the FY 2012.

## FY 2011 Publications/Presentations

- 2011 DOE Annual Peer Review Meeting Presentation, May 9<sup>th</sup>-13<sup>th</sup>, 2011, Washington DC, USA.
- DOE-USABC Electrolyte Workshop, Invited Presentation, August, 18<sup>th</sup>-19<sup>th</sup>, 2011, Southfield, MI, USA.
- 6<sup>th</sup> International Forum on Lithium-ion Battery Technology and Industry development, Invited Talk, September 19<sup>th</sup>-20<sup>th</sup>, 2011, Beijing, China.
- EV Battery Tech USA 2011, September 27<sup>th</sup>-28<sup>th</sup>, Invited Talk, Troy, MI, USA.
- High Voltage Electrolyte for Lithium Ion Battery. Manuscript in preparation.

## IV.B.4.4 High Voltage Electrolytes for Li-ion Batteries (ARL)

Kang Xu, Arthur von Cresce, Jan L. Allen, Oleg Borodin, T. Richard Jow

Point of Contact:

T. Richard Jow/Kang Xu

U.S. Army Research Laboratory

2800 Powder Mill Road

Adelphi, MD 20783

Phone: (301) 394-0340/(301) 394-0321

Fax: (301) 394-0273

E-mail: [t.r.jow.civ@mail.mil](mailto:t.r.jow.civ@mail.mil)/  
[conrad.k.xu.civ@mail.mil](mailto:conrad.k.xu.civ@mail.mil)

Start Date: August 15, 2008

Projected End Date: September 30, 2014

### Objectives

- Develop high voltage electrolytes that enable the operation of Li-ion batteries with high voltage cathodes for enhanced energy density for PHEVs.

### Technical Barriers

This project addresses the following technical barriers of today's Li-ion batteries:

- State of the art electrolytes based on carbonate solvents decompose below 4.5 V;
- Sulfone-based solvents showed anodic stability up to 5.8 V but:
  - SEI chemistry from reduction of sulfones does not provide protection of graphitic anodes
  - Most sulfones such as dimethyl sulfone and sulfolane are viscous liquids with melting point near RT.
- Lack of a reliable 5 V cathode as characterization platform.
- High voltage cathode materials today do not have suitable high voltage electrolytes for realizing their capacity and achieving long cycle and storage life.
- Lack of guides in developing electrolyte components enabling the cycling of high voltage cathodes.

### Technical Targets

- Synthesize improved sulfone based solvents with and without unsaturated bonds and evaluate their electrochemical properties.

- Identify and synthesize additives for electrolytes based on sulfone solvents for Li-ion cells.
- Identify and synthesize additives for electrolytes based on carbonate solvents for Li-ion cells.
- Formulate, test and evaluate electrolytes containing synthesized additives in Li half cells.
- Select promising formulations, test and demonstrate in complete cells in button cell or in prototype cell configurations.

### Accomplishments

- Explored fluorinated phosphate esters of different fluorine/hydrogen (F/H) ratios as additives for carbonate based electrolytes and tested their effectiveness in retaining capacity of the 4.7 V  $\text{LiNi}_{0.5}\text{Mn}_{1.5}\text{O}_4/\text{Li}$  half cells.
- The cycling of  $\text{LiNi}_{0.5}\text{Mn}_{1.5}\text{O}_4/\text{Li}$  cells indicated that tris(hexafluoroisopropyl) phosphate, HFIP, with the highest F/H ratio of 6 is mostly effective in retaining capacity to 200 cycles.
- Achieved stable capacity retention over 160 cycles for the cycling of  $\text{LiNi}_{0.5}\text{Mn}_{1.5}\text{O}_4/\text{graphite}$  full cells in 1.2 M  $\text{LiPF}_6$  in EC-EMC (3:7 v/o) with 0.5 mM HFIP while the capacity of the same cells in the same electrolyte without additives showed steady decline.
- Enabled  $\text{LiNi}_{0.5}\text{Mn}_{1.5}\text{O}_4/\text{graphite}$  cells to be cycled in  $\text{LiPF}_6$  in linear carbonate, ethyl methyl carbonate (EMC), solvent alone with the addition of HFIP. This demonstrated that HFIP plays a critical role in on forming effective SEIs.
- Developed a 4.8 V Fe substituted  $\text{LiCoPO}_4$  cathode, in which a portion of the Co is substituted by  $\text{Fe}^{2+}$  and  $\text{Fe}^{3+}$ . This cathode showed good structural stability and retained 80% original capacity over 500 cycles in 1 m  $\text{LiPF}_6/\text{EC}:\text{EMC}(3:7 \text{ w/o})$  with 1 wt% HFIP.
- Influence of anion on the electrolyte solvent oxidative stability and initial decomposition reactions was explored using quantum chemistry calculations.

◇ ◇ ◇ ◇ ◇

### Introduction

Achieving higher energy density using the new generation of high voltage cathodes with voltages from 4.5 to 5.0 V such as  $\text{LiNi}_{0.5}\text{Mn}_{1.5}\text{O}_4$  and  $\text{LiCoPO}_4$  for Li-ion batteries for PHEV will need compatible high voltage electrolytes. The state-of-the-art electrolytes made of

LiPF<sub>6</sub> in carbonate solvent mixtures decompose at voltages below 4.5 V and are unable to realize the higher energy density and achieve long cycle and storage life. The development of compatible high voltage electrolytes is urgently needed.

## Approach

Instead of using the state-of-the-art carbonate based solvent systems, our approach is to explore the use of sulfone based solvent systems and additives for both the sulfone based and the carbonate based solvent systems. The sulfone solvents with unsaturated bonds would also be good candidates as additives for both sulfone and carbonate based electrolytes. It has been reported that the electrolytes containing sulfone based solvents are anodically stable up to about 5.8 V. However, they lack the ability to form a protective SEI at the anode. Furthermore, the commercially available sulfones such as dimethyl sulfone and sulfolane are viscous. To allow the operation of the high voltage cathode materials, we will develop electrolytes based on improved sulfone based solvents.

To improve both sulfone based and carbonate based solvent systems, our approaches include the following:

- Explore asymmetric sulfone with different functional groups for lower melting points and low viscosity.
- Explore sulfone solvents with functional groups containing un-saturated bonds as solvents and as additives.
- Explore the use of other additives from the chemicals that have the ability for forming the protective layers on cathodes.
- Develop high voltage LiCoPO<sub>4</sub> based cathode for the evaluation of high voltage electrolytes
- Employ quantum chemistry calculations to predict oxidative stability and decomposition reactions of electrolytes and additives

## Results

**Phosphate Ester Additives and the Benefit of Increasing Degree of Fluorination.** The phosphate esters used as additives at ARL to enhance the high-voltage stability of organic carbonate electrolytes seem to benefit from greater amounts of fluorination. Our current additive, tris(hexafluoroisopropyl)phosphate (called HFiP) [3], is a highly fluorinated phosphate ester with a fluorine/hydrogen (F/H) ratio of 6. Several other phosphates esters, with varying F/H ratios, were also tested as additives. Interestingly, the performance of those cells seemed to relate directly to the F/H ratio of each additive. We took capacity retention at the 175th cycle as our performance marker. Low F/H ratio additives did not retain as much capacity at cycle 175 as did those with high

F/H ratio, led by the most fluorinated phosphate ester HFiP (Figure IV - 94).

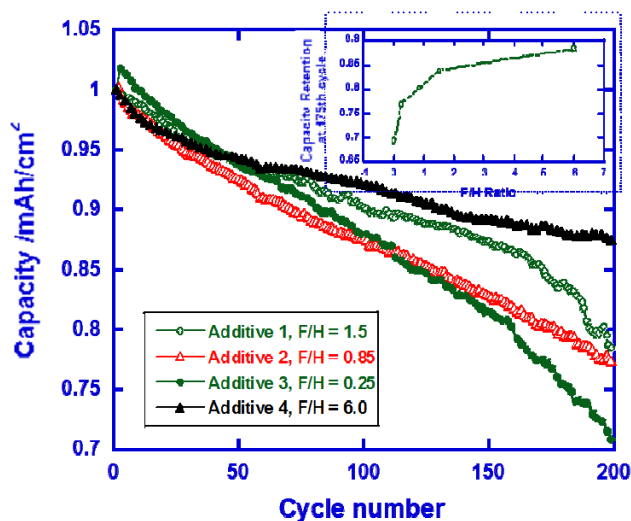


Figure IV - 94: Capacity as a function of cycle number plots at room temperature for LiNi<sub>0.5</sub>Mn<sub>1.5</sub>O<sub>4</sub>/Li half cells in 1 M LiPF<sub>6</sub>/EC:EMC (3:7 w/o) with various fluorinated phosphate esters of different fluorine/hydrogen (F/H) ratios.

**Performance of HFiP in Full-cell Configuration with a 4.7V LiNi<sub>0.5</sub>Mn<sub>1.5</sub>O<sub>4</sub> Cathode and Graphite Anode.** We have successfully cycled LiNi<sub>0.5</sub>Mn<sub>1.5</sub>O<sub>4</sub> versus lithium in 1.2 M LiPF<sub>6</sub>/EC:EMC (3:7 v/o) with 1 mM HFiP. Subsequent tests of HFiP-containing electrolytes showed that HFiP was also compatible with graphite anodes. It was found that Li<sup>+</sup> could be intercalated into graphite reversibly in LiPF<sub>6</sub> in propylene carbonate (PC) with HFiP. This could not be achieved without HFiP as PC co-intercalates into graphite and the reduction products of PC exfoliate graphite. Because of this positive anode result, we constructed full cells consisting of a LiNi<sub>0.5</sub>Mn<sub>1.5</sub>O<sub>4</sub> cathode and the A12 graphite anode made from Conoco Philips graphite. The test results are shown in Figure IV - 95. Our results, while not as dramatic as those seen in the half-cell configuration, again showed that HFiP can slow the capacity loss during cycling of a full Li-ion cell. The primary difference between the full and half cell configuration was the lower initial capacity utilization in electrolytes containing HFiP as compared to the standard Generation 2 electrolyte, 1.2 M LiPF<sub>6</sub>/EC:EMC (3:7 v/o). This initial penalty, though, was erased upon cycling as the standard electrolyte consistently lost capacity during cycling at a higher rate than the HFiP containing electrolyte. After 50 cycles, cells with HFiP electrolytes have lost very little capacity while the standard electrolytes have lost nearly 20% of initial capacity. Due to the behavior of HFiP in standard electrolytes, and in PC, we think that HFiP is helping to form a tougher SEI layer that is better able to resist electrochemical redox reactions. This may be the cause of the initial capacity penalty seen in the full cell results. The current additive, HFiP, is a highly

fluorinated phosphate ester with a F/H ratio of 6. Several other phosphates esters, with varying F/H ratios, were also tested as additives.

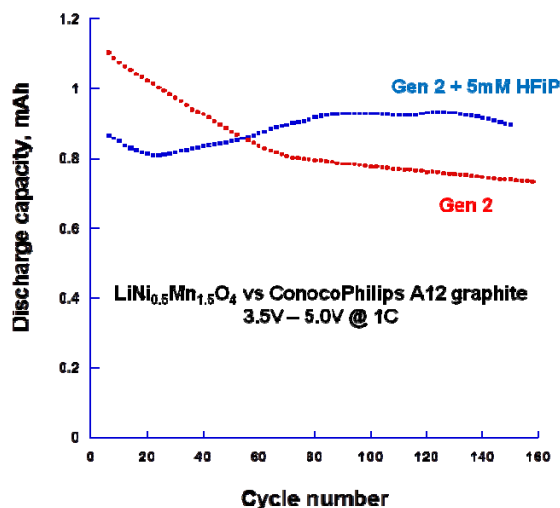


Figure IV - 95: A comparison of capacity retention of  $\text{LiNi}_{0.5}\text{Mn}_{1.5}\text{O}_4/\text{A12}$  full cells in 1.2 M  $\text{LiPF}_6/\text{EC}:\text{EMC}$  (3:7 v/o) with and without 5 mM HFIP versus cycle number at 1C between 3.5 and 5.0 V at room temperature.

**Impact of HFIP in 0.8 M  $\text{LiPF}_6$  in EMC Electrolyte on Cycling of 4.7V  $\text{LiNi}_{0.5}\text{Mn}_{1.5}\text{O}_4$  Cathode against Graphite Anode.** Another benchmark test of HFIP was its ability to cycle a linear carbonate, EMC, in a solution without EC in a full cell configuration. Normally, EMC is used as a viscosity-lowering co-solvent. Our group has identified that it does not fully participate in the solvation of  $\text{Li}^+$  and generally displays poor electrochemical properties, such as resistance to redox decomposition and formation of a lithium-conducting SEI layer on anode or cathode. Because of its extremely poor SEI forming qualities, we added 5mM HFIP to a purely EMC electrolyte and compared that, in a full cell configuration, with a plain EMC electrolyte. The differences are immediately apparent; the cell in EMC electrolyte without HFIP starts with a higher capacity but quickly fades and fails by cycle 100. The cell containing EMC and 5mM HFIP maintained close to 95% of initial cycling capacity beyond the 100th cycle (Figure IV - 96). This is a very important result because it plainly shows that HFIP can influence the performance of a weak electrolyte, even at very low concentrations.

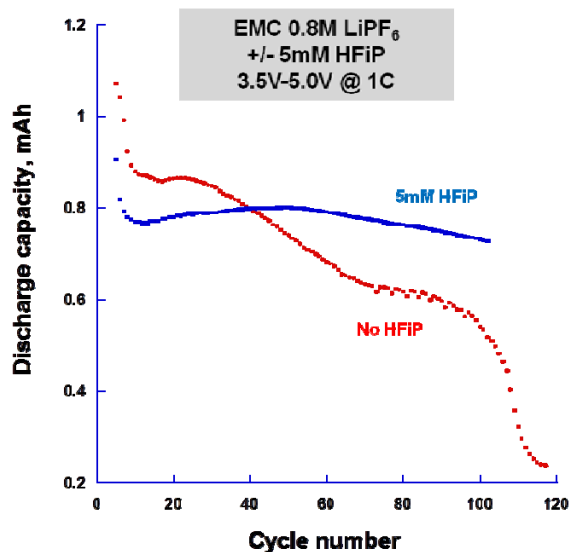


Figure IV - 96: A comparison of capacity retention of  $\text{LiNi}_{0.5}\text{Mn}_{1.5}\text{O}_4/\text{A12}$  full cells in 0.8 M  $\text{LiPF}_6/\text{EMC}$  with and without 5 mM HFIP versus cycle number.

**Development of High Voltage  $\text{LiCoPO}_4$  Cathode for Evaluation of High Voltage Electrolytes.**  $\text{LiCoPO}_4$  is a 4.8 V cathode material with potentially 40% higher energy density than  $\text{LiFePO}_4$  and is an ideal test vehicle for high voltage electrolyte development. However, its relatively poor cycle life resulting from lack of structural stability plus compatible high voltage electrolytes became a challenge for using this material. We developed a Fe-doped  $\text{LiCoPO}_4$  in which a portion of the Co is substituted by  $\text{Fe}^{2+}$  and  $\text{Fe}^{3+}$ . The novel material was characterized by ICP-MS, Mössbauer spectroscopy (Figure IV - 97), FT-IR, XPS and XRD to confirm this substitution with the olivine structure. Long term cycling of cells in electrolyte containing HFIP is shown in Figure IV - 98[7].

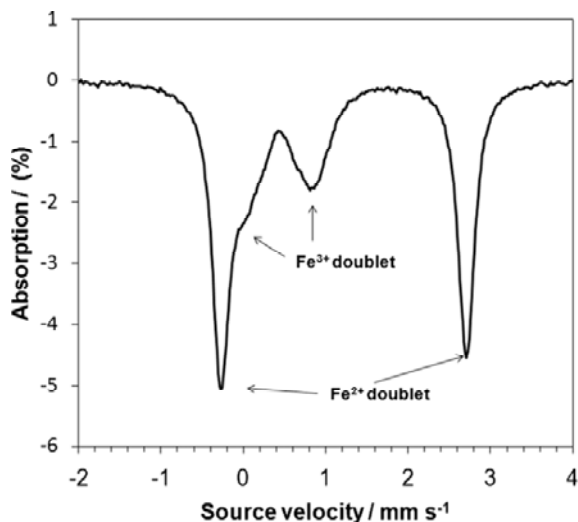


Figure IV - 97: Mössbauer spectrum of Fe-substituted  $\text{LiCoPO}_4$ .

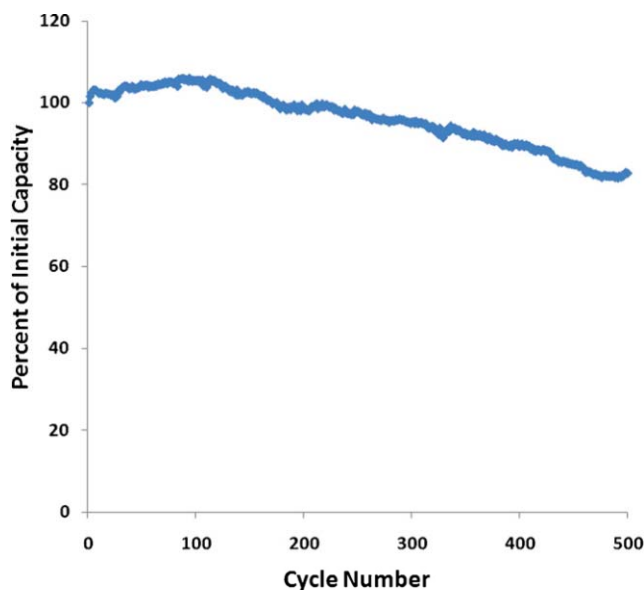


Figure IV - 98: Long term cycling of Fe-substituted  $\text{LiCoPO}_4$  against Li in 1 m  $\text{LiPF}_6/\text{EC}:\text{EMC}$  (3:7 w/o) with 1% HFIP additive.

**Oxidation Stability Limits of Solvents.** The calculation of oxidation stability potential limits of solvents using density functional theory (DFT) with M05-2X functional and cc-pvTz basis set indicates that oxidation potential limits are about 1 V too high compared with the experimental values obtained using linear voltammetric scan method using glass carbon electrode. However, the calculated values agree with the experimental values when the anion of the salt is included in the calculation as discussed in ref.[6]. Moreover, the oxidative stability of the solvent-anion complexes increases with increasing solvent dielectric constant, while the opposite trend is observed for pure solvents.

Investigation of the influence of anions ( $\text{PF}_6^-$ ,  $\text{ClO}_4^-$ ) on the oxidative decomposition reaction of PC were completed using DFT in collaboration with Lidian Xing

and Grant Smith of University of Utah. DFT calculations were performed in gas phase (dielectric constant  $\epsilon=1$ ) and in the implicit solvent using polarized continuum model (PCM) with  $\epsilon=20.5$ . It has been found that the presence of  $\text{PF}_6^-$  and  $\text{ClO}_4^-$  anions significantly reduces PC oxidation stability, stabilizes the PC-anion oxidation decomposition products and changes the order of the oxidation decomposition paths. Formation of HF and  $\text{PF}_5$  was observed upon the initial step of  $\text{PC-PF}_6^-$  oxidation while  $\text{HClO}_4$  formed during oxidation of  $\text{PC-ClO}_4^-$ . The most probable reaction paths for the initial decomposition of the oxidized  $\text{PC-PF}_6^-$  and  $\text{PC-ClO}_4^-$  complexes are shown in Figure IV - 99. The primary oxidative decomposition products of  $\text{PC-PF}_6^-$  and  $\text{PC-ClO}_4^-$  at room temperature were  $\text{CO}_2$  and acetone radical.

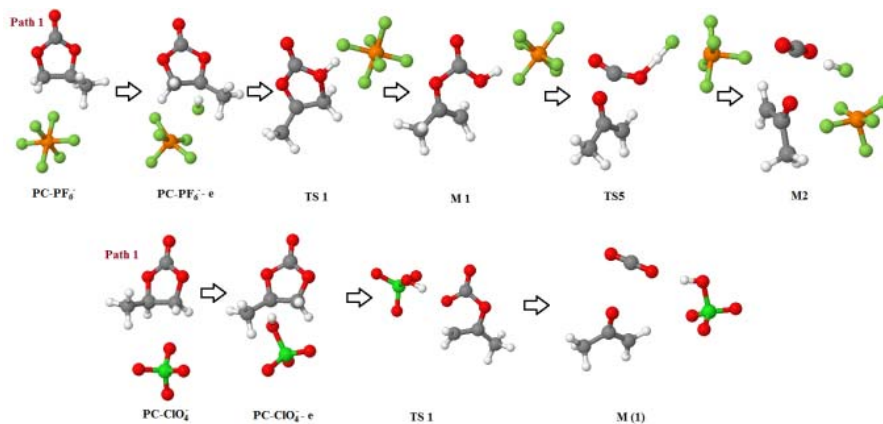


Figure IV - 99: The lowest barrier pathway for oxidative decomposition reaction of  $\text{PC-PF}_6^-$  and  $\text{PC-ClO}_4^-$ .

The pathway with the second lowest barrier for the PC-PF<sub>6</sub><sup>-</sup> oxidative ring opening resulted in a formation of fluoro-organic compounds suggesting that these compounds form at elevated temperatures under oxidizing conditions [7]. Influence of PF<sub>6</sub><sup>-</sup> anion on the HFiP additive intrinsic oxidative stability was explored, indicating a spontaneous fluorine transfer from PF<sub>6</sub> to phosphorus of HFiP upon oxidation.

## Conclusions and Future Directions

We have identified effective additives, fluorinated phosphate esters, for the carbonate based electrolyte formulations. With the addition of 0.5 mM HFiP in the baseline electrolytes, 1.2 M LiPF<sub>6</sub>/EC:EMC(3:7 v/o), a steady capacity retention of LiNi<sub>0.5</sub>Mn<sub>1.5</sub>O<sub>4</sub>/graphite full cells has been demonstrated. The Fe substituted LiCoPO<sub>4</sub> cycled against Li in the baseline electrolyte with 1 wt% HFiP has showed improved capacity retention and cycle life. Our planned works include the following.

- Synthesis of new phosphate ester variants that are perfluorinated and contain no protons for the evaluation of the effectiveness of forming protective layers on electrodes.
- Evaluation of HFiP containing electrolytes at elevated and low temperatures for stability and rate performance of LiNi<sub>0.5</sub>Mn<sub>1.5</sub>O<sub>2</sub>/graphite full cells.
- Evaluation of Fe modified LiCoPO<sub>4</sub> in a full cell configuration in electrolytes containing additives including fluorinated phosphate esters.
- Understanding of the mechanism of how HFiP works for developing more effective additives.
- Adding computational efforts for basic understanding of decomposition of electrolyte components and reactive pathway of forming interfacial layers. This effort could potentially provide guidance in design better electrolyte components.
- Evaluation of linear sulfone based electrolytes formulated with other solvent mixtures and additives.

## FY 2011 Publications/Presentations

6. "Preferential Solvation of Li<sup>+</sup> Directs Formation of Interphase on Graphitic Anode", A. v. Cresce, and K. Xu, *Electrochem. and Solid State Letters*, 2011, 14, A154-156
7. "Interfacing electrolytes with electrodes in Li Ion Devices", K. Xu and A. v. Cresce, invited contribution to Special Issue on Materials for Li Ion Batteries, *J. Mater. Chem. (RSC)*, 2011, 21, 9849-9864
8. "Electrolyte Additive in Support of 5 V Li Ion Chemistry", A. v. Cresce, and K. Xu, *J. Electrochem. Soc.* 2011, 158, A337-342.

9. "Improved cycle life of Fe-substituted LiCoPO<sub>4</sub>" J. L. Allen, T. R. Jow, J. Wolfenstine, *J. Power Sources*, 2011, 196, 8656-8661.
10. "Distinguishing Charge Transfer Kinetics at the Electrolyte/NCA Cathode and the Electrolyte/Graphite Anode Interfaces in Li-ion Cells", T. R. Jow, M. Marx, J. L. Allen, *ECS Transactions*, 2011, 38(23), 1-13.
11. "Quantum Chemistry Studies of the Oxidative Stability of Carbonate, Sulfone and Sulfonate-Based Electrolytes Doped with BF<sub>4</sub><sup>-</sup>, PF<sub>6</sub><sup>-</sup> Anions", O. Borodin, T. R. Jow, *ECS Transactions*, 2011, 33 (28), 77-84.
12. "A Density Function Theory Study of the Role of Anions on the Oxidative Decomposition Reaction of Propylene Carbonate", L. Xing, O. Borodin, G. D. Smith, W. Li, *J. Phys. Chem. A*, 2011 (ASAP, published on the web).
13. "Phosphate-Based Compounds as Additives for 5-Volt Lithium-Ion Electrolytes", A. V. Cresce, K. Xu, *Electrochemical Society Fall Meeting 2011*, Boston, MA.
14. "Direct Mapping of Li<sup>+</sup>-Solvation Sheath Structure through a Mass Spectrum Technique", K. Xu, A. V. Cresce, *Electrochemical Society Fall Meeting 2011*, Boston, MA.
15. "LiCoPO<sub>4</sub> as Li-ion Cathode," J. L. Allen, J. Wolfenstine, T. R. Jow, *Electrochemical Society Fall Meeting 2011*, Boston, MA.
16. "Li<sup>+</sup>-solvation/desolvation directs interphasial process in Li ion batteries", K. Xu, DOE/USABC Workshop on Electrolytes, Detroit, MI (August 17-19, 2011).
17. "Low Temperature Electrolytes", T. R. Jow, DOE/USABC Workshop on Electrolytes, Detroit, MI (August 17-19, 2011)
18. "5 V Electrolyte Solvents and Additives", K. Xu, invited talk at Navy Electrochemical Power Sources Workshop, Monterey, CA (June 20-23, 2011)
19. "Interphasial Chemistries directed by Li<sup>+</sup>-Solvation Shell", K. Xu, invited talk at Pacific Northwest National Laboratory, Richland, WA (June 6, 2011)
20. "Interfacing Electrolytes with Electrodes in Li Ion Batteries", K. Xu, invited talk at ACS Mid-Atlantic Region Symposium, College Park, MD (May 23, 2011)
21. "Li<sup>+</sup>-Solvation and Desolvation in Non-aqueous Electrolytes and Its Implication in Interphasial Chemistry", K. Xu, A. v. Cresce, invited talk at MRS Spring Meeting, San Francisco, CA (April 25, 2011).
22. "Progress towards using LiCoPO<sub>4</sub> as Li-Ion Battery Cathode" J. L. Allen, J. Wolfenstine, T. R. Jow, *Materials Research Society, Fall Meeting 2010*, Boston, MA.
23. "High Cycle Life Cathode for High Voltage (5V) Lithium Ion Batteries," *WBT Innovation Marketplace*, Arlington, TX, March 2011.

24. “Insight into Transport Properties and Oxidative Decomposition Pathways of Lithium Battery Electrolytes from MD Simulations and DFT” (invited talk) O. Borodin, L. Xing, R. Jow, ACS Meeting, Denver, August 26, 2011-September 1, 2011
25. “Modeling of Liquid and Ionic Liquid Electrolytes for Energy Storage Applications” O. Borodin (invited talk) 10X Advanced Battery R&D, Future Storage Platforms, January 10-12, 2010 at Techmart in Santa Clara, CA
26. “Molecular Insight into Ionic Liquid Behavior in Double Layer Capacitors and in Electrolytes for Lithium Batteries” (invited talk) O. Borodin, J. Vatamanu, G. Smith 4<sup>th</sup> Congress on Ionic Liquids (COIL-4), June 15-18, 2011, Crystal City Hilton, Arlington, Virginia
27. “Understanding Electrolyte Stability from DFT Calculations and Double Layer Structure from MD Simulations” Lidan Xing, Jenel Vatamanu, Oleg Borodin, Grant D Smith 4th Symposium on Energy Storage : Beyond Lithium Ion, Pacific Northwest National Laboratory, June 7-9, 2011
28. Influence of Anions on Propylene Carbonate Oxidative Decomposition Pathways from DFT Calculations L. Xing, O. Borodin, G. D. Smith, W. Li *220th Electrochemical Society Fall Meeting 2011*, October 9-14, 2011, Boston, MA

## IV.B.4.5 Development of Novel Electrolytes for Use in High Energy Lithium-Ion Batteries with Wide Operating Temperature Range (JPL)

Marshall C. Smart  
Electrochemical Technologies Group  
Power and Sensor Systems Section  
Jet Propulsion Laboratory  
California Institute of Technology  
4800 Oak Grove Drive, M/S 277-207  
Pasadena, CA 91109-8099  
(818) 354-9374 (Phone)  
(818) 393-6951 (Fax)  
E-Mail : [Marshall.C.Smart@jpl.nasa.gov](mailto:Marshall.C.Smart@jpl.nasa.gov)

Start Date: Oct 1, 2009  
Projected End Date: September 30, 2014

### Objectives

- Develop a number of advanced Li-ion battery electrolytes with improved performance over a wide range of temperatures (-30° to +60°C) with projected long-life characteristics (5,000 cycles over 10-yr life span).
- Improve the high voltage stability of these candidate electrolyte systems to enable operation up to 5V with high specific energy cathode materials.
- Define the performance limitations at low and high temperature extremes, as well as life-limiting processes.
- Demonstrate the performance of advanced electrolytes in large capacity prototype cells.

### Technical Barriers

This project addresses the following technical barriers associated with the development of PHEVs:

- (A) Narrow operating temperature range
- (B) Limited life
- (C) Poor abuse tolerance.

### Technical Targets

- The technology development program is focused on enabling 10 s discharge power, and is associated with a number of technical targets, including:
  1. 750 W/kg (10 mile) and 316 W/kg (40 mile)
  2. Cold cranking capability to -30°C,

3. Cycle life: 5000 cycles (10 mile) and 3000 cycles (40 mile)
4. Calendar life: 15 years (at 35°C);

### Accomplishments

- Demonstrated improved performance with wide operating temperature electrolytes containing methyl butyrate) in A123 LiFePO<sub>4</sub>-based prototype cells.
- Demonstrated >11C discharge rates at -30°C, with over 90% of the room temperature capacity being delivered in A123 LiFePO<sub>4</sub>-based prototype cells containing methyl butyrate-based electrolytes.
- Observed good performance to temperatures as low as -60°C, with 80% of the room temperature capacity being delivered using a C/10 rate.
- Demonstrated operational capability over a wide temperature range (-60° to +60°C), with good life characteristics being observed at ambient and high temperatures.
- Formulations possessing mono-fluoroethylene carbonate (FEC), lithium bis(oxalato) borate (LiBOB), lithium oxalate, and vinylene carbonate have shown promise in experimental cells.
- Investigated the use of methyl butyrate-based electrolyte containing additives in conjunction with LiNi<sub>1/3</sub>Co<sub>1/3</sub>Mn<sub>1/3</sub>O<sub>2</sub>, Li(Li<sub>0.17</sub>Ni<sub>0.25</sub>Mn<sub>0.58</sub>)O<sub>2</sub>, LiNi<sub>0.50</sub>Mn<sub>1.50</sub>O<sub>2</sub> (LMNO), LiNiMnCoO<sub>2</sub> cathode materials in experimental cells, with good performance being exhibited thus far.
- In three electrode cells, the presence of additives (i.e., FEC, VC, and lithium oxalate) have been observed to have a beneficial effect upon the anode characteristics (lithium intercalation kinetics) after exposure to high temperatures, which is manifested in lower film (SEI) and charge transfer resistances.

◇ ◇ ◇ ◇ ◇

### General Approach

The development of electrolytes that enable operation over a wide temperature range, while still providing the desired life and resilience to high temperature (and voltage) remains a technical challenge. To meet the proposed objectives, this electrolyte development project will include the following general approaches: (1)

optimization of carbonate solvent blends, (2) use of low viscosity, low melting ester-based co-solvents, (3) use of fluorinated esters and fluorinated carbonates as co-solvents, (4) use of novel “SEI promoting” and thermal stabilizing additives, (5) use of novel non-fluorine based salts (with Materials Methods and LBNL). Many of these approaches will be used in conjunction in multi-component electrolyte formulations (i.e., such as the use of low viscosity solvents and novel additives and salts), which will be targeted at improved operating temperature ranges while still providing good life characteristics.

### Electrolyte Characterization Approach

The candidate electrolytes are characterized using a number of approaches, including performing ionic conductivity and cyclic voltammetry measurements, and evaluating the performance characteristics in ~400 mAh three-electrode cells. Initially, cells are fabricated with either (a) MCMB /LiNi<sub>0.8</sub>Co<sub>0.2</sub>O<sub>2</sub> or (b) graphite/LiNi<sub>1/3</sub>Co<sub>1/3</sub>Mn<sub>1/3</sub>O<sub>2</sub> electrode couples. Other chemistries are evaluated depending upon availability from collaborators. In addition to performing charge/discharge characterization over a wide range of temperatures and rates on these cells, a number of electrochemical characterization techniques will be employed, including: (1) Electrochemical Impedance Spectroscopy (EIS), (2) DC linear (micro) polarization, and (3) Tafel polarization measurements. The electrochemical evaluation in three-electrode test cells enables electrochemical characterization of each electrode (and interface) and the identification of performance-limiting mechanisms. Electrodes are easily harvested from these test cells and samples are delivered to collaborators (i.e., URI and Hunter College). In addition to evaluating candidate electrolytes in spirally wound experimental cells, studies are also performed in coin cells, most notably in conjunction with high voltage cathode materials.

### Performance Demonstration

Performance testing of large capacity prototype cells containing candidate advanced electrolytes will be performed and evaluated under a number of conditions (i.e., assessment of wide operating temperature capability and life characteristics). JPL has on-going collaborations with a number of battery vendors and also has the capabilities to perform extensive testing. Typical prototype cells that will be considered include (i) Yardney 7 Ah prismatic cells, (ii) Quallion prismatic cells (0.300Ah

size), and (iii) A123 2.2 Ah cylindrical cells. Cells will be procured and obtained through on-going collaborations

### Results

We have investigated a number of ester containing electrolytes, namely methyl propionate and methyl butyrate-based electrolytes, in conjunction with electrolyte additives, with the intent of providing improved low temperature performance while still delivering acceptable high temperature resilience. More specifically, we have focused upon formulations consisting of LiPF<sub>6</sub> in ethylene carbonate (EC) + ethyl methyl carbonate (EMC) + methyl propionate (MP) or methyl butyrate (MB) (20:20:60 vol %) with and without electrolyte additives, including lithium oxalate, mono-FEC VC, and LiBOB. The identification of these esters, as well as the optimization of their concentrations in EC+EMC-based solutions, was based upon studies with MCMB-LiNiCoO<sub>2</sub> and LiNiCoAlO<sub>2</sub> systems.

Based upon these approaches, a number of methyl butyrate-based electrolytes were investigated with the anticipation that the high temperature resilience will be improved. These electrolytes have been shown to have improved performance in MCMB-LiNiCoO<sub>2</sub> and graphite-LiNi<sub>1/3</sub>Co<sub>1/3</sub>Mn<sub>1/3</sub>O<sub>2</sub> Li-ion cells, as described below. It should be noted that the use of these additives, in some cases, improved the low temperature rate capability (reported in FY'11).

After fully characterizing the low temperature performance and electrochemical characteristics at low temperature, the MCMB-LiNiCoO<sub>2</sub> cells containing methyl butyrate-based electrolytes were subjected to high temperature cycling (60°C and 80°C) and subsequent electrochemical characterization. A number of electrolyte additives improved the stability of the methyl butyrate system, especially FEC and VC, when exposed to high temperature cycling, especially on the MCMB anodes as evident from a low interfacial resistance from the EIS measurements (Figure IV - 100).

With respect to the LiNi<sub>x</sub>Co<sub>1-x</sub>O<sub>2</sub> cathodes, the cell containing the electrolyte with lithium oxalate was observed to display the lowest film and charge transfer resistance, as shown in Figure IV - 101, in contrast to the other additives studied. This suggests that either the lithium oxalate effectively retards the catalytic decomposition of the electrolyte salt anion (PF<sub>6</sub>) as anticipated, or it is beneficially participating in the cathode film formation process.

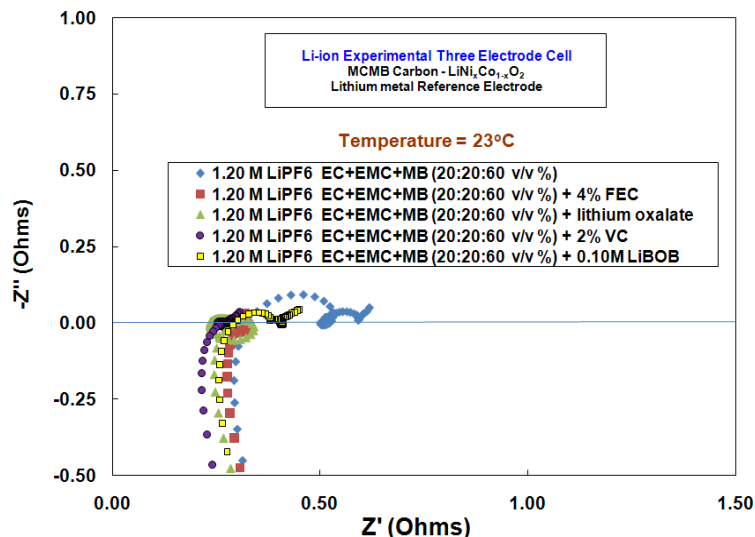


Figure IV - 100: EIS characteristics of MCMB anodes from MCMB-LiNi<sub>x</sub>Co<sub>1-x</sub>O<sub>2</sub> cells containing 1.0M LiPF<sub>6</sub> EC+EMC+MB (20:20:60 vol %) electrolytes with and without additives after high temperature cycling.

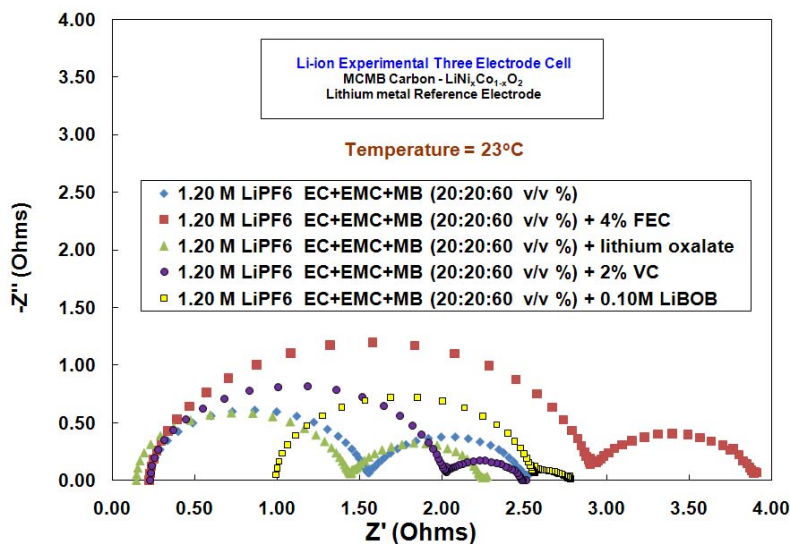


Figure IV - 101: EIS characteristics of LiNi<sub>x</sub>Co<sub>1-x</sub>O<sub>2</sub> cathodes from MCMB-LiNi<sub>x</sub>Co<sub>1-x</sub>O<sub>2</sub> cells containing 1.0M LiPF<sub>6</sub> EC+EMC+MB (20:20:60 vol %) electrolytes with and without additives after high temperature cycling.

Methyl butyrate-based electrolytes (with and without additives) have also been evaluated over a wide temperature with graphite-LiNi<sub>1/3</sub>Co<sub>1/3</sub>Mn<sub>1/3</sub>O<sub>2</sub> cells. In a similar fashion, the use of additives was observed to improve the low temperature rate capability as well as the high temperature resilience of the cells. The use of FEC and lithium oxalate were observed to improve the discharge rate capability at -40°C compared to the methyl butyrate system without any additive, as well as the all carbonate-based baseline electrolyte (i.e., 1.2M LiPF<sub>6</sub> in EC+EMC (30:70 vol%). The use of the electrolyte

additives were also observed to preserve the lithium kinetics at the anode after being subjected to cycling, as displayed by the dramatic difference in limiting current densities determined using Tafel polarization measurements on the graphite electrodes, Figure IV - 102. This finding suggests that either the electrolyte additives are resulting in a more desirable, protective SEI layer on the graphite anodes, or they are participating in a filming process at the LiNi<sub>1/3</sub>Co<sub>1/3</sub>Mn<sub>1/3</sub>O<sub>2</sub> electrodes which results in decreased electrolyte degradation and subsequent deposition of byproducts on the anode.

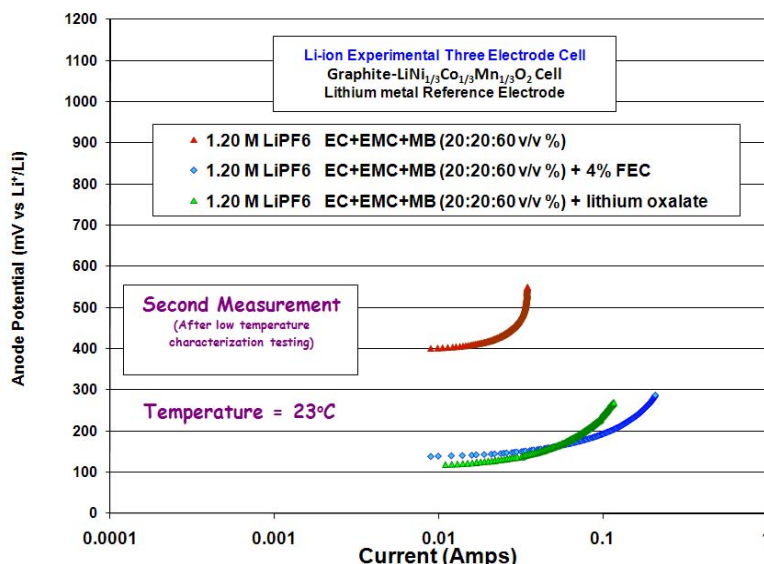


Figure IV - 102: Tafel polarization measurements performed at 23°C on graphite electrodes in contact with different MB-based electrolytes.

In collaboration with A123 Systems, two of the promising methyl butyrate-based electrolytes have been incorporated into 26650  $\text{LiFePO}_4$ -based Li-ion cells (2.20 Ah size) for evaluation (i.e., 1.20M  $\text{LiPF}_6$  in EC+EMC+MB (20:20:60 v/v %) + 4% FEC and 1.20M  $\text{LiPF}_6$  in EC+EMC+MB (20:20:60 v/v %) + 2% VC). A number of performance tests are on-going to assess the performance, including: (a) discharge rate performance at various temperatures (-60 to +25°C), (b) cycle life performance at various temperatures (i.e., 23°, 40°, and 50°C), (c) variable temperature cycling, and (d) current interrupt impedance measurements at various temperatures.

As part of the testing, we have performed discharge rate characterization over a wide temperature range (-60 to +20°C) using a number of rates (ranging from C/20 to 11.4C). Although the cells with the baseline electrolytes were observed to deliver negligible capacity at -40°C, excellent performance was demonstrated with the cells containing the methyl butyrate-based electrolytes, as shown in Figure IV - 103 and Figure IV - 104. The performance corresponds to over 90% of the room temperature capacity being delivered at -40°C at a 11.2C discharge rate (57-59 Wh/kg under these conditions). These systems have also

been observed to support up to 10C rates at temperatures as low as -50°C and C rates at -60°C.

The cycle life performance of these systems is also promising, with over 3,500 cycles (100% depth of discharge) being delivered at room temperature with over 90% of the initial capacity remaining (1.0C rate charge and discharge). Effort has also been focused upon evaluating the high temperature resilience of these systems by implementing a number of additional cycle life tests (i.e., at 40° and 50°C), as shown in Figure IV - 105. Thus far, the performance is encouraging with over 1600 cycles being delivered, with the cells containing the 1.20M  $\text{LiPF}_6$  in EC+EMC+MB (20:20:60 vol %) + 2% VC electrolyte behaving comparably to the baseline system, and the FEC containing variant displaying modestly increased capacity fade. We have also performed tests in which the cells are cycled between two temperature extremes (i.e., +40° and -20°C) to determine the impact of the high temperature exposure upon the low temperature performance. As shown in Figure IV - 106, the cell containing the methyl butyrate+VC performed comparably to the baseline system, illustrating promising lifetime characteristics over harsh conditions.

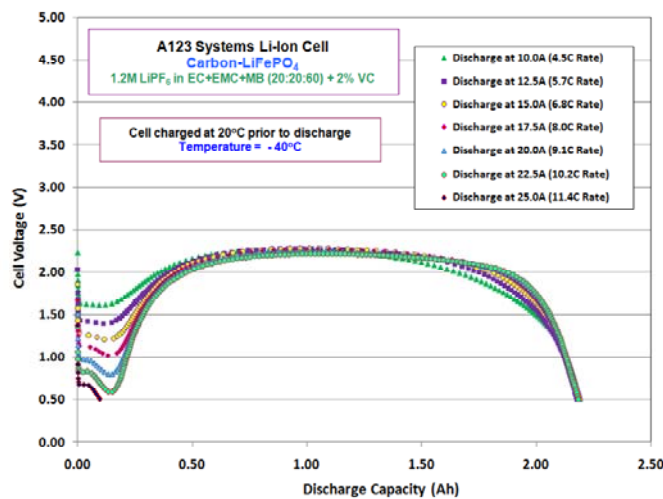


Figure IV - 103: Discharge rate characterization of a LiFePO<sub>4</sub>-based A123 cell at -40°C using high rate (4.5C to 11.2C). Cells contains 1.0M LiPF<sub>6</sub> EC+EMC+MB (20:20:60 vol %) + 2% VC. Cell was charged at room temperature prior to discharge.

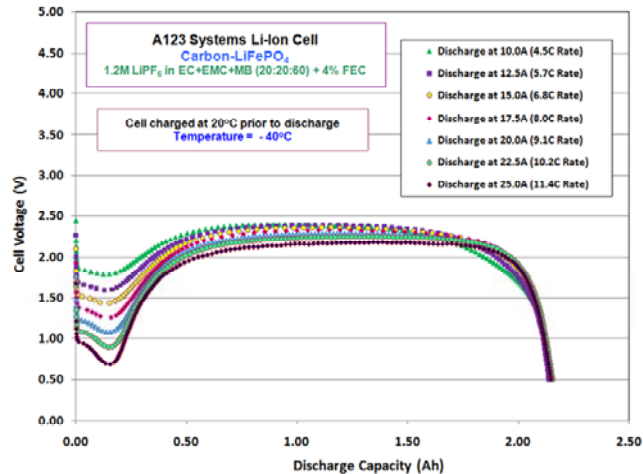


Figure IV - 104: Discharge rate characterization of a LiFePO<sub>4</sub>-based A123 cell at -40°C using high rate (4.5C to 11.2C). Cells contains 1.0M LiPF<sub>6</sub> EC+EMC+MB (20:20:60 vol %) + 4% FEC. Cell was charged at room temperature prior to discharge.

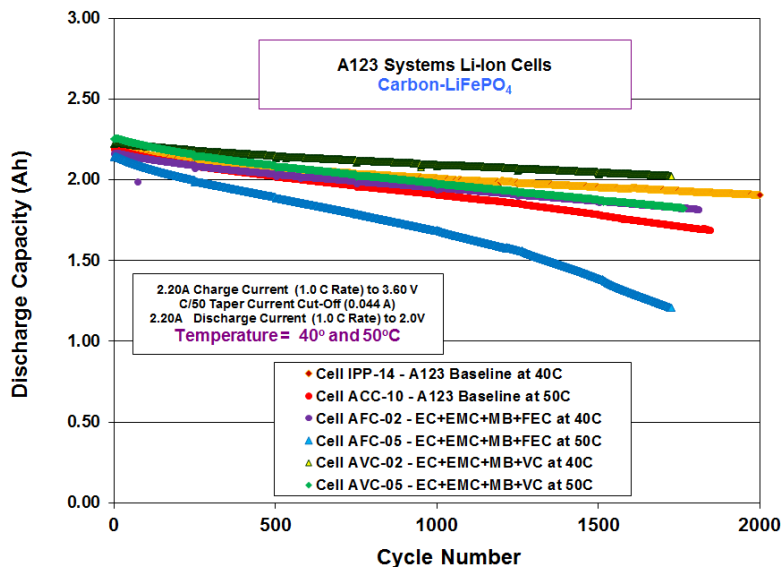


Figure IV - 105: Cycle life performance of LiFePO<sub>4</sub>-based A123 cells containing various electrolytes at +40°C and +50°C

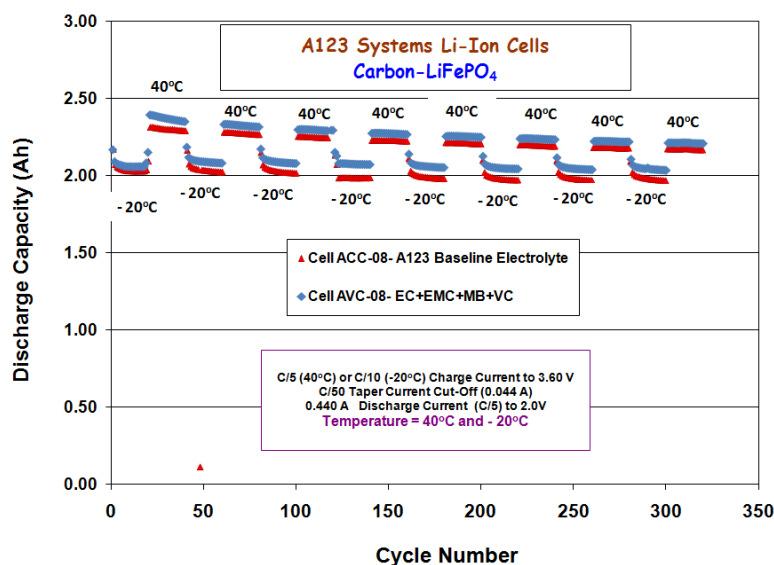


Figure IV - 106: Variable temperature cycling (+40° to -20°C) of LiFePO<sub>4</sub>-based A123 cells containing 1.20M LiPF<sub>6</sub> EC+EMC+MB (20:20:60 vol %) + 2% VC and the baseline electrolyte.

Continued efforts have been focused upon investigating the effect of using additional lithium electrolyte salts in conjunction with LiPF<sub>6</sub> to serve as electrolyte additives, with the intent of improving the high temperature resilience of the cells. Specifically, we have studied electrolytes that contain LiBOB, lithium hexafluoro isopropoxide, and a lithium malonate borate-based salt (LiDMMDFB) developed by LBNL and the URI (Li Yang, John Kerr, and Brett Lucht). With MCMB-LiNiCoO<sub>2</sub> cells containing these electrolytes, we have performed the electrochemical evaluation (i.e., EIS, linear and Tafel polarization), discharge rate characterization, and exposure to high temperature. These electrolyte

additives have been investigated in various formulations, including both ester based and all carbonated-based electrolytes.

We have also focused on evaluating various ester-based electrolytes in conjunction with high voltage cathode materials. For example, we have investigated the performance of a number of electrolytes with the MPG-111 graphite/Toda LiNiMnCoO<sub>2</sub> system. It should be noted that emphasis was placed upon utilizing commonly used carbonaceous anode materials, rather than lithium metal, to establish the compatibility of the electrolyte systems. Good reversibility was observed with methyl

butyrate-based electrolytes, with over 230 mAh/g capacity delivered (based on active cathode material). When a number of cells were subjected to 100% DOD cycling using C/10 rates (4.60V to 3.0V), cells containing a methyl-butyrates based solution containing LiBOB as an electrolyte additive outperformed the baseline all carbonate-based blend.

Recent work has also focused upon developing a number of wide operating temperature range electrolytes that operate well with the high voltage  $\text{LiNi}_{0.50}\text{Mn}_{1.50}\text{O}_2$  (LMNO) cathode. A number of  $\text{Li}_4\text{Ti}_5\text{O}_{12}$  (LTO)/LMNO cells were fabricated with electrodes provided by ANL. Preliminary results with a methyl butyrate electrolyte solution are very encouraging, with comparable formation characteristics and rate capability observed to the baseline electrolyte. Furthermore, when the cells were subjected to 100% DOD cycle life testing, the cells containing the methyl butyrate-based electrolyte outperformed the all carbonate-based blend, as shown in Figure IV - 107. Current efforts are focused upon evaluating the effectiveness of utilizing various electrolyte additives with these electrolytes to improve the cycle life performance of this system, while also providing the capability to operate over a wide temperature range. Furthermore, these efforts will be extended to other high voltage systems recently received from ANL (e.g.,  $\text{LiNiCoMnO}_2$ ) and similar materials obtained from in-house programs.

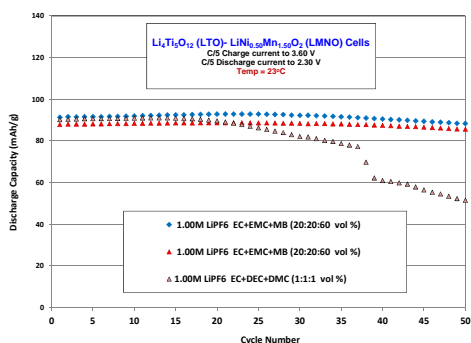


Figure IV - 107: Cycle life performance of LTO/ LMNO cells containing various electrolytes.

## Collaborations

During the course of this program, we have collaborated with a number of institutions, including: (a) Univ. Rhode Island (Brett Lucht: perform analysis of harvested electrodes, on-going collaborator), (b) ANL (Khalil Amine: source of electrodes, on-going collaborator), (c) LBNL (John Kerr) (evaluation of novel salt), (d) A123 Systems, Inc. (electrolyte development, on-going collaborator), (e) Quallion, LCC. (electrolyte development, on-going collaborator), (f) Yardney Technical Products (electrolyte development, on-going collaborator), (g) Saft America (collaborator, industrial

partner under NASA program), (h) NREL (Smith/Pesaran) (supporting NREL in model development by supplying data), and (i) the Univ. of Southern California (Prof. Prakash, electrolyte salt development).

## FY 2011 Publications/Presentations

1. M. C. Smart, B. V. Ratnakumar, K. B. Chin, and L. D. Whitcanack, "Lithium-Ion Electrolytes Containing Ester Cosolvents for Improved Low Temperature Performance", *J. Electrochem. Soc.*, **157** (12), A1361-A1374 (2010)
2. N. Leifer, M. C. Smart, G. K. S. Prakash, L. Gonzalez, L. Sanchez, P. Bhalla, C. P. Grey, and S. G. Greenbaum, " $^{13}\text{C}$  Solid State NMR Study of SEI Formation in Carbon Lithium Ion Anodes Cycled in Isotopically Enriched Electrolytes Suggests Unusual Breakdown Products", *J. Electrochem. Soc.*, **158** (5), A471-A480 (2011).
3. M. C. Smart and B. V. Ratnakumar, "Effect of Cell Design Parameters on Lithium Plating in Lithium-Ion Cells", *J. Electrochem. Soc.*, **158** (4), A379-A389 (2011).
4. M. C. Smart, B. V. Ratnakumar, W. C. West, and E. J. Brandon, "Primary and Secondary Lithium Batteries Capable of Operating at Low Temperatures for Planetary Exploration", Lunar Superconductor Applications, 1<sup>st</sup> International Workshop, Houston Texas, March 3-5, 2011.
5. M. C. Smart, A. S. Gozdz, L. D. Whitcanack, and B. V. Ratnakumar, "Improved Wide Operating Temperature Range of High Rate Nano-Lithium Iron Phosphate Li-Ion Cells with Methyl Butyrate-Based Electrolytes", 220<sup>th</sup> Meeting of the Electrochemical Society, Boston, MA, October 11, 2011.
6. S. Dalavi, M. C. Smart, B. L. Lucht, F. C. Krause, and B. V. Ratnakumar, 220<sup>th</sup> Meeting of the Electrochemical Society, Boston, MA, October 10, 2011.

The work described here was carried out at the Jet Propulsion Laboratory, California Institute of Technology, under contract with the National Aeronautics and Space Administration (NASA).

---

## IV.B.4.6 Novel Phosphazene-Based Compounds to Enhance Electrolyte Safety and Stability for High Voltage Applications (INL)

Kevin L. Gering, PhD

Idaho National Laboratory  
2525 N. Fremont Ave.  
Idaho Falls, ID 83415-2209  
Phone: (208) 526-4173; Fax: (208) 526-0690  
E-mail: [kevin.gering@inl.gov](mailto:kevin.gering@inl.gov)

Collaborators (INL): Mason K. Harrup, Harry W. Rollins, Sergiy V. Sazhin, Fred F. Stewart  
(non-INL): John Burba, Princess Energy Systems

Contract No. DE-AC07-05ID14517

Start Date: January, 2009  
Projected End Date: ongoing

### Objectives

Our focus is on producing electrolyte compounds resilient in both temperature and voltage regimes, while meeting a competitive baseline performance in transport properties and SEI characteristics. We seek compounds that will:

- enable prolonged usage of advanced higher-voltage electrode couples,
- promote better safety performance under abuse conditions,
- enhance cell life.

Another objective is to gain fundamental understanding of molecular-scale interactions between phosphazenes and other electrolyte species and cell components.

### Technical Barriers

Safety and longevity of Li-ion batteries continues to be an issue for vehicular applications. This is complicated by the drive toward higher voltage cells (5V+) and some usage patterns and conditions that would cause batteries to operate at higher temperatures. A viable alternative electrolyte for Li-ion batteries must simultaneously meet multiple criteria regarding transport properties, SEI film formation, voltage stability, flammability, aging mechanisms, chemical compatibility, performance at high and low temperatures, etc. A fundamental challenge remains to produce electrolyte components that will

provide noteworthy levels of flame retardance while reducing viscosity to competitive levels to maintain attractive transport properties, and some success has been had at the INL toward that goal. Also, since this work involves numerous analysis techniques, chemical synthesis, and cell testing, it requires considerable commitment of resources in terms of qualified personnel in diverse areas.

### Technical Targets

With regard to higher voltage systems, our targets are split between three primary classifications:

- *Phosphazenes as primary solvents* (>40%) to greatly reduce electrolyte flammability. These must meet specific requirements for the resultant electrolyte blends to approach a competitive basis. Our requirements for the pure phosphazene (with lithium salt) to be viable as a primary solvent: room temperature viscosity less than 5 cP, conductivity greater than 4 mS/cm, and lithium salt (LiPF<sub>6</sub>) solubility at least 0.6 M.
- *Phosphazenes as cosolvents* (10-40%) to provide mixed benefits of reduced electrolyte flammability and prolonged cell life. Properties for the pure salted phosphazene to be defined as a cosolvent: room temperature viscosity within 5-40 cP, conductivity 0.2-4 mS/cm, and lithium salt solubility within 0.2-0.6 M.
- *Phosphazenes as additive solvents* (≤10%) to enhance chemical/thermal stability of the bulk electrolyte and improve SEI properties in terms of thermal runaway and stability over life. Viable cosolvent candidates are defined as follows: room temperature viscosity exceeds 40 cP, conductivity ≤ 0.2 mS/cm, and lithium salt solubility < 0.2 M.
- Candidate INL phosphazene additives must be compatible with the cell environment, promoting stability/longevity of cell components, particularly in terms of the operating voltage window of the electrode couple. INL testing and abuse testing at SNL looks squarely at how these compounds provide benefit to cell operation, safety, and life.
- We have initiated dialog with DOE and ANL regarding scale-up of best phosphazene candidates.

## Accomplishments

- Early generations of heterocyclic phosphazene compounds have been synthesized, characterized, and tested in coin cells, including our first series of ionic liquid solvents. More efficient and economical synthesis routes have been found for some classes of compounds to decrease manufacturing costs.
- Further studies confirmed that low amounts of phosphazenes (as low as 1%) greatly enhance the chemical/thermal stability of the baseline electrolyte, as evidenced in prolonged studies performed at 60 °C.
- Abuse testing at SNL began with three INL additives (SM6, FM2, PhIL-2) shipped, and we await results for ARC and flammability testing. Best candidates from abuse testing are candidates for the ANL Materials Scale-up facilities.
- Extensive coin cell testing has been performed, using the INL electrolyte blends against ABR-relevant electrode couples, including LNMO/LTO, NMC (3M)/graphite, and NMC (Toda)/graphite. To date, results show good compatibility of phosphazenes with the various cell environments, promoting stability at elevated temperatures.
- We improved and expanded our methods for voltammetric electrolyte and interface characterization, which has the potential of being an important new tool for materials selection.
- DFT modeling has established trends between molecular configuration and solvent-to-lithium binding energy. Our ionic liquid additives show appreciable decreases in association with lithium, which will improve charge transfer efficiency.



## Introduction

Electrolytes play a central role in performance and aging in most electrochemical systems. As automotive and grid applications place a higher reliance on electrochemical stored energy, it becomes more urgent to have electrolyte components that enable optimal battery performance while promoting battery safety and longevity. Safety remains a foremost concern for widespread utilization of Li-ion technology in electric-drive vehicles, especially as the focus turns to higher voltage systems (5V). This work capitalizes on the long established INL expertise regarding phosphazene chemistry, aimed at battery-viable compounds that are highly tolerant to abuse. Various references document or relate to this work [1-4].

## Approach

The general heterocyclic phosphazene structure is given as shown in

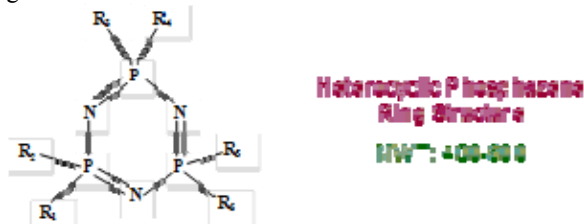


Figure IV - 108.

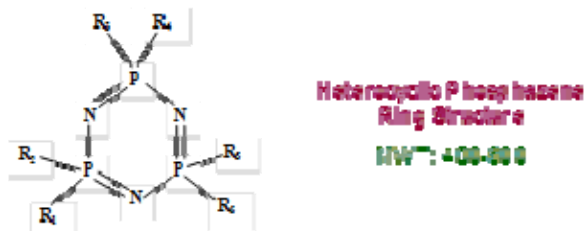


Figure IV - 108: General Heterocyclic Phosphazene Structure

A change of chemical structure in the ring pendant arms has a strong influence on electrolyte properties, performance, and longevity in a higher-voltage system (5V+) and at higher temperatures. By customizing the pendant structures we seek to improve transport properties while increasing flash point and having acceptable SEI characteristics and cell aging. We are seeing progress in this fundamental challenge as we advance our knowledge of structure-property relationships. Benefits include inherent stability and non-flammability, very low vapor pressure, good lithium salt dissolution, and choice of R groups (pendant arms) can be customized to precisely engineer properties. Challenges would include high viscosity and the need to attenuate N:Li<sup>+</sup> attraction that occurs due to electron doublet transfer. To date our numerous compounds derive from the following four groups:

- SM:** ether groups attached to the phosphorus centers
- AL:** unsaturated analogues of the SM series
- FM:** fluorinated analogues of the SM series
- PhIL:** based on an ionic liquid structure.

The ionic liquid series helps to mitigate some of the limitations seen with traditional cyclic phosphazenic solvents, such as N:Li<sup>+</sup> association that can adversely affect conductivity. Non-cyclic phosphazene compounds are also being targeted, and salts other than LiPF<sub>6</sub> are being considered.

We employ a number of diverse testing and characterization methods to determine viability of candidate compounds, including advanced voltammetry techniques, coupled viscosity and conductivity analysis, flash point, EIS, cell testing, as well as DFT modeling. Coin cells (type 2032) are used to test candidate

electrolytes in an actual cell environment, covering crucial issues of formation, interfacial impedance, polarization testing, and aging.

## Results

Summarized below are salient results from 2011 research. For brevity, only representative samplings are given. The baseline (BL) electrolyte in all cases is 1.2M  $\text{LiPF}_6$  in EC-EMC (2:8, wt.).

Figure IV - 109 attests that INL SM-series phosphazene additives extend the electrochemical window (EW) past what is achievable with the BL electrolyte. Presence of the phosphazene more than doubles the EW past the BL value. In a sense, these additives act to moderate the oxidative processes at the positive electrode, and hence enhance stability at higher voltages. In these studies Ni metal was the working electrode at potentials negative to OCV, while Al was used positive to OCV. Li metal served as both the counter and reference electrodes.

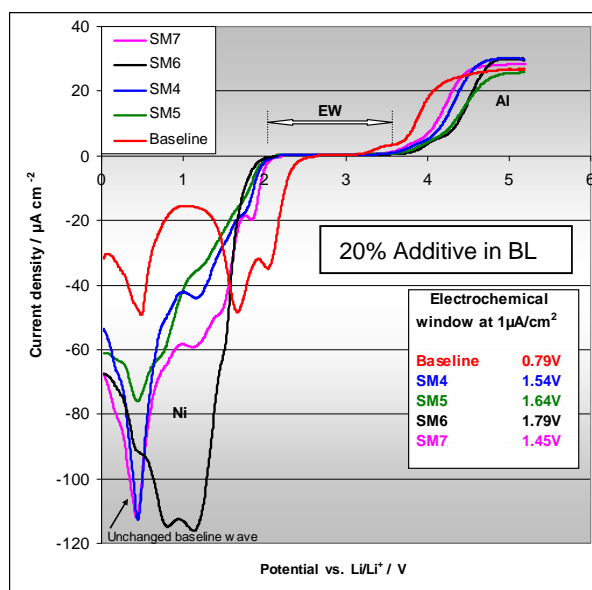


Figure IV - 109: Electrochemical Properties of SM-series Phosphazene Additives

INL phosphazene additives promote chemical stability of the baseline electrolyte, making it more tolerant to higher temperatures. In Figure IV - 110, our stability testing is summarized for selected SM compounds for tests maintained at 60°C for a minimum of 60 days. The coloration of the baseline electrolyte over time is due to degradation processes, resulting in a thick, dark mass at 60 days, while the colors of the phosphazene containing samples were largely unchanged over the study, even at levels as low as 1% (the SM7 samples were known to contain tens of ppm water, and hence underwent a higher degree of degradation). These results complement those of 2010, wherein similar results were seen for other SM and FM compounds.

Cell testing was performed using 2032-type coin cells to judge performance of the electrolytes using a number of metrics. The electrode couples included

- $\text{LiNi}_{0.5}\text{Mn}_{1.5}\text{O}_4 / \text{Li}_4\text{Ti}_5\text{O}_{12}$ ,
- $\text{LiNi}_{1/3}\text{Mn}_{1/3}\text{Co}_{1/3}\text{O}_2$  (3M) / Graphite, and
- $\text{LiNi}_x\text{Mn}_y\text{Co}_z\text{O}_2$  (Toda) / Graphite.

Figure IV - 111(A) and Figure IV - 111(B) summarize the early life capacity performance of coin cells using the first two couples above, having SM4, SM6, FM2, and PhIL-1 at 10 and/or 3 wt% in the baseline. In Figure IV - 111(A), cell polarization is most evident at highest cycling rate and highest additive content (10%). Final C/10 capacities are all higher than initial set, with no apparent cell aging.

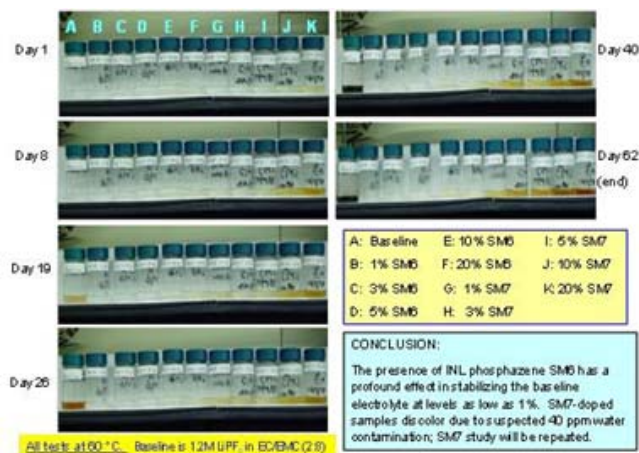


Figure IV - 110: Summary of Stability Testing for Selected SM Compounds

Whereas Figure IV - 111(B) shows that cell polarization is higher for the NMC/graphite set, probably due to impedance tied to EIS HF arc. Final C/10 capacities are slightly lower than initial set. Lastly, Figure IV - 111(B) indicates that all additives yield similar cell performance, with only subtle differences noted between electrolytes having 3 and 10% additives, and at each rate. Work with NMC (Toda)/graphite is ongoing, and  $\text{LiNi}_{0.8}\text{Co}_{0.15}\text{Al}_{0.05}\text{O}_2$  (Toda) / Graphite will be tested early in 2012.

To aid molecular design, DFT modeling was performed to look at molecular interactive properties of phosphazene electrolyte materials. This was performed using Gaussian03, B3LYP, 6311-G(d,p) basis set. All structures are minima with no imaginary frequencies. Several representative phosphazenes were modeled that

contained various pendent groups (ethoxy, isopropoxy, etc.), and the binding enthalpies were found to vary between 65-98 Kcal/mol for several cases of charge-neutral solvent molecules. This exceeds the single-ligand binding between ethylene carbonate and lithium, ( $\approx 50$  Kcal/mol). Thus, we sought to produce compounds that would greatly diminish this interaction, since high binding energies would prove problematic in the lithium desolvation step and cause charge transfer to be less efficient. Figure IV - 112 shows the results for DFT modeling of our early ionic liquid phosphazene additive, wherein we investigated the relative distance of the cationic moiety from the phosphazene core.

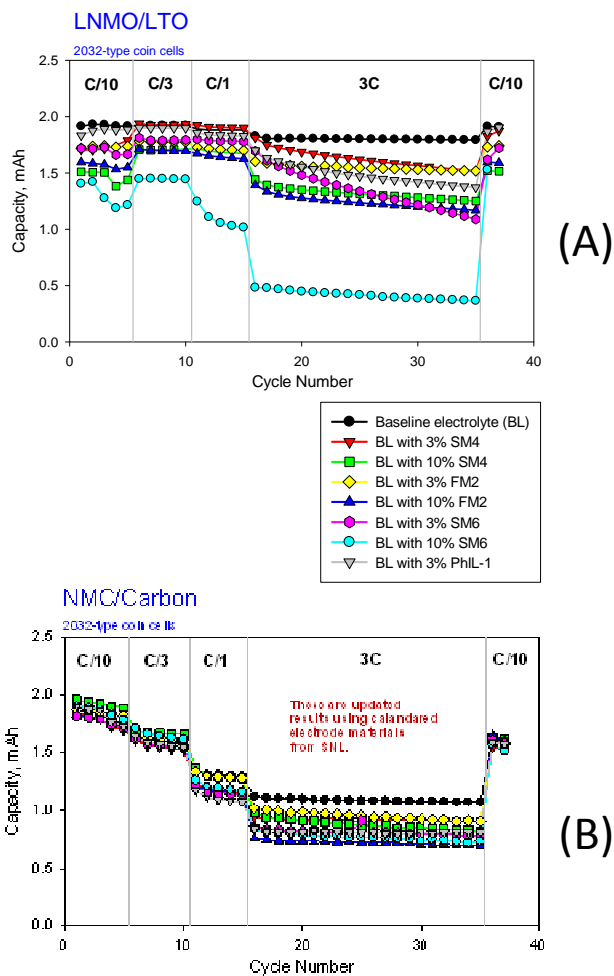


Figure IV - 111: Early life Capacity Performance of Coin Cells: (A) Cell Polarization Evident at Highest Cycling Rate and Highest Additive Content (10%), and (B) Cell Polarization for the NMC/graphite set.

Lastly, Figure IV - 113 demonstrates part of our expanded capability to synthesize phosphazene compounds, demonstrating our commitment to provide sufficient

amounts of materials for testing and characterization at INL, SNL, and other DOE-partnered labs.

DFT Results for Nitrogen-to-Li<sup>+</sup> Binding Energy for Various Design Configurations of Gen1 Ionic Liquid Phosphazene (strongest binding site shown)

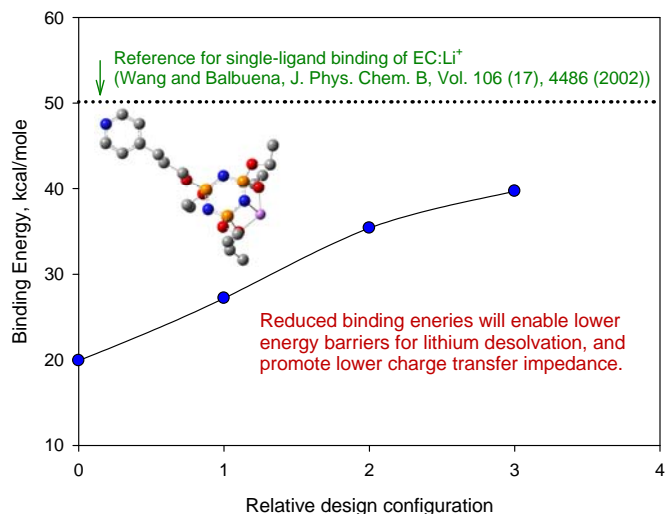


Figure IV - 112: Results of DFT modeling of INL Early Ionic Liquid Phosphazene Additive



Figure IV - 113: Expansion of INL Capabilities to Synthesize Phosphazene Compounds

## Conclusions and Future Directions

INL phosphazene materials improve electrolyte stability at higher voltage and elevated temperatures. The choice of the pendant R groups profoundly influences electrolyte properties tied to fate and performance in Li-ion cells, and is used to customize these molecules. Ionic liquid phosphazenes drastically reduce the inherent association between nitrogen and Li<sup>+</sup>. In FY 12 we will explore electrolytes having mostly phosphazene solvents to exploit their low flammability, wherein non-cyclic phosphazene compounds will be targeted to reduce viscosity. Newer compounds within the FM and PhIL series will indicate whether these structures provide superior benefit compared to other phosphazenes. NMR studies will be performed with a new probe that is capable

of 2-dimensional experiments with fluorine in combination with any other nucleus. Half-cell studies on SEI will be considered. Initial SNL abuse-tolerance testing will be completed, and we will collaborate with ANL regarding scale-up of INL phosphazene compounds.

## FY 2011 Publications/Presentations

1. K. L. Gering, "Novel Compounds for Enhancing Electrolyte Stability and Safety of Lithium-ion Cells", 2011 DOE-VTP Annual Merit Review Meeting Presentation, Project ES027.
2. S. V. Sazhin, M. K. Harrup, K. L. Gering, "Characterization of low-flammability electrolytes for lithium-ion batteries". *J. Power Sources*, v. 196 (2011) 3433-3438.
3. Sergiy V. Sazhin, Mason K. Harrup, Harry W. Rollins, Kevin L. Gering, "Investigation of Phosphazene-based Low Flammability Electrolytes for PHEV Batteries", Pacific Power Source Symposium, January 10-14, 2011. (Waikoloa, HI).
4. U. S. Patent Application 13/253,707, "IONIC LIQUIDS, ELECTROLYTE SOLUTIONS INCLUDING THE IONIC LIQUIDS, AND ENERGY STORAGE DEVICES INCLUDING THE IONIC LIQUIDS", K. L. Gering, M. K. Harrup, and H. W. Rollins (Idaho National Laboratory), 2011.

---

## IV.C Calendar and Cycle Life Studies

### IV.C.1 Diagnostics and Modeling

#### IV.C.1.1 Electrochemistry Cell Model (ANL)

Dennis Dees and Kevin Gallagher

Argonne National Laboratory  
9700 South Cass Avenue  
Argonne, IL 60439-4837  
Phone: (630) 252-7349; Fax: (630) 972-4520  
E-mail: [dees@anl.gov](mailto:dees@anl.gov)

**Collaborators:**

Daniel Abraham, Argonne National Laboratory  
Sun-Ho Kang, Argonne National Laboratory  
Andrew Jansen, Argonne National Laboratory  
Wenquan Lu, Argonne National Laboratory  
Kevin Gering, Idaho National Laboratory

Start Date: October, 2008

Projected End Date: September, 2014

#### Objectives

- The objective of this work is to correlate analytical diagnostic results with the electrochemical performance of advanced lithium-ion battery technologies for PHEV applications.
- Link experimental efforts through electrochemical modeling studies.
- Identify performance limitations and aging mechanisms.

#### Technical Barriers

The primary technical barrier is the development of a safe cost-effective PHEV battery with a 40 mile all electric range that meets or exceeds all performance goals.

- Interpreting complex cell electrochemical phenomena.
- Identification of cell degradation mechanisms.

#### Technical Targets

- Advance development of PHEV focused electrochemical models in support of programmatic goals. (September, 2014)
- Identify new differential algebraic equation solver package with enhanced capabilities and complete conversion of existing models to newly adopted package. (September, 2011)
- Complete implementation and initial testing of full SEI growth model. (December, 2012)
- Initiate parameter estimation of high-energy NMC/graphite system. (March, 2012)

#### Accomplishments

- Adopted new differential equation solver software (PSE gPROMS) to address several long term issues limiting model advancement.
  - Integrating complex dynamic interfaces into full cell Li-ion models to examine factors limiting performance and life.
  - Streamlining parameter estimation for new cell chemistries.
  - Implementing the AC impedance version of model with increasingly more intricate interfacial and bulk active particle phenomena.
- Implemented SEI growth model on the negative electrode to analyze capacity fade mechanisms including cross-interactions with positive electrode.
- Developed 3D electrochemical model to examine primary-secondary active particle microstructure and properties affecting impedance (e.g. porosity, surface area, electronic conductivity, electronic contacts, geometry, and electrolyte wetting).
- Utilized electrochemical model to further examine electrode thickness limitations.



## Introduction

The electrochemical modeling effort is aimed at associating electrochemical performance measurements with post-test diagnostic studies conducted on lithium-ion cells. The methodology for the electrochemical model is described in detail in the literature.<sup>19,20,21</sup> Two versions of the model are utilized in this effort. One version of the electrochemical cell model is used to simulate the cell response from Electrochemical Impedance Spectroscopy (EIS) studies, and the other model version is utilized for examining DC studies, such as controlled current or power cycling and diagnostic HPPC tests. The underlying basis for both models is the same, as well as their parameter set.

The general methodology for the electrochemical model follows the work of Professor Newman at Berkeley. Continuum based transport equations using concentrated solution theory describe the movement of salt in the electrolyte. Volume-averaging of the transport equations accounts for the composite electrode geometry. Electrode kinetics, thermodynamics, and diffusion of lithium in the active material particles are also included. The detailed theoretical description of the active material/electrolyte interface, commonly referred to as the solid electrolyte interphase or SEI, is based on post-test analytical diagnostic studies. The SEI region is assumed to be a film on the active material and layer at the surface of the active material. The film is taken to be an ill-defined mixture of organic and inorganic material through which Li-ions from the electrolyte must diffuse and/or migrate across to react electrochemically at the surface of the active material. The lithium is then assumed to diffuse through the surface layer and into the bulk active material in the particle. Capacitive effects are incorporated into the model at the electrochemical interfaces and a localized electronic resistance between the current carrying carbon and the oxide interface can also be included. The model can also accept multiple particle fractions with unique characteristics.

## Approach

The approach for electrochemical modeling activities is to build on earlier successful characterization and modeling studies in extending efforts to new PHEV technologies. The earlier studies involved developing a model based on the analytical

diagnostic studies, establishing the model parameters, and conducting parametric studies with the model. The parametric studies were conducted to gain confidence with the model, examine degradation mechanisms, and analyze cell limitations. Efforts this year have focused on expanding and improving the model's capabilities.

## Results

**Electrochemical Active Material Particle Model Development and Simulation.** A three-dimensional electrochemical model was developed to examine primary-secondary active particle microstructure and properties affecting impedance (e.g. porosity, surface area, electronic conductivity, electronic contacts, and electrolyte wetting). Microscopy and other analytical studies on many positive active materials indicate that their secondary particle microstructure has some degree of porosity, such that electrochemical reactions can penetrate into the secondary particles. A previously developed electrochemical model with a simplified SEI relation was applied on the particle scale. A secondary particle was assumed to be made of primary particles with independent core and outer layer characteristics. The particle porosity allows access of electrolyte and ionic current to reach into the particle core.

A wealth of diagnostic studies and associated model development for NCA active material with Gen 2 (EC/EMC/LiPF<sub>6</sub>) electrolyte was utilized to create a baseline parameter set and particle characteristics. Simple relations were also developed for the active material surface area and tap density based on changes in particle porosity. Two specific impedance terms were used to describe particle performance: area specific impedance (ASI), based on particle active area (i.e. not the electrode area), and particle mass specific impedance (MSI). In general, when the ratio of active area to mass is fixed then both impedance effects behave similarly, as is the case for the change in particle impedance with applied voltage.

The impact of electronic conductivity on particle performance is shown in Figure IV - 114. At effective electronic conductivities less than about  $10^{-5} \Omega^{-1} \text{ cm}^{-1}$  the particle impedance is a strong function of conductivity, while the impedance is governed by other phenomena at greater conductivities. Similarly, the particle impedance is relatively independent of the number of contacts and the diameter of the particle contacts for effective electronic conductivities greater than  $10^{-4} \Omega^{-1} \text{ cm}^{-1}$ .

<sup>19</sup> D. Dees, E. Gunen, D. Abraham, A. Jansen, and J. Prakash, *J. Electrochem. Soc.*, **152** (7) (2005) A1409.

<sup>20</sup> D. Abraham, S. Kawauchi, and D. Dees, *Electrochim. Acta*, **53** (2008) 2121.

<sup>21</sup> D. Dees, E. Gunen, D. Abraham, A. Jansen, and J. Prakash, *J. Electrochem. Soc.*, **155** (8) (2008) A603.

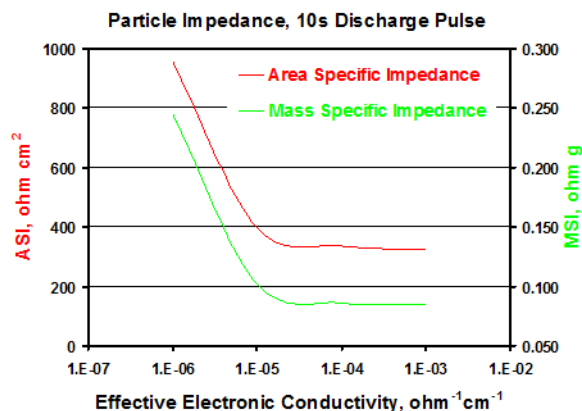


Figure IV - 114: Impact of electronic conductivity on particle performance.

It is much easier for Li ions to diffuse through the liquid electrolyte than the solid-state oxide active material by a factor of about  $10^4$ . Therefore, even a small amount of electrolyte in the oxide particle pores can enhance the overall electrochemical reaction in the core of the particle and reduce its impedance. As the particle porosity increases, its active surface area rises dramatically reducing the particle impedance on a gravimetric basis. However, for a fixed applied polarization, the particle impedance on an active area basis rises significantly with increasing porosity. As the porosity increases, there is less active material available for the lithium to diffuse into, resulting in increasingly higher concentration polarization and ASI.

The three-dimensional electrochemical particle model, described above, was further modified to study spheroid shaped particles. To simplify the studies three types of particle shapes were examined: spherical (adopted in original modeling study with an aspect ratio = 1), potato ( $1 < \text{aspect ratio} < 4$ ), and saucer ( $1 < \text{aspect ratio} < 4$ ). As an initial test case for this model, the spherical-particle-shaped carbon anode material being developed in this program was examined. An approximate sloping voltage discharge curve was estimated from half-cell cycling data with the graphitized material. A reasonable estimate was made for the diffusion coefficient of lithium through the carbon, based on previous work on graphite negative electrodes. Initial studies were conducted assuming isotropic transport properties, an assumption that can be changed for examining highly graphitized material. The core of the particle was considered dense and a relatively thin shell was added with limited porosity to account for the measured surface area.

Initial simulations with the three particle shapes were conducted with all particles having the same volume and active area. The particle impedances are given in Figure IV - 115 for a ten minute step in potential

applied to each of the particles. In general, the transport of lithium through the electrolyte around the particle is much faster than the solid-state transport of lithium through the carbon. This combined with the relatively high interfacial impedance makes the current distribution across the active area relatively uniform, despite changes in the particle shape. For short times, the impedance of all three particle shapes is similar. As the time increases, the concentration gradients reach further into the particles and the shorter diffusion length of the non-spherical particles is advantageous. These simulations are continuing by examining the impact of anisotropic solid-state diffusion coefficients.

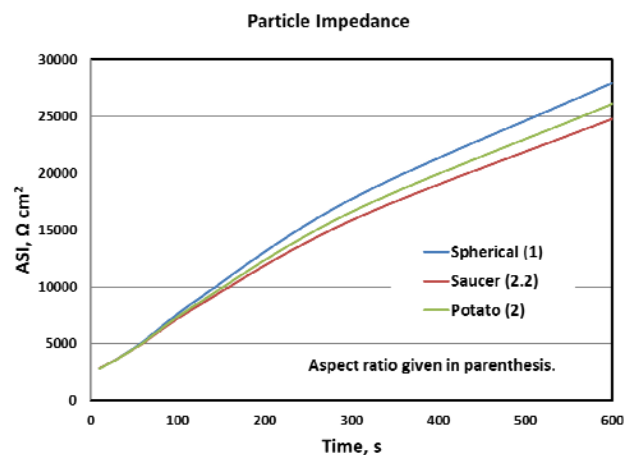


Figure IV - 115: Impact of particle shape on performance.

**Electrochemical Cell Model Utilized to Examine Electrode Thickness Limitations.** Battery design studies point out the advantages of going to thicker electrode coatings. The electrochemical model was utilized to further examine electrode thickness limitations. As shown in Figure IV - 116, the cell discharge capacity effectively reaches a limiting capacity with increasing electrode thickness. Lowering the discharge current allows for a greater fraction of the electrode capacity to be utilized. As electrode thickness increases transport of salt in electrolyte limits the constant C-rate discharge capacity (i.e. the salt concentration in the positive electrode approaches zero). Increasing the electrode thickness also affects the current distribution in the electrodes. Because Li-ion electrodes typically have a large interfacial impedance compared to other impedance phenomena in the cell, thinner electrodes (i.e.  $\sim \leq 150 \mu\text{m}$  for 1C discharge) have a relatively uniform current distribution. However, electrolyte transport limitations in thick electrodes shifts the initial current towards the separator, which gradually changes throughout the discharge.

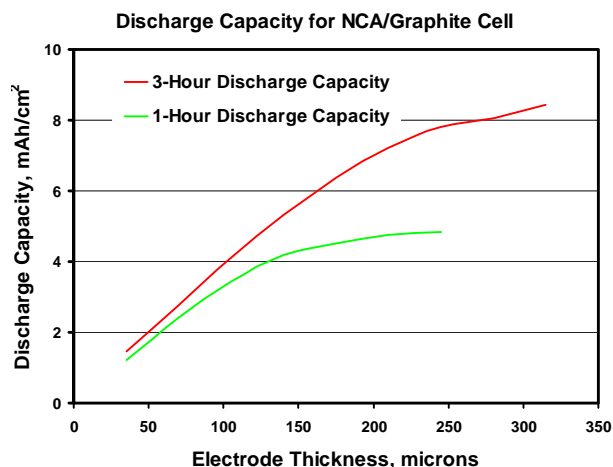


Figure IV - 116: Li-ion cell discharge capacity as a function of electrode thickness.

As shown in Figure IV - 117, the electrode impedance is relatively constant over a wide thickness range. The impedance of thin electrodes increases as the active area decreases, and for thick electrodes the cell impedance increases resulting from electrolyte transport limitations. However, the primary performance limitation for thick electrodes is that thicker graphite negatives can dip below the lithium deposition voltage during regen charging pulses.

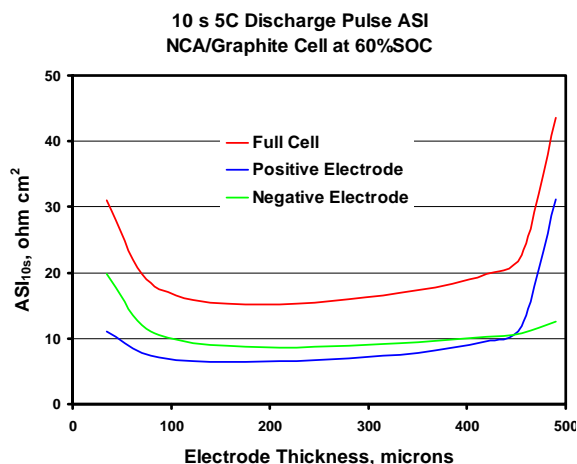


Figure IV - 117: Cell and electrode impedance.

**Efficiently Solving Increasingly Complex Electrochemical Cell Models.** This project has been continually challenged by finding efficient ways to solve increasingly complex electrochemical cell models that are typically comprised of dynamic coupled one-dimensional multi-scale subsystems. A search for a new solver program was initiated. As a result, a new differential equation solver package (PSE gPROMS) was identified. This package should be able to address several long term issues limiting model advancement. These challenges include: integrating complex dynamic

interfaces into full cell Li-ion models to examine factors limiting performance and life; streamlining parameter estimation for new cell chemistries; and implementing the AC impedance models with increasingly more intricate interfacial and bulk active particle phenomena.

Previously, coupled multi-scale problems were solved using a multi-dimensional solver. The new solver program explicitly treats each length scale to allow for greater stability and increased dynamic complexity. As an example, in the past full cell DC modeling studies with complex interfacial phenomena could not be conducted without considerable stability problems. The new solver program is able to recreate the earlier studies without the troubling stability issues.

Parameter estimation is always a serious challenge when dealing with the complex phenomenological modeling used in this project. Previous efforts used a “hand-fit” approach where the modeler systematically varied parameters to find a “best-fit” to the eye of the user. The new software package has parameter estimation algorithms and statistical assessment of the solution. Parameter estimations for new chemistries in both the DC and AC versions of the model will be streamlined enabling greater speed in modeling chemistries being evaluated in the program. We have set-up the parameter estimation for the DC model and begun evaluating some of the previous values used.

**SEI Growth Model Development.** Work is progressing on implementing the SEI growth model necessary to understand power and energy fade in future Li-ion cell builds. Differing negative electrode aging behavior between battery technologies is being examined to establish a baseline set of parameters. The deposition of cations into the SEI is known to accelerate capacity fade; although, the exact mechanism has yet to be proven. We suggest that the mobility of the negative charge carrier in the SEI is the limiting factor for capacity fade during calendar-life testing at moderate and high states of charge. The reduction of cations to metals under certain conditions will lead to an enhanced mobility of negative charge in the SEI. Current model development involves inclusion of the appropriate equations to capture this side reaction that may govern an interplay between the cathode and anode.

## Conclusions and Future Directions

It is apparent from experimental studies on lithium and manganese rich NMC materials that particle size and morphology plays a critical role in its performance. While not initially applied to these advanced high energy cathode materials, the electrochemical particle model developed here has already been very useful in establishing the impact of porosity and other parameters on performance.

Battery design studies point out the advantages of going to thicker electrode coatings. Simulations with the electrochemical cell model indicate that transport limitations show up first in the cathode during discharge. However, potentially more significant, is the anode limitation on electrode thickness resulting from the chance of lithium plating during regenerative braking charge pulses.

With most lithium-ion PHEV technology battery packs having excess power, the primary concern for performance degradation becomes capacity loss. Development of a capacity loss degradation model is continuing into the next fiscal year. Critical to this effort is the utilization of the newly adopted differential equation solver package (PSE gPROMS). Also, efforts to convert existing models to the new solver are

progressing and will continue into the next fiscal year. Further, continued development of PHEV technology electrochemical models is needed such as examining alternative materials, additives, and testing protocols.

Other ABR projects will be supported as needed. As an example, two multi-dimensional heat transfer models were developed this year to support the battery Design Modeling effort. Also, an electrochemical model is being developed to examine edge effects in the prototype cells.

### **FY 2011 Publications/Presentations**

1. 2011 DOE Annual Peer Review Meeting Presentation, May 9<sup>th</sup>-13<sup>th</sup> 2011, Washington DC.

## IV.C.1.2 Battery Design Modeling (ANL)

Kevin G. Gallagher, Paul A. Nelson & Dennis W. Dees

Argonne National Laboratory  
9700 South Cass Avenue  
Argonne, IL 60439-4837  
Phone: (630) 252-4473; Fax: (630) 972-4520  
E-mail: kevin.gallagher@anl.gov

### Collaborators:

Ira Bloom, Argonne National Laboratory  
Wenquan Lu, Argonne National Laboratory  
Dan Santini, Argonne National Laboratory  
Fritz Kalhammer, Electric Power Research Institute  
Satish Rajagopalan, Electric Power Research Institute

Start Date: August 2010

Projected End Date: September 2014

### Accomplishments

- Created version 1.0 of BatPaC: Battery Performance and Cost model for lithium-ion transportation batteries
- Updated, documented, and modified earlier design and cost modeling based upon multiple public and private peer review sessions with academics, industry and other research organizations.
- Continually interacted with ABR program participants to quantify the effect of materials development on cost.
- Successfully supported the EPA and DOT in refining BatPaC to enable use in the 2017-2025 rule making process for CAFE and GHG regulations. Public distribution was enabled in November 2011 from [www.cse.anl.gov/batpac](http://www.cse.anl.gov/batpac)

### Objectives

The objective of this task is to develop and utilize efficient simulation and design tools for advanced lithium-ion batteries capable of predicting precise overall and component weight and dimensions, as well as cost and performance characteristics.

### Technical Barriers

The primary technical barrier is the development of a safe cost-effective PHEV battery with a 40 mile all electric range that meets or exceeds all performance goals. The major challenge specific to this project is accurately predicting the impact of promising new battery materials on the performance and cost of advanced full-size lithium-ion batteries for transportation applications.

### Technical Targets

- Develop a model for calculating total battery mass, volume, & cost from individual components.
- Predict methods & materials that enable manufacturers to reach goals.
- Evaluate the interplay between performance and cost for advanced materials, such as anodes and cathodes, on end battery pack cost.
- Support policy making process of U.S. Government
- Document and publically distribute model.



### Introduction

The recent penetration of lithium-ion (Li-ion) batteries into the vehicle market has prompted interest in projecting and understanding the costs of this family of chemistries being used to electrify the automotive powertrain. Additionally, research laboratories throughout the DOE complex and various academic institutions are developing new materials for Li-ion batteries every day. The performance of the materials within the battery directly affects the energy density and cost of the battery pack. The development of a publically available model that can project bench-scale results to real world battery pack values would be of great use. This first version of the model, the battery performance and cost (BatPaC) model, represents the only public domain model that captures the interplay between design and cost of Li-ion batteries for transportation applications.

### Approach

The starting point for this work is based on the decades of battery design work headed by Paul Nelson at Argonne National Laboratory (Argonne). These design models were based in Microsoft Office Excel resulting in a flexible and straightforward format. The current effort builds on this previous experience by adding a manufacturing cost calculation as well as increasing the fidelity of the performance calculations all while

maintaining efficient calculations (e.g. fractions of a second).

The cost of a battery will change depending upon the materials chemistry, battery design, and manufacturing process. Therefore, it is necessary to account for all three areas with a bottom-up cost model. Other bottom-up cost models exist but are not generally available and have not been explicitly detailed in a public document. The motivation for our approach is based on a need for a battery performance and cost model that meets the following requirements:

1. Open and available to the entire community
2. Transparent in the assumptions made and method of calculation
3. Capable of designing a battery specifically for the requirements of an application
4. Accounts for the physical limitations that govern battery performance
5. Based on a bottom-up calculation approach to account for every cost factor.

Our approach is to first assume a standard cell, module, and battery format, Figure IV - 118a. However, the materials requirements are specifically calculated based upon the performance of the materials being evaluated. In other words, the model calculates the exact electrode loading and separator area to meet a specified power and energy requirement. The prismatic design used for these calculations only has a minor effect on the end cost as compared to costs for other design formats (e.g. spiral or flat wound). From the battery design calculations, a bill of materials is generated. The cost for a battery company to purchase every item has been determined from private conversations with suppliers and original equipment manufacturers (OEMs). When no values were available, engineering estimates were used.

The manufacturing cost for producing the finished product is calculated by assuming a baseline manufacturing facility that accounts for the capital, area, and labor requirements for every step of the standard battery production process, Figure IV - 118b. The throughput and thus cost for each step will change depending on the battery performance requirements and the materials chemistry chosen to meet those requirements. The costs and overhead for these processes have also been determined from conversations with industry.

The model does not try to calculate the high costs of batteries today or all of the aspects of the learning curve to an established, competitive marketplace. The battery pack

design and cost calculated in BatPaC represent projections of a 2020 production year and a specified level of annual battery production, 20,000-500,000. As the goal is to predict the future cost of manufacturing batteries, a mature manufacturing process is assumed. The model designs a manufacturing plant with the sole purpose of producing the battery being modeled. The assumed battery design and manufacturing facility are based on common practice today but also assume some problems have been solved to result in a more efficient production process and a more energy dense battery. In general, a high-degree of automation has been assumed whereas today's manufacturing environment relies on semi- or non-automated approach to certain processes such as pack assembly. Another example is the higher throughput assumed for cell-stacking; today's best practices are slower than what we believe will be achieved through innovative new processes developed to compete in a mature marketplace. Our proposed solutions do not have to be the same methods used in the future by industry. We simply assume the leading battery manufacturers, those having successful operations in the year 2020, will reach these ends by some means.

## Results

**BatPaC v1.0.** A single spreadsheet has been developed to calculate the battery performance and cost for all of the components that will compose a battery for a high volume, established battery industry. The battery and manufacturing facility are redesigned for each individual battery to meet the specified power and energy requirement for a specific application and cell chemistry. The model contains six common electrochemical couples but almost any value may be overridden by the user to represent a different materials couple.

The design assumptions and methodologies have been documented and reported in a number of formats.<sup>1-6</sup> The most notable of which is the 100+ page public report that accompanies the model.<sup>6</sup> This report was completed to support the use of the model by the EPA and DOT in the 2017-2025 CAFE and GHG regulations. Through that process, the model and documentation were subjected to a public peer-review and multiple private peer-reviews. The model was altered in response to the comments to create a more accurate and powerful tool. These peer-reviews serve as a validation for both the design methodology and also the cost inputs and calculations. The use of active liquid thermal management was included in response to the peer-review.

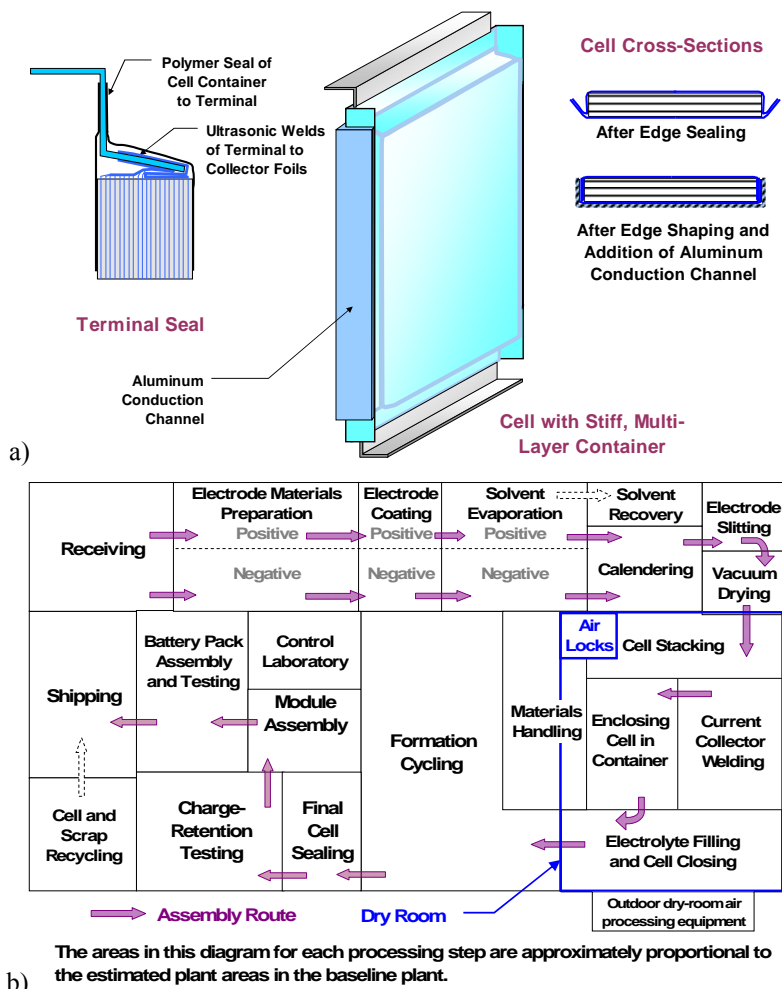


Figure IV - 118: a) assumed stiff pouch cell format b) schematic of baseline manufacturing facility.

**Efficient Impedance Calculation.** A new approach to calculating the impedance of Li-ion cell was necessary to capture physical processes occurring between the electrode but still reaching a solution in a fraction of a second. This simplified area-specific impedance (ASI) calculation is detailed in Ref (2). Figure IV - 119 and Figure IV - 120 demonstrate good agreement between the new impedance calculation and experimentally measured results. This serves as a verification of this approach to real-world cells.

The impedance calculation is necessary to adequately determine the power capability of a battery design. In BatPaC, the model iterates around electrode thickness and separator area to determine the proper design that meets both energy and power requirements. This is one of the key components of the model that enables the design of HEVs through EVs.

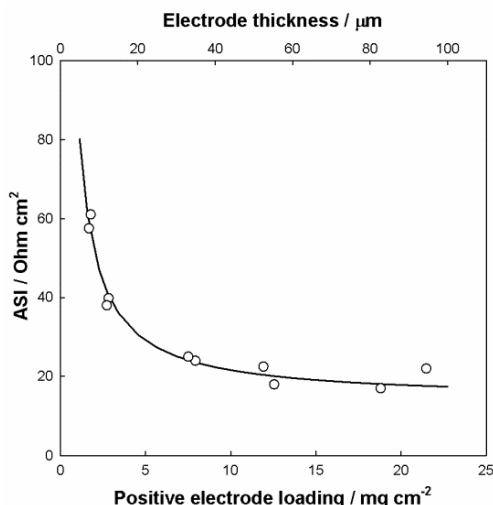


Figure IV - 119: Calculated (solid line) and experimental (open circles) area-specific impedance (ASI) for a NCA/Graphite couple with varying electrode loading. Model captures the physical origin of the ASI as a function of active material at constant C-rate.

**Correlation Between Performance and Cost.** The correlation between performance and cost is highlighted in Figure IV - 121a and Figure IV - 121b. While the total values are shown here, BatPaC is able to quantify the cost, mass and volumetric breakdown of a Li-ion transportation battery. There is a clear change in battery price and mass for differing power and energy requirements. One of the more interesting aspects captured by BatPaC is that a minimal energy requirement exists for a certain power requirement. In other words, the physical limitation of how fast one can remove Li-ions from a material is captured with this approach. If the specified energy and power approach this limitation, the design begins to result in a more expensive battery. Hence, an optimum design point exists for high power to energy ratio batteries. A secondary observation is that a strong correlation exists between battery price and mass. Even at low total energy, the correlation between mass and battery price exists.

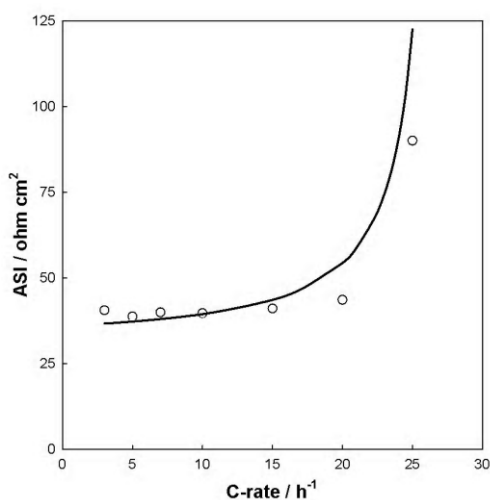
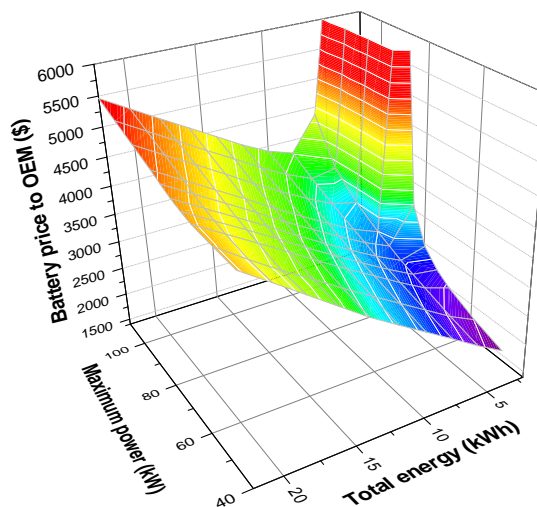


Figure IV - 120: Calculated (solid line) and experimental (open circles) area-specific impedance (ASI) for a NCA/Graphite couple operated at increasing C-rate. The model is able to capture physical limitations within battery.

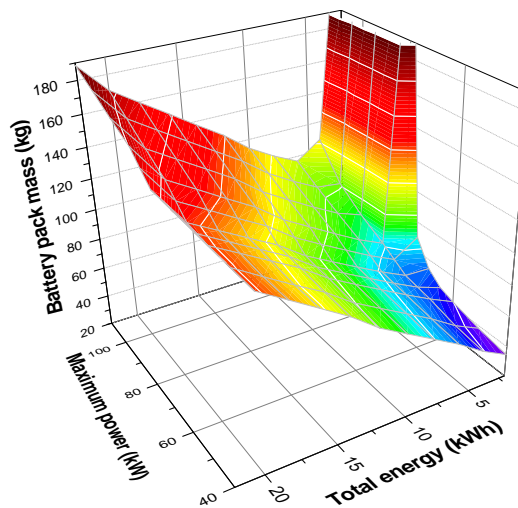
Another valuable aspect of BatPaC is the ability to guide research and development efforts. The lithium and manganese rich transition metal oxide cathode materials (LMR-NMC) are a very promising approach to lower the cost and increase the energy density of PHEV batteries. One issue with this class of materials is a high ASI at low states-of-charge (SOC). This is problematic for PHEV applications due to the charge-sustaining region near 20-30% SOC. Material scientists working to advance this class of materials have often asked what ASI is necessary to meet the DOE goals. Figure IV - 122 is one attempt to answer this question. The ASI allowed is a direct function of the power requirement of the vehicle battery. More powerful batteries are more sensitive to the electrochemical couple ASI. Therefore, for lower power applications that might exist in a parallel configuration PHEV, a higher ASI might be allowable. However, for a

series PHEV requiring 100 kW, a low valued ASI is necessary.

Analysis of PHEV cost also detailed as a part of the PHEV Battery Cost Assessment in section III.C.8 and III.C.2.



a)



b)

Figure IV - 121: a) Battery price and b) mass as a function of demanded power (W) and energy (kWh) for an NMC333/Graphite couple. High power batteries with too low of energy (active material) will result in an undesirable (expensive) battery: an optimum design point exists.

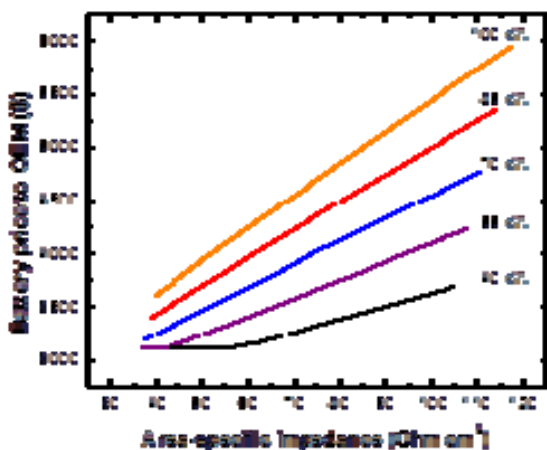


Figure IV - 122: Price of LMR-NMC/Graphite

5. K. G. Gallagher, P. A. Nelson, I. Bloom, D. J. Santini, and D. W. Dees "Predicting the Cost and Energy Density of Lithium-Ion Batteries for Hybrid, Plug-in and Full Electric Vehicles" 5th International Conference on Polymer Batteries and Fuel Cells, Argonne National Laboratory, Argonne, IL USA, Aug 1 – Aug 5, 2011. Poster presentation
6. P. A. Nelson, K. G. Gallagher, I. Bloom, and D. W. Dees "Modeling the Performance and Cost of Lithium-Ion Batteries for Electric Vehicles" Chemical Sciences and Engineering Division, Argonne National Laboratory, ANL-11/32, Argonne, IL USA (2011).

## Conclusions and Future Directions

The first public distribution of BatPaC is expected to involve some level of support from the PIs. As the visibility of the model increases, stakeholders (OEMs and cell developers) will have greater interest in learning about the model's capabilities and providing their view of what cost inputs may be in a future, well-established transportation Li-ion battery industry. Interaction with these partners will be nurtured in an effort to build buy-in from the community and improve the fidelity of the model. Continuing from previous years, more sophisticated modeling and simulation techniques will be integrated into the model in a manner that will not sacrifice flexibility or efficiency. Areas of increasing interest are those related to thermal management and durability (limitations due to lithium plating, etc). As always, BatPaC will continue to be utilized to evaluate the impact on cost and battery performance of new materials developed and/or identified under the ABR and BATT programs.

## FY 2011 Publications/Presentations

1. D. J. Santini, K. G. Gallagher, and P. A. Nelson, "Modeling of Manufacturing Costs of Lithium-Ion Batteries for HEVs, PHEVs, and EVs" Electric Vehicle Systems 25, Shenzhen, China, Nov. 5-9, 2010.
2. K. G. Gallagher, P. A. Nelson, and D. W. Dees "Simplified Calculation of the Area Specific Impedance for Battery Design" Journal of Power Sources 196, 2289-2297 (2011).
3. S.-H. Kang, W. Lu, K. G. Gallagher, S.-H. Park, and V. G. Pol "Study of  $\text{Li}_{1-x}(\text{Mn}_{4/9}\text{Co}_{1/9}\text{Ni}_{4/9})_{1-x}\text{O}_2$  Cathode Materials for Vehicle Battery Applications" Journal of the Electrochemical Society 158, A936-A941 (2011)
4. 2011 DOE Annual Peer Review Meeting Presentation.

## IV.C.1.3 Diagnostic Studies on Li-Battery Cells and Cell Components (ANL)

Daniel P. Abraham

Argonne National Laboratory  
9700 South Cass Avenue  
Argonne, IL 60439-4837  
Phone: (630) 252-4332; Fax: (630) 972-4406  
E-mail: [abraham@anl.gov](mailto:abraham@anl.gov)

### Collaborators:

Dennis Dees, Argonne National Laboratory  
Andrew Jansen, Argonne National Laboratory  
Bryant Polzin, Argonne National Laboratory  
Wenquan Lu, Argonne National Laboratory  
Javier Bareno, Argonne National Laboratory  
Martin Bettge, Argonne National Laboratory  
Ivan Petrov, University of Illinois  
Brett Lucht, University of Rhode Island

Start Date: October, 2008

Projected End Date: September, 2012

### Objectives

- Various electrochemical couples are being examined for use in lithium-ion cells for PHEV applications. The objectives of this study are as follows:
- To identify factors that contribute to cell performance and performance degradation (capacity fade, impedance rise) on long-term storage/cycling of these various electrochemical couples;
- To recommend solutions, which improve performance and minimize performance degradation of materials, electrodes, and cells.

### Technical Barriers

- This project addresses the following technical barriers to the development of a PHEV battery with a 40 mile all electric range that meets or exceeds all performance goals.
- Performance and Performance Degradation Mechanisms that affect cell life.

### Technical Targets

- Complete accelerated aging studies of PHEV-baseline electrochemical cells.
- Complete physicochemical examination of PHEV-baseline cells and cell constituents.

- Initiate characterization and aging experiments on ABR-1 electrodes and electrode constituents.

### Accomplishments

- “Wrapped-up” characterization of PHEV baseline electrodes and aging studies on cells with these electrodes
  - Electrochemical cycling and impedance (EIS and HPPC) data were obtained on electrodes and full cells. Data obtained on these electrodes and cells are similar to those obtained for cells with ATD-Gen2 chemistry, which have a comparable chemistry.
  - Conducted cell disassembly, then electrochemical and physicochemical characterization of harvested cell components.
  - Identified sources of performance degradation
- Initiated characterization of ABR-1 electrodes and initiated aging studies on cells with these electrodes
  - Electrochemical cycling and impedance (EIS and HPPC) data were obtained on electrodes and full cells.
- Determined features and challenges associated with the high-energy density oxides.



### Introduction

The performance and performance degradation of materials and cells being developed for PHEV applications are being studied. These cells contain (a) electrode materials that are new or modified versions of current chemistries, (b) novel electrolytes, or additives to current electrolytes, to enhance cell performance and life, (c) changes in cell testing conditions that include wider voltage windows and greater state-of-charge (SOC) swings, etc. The degradation mechanisms associated with various cell chemistries and testing conditions will be identified to determine suitable electrode-electrolyte combinations that will meet the target goals of PHEV batteries. We will also continue examining electrode surface films after formation cycling in cells containing various electrolytes and electrolyte additives. Some of these experiments will be conducted on model electrodes, such as binder-free graphite electrodes and binder- and carbon-free oxide electrodes.

## Approach

We typically employ electrochemical and physicochemical techniques for our diagnostic studies. Our electrochemical measurements are conducted in cells that include coin cells, pouch cells, and reference electrode cells to determine cell performance, performance degradation characteristics, and degradation sources. Our physicochemical examinations employ a combination of spectroscopy, microscopy, diffraction and chemical analysis techniques that include scanning and transmission electron microscopy, energy dispersive spectroscopy, electron energy loss spectroscopy, X-ray diffraction, X-ray photoelectron spectroscopy, Fourier Transform InfraRed spectroscopy (FT-IR) with Attenuated Total Reflectance (ATR), and Nuclear Magnetic Resonance (NMR) spectroscopy.

## Results

**PHEV-baseline electrodes and cells.** Cells with the PHEV baseline chemistry contain  $\text{LiNi}_{0.8}\text{Co}_{0.15}\text{Al}_{0.05}\text{O}_2$ -based positive electrodes, Mag10 Graphite-based negative electrodes, Celgard 2325 separator, and EC:EMC (3:7, by wt.) + 1.2M  $\text{LiPF}_6$  electrolyte. The performance of as-prepared cells was characterized using a series of electrochemical charge-discharge cycling and impedance experiments. The cells were then cycle-life aged at  $45^\circ\text{C}$ ; capacity and impedance data were obtained periodically to characterize performance degradation.

Figure IV - 123 shows AC impedance data obtained on a cell containing a reference electrode that underwent 4000 cycles between 3.6 and 4.0V, then 500 cycles between 3.3 and 4.0V at a C/1 rate. The data show that the full cell impedance increases on aging. Furthermore, all of the impedance rise can be attributed to the positive electrode; the negative electrode contribution is minimal. The positive electrode impedance rise can be attributed to processes (i) at the electrode-electrolyte interface, which is seen from growth of the mid-frequency arc (ii) within oxide bulk, which is observed in the Warburg diffusion tail obtained to low-frequencies (data not shown). This impedance result is very similar to that previously reported for other NCA/graphite cells that were aged under testing conditions relevant to HEV (high-power) applications.

Figure IV - 124a and Figure IV - 124b show capacity and impedance data obtained on a cell that underwent 4000 cycles between 3.6 and 4.0V, then 2000 cycles between 3.3 and 4.0V at a C/1 rate. The figures show that the rate of capacity fade and impedance rise is greater for the 3.3-4.0V cycling compared to the 3.6-4.0V cycling. That is, cell performance degradation is greater for wider voltage cycling windows; i.e., when a larger proportion of the  $\text{Li}^+$  inventory is shuttled between the electrodes. Wider voltage cycling windows are typical of PHEV profiles because of the need to access higher capacities that are required to

drive longer distances; in comparison, shallow voltage cycles are more typical of HEV profiles, wherein the need is for high-power from cells.

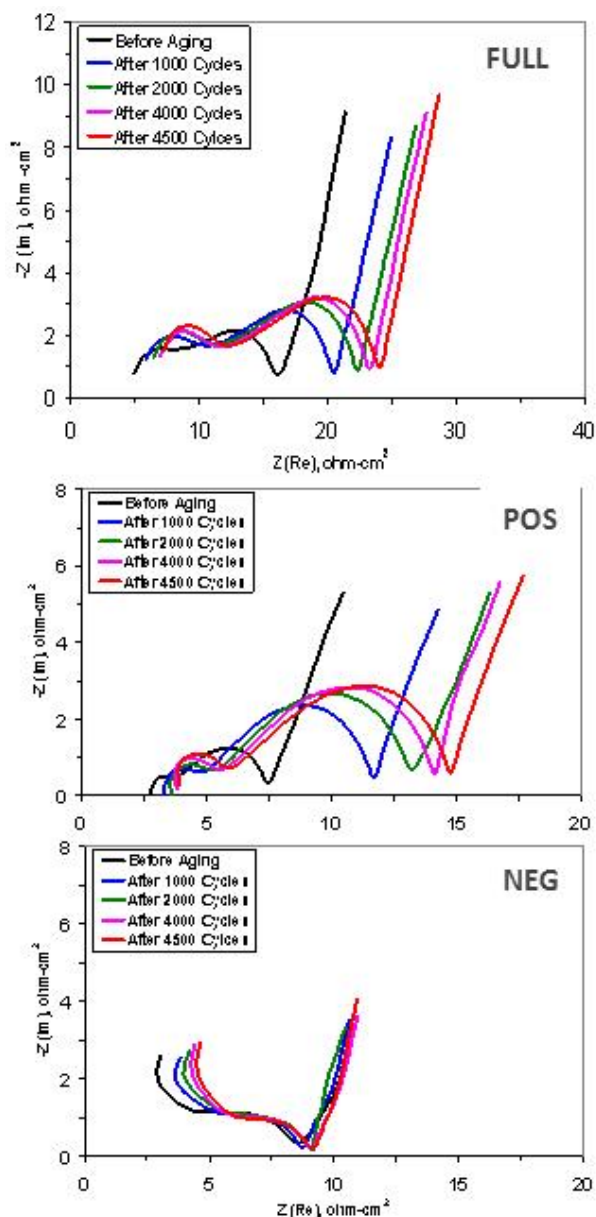


Figure IV - 123: AC impedance data obtained on a NCA/graphite cell with a Li-Sn reference electrode. The data were obtained at  $30^\circ\text{C}$ , 3.75V full cell voltage, in the 100KHz-10 mHz frequency range

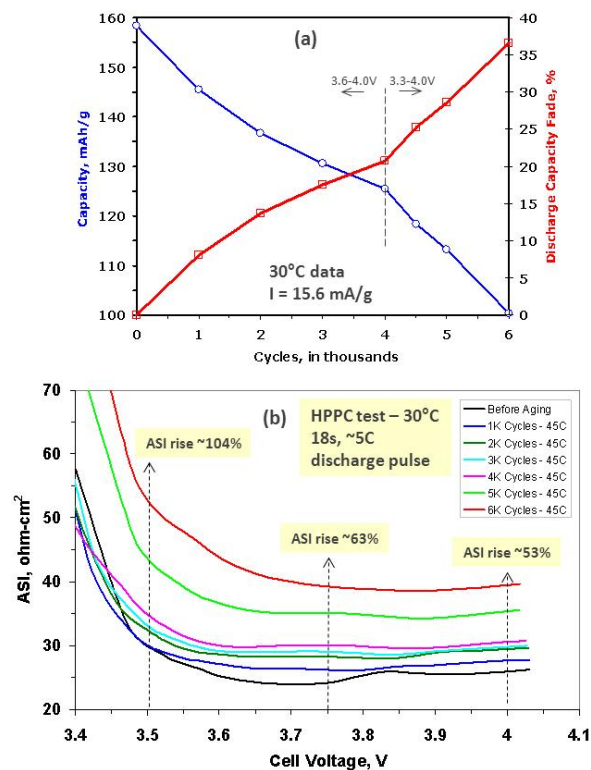


Figure IV - 124: (a) Capacity/capacity fade data obtained from capacity-voltage plots, and (b) impedance data from HPPC tests, from a cycle-life aged cell. All data were acquired at 30°C.

To determine the source of capacity fade we conducted experiments on positive electrodes that were harvested from “formed” and “aged” full cells. The data shown in Figure IV - 125 is from a “formed” cell that was cycled three times between 3 and 4.1V at 30°C; the “aged” data is from the cell that underwent 6000 cycles at 45°C, as described earlier.

The data shown in Figure IV - 125 are from coin cells containing the “harvested” positive electrode, Li metal counter electrode, and the baseline electrolyte; the data were obtained at 30°C, in the 3 – 4.3V voltage range at a  $\sim C/30$  rate. It is evident from the figure that the lithiation capacity of the aged cell electrode is only slightly ( $\sim 7\%$ ) smaller than that of the formed cell electrode; furthermore, the  $dQ/dV$  profiles are also very similar. These data indicate that the “electronic isolation” of oxide particles is small, i.e., most oxide particles in the positive electrode can contribute to cell capacity when cell cycling is conducted at very slow rates. Therefore, the positive electrode contribution to “true” capacity fade is small – the cell capacity fade can be attributed to  $\text{Li}^+$  consuming processes at the negative electrode.

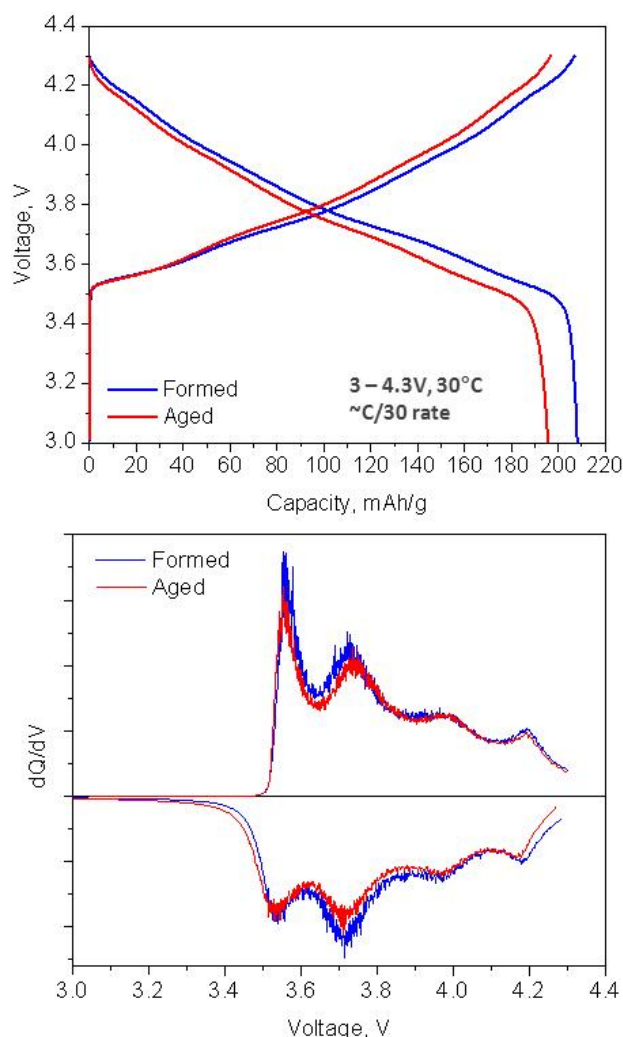


Figure IV - 125: Capacity-voltage, and corresponding  $dQ/dV$ , plots from harvested electrode vs. Li cells.

To determine the source of impedance rise we conducted experiments on positive electrodes that were harvested from various full cells. Figure IV - 126 contains XRD data on positive electrode samples harvested from “Formed” and “Aged” full cells discharged to  $< 2V$ . The measured peak shifts indicate c-axis expansion and a-axis contraction on aging. These data indicate that the aged samples contain Li-deficient oxides. The observed changes in the bulk oxide structure indicate Li-loss from the oxides, which is consistent with the capacity loss displayed by the cells.

To determine the source of capacity fade we examined the negative electrodes that were harvested from various full cells. X-ray diffraction data obtained on the negative electrodes showed that the graphite bulk structure was not damaged by the cell aging process – the graphite lattice parameter and peak shape changes on aging were very small. However, Raman spectroscopy data (see Figure IV - 127) show significant changes in the  $I(D)/I(G)$  ratio –

the ratio increases from 0.21 in as-prepared electrodes to 0.93 in highly-aged electrodes, which indicates that the amount of graphite disorder increases on aging. Because XRD data do not indicate changes to graphite bulk this increased disorder is probably at the graphite particle edges and may be the result of nano-fracturing at high charge-discharge rates. Such nano-fractures may passivate, that is, form an SEI layer that consumes lithium and increases cell capacity fade.

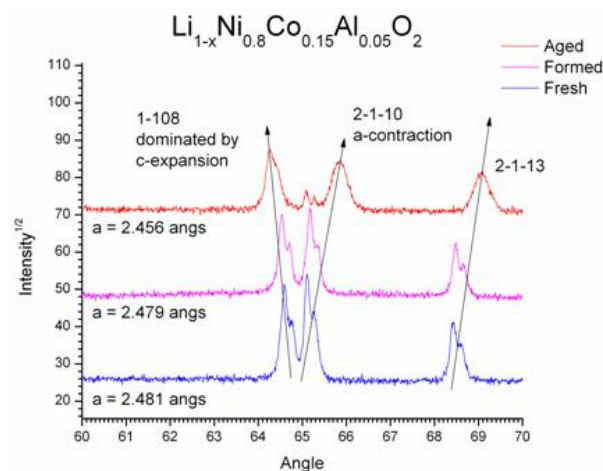
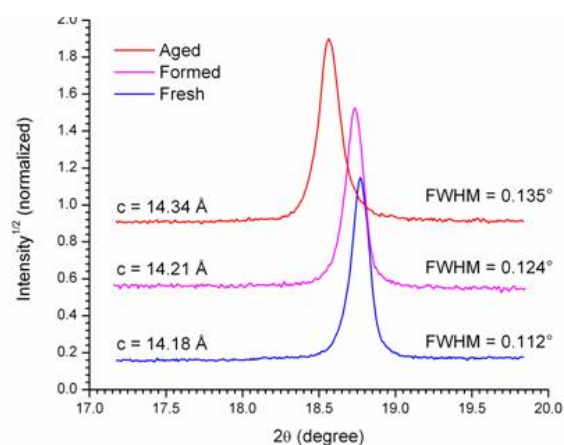


Figure IV - 126: X-ray diffraction data obtained on the positive electrode

**ABR-1 electrodes and cells.** Cells with the ABR-1 chemistry contain  $\text{Li}_{1.2}\text{Ni}_{0.15}\text{Co}_{0.1}\text{Mn}_{0.55}\text{O}_2$ -based positive electrodes, ConocoPhillips A12 graphite-based negative electrodes, Celgard 2325 separator, and EC:EMC (3:7, by wt.) + 1.2M  $\text{LiPF}_6$  electrolyte. The performance of as-prepared cells was characterized using a series of electrochemical charge-discharge cycling and impedance experiments.

The  $\text{Li}_{1.2}\text{Ni}_{0.15}\text{Co}_{0.1}\text{Mn}_{0.55}\text{O}_2$ -based positive electrodes deliver low capacities ( $\sim 70$  mAh/g) in a voltage window ( $\sim 2$ -4.1V vs. Li) that is typical for layered oxides. In comparison,  $\text{LiNi}_{0.8}\text{Co}_{0.15}\text{Al}_{0.05}\text{O}_2$ -based positive electrodes yield a discharge capacity  $\sim 150$  mAh/g in the

same voltage window. Cycling over a wider voltage window is needed to obtain higher capacities, as shown in Figure IV - 128. After oxide “activation”, however, the charge and discharge profiles are no longer symmetric. For example, charge capacity (3.2-4.7V) is  $\sim 265$  mAh/g, whereas discharge capacity in the same window is only  $\sim 235$  mAh/g.

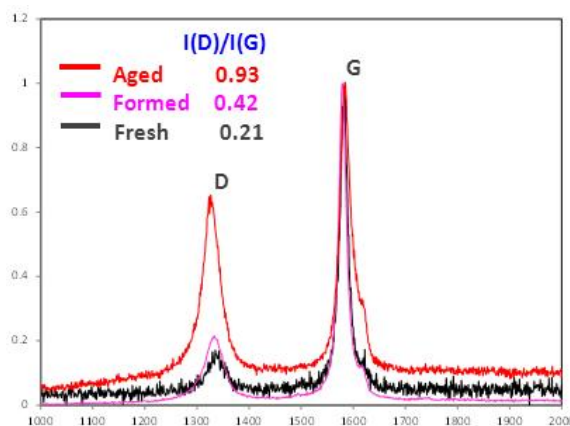


Figure IV - 127: Raman spectroscopy obtained on fresh and harvested negative electrodes.

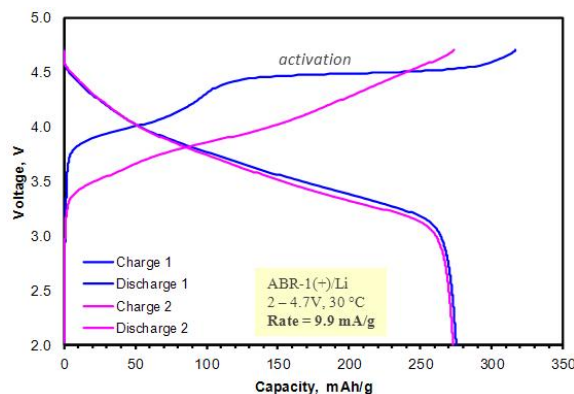


Figure IV - 128: First 2 cycles of a Li-metal cell containing a  $\text{Li}_{1.2}\text{Ni}_{0.15}\text{Co}_{0.1}\text{Mn}_{0.55}\text{O}_2$ -based positive electrode.

Figure IV - 129 shows electrochemical cycling data obtained on a Li-metal cell containing a  $\text{Li}_{1.2}\text{Ni}_{0.15}\text{Co}_{0.1}\text{Mn}_{0.55}\text{O}_2$ -based positive electrode – the cell was cycled in the 2 – 4.7V window, at 30°C, at a rate of 9.9 mA/gm. The data indicate changes in the voltage profile during cycling – this “depression” of the voltage profile, seen on both charging and discharging, is significant during the early cycles and slows with cycle number. This behavior appears to be triggered by changes to the oxide structure during the first charge cycle and is believed to result from phase changes in the oxide.

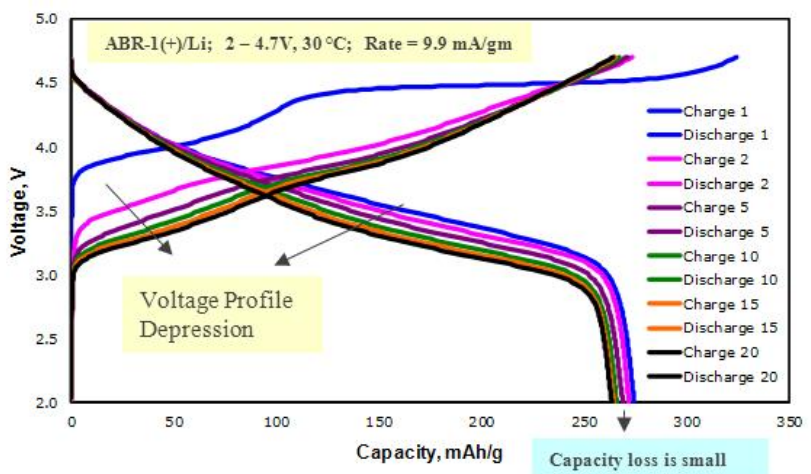


Figure IV - 129: Electrochemical cycling data obtained on a Li-metal cell containing a  $\text{Li}_{1.2}\text{Ni}_{0.15}\text{Co}_{0.1}\text{Mn}_{0.55}\text{O}_2$ -based positive electrode.

## Conclusions and Future Directions

We have been studying the performance degradation of electrodes and cells with the PHEV baseline chemistry. Our data show that cell impedance rise on aging arises from processes at the positive electrode, whereas cell capacity loss can be attributed to processes at the negative electrode. The impedance rise can be correlated to structural defects within oxide particles and the increasingly inorganic nature of positive electrode surface films, whereas cell capacity fade appears to result from Li loss during graphite SEI dissolution/reformation.

Our results on the high-energy density oxide cells show the following: (i) the oxide has to be “activated” to obtain the high capacities; (ii) on activation, the voltage profile becomes asymmetric; (iii) “depression” of the voltage profile is observed both on charge and discharge; it is significant during the early cycles and slows with cycle number.

## FY 2011 Publications/Presentations

1. 2011 DOE Annual Peer Review Meeting Presentation, May 9<sup>th</sup>-13<sup>th</sup> 2011, Washington DC.
2. D.P. Abraham, Invited Speaker, 11th Advanced Automotive Battery Conference (AABC 2011), “Performance Degradation of Lithium-Ion Batteries”, Pasadena, California, January 24-28, 2011.
3. D.P. Abraham, Invited Speaker, Performance and Performance Degradation of Lithium-Ion Batteries”, Dow Chemical Company, Midland, MI, October 12, 2010.
4. D.P. Abraham, Invited Speaker, 1<sup>st</sup> NEDO-Argonne Workshop, “Diagnostic Studies on Lithium-ion cells at Argonne - An Overview”, Argonne, IL, October 6 – 8, 2010.

## IV.C.1.4 Structural Investigations of Layered Oxide Materials for PHEV

### Applications (ANL)

Daniel P. Abraham

Argonne National Laboratory  
9700 South Cass Avenue  
Argonne, IL 60439-4837  
Phone: (630) 252-4332; Fax: (630) 972-4406  
E-mail: [abraham@anl.gov](mailto:abraham@anl.gov)

#### Collaborators:

Javier Barenó, Argonne National Laboratory  
Sun-Ho Kang, Argonne National Laboratory  
Mahalingam Balasubramanian, Argonne National Laboratory  
Ivan Petrov, University of Illinois  
Jian-Guo Wen, University of Illinois

Start Date: October, 2008

Projected End Date: September, 2012

### Objectives

The structure and structural rearrangements in Li-bearing Mn-based layered oxides, which show anomalously high-capacities when cycled to high-voltages, have a significant effect on cell performance, calendar-life, and safety. The objective of this work is to obtain a detailed structural understanding of  $\text{Li}_{1+a}(\text{TM}_{1-x}\text{Mn}_x)_{1-a}\text{O}_2$ ; TM=transition metal (Ni, Co, Cr, Fe, etc.). These oxides display significant differences between the long range crystal structure and local arrangements around individual atoms, which are important because the local atomic environments affect Li-ion transport, and hence rate capability of the oxide.

### Technical Barriers

This project addresses the following technical barriers to the development of a PHEV battery with a 40 mile all electric range that meets or exceeds all performance goals.

- Oxide/Positive Electrode/Cell Performance
- Cell Calendar Life
- Oxide Stability/Cell Safety

### Technical Targets

- Our experiments are designed to answer various questions that include the following:

- What are the local atomic arrangements in the as-prepared oxides and how are these arrangements influenced by composition?
- What are the charge compensation mechanisms during oxide delithiation & lithiation, i.e., during electrochemical cycling?
- What phase transformations result on cycling/aging? How does this affect the oxide's capacity and rate performance?
- What are the correlations between the composition, structure, and performance for the various oxides?

### Accomplishments

- Completed structural study of as-prepared  $\text{Li}(\text{Li}_{0.2}\text{Mn}_{0.4}\text{Co}_{0.4})\text{O}_2$ 
  - Determined that the oxide contains a mixture of  $\text{Li}_2\text{MnO}_3$ -like and  $\text{LiCoO}_2$ -like areas, which are integrated and interconnected at the atomic scale
- Initiated structural study of cycled  $\text{Li}(\text{Li}_{0.2}\text{Mn}_{0.4}\text{Co}_{0.4})\text{O}_2$  samples.
- Observed differences in local atom arrangements between as-prepared and cycled samples may be responsible for changes in the oxides' voltage profile



### Introduction

Lithium-bearing manganese-based layered oxides are promising positive electrode active material candidates to achieve high energy and power density lithium-ion batteries. However, the performance and calendar life of existing materials needs to be improved before widespread applications in PHEVs and EVs can be realized. Despite considerable materials research over the last decade, the structure of common positive electrode materials, as well as its evolution upon cycling, and the atomistic mechanisms responsible for these changes remains the subject of debate.

This project combines advanced structural characterization techniques, including X-ray diffraction, X-ray absorption spectroscopy (XAS), and analytical electron microscopy (AEM) to investigate atomistic rearrangements in lithium-bearing layered oxide materials during and after electrochemical cycling. Fundamental insights into the tradeoffs between oxide performance and

stability will help define new design strategies for the next-generation of high-performance long-lasting batteries.

## Approach

We have embarked on a multi-institution effort to synthesize, characterize, and model these complicated oxide structures. After oxide synthesis, structure examination by XRD and initial electrochemical performance examination, we conduct both *ex situ* and *in situ* XAS measurements on the samples. These XAS studies, conducted at Argonne's Advanced Photon Source (APS) provide information on transition metal (TM) oxidation states, coordination characteristics around the TM atoms, and changes in these parameters during electrochemical cycling. Because the information obtained by XAS is an average over several grains, the data provides a snapshot of the oxide bulk that is used as a guide for AEM study, which provides information on the local (<2 nm) structure and composition in the oxides. The AEM study includes electron diffraction and high angle annular dark field (HAADF) electron microscopy to examine the oxide's crystal structure at near-atomic spatial resolution and electron energy loss spectroscopy to examine composition variations in the 1 to 10 nm scale range.

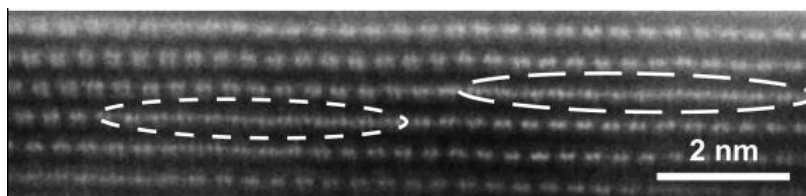


**Figure IV - 130:** HAADF-STEM image of  $\text{Li}_{1.2}\text{Co}_{0.4}\text{Mn}_{0.4}\text{O}_2$ , that reveal the coexistence of  $\text{Li}_2\text{MnO}_3$ -like (dot contrast) and  $\text{LiCoO}_2$ -like (continuous contrast) areas within (0001) transition metal planes.

Electron diffraction also revealed the coexistence of monoclinic  $\text{Li}_2\text{MnO}_3$ -like and rhombohedral  $\text{LiCoO}_2$ -like crystal structures, consistent with the HAADF-STEM observation of Li-ordering at TM planes of the host rhombohedral lattice. EELS data showed the presence of Co and Mn in all areas of the sample. The compositional variations across dotted and continuous contrast areas of STEM images was about 10 %, which is too small to be compatible with perfect, or close to perfect, segregation into pure  $\text{LiCoO}_2$  and  $\text{Li}_2\text{MnO}_3$  over length scales longer than the sample thickness.

EXAFS revealed distinct segregation of Mn and Co into nearly undistorted  $\text{LiCoO}_2$ -like and  $\text{Li}_2\text{MnO}_3$ -like atomic environments over length scales of at least  $7\text{\AA}$ . In contrast, EELS analysis revealed a coexistence of Co and Mn on roughly equal proportion over length scales less than 1 nm. This apparent contradiction is resolved by a proposed model (see Figure IV - 131) consisting of well integrated  $\text{LiCoO}_2$  and  $\text{Li}_2\text{MnO}_3$  nanoclusters which, for

## Results

$\text{Li}_{1.2}\text{Co}_{0.4}\text{Mn}_{0.4}\text{O}_2$  was synthesized from stoichiometric amounts of  $\text{Li}_2\text{CO}_3$  and  $(\text{Co}_{0.5}\text{Mn}_{0.5})\text{CO}_3$  precursors that were thoroughly mixed and calcined at  $900^\circ\text{C}$  for 12 h in air. To elucidate the atomic structure of  $\text{Li}_{1.2}\text{Co}_{0.4}\text{Mn}_{0.4}\text{O}_2$  ( $0.5\text{Li}_2\text{MnO}_3 \bullet 0.5\text{LiCoO}_2$  in the two-component notation) we obtained detailed crystallographic data, both in direct and reciprocal space, on as-prepared samples by analytical electron microscopy (AEM). The studies were conducted using a combination of techniques that included high-resolution electron microscopy (HREM), high-angle annular dark-field imaging in scanning transmission electron microscopy (HAADF-STEM), and selected-area electron diffraction (SAED). Elemental compositions were determined using X-ray energy dispersive spectroscopy (EDS) and electron energy loss spectroscopy (EELS).

SEM and XRD data showed that the  $\text{Li}_{1.2}\text{Co}_{0.4}\text{Mn}_{0.4}\text{O}_2$  sample possesses an overall R-3m structure similar to  $\text{LiCoO}_2$ , and that  $\approx 0.2 - 0.5\ \mu\text{m}$  primary particles agglomerate to form bigger, approximately  $7\ \mu\text{m}$ , secondary particles. The sample was found to possess a rhombohedral ( $R\bar{3}m$ )  $\text{LiCoO}_2$ -like overall structure, with excess Li at TM planes forming ordered areas with local monoclinic (C2/m)  $\text{Li}_2\text{MnO}_3$ -like structure (see Figure IV - 130).

compositions close to  $0.5\ \text{Li}_2\text{MnO}_3 \cdot 0.5\ \text{LiCoO}_2 = \text{Li}_{1.2}\text{Co}_{0.4}\text{Mn}_{0.4}\text{O}_2$  presents a microstructure composed of well integrated dendritic clusters. The small width of the dendrites ( $\approx 1\ \text{nm}$ ) accounts both for the near perfect segregation into  $\text{LiCoO}_2$  and  $\text{Li}_2\text{MnO}_3$  at EXAFS scales and the nearly homogeneous concentration of Mn and Co at EELS scales. The dendritic nature of the clusters, allowing them to retain continuity over long distances in the TM(0001) plane accounts for the large lateral extension of the  $\text{Li}_2\text{MnO}_3$ -like contrast regions observed in HAADF-STEM.

Because no specific atomic interactions were used in obtaining the atomistic models, we expect the proposed microstructures to be valid for other  $\text{Li}_{1+a}(\text{Mn}_x\text{M}'_z)\text{O}_2$  materials that display Li-ordering within the TM(0001) planes of a host rhombohedral structure.

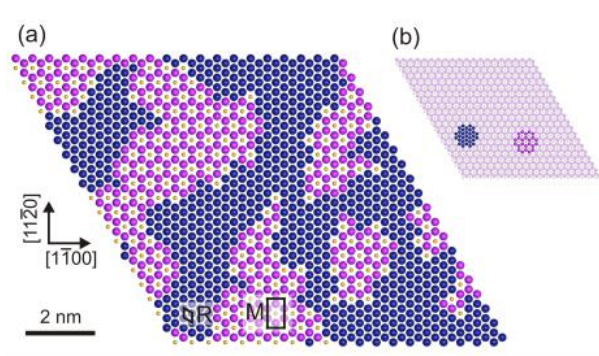


Figure IV - 131: (a) Schematic model structure of TM plane in  $\text{Li}_{1.2}\text{Co}_{0.4}\text{Mn}_{0.4}\text{O}_2$  showing coexistence of Co and  $\text{LiMn}_2$  domains. Big blue and magenta spheres represent Co and Mn atoms, respectively; small yellow spheres represent Li atoms. In-plane sections of the rhombohedral (R) and monoclinic (M) unit cells are indicated in the figure. Periodic boundary conditions connect the top and left edges of the figure with the bottom and right edges, respectively. Therefore, the particular model shown contains only one Co and two  $\text{LiMn}_2$  separate clusters. Additionally, projected atomic columns along  $\langle -1-100 \rangle$  (e.g. left to right) contain approximately equal amounts of Co and X atoms, where X varies across columns following a Mn-Mn-Li sequence consistent with STEM results. (b) Illustration of the early stages of model generation showing one  $\text{LiMn}_2$  and one Co cluster randomly placed on the board. Empty sites are indicated by faded colors.

AEM and XAS of cycled  $\text{Li}_{1.2}\text{Mn}_{0.4}\text{Co}_{0.4}\text{O}_2$  samples are in progress. Figure IV - 132 shows charge-discharge cycles for the first, second and 40<sup>th</sup> cycle, between 2.0 V and 4.7 V vs. Li. The long plateau observed during the first charge cycle is believed to result from a crystal structure change that includes the evolution of oxygen from the sample. A depression of the voltage profile is observed on extended cycling.

XRD data provide information on long-range (average) structure of crystal lattice. Figure IV - 133 presents a comparison of XRD spectra from  $\text{Li}_2\text{MnO}_3$ , and  $\text{LiCoO}_2$  powder samples with  $\text{Li}_{1.2}\text{Co}_{0.4}\text{Mn}_{0.4}\text{O}_2$  laminates, both as-prepared, and after one and forty electrochemical cycles in a cell employing a Li anode. The cycled  $\text{Li}_{1.2}\text{Co}_{0.4}\text{Mn}_{0.4}\text{O}_2$  spectra present an overall shift to lower  $2\theta$  values, indicative of an increase in lattice parameters, and decreased crystal quality, as evidenced by reduced signal to noise ratio and broadened reflections. The data show no

obvious evidence of new oxide phase formation after extended cycling. However, the graphite peak, evident at  $\sim 26.5^\circ$  in the as-prepared sample, shows significant broadening after the 1<sup>st</sup> cycle, and is not seen in the 40-cycle sample. The disappearance of the peak may be related to the intercalation of  $\text{PF}_6^-$  ions into the graphite, which is an electron-conducting additive in the positive electrode.

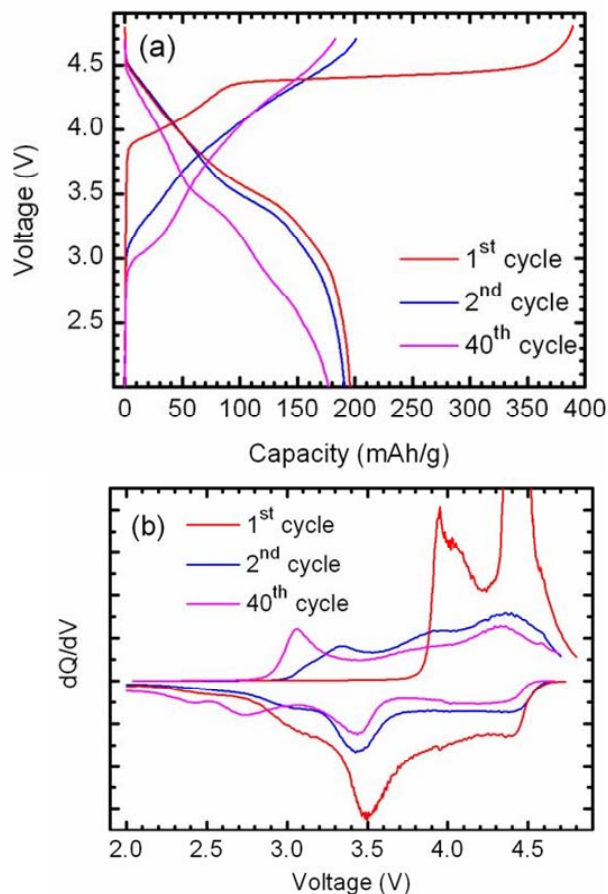


Figure IV - 132: a) Charge-discharge profiles and (b)  $dQ/dV$  plots of  $\text{Li}(\text{Li}_{0.2}\text{Mn}_{0.4}\text{Co}_{0.4})\text{O}_2$  vs. Li cell between 2 and 4.7V.

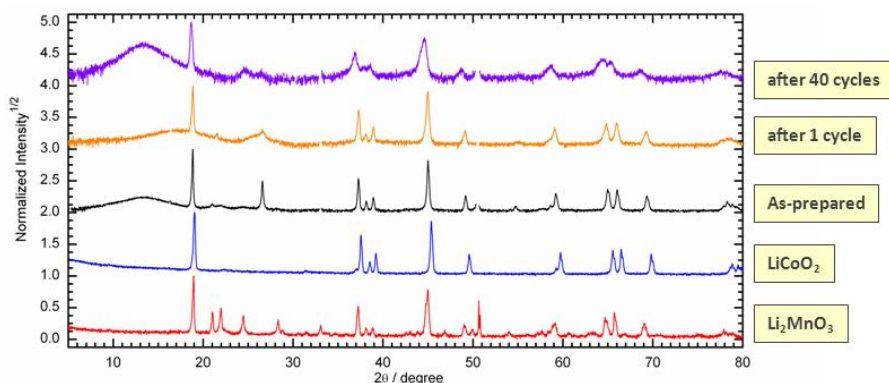


Figure IV - 133: X-ray diffraction data on  $\text{Li}(\text{Li}_{0.2}\text{Mn}_{0.4}\text{Co}_{0.4})\text{O}_2$  samples. Data from  $\text{LiCoO}_2$  and  $\text{Li}_2\text{MnO}_3$  are shown for comparison.

Local atomic structure in the sample was studied by X-ray and Electron Beam Techniques. XAS data provide information on local arrangements in lattice. XAS data from cycled  $\text{Li}(\text{Li}_{0.2}\text{Mn}_{0.4}\text{Co}_{0.4})\text{O}_2$  samples showed evidence of Mn-reduction (see Figure IV - 134).

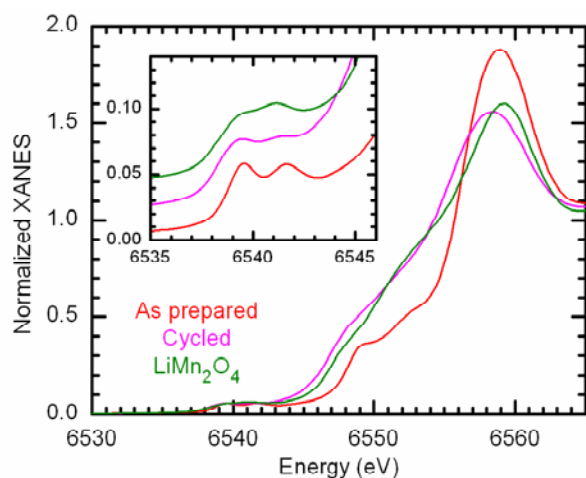


Figure IV - 134: XAS data on as-prepared and cycled  $\text{Li}(\text{Li}_{0.2}\text{Mn}_{0.4}\text{Co}_{0.4})\text{O}_2$  samples. Data from  $\text{LiMn}_2\text{O}_4$  are shown for comparison.

Z-contrast STEM (HAADF) images from cycled  $\text{Li}(\text{Li}_{0.2}\text{Mn}_{0.4}\text{Co}_{0.4})\text{O}_2$  samples showed periodicity in Li layers that is characteristic of a spinel structure (Figure IV - 135). We believe that the voltage profile changes observed in oxides from cycled/aged cells may be caused by the development of these spinel-like crystal structures.

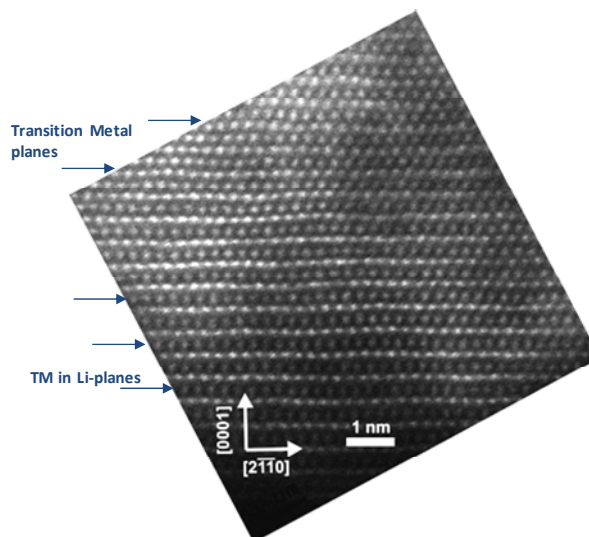


Figure IV - 135: Z-contrast STEM (HAADF) image from cycled  $\text{Li}(\text{Li}_{0.2}\text{Mn}_{0.4}\text{Co}_{0.4})\text{O}_2$  samples.

## Conclusions and Future Directions

We have been studying the structure and structural rearrangements in layered  $\text{Li}(\text{Li}_x\text{Mn}_a\text{Ni}_b\text{M}'_c)\text{O}_2$  compounds using X-ray, electron beam, and electrochemical techniques.  $\text{Li}(\text{Li}_{0.2}\text{Mn}_{0.4}\text{Co}_{0.4})\text{O}_2$  is a model compound from this family of oxides. Our data show that as-prepared  $\text{Li}(\text{Li}_{0.2}\text{Mn}_{0.4}\text{Co}_{0.4})\text{O}_2$  contain an intimate mixture of  $\text{Li}_2\text{MnO}_3$ -like and  $\text{LiMO}_2$ -like ( $\text{M}=\text{Co}, \text{Ni}$ ) areas,  $\sim 1\text{-}2$  nm size, which are integrated and interconnected at the atomic scale. The voltage-profile depression displayed by these oxides may be related to spinel-like phases that form during cycling/aging.

We intend to continue structure investigations of  $\text{Li}(\text{Li}_x\text{Mn}_a\text{Ni}_b\text{M}'_c)\text{O}_2$  compounds. We will continue to identify causes and recommend solutions to mitigate crucial challenges that may hinder commercialization, which include first cycle irreversibility, structural stability, and power delivery capability. Even more important is the

“voltage depression” displayed by these oxides during cycling at high voltages. Such voltage fade can lower the energy density of the oxides, and create unpredictability in the oxide’s voltage profile behavior.

### FY 2011 Publications/Presentations

1. 2011 DOE Annual Peer Review Meeting Presentation, May 9<sup>th</sup>-13<sup>th</sup> 2011, Washington DC.
2. J.-G. Wen, J. Bareño, C. Lei, S.-H. Kang, M. Balasubramanian, I. Petrov, D.P. Abraham, “Analytical Electron Microscopy of  $\text{Li}_{1.2}\text{Co}_{0.4}\text{Mn}_{0.4}\text{O}_2$  for Lithium-ion Batteries”, *Solid State Ionics* 182 (2011) 98-107.
3. J. Bareño, M. Balasubramanian, S.-H. Kang, J.-G. Wen, C. Lei, S.V. Pol, I. Petrov, D.P. Abraham, “Long-Range and Local Structure in the Layered Oxide  $\text{Li}_{1.2}\text{Co}_{0.4}\text{Mn}_{0.4}\text{O}_2$ ”, *Chem. Mater.* 23 (2011) 2039-2050.
4. D.P. Abraham, J. Bareño, J.G. Wen, I. Petrov, Invited Speaker, “Structural Changes Induced by Aging in Oxide Materials for Lithium-Ion Batteries”, *Microscopy & Microanalysis 2011*, Nashville, TN, August 7 – 11, 2011.
5. J.G. Wen, J. Bareño, C.H. Lei, I. Petrov, D.P. Abraham, “Direct Observation of Cation Ordering in  $\text{Li}_{1.2}\text{TM}_{0.4}\text{Mn}_{0.4}\text{O}_2$  (TM: Co, Fe) Lithium-Ion Battery Materials Using Aberration-corrected TEM”, *Microscopy & Microanalysis 2011*, Nashville, TN, August 7 – 11, 2011.
6. N.K. Karan, M. Balasubramanian, D.P. Abraham, “Local distortions and clustering tendencies in Cr substituted layered  $\text{LiMn}_{0.5}\text{Ni}_{0.5}\text{O}_2$  cathodes for rechargeable Li-ion batteries”, *MRS meeting*, San Francisco, CA, April 26, 2011.

## IV.C.1.5 Electrochemistry Diagnostics of Baseline and New Materials (LBNL)

Robert Kostecki, Thomas Richardson

Environmental Energy Technologies Division  
Lawrence Berkely National Laboratory  
1 Cyclotron Road, MS 90-3026D  
Berkeley, CA 94720  
Phone: (510) 486-4636; Fax: (510) 486-4260  
E-mail: [r\\_kostecki@lbl.gov](mailto:r_kostecki@lbl.gov)

### Collaborators

Daniel Abraham, Argonne National Laboratory

Start Date: October 1, 2010

Projected End Date: September 30, 2011

### Objectives

- Enable increased cell specific energy by addressing the impact of high potentials on carbons in the cathode
  - Identify physico-chemical changes of carbon additives when subjected to high potentials, and suggest approaches to improved carbon stability
  - Investigate surface treatment regimens to reduce side reactions
  - Develop strategies to minimize irreversible cell capacity losses
- Determine the key factors that contribute to the degradation mechanism in the PHEV test cells and individual cell components
  - Carry out post-test characterization of components from ABR test cells
- Characterize SEI formation on model electrode surfaces to improve understanding of key interfacial phenomena in PHEV cells

### Technical Barriers

- PHEV battery durability and safety, as well as the need for efficient cell-formation processes, are the major barriers addressed by LBNL diagnostic work
- The primary LBNL role in the ABR Program is to carry out specific diagnostic evaluations to determine the changes in cell components that accompany Li-ion cell power fade, capacity fade, and/or failure
- LBNL also seeks to identify electrode and electrolyte processes that are significantly influenced by various cell-formation protocols

### Technical Targets

- Cycle life: 5000 (deep) and 300,000 (shallow) cycles (40 mile)
- Available energy: 96 Wh/kg (40 mile)
- Calendar life: 15 years

### Accomplishments

- Completed electrochemical characterization study of common carbon black additives at anodic potentials
- Determined interfacial instability of carbon black in composite high-voltage cathodes
- Elucidated the mechanism of carbon black structural degradation
- Identified an approach to carbon black additive stabilization



### Introduction

A primary aim of this project is to develop and use advanced diagnostic techniques to characterize basic physico-chemical properties of electrode active and passive components in ABR Program cells that are being developed for use in PHEV and EV applications. The focus of this task is to correlate fundamental processes that occur in Li-ion batteries with the electrochemical performance. The diagnostic results are used to determine cell failure mechanisms, anticipate the system lifetime as well as to suggest new approaches to design more-stable materials, composites and electrodes.

### Approach

- Strategies to minimize irreversible capacity losses
  - Determine the mechanisms for carbon damage and migration at high potentials
  - Investigate mitigating treatments, additives, and procedures
- Diagnostic evaluation of ABR Program lithium-ion cell chemistries
  - Carry out post-test spectroscopic, microscopic and diffraction diagnostic evaluation of components from ABR test cells and model cells (no test cells have been sent to LBNL in FY11)

- Understand factors that can enhance the stability of SEI layers
  - Use results to suggest approaches to stabilize interfaces
- Establish and investigate degradation mechanisms of PHEV cells

## Results

The electrochemical properties of standard carbon additives and possible implications for the performance of high-voltage cathodes were investigated. We rigorously examined different types of carbon black (Super P, Shawinigan and Denka), which constitute common conductive additives in Li-ion composite cathodes.

Various characterization techniques, such as BET surface area measurements, Raman spectroscopy, SEM, and cyclic voltammetry (CV) were used to assess the structure, stability, and electrocatalytic response of carbon

blacks in organic carbonate electrolytes at potentials that correspond to the operating conditions of high-voltage cathodes such as  $\text{LiMn}_{1.5}\text{Ni}_{0.5}\text{O}_4$  (LMNO). CVs of pure carbon black electrodes revealed side effects that could interfere with the main charge-discharge process in composite high-voltage cathodes, namely,  $\text{PF}_6^-$  intercalation into carbon and electrolyte oxidation.

This anion intercalation into carbon black was monitored *in situ* using Raman microscopy (Figure IV - 136). The intercalation of  $\text{PF}_6^-$  ions in amorphous carbons has been found to occur at potentials ca. 4.1 V vs.  $\text{Li}/\text{Li}^+$ , which is significantly lower than in graphite (4.45 V). Larger spacing between short and disordered graphene planes in amorphous carbons is mainly responsible for this effect. The potentials at which  $\text{PF}_6^-$  intercalation in carbonaceous materials occurs is directly related to the distance between the grapheme sheets and the degree of structural disorder in the carbonaceous material.

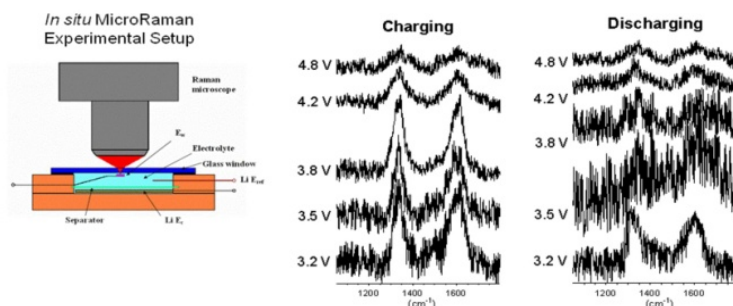


Figure IV - 136: In situ Raman of  $\text{PF}_6^-$  intercalation in carbon black

The electrocatalytic properties of carbon toward the organic electrolytes depend on the carbon atom coordination at the surface, the presence of surface functional groups, and the possible presence of contaminants. Prolonged carbon drying and surface-treatment processes such as heat treatment under  $\text{Ar}/\text{H}_2$  atmosphere can be used to remove volatile contaminants

and oxygen-containing surface groups from the carbon material. CVs of the pristine and heat-treated carbon black electrodes are shown in Figure IV - 137. No change in electrochemical response can be observed after HT treatment. Thus electrolyte oxidation at the surface of the carbon additive is not related to the presence of volatile contaminants, e.g. residual water, or oxygen-containing surface groups.

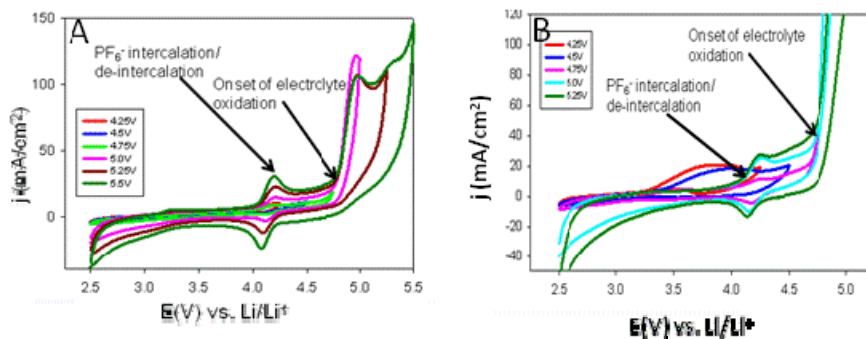


Figure IV - 137: CVs of carbon black electrodes before (A) and after (B) surface treatment with  $\text{Ar}/\text{H}_2$  at  $900^\circ\text{C}$

In an effort to evaluate the potential application of this technology in high-voltage Li-ion cells, a common carbon

black powder (Denka) was subjected to the same surface oxidation procedure. A small carbon sample was placed in

a tubular furnace under a constant flow of nitrogen and heated to 900°C. When the temperature of the furnace reached 900°C, N<sub>2</sub> was replaced with CO<sub>2</sub>. After 1 hour, the CO<sub>2</sub> flow was stopped and nitrogen was introduced again while the furnace was allowed to cool down to room temperature. BET surface area measurements of the pristine and the oxidized carbon powders were performed using nitrogen adsorption at -196°C. The BET surface areas of the pristine and oxidized samples were 50 m<sup>2</sup>/gr and 70 m<sup>2</sup>/gr, respectively. This difference is likely due to a different structure and morphology of Denka carbon black as compared to the carbon film pyrolyzed from polyimide at 1000°C.

To evaluate the electrochemical properties of the heat-treated carbon black material, composite electrodes were prepared. 90% of carbon powder and 10% of PVdF were mixed in NMP for 12 hours. The resulting slurry was drop casted onto an aluminum current collector and allowed to dry at 80°C. The electrodes were then placed in a vacuum oven and dried at 120°C for 12 hours. A three-electrode

cell was assembled with lithium-foil reference and counter electrodes, and filled with 1M LiPF<sub>6</sub>, EC:DEC (wt. 1:2). Cyclic voltammetry measurements were performed at a scan rate of 5 mV/sec.

Figure IV - 138 shows the CVs of the pristine and oxidized carbon black electrodes. The double layer capacities of the pristine sample and oxidized sample were 2 F/gr and 3 F/gr, respectively. This difference in capacitance is consistent with the 40% increase of surface area upon carbon oxidation treatment.

The current at the anodic potential vertex is an excellent indication of the extent of electrolyte oxidation taking place at that potential. As can be seen from Figure IV - 138, the anodic vertex current in the pristine carbon black is significantly higher compared to the oxidized sample. The difference in the anodic vertex current becomes more pronounced as the electrodes were polarized to higher anodic potentials. When the potential span was higher than 5 V, a cathodic peak appeared at 4.2 V (in both samples) and was attributed to the deintercalation of PF<sub>6</sub><sup>-</sup> anions.

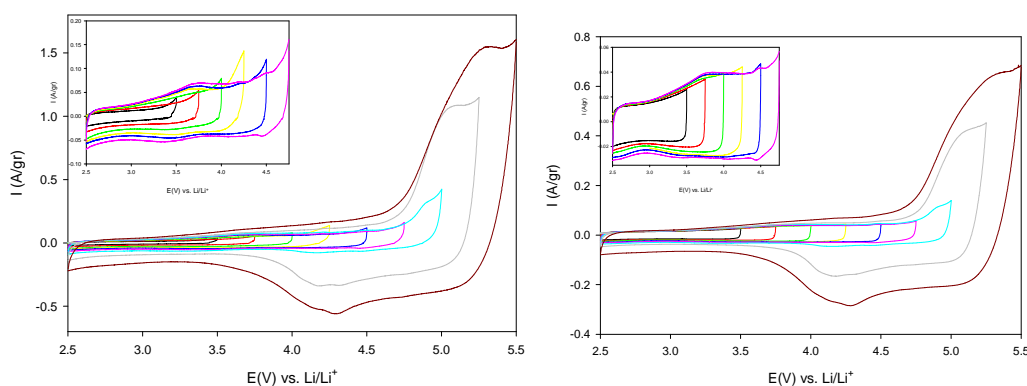


Figure IV - 138: CV's of pristine Denka carbon black (a), and oxidized Denka carbon black

Based on these results, we postulate that carbon surface structure modification due to the oxidation process inhibits both electrolyte oxidation and anion intercalation. Interestingly, this deactivation effect is observed despite the significant surface area increase, which should produce the opposite current trend. It is likely that the presence of surface groups created during the oxidation treatment is responsible for improved electrolyte stability.

## Conclusions and Future Directions

### Conclusions

- Electrolyte oxidation and PF<sub>6</sub><sup>-</sup> intercalation in standard carbon black additives prevents the implementation of high-voltage cathodes

- Pyrolysis of organic precursors at relatively low temperatures (1000°C) leads to the formation of amorphous carbon, which does not allow PF<sub>6</sub><sup>-</sup> intercalation
- CO<sub>2</sub>-activation at elevated temperatures (900°C) leads to more than two orders of magnitude higher carbon surface area
- High-surface-area carbon electrode shows increased stability toward electrolyte oxidation

### Future Directions

- Continue studies of degradation modes of high-voltage cathodes
- Continue search for remedies that decrease irreversible capacity losses and improve coulombic efficiency during cycling

- Reduce the irreversible charge required to form surface layers
- Investigate pretreatment regimens to reduce side reactions
- **Diagnostics of ABR Program cell components.**
- Carry out post-test characterization of components from ABR cells
- Examine electrode composition, structure, and surface films
  - Understand factors that can enhance the stability of SEI layers
  - Establish and investigate degradation mechanisms of PHEV cells
  - Compare degradation mechanisms in ATD vs. ABR cells
- Continue studies of ABR cell components and electrode/electrolyte interface stabilization in collaboration with ABR Program partners
- Carry out post-test characterization of components from ABR cells
  - Examine electrode composition, structure, and surface films
  - Understand factors that can enhance the stability of SEI layers
- Establish and investigate degradation mechanisms of PHEV cells

### FY 2011 Publications/Presentations

1. Vijay A. Sethuraman, Laurence J. Hardwick, Venkat Srinivasan, Robert Kostecki, “Surface structural disordering in graphite upon lithium intercalation/deintercalation”, *Journal of Power Sources* 195 (2010) 3655–3660
2. Robert Kostecki, “*In situ* SPM of Local Interfacial Phenomena in Li-ion Batteries”, International Workshop on SPM for Energy Applications, Oak Ridge National Laboratory, September 16, 2010
3. Robert Kostecki, “Batteries for Automotive Applications”, 2<sup>nd</sup> Annual Workshop on Energy Research Energy Research Institute @ NTU, Singapore, June 16, 2010, (invited talk)

---

## IV.C.1.6 Mechanistic, Molecular, and Thermodynamic Modeling/Diagnostics in support of ABR Cell Performance and Aging Studies (INL)

Kevin L. Gering, PhD  
Idaho National Laboratory  
2525 N. Fremont Ave.  
Idaho Falls, ID 83415-2209  
Phone: (208) 526-4173; Fax: (208) 526-0690  
E-mail: [kevin.gering@inl.gov](mailto:kevin.gering@inl.gov)

Collaborators (INL): David K. Jamison, Christopher J. Michelbacher, Sergiy V. Sazhin

Contract No. DE-AC07-05ID14517

Start Date: April, 2008

Projected End Date: ongoing

### Objectives

- Develop advanced modeling tools that will complement Developmental and Applied Diagnostic Testing (DADT), based on fundamental principles of molecular interactions, chemical physics, reaction kinetics, and thermodynamics.
- Deploy these modeling tools to examine mechanistic contributions to cell performance, cell aging and path dependence (PD) thereof, to support technological advances of materials, and to improve battery management.
- Use INL modeling tools to develop/optimize operational protocol to manage and minimize the aging processes for lithium-ion cells within a given application and geographic location (chemistry-specific, but with generalized approach).

### Technical Barriers

Batteries employed in electric drive applications (HEV, PHEV, or EV) will undergo diverse usage patterns during their service life, where the extent of aging over time depends on several factors tied to severity of the duty cycle, environmental conditions, and the onboard thermal management scheme. Path dependence of aging is then a premier consideration for understanding and prolonging the life of batteries in their primary, secondary, and later applications. If indeed a strong path-dependent correlation exists for battery aging rates, this will have a sobering consequence toward meeting battery warranties for HEV, PHEV, and EV systems, since in many such cases battery

life is elucidated by the industry from a series of isothermal or other equally oversimplified studies.

Thus, there has been a need for modeling tools that describe physics-level phenomena within electrochemical systems over multiple domains, since such tools have generally not kept pace with lithium-ion materials technology worldwide. Of keen interest is to develop a purely scientific and mechanistic-based approach to describing aging processes in such systems, where the foundational theories and mathematics lend themselves to true predictive analysis over arbitrary aging conditions. Seeing this need, this work has produced a generalized physics-based modeling platform that can be used for truly predictive analysis of aging mechanisms, wherein this capability looks squarely at the issue of aging path dependence. Added to this is a unique INL molecular-based software tool known as the Advanced Electrolyte Model (AEM) that saw further expansion during 2011 to cover more chemical systems, additional molecular phenomena, and application toward more private sector customers.

### Technical Targets

- Develop and validate computer modeling and simulation tools that yield accurate interpretation of aging and performance data in terms of meaningful physical and chemical quantities. Demonstrate INL diagnostic/predictive modeling capabilities through software that integrates key modules regarding cell performance over life (INL CellSage).
- Deploy modeling tools toward optimizing battery usage and life given operational and environmental conditions, including geographic location.
- Develop and demonstrate DADT tools that enable materials-level investigations of cell performance.
- Integrate modeling protocols into a chipset to provide real-time dynamic monitoring, diagnosis and evaluation, and prediction of key metrics such as useful life remaining.
- Continue deployment of AEM to support the DOE ABR program and the private sector.

### Accomplishments

- Key computational methods have been developed and benchmarked on Gen2 and other Li-ion cell performance and aging data. Our framework adapts

these tools to PD scenarios and will be applied to our various DADT data. These methods cover losses of capacity and cell conductance over aging, kinetic performance over multiple domains, and other diagnostic data.

- Mechanistic analysis is supported, allowing quantification of predominant contributions to aging metrics such as capacity loss.
- Prediction of aging trends under arbitrary conditions has been accomplished, using a generalized physics and thermodynamics-based scheme. This capability allows direct consideration of aging path dependence.
- PD effects from various scenarios involving temperature, SOC, and cycling regime have been investigated with these modeling tools, using Gen2 NCA/graphite cell performance as a benchmark.
- Multi-year simulations were performed for lithium-ion cells operating at Phoenix, Arizona, where the annual temperature cycle and HEV duty cycling were considered through the modeling framework, as well as variable SOC and thermal management scenarios. The results support optimizing battery usage conditions to prolong life.



## Introduction

Domestic and worldwide vehicle designs are going more toward electric-drive platforms based on advanced batteries (Li-ion), causing a commensurate need for a rational foundation for understanding how battery usage conditions affect the aging rates and the effective service life of batteries. Batteries in vehicle service will encounter diverse usage conditions, and may be placed in secondary or tertiary applications once their performance in vehicles has reached predefined limits. Non-vehicle utilization of advanced batteries will involve several million cells under an inexhaustible assortment of applications and conditions. This collective landscape exposes an obvious need for physical models that can facilitate intelligent, science-based diagnostic analysis and prediction of performance and aging trends for electrochemical cells and cell materials operated at arbitrary conditions.

In 2011 INL successfully demonstrated capability toward meeting this fundamental need. We utilize capabilities at INL to answer fundamental questions on aging processes, path dependence thereof, and how to mitigate performance limitations over life. Recent references document or relate to this work [1-3].

## Approach

This work aims to leverage laboratory test data toward elucidating aging under actual yet arbitrary PHEV field

conditions through physical (physics-based) models by isolating the predominant aging stress factors of Li-ion cells in EDV service, which would include, for example, the nature and frequency of duty cycles, annual thermal cycles, as well as the frequency and severity of daily thermal cycles. At INL, such factors are studied in controlled and repeatable laboratory conditions to enable mechanistic evaluation of aging processes and path dependence thereof.

Modeling tools developed and employed are those that promote diagnostic analysis of aging mechanisms over multiple domains. Model parameters strictly represent physical, chemical, electrochemical, or molecular quantities, and the mathematical framework incorporates key governing equations covering thermodynamics and chemical kinetics. These tools are supported by a suite of diagnostic testing (for sake of model validation), naturally lend themselves to PD scenarios, and have intellectual property status. Testing is in progress to establish path dependence behavior as functions of temperature and SOC, thereby providing further means toward model validation.

**Path Dependence (PD) of Cell Aging.** The extent and rate of cell aging over time depends on specific operational conditions (stress factors) encountered over the timeline. Path dependence asserts that the *sequence* of aging conditions as well as the nature of conditions has a direct influence on the rate of aging and net aging along the timeline (akin to performance of a “batch reactor”). A change in aging conditions can accelerate or decelerate degradation mechanisms, and can initiate new ones. Principles of reaction kinetics and thermodynamics are key to understanding the aging process along the path. INL aging models are easily adaptable to PD scenarios.

**Modeling Aging Cells as Batch Reactors.** Contributions from chemical kinetics and thermodynamics to cell degradation processes determine the effective rate and extent that cells age, affecting losses in capacity, power, general performance, and ancillary quantities over service life of electrochemical cells (Figure IV - 139). Sigmoidal rate expressions are well suited to describe these processes within a batch reactor scenario, e.g., for capacity loss at aging condition  $i$  ( $\Psi_i$ ) we have:

$$\Psi_i = \sum_j 2M_j \left[ \frac{1}{2} - \frac{1}{1 + \exp(a_j t^{b_j})} \right]_i$$

- $a_j$  : rate constant attributable to mechanism  $j$ ,
- $b_j$  : related to the order of reaction for mechanism  $j$ ,
- $M_j$  : theoretical maximum limit of capacity loss under mechanism  $j$  considering the thermodynamic limit of degradation under  $j$  for a batch system.



Figure IV - 139: Modeling Aging Cells as batch reactors

These mathematical expressions are self-consistent, properly bounded, adaptive, relevant to cell environments, and easily lend themselves to a comprehensive degradation rate analysis of performance data. This basis enables rendering of the constituent (mechanistic) sources of performance loss.

## Results

FY 2011 was a key year in mobilizing computational tools for evaluating aging mechanisms and related path dependence, and for deployment of the AEM for additional use within ABR and the private sector. Our key findings are summarized below for 2011, using the Gen2 cell chemistry as a basis:

Simulations were done where SOC was used as the PD parameter over temperature for HEV cycle-life conditions. Figure IV - 140 and Figure IV - 141 show the C/25 and C/1 capacity losses, respectively, wherein the red curves represent the case where the effective SOC was at 100% for the first two years, then switched to 60% SOC for the remaining two years. The blue curves reverse this SOC trend. The solid curves are aging at 25°C while the dashed curves represent aging at 45°C. Thus, at a given temperature the simulation imposes identical net conditions by the end of four years. The shown predicted curves are composite capacity losses for a two-mechanism degradation process involving loss of lithium inventory (LLI) and loss of active host material (LAHM). From both figures it is evident that there is a stronger PD effect for aging at 45°C, as seen by the larger difference in the final capacity fade. The occurrence of path dependence implies the opportunity of path optimization. PD should be exploited when feasible to optimize cell life. In this case starting at a lower SOC then moving to a higher one yields overall lower capacity loss by the end of the simulations.

Aging simulations were performed to investigate the aging trends of Gen2 cells at Phoenix, Arizona, considering the annual temperature cycle at that locale (Figure IV - 142). Figure IV - 143 and Figure IV - 144 show HEV cycle-life and calendar-life results for Gen2 cells aging under the Phoenix monthly temperatures (red curves) compared to baseline cycle-life results at 25°C (black curves). The heavy dashed curves represent the total capacity loss over time while the solid and dotted curves are from the mechanisms of LLI and LAHM, respectively. Stairstepping of capacity loss is seen as the

higher summer temperatures cause losses to increase while the colder fall and winter months cause a commensurate decrease in aging rates. Figure IV - 145 reveals PD behavior in C/1 capacity loss in varying the SOC over the four year simulation for Phoenix. Similar to Figs. 4 and 5, Fig. 6 shows that less capacity is lost if SOC starts lower and is increased over time. Finally, Figure IV - 146 and Figure IV - 147 show results for PD simulations having a presumed thermal management scheme for Phoenix, as defined by a maximum permissible temperature under thermal management (y axes). Thermal management provides substantial increase in cell life for the C/25 case, particularly below 40°C, but less so for C/1 due to polarization effects which persist over temperature. Such results can be used to support design of thermal management systems for battery packs destined for various geographic locations.

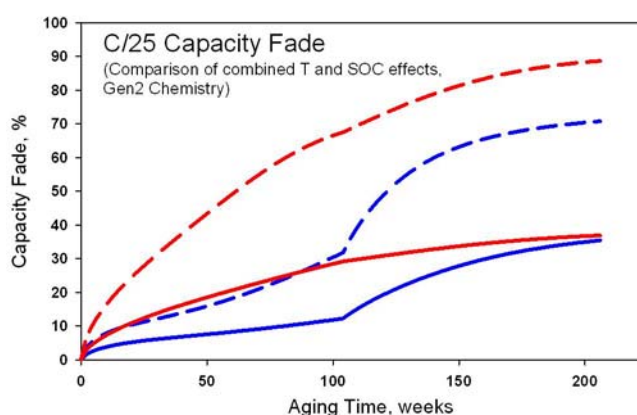


Figure IV - 140: C/25 Capacity Fade Curve

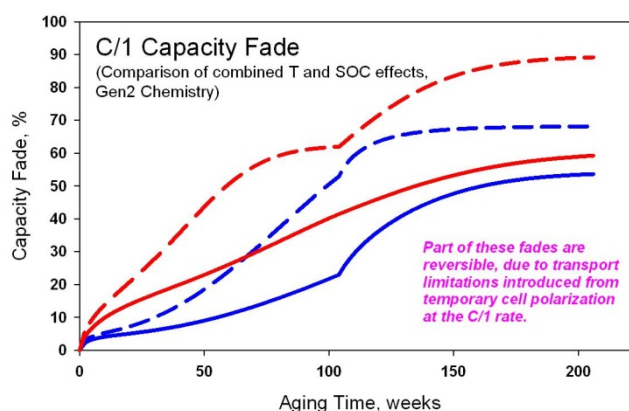


Figure IV - 141: C/1 Capacity Fade Curve

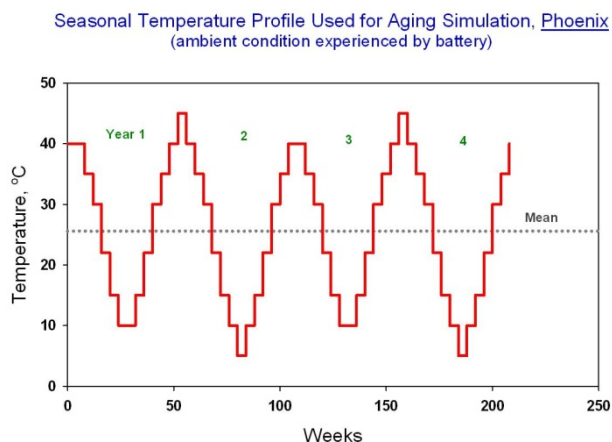


Figure IV - 142: Seasonal Temperature Profile Used for Aging Simulation (Phoenix)

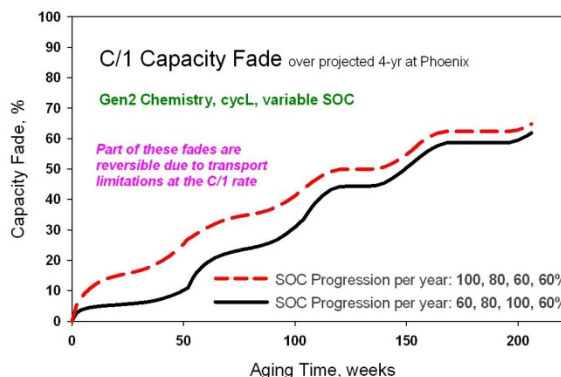


Figure IV - 145: PD behavior in C/1 capacity loss in varying the SOC over four year simulation (Phoenix)

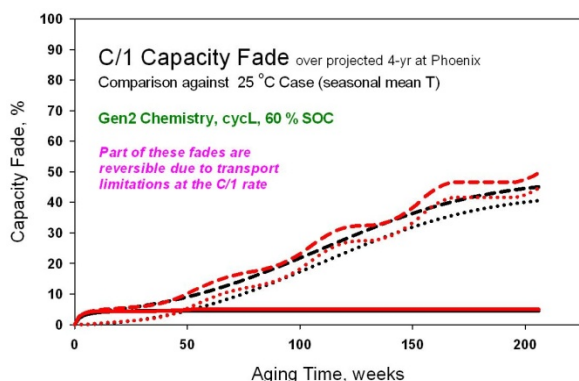


Figure IV - 143: HEV cycle-life results for Gen2 cells aging (Phoenix monthly temperatures)

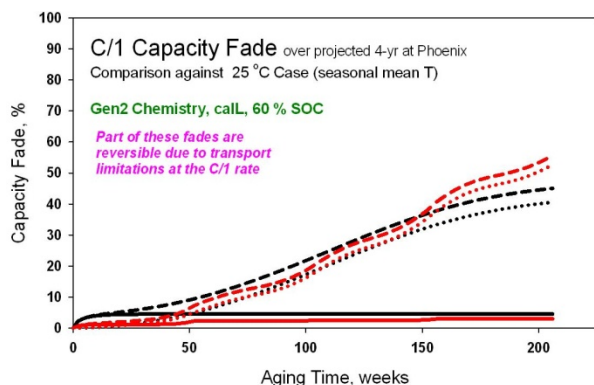


Figure IV - 144: HEV calendar-life results for Gen2 cells aging (Phoenix monthly temperatures)

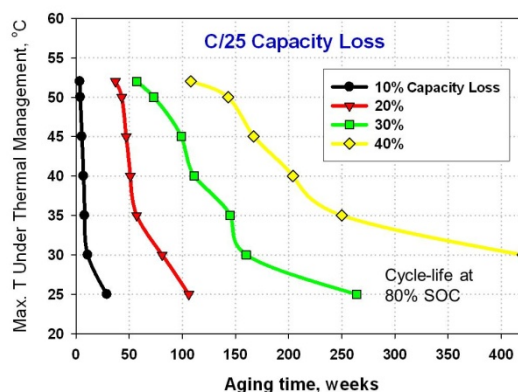


Figure IV - 146: PD simulations with thermal management scheme for Phoenix – C/25 Capacity Fade

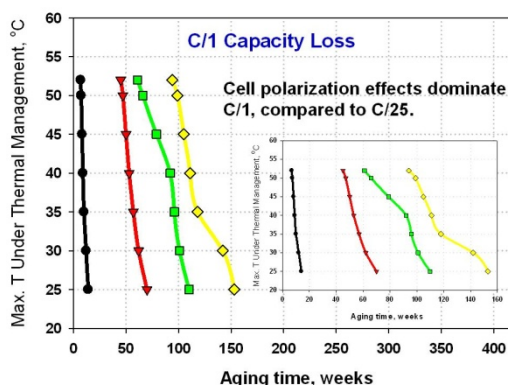


Figure IV - 147: PD simulations with thermal management scheme for Phoenix – C/1 Capacity Fade

### Conclusions and Future Directions

INL has developed strategic computational tools used to diagnose, model and predict performance and aging of electrochemical cells and cell components. These tools have been used to guide research by targeting more relevant experimental conditions. Within the context of cell aging under PHEV protocols, these tools are revealing

mechanisms of cell degradation, related path dependence, and chief causes and conditions of performance loss. The immediate benefits of this work are (1) to provide more realistic and accurate life predictions by accounting for the influence of thermal cycling effects and related path dependence on aging mechanisms, and (2) enable accelerated battery development, design, and management

Future simulation work toward path dependence studies could involve other duty-cycles (e.g., FUDS, DST), other temperature parameters defined for a particular city or region, the effect of daily thermal cycling, and other Li-ion cell chemistries. Optimizing battery life is an abiding goal of this work, a goal that is reachable through INL intelligent physical models.

### **FY 2011 Publications/Presentations**

1. K. L. Gering, “Efficient and Accurate Computational Tools for Evaluating Performance Targets of Lithium-ion Cells and Cell Components”, Lithium Mobile Power 2010, Nov. 5, 2010 (Boston, MA).
2. K. L. Gering, “Advanced Electrolyte Modeling Methods: Foundations and Capabilities”, Pacific Power Sources Symposium, Jan. 13, 2011 (Waikoloa, Hawaii).
3. K. L. Gering, “How “Old” is Your Battery? Metrics and Methods for Determining Battery Performance over Aging”, 12th Electrochemical Power Sources R&D Symposium, June 21, 2011 (Monterey, CA).

## IV.C.1.7 Mechanistic, Molecular, and Thermodynamic Modeling/Diagnostics in support of ABR Cell Performance and Aging Studies (ORNL)

Claus Daniel

Oak Ridge National Laboratory  
1 Bethel Valley Rd.  
P.O. Box 2008, MS-6472  
Oak Ridge, TN 37831-6472  
Phone: (865) 241-9521; Fax: (865) 241-5531  
E-mail: [danielc@ornl.gov](mailto:danielc@ornl.gov)

### Collaborators:

Nancy Dudney, ORNL  
Andrew Payzant, ORNL  
Robbie Meisner, ORNL  
Daniel Abraham, ANL  
Sean Hearne, SNL  
Donald Siegel, University of Michigan

Start Date: January, 2009  
Projected End Date: September 2011

### Objectives

- Develop cost effective *in situ* characterization tools for the validation of degradation mechanisms
- Develop an understanding of degradation mechanisms in anodes and cathodes

### Technical Barriers

The primary technical barriers are a lack of understanding of the contribution of mechanical degradation to the life time limitation of batteries and their capacity fade.

### Accomplishments

- Developed a laboratory-scale methodology for using acoustic emission (AE) and x-ray diffraction (XRD) for monitoring degradation in lithium ion batteries (LIBs).
- *In situ* AE-XRD uses safe, inexpensive components that can be tailored to work with either anode or cathode materials, making the design useful in a wide variety of situations.
- Lattice strain and phase transformation analysis in cathodes ( $\text{LiNi}_x\text{Mn}_y\text{Co}_z\text{O}_2$  [NMC],  $\text{Li}(\text{Mn}_{1.5}\text{Ni}_{0.5})\text{O}_4$  [MNO], and  $\text{Li}_{1.2}\text{Ni}_{0.15}\text{Mn}_{0.55}\text{Co}_{0.1}\text{O}_2$  [HE5050]) and

Sn anodes was measured and correlated well with the observed AE activity.

◇ ◇ ◇ ◇ ◇

### Introduction

Electrode materials for LIBs undergo many changes as they are cycled, including lattice strain and particle fracture. The role of mechanical degradation in overall LIB performance is not thoroughly understood but is likely to play an important role in the development of next-generation active materials and cell design. However, the progress of work in this area is limited by current characterization techniques. A novel *in situ* technique that combines AE and XRD has been developed and tested on both anode and cathode materials.

### Approach

AE has been used to detect, sort, and classify mechanical events such as particle fracture inside cycling LIBs. In order to directly correlate the observed fracture events with strain in the active materials, special *in situ* methods of XRD can be used. A novel beryllium-free *in situ* AE-XRD cell has been devised which uses a metalized Mylar or Kapton window to allow X-ray penetration during cycling in standard coin cell hardware. More details can be found in our last year's report. This technique provides a safe, inexpensive alternative to current *in situ* XRD methods. It also provides data for a depth of understanding which before was possible only with special miniature cells and very short synchrotron beam time. The new cell allows for extended beam time in inexpensive laboratory-scale diffractometers. Mylar or Kapton disks sputtered with compatible metals can be used in direct contact with active materials. Studies using this combined technique will allow for further fundamental understanding of material degradation mechanisms and how they are correlated with capacity fade and cell failure.

### Results

**$\text{Li}(\text{Mn}_{1.5}\text{Ni}_{0.5})\text{O}_4$  (MNO):** We showed that at 4.7V, stepwise transformations between tetragonal spinel phases occurred as Ni was oxidized or reduced during charge and discharge respectively. At low potentials near 2.7V a Jahn Teller distortion was observed that creates a distorted spinel phase. AE experiments were conducted using the

same MNO materials and cycling parameters as used in Publication 1, referenced at the end of this section.

The total number AE hits recorded during each charge and discharge step are shown plotted with capacity in Figure IV - 148. The most striking feature of this figure is that almost all of the AE activity occurs during charging when lithium is being removed from the MNO particles. As lithium is removed the particle surface comes under tension while the core experiences compression. This likely indicates that cracks are forming on the particle surface. Another interesting observation is that major AE activity is not observed until about the 7<sup>th</sup> cycle, peaks at the 11<sup>th</sup> cycle, and decreases thereafter. This indicates a fatigue type behavior where the material undergoes a pile up of dislocations and defects during the initial cycles which result in fracture after a critical point.

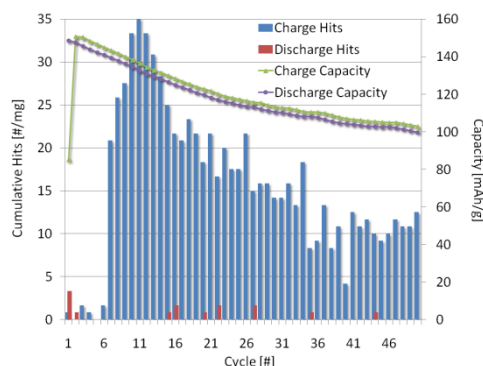


Figure IV - 148: Bar graph of AE activity for each charge and discharge step. A clear majority of events were observed during charging and a fatigue type AE activity onset was seen.

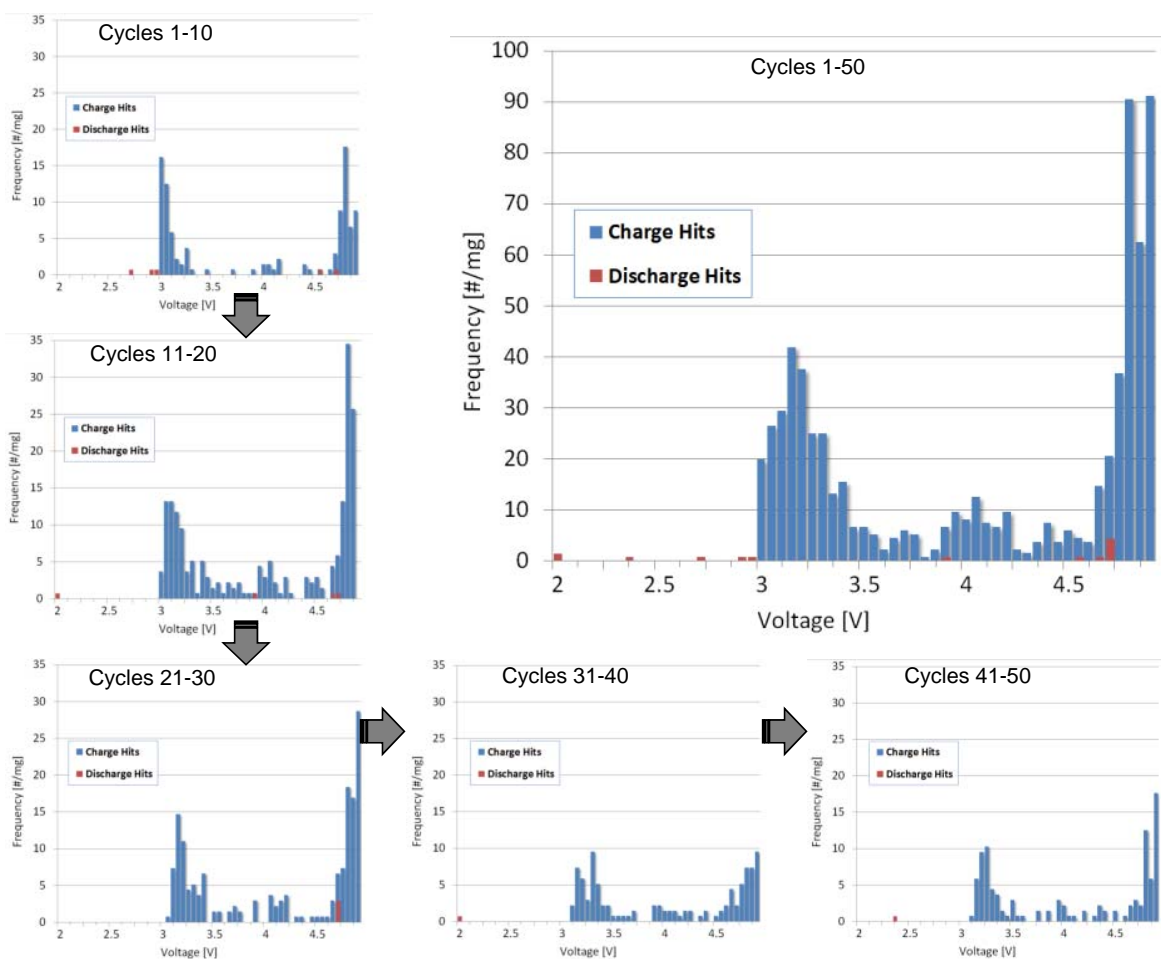


Figure IV - 149: Bar graph of AE activity binned by cell potential. Three activity regions were noted including those related to Ni oxidation (4.7V), Mn Jahn Teller distortion (2.7V), and cation ordering (4.0V). The 4.7V group showed the most dependence on cycle number and is likely the source of the fatigue onset type behavior.

Figure IV - 149 was created by binning the AE activity as a function of voltage over sets of 10 cycles. Here it clear that a majority of AE hits were detected in the 4.7V region where transition between the difference Ni oxidation states

occurs. A significant population of AE hits was also detected in the low potential region near 2.7V which is related to the Mn Jahn Teller distortion. A minority group near 4.0V seems to correspond with the voltage plateau

observed when cycling ordered MNO and may be related to material damage arising from cation reordering processes. The high potential AE group is most affected by cycle number and it peaks between 11-20 cycles before decreasing.

**Li<sub>1.2</sub>Ni<sub>0.15</sub>Mn<sub>0.55</sub>Co<sub>0.1</sub>O<sub>2</sub> (HE5050):** During the end of this fiscal year, we started to work on this new cathode material in collaboration with Dan Abraham of ANL. The two questions we pursued were: (1) When is the major mechanical degradation and how is it associated with the lattice constant development during slow and fast charge/discharge? (2) The material experiences a dramatic impedance change after cycling during a hold time at a voltage of 4.5 to 4.6V. Is the material considerably

mechanically degrading during this time and what is the lattice parameter development?

During the mechanical degradation quantification, we only counted acoustic emissions contributing to crack formation and propagation in typical signatures of single and sequential cracking events. Figure IV - 150 shows that a low current of 9.9 mA/g does not contribute to significant mechanical degradation, while a high current of 30mA/g shows considerable mechanical degradation during delithiation. This is contrary to earlier results on high capacity anode materials and indicates that anodes and cathodes degrade simultaneously (anodes are lithiated at the time of cathode delithiation).

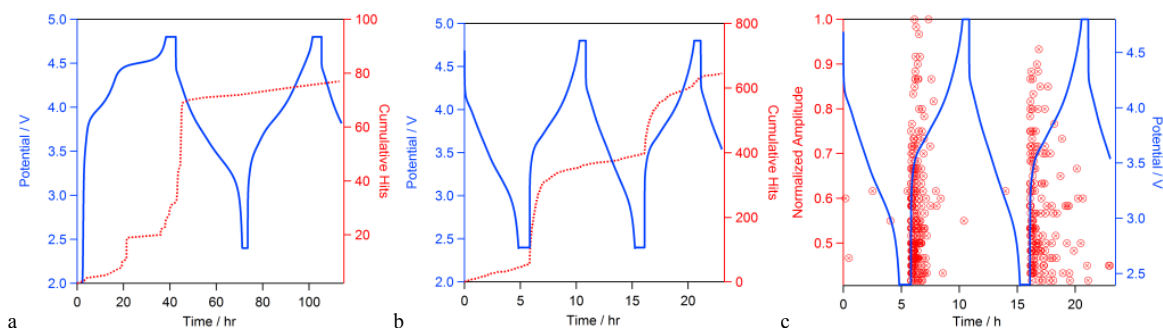


Figure IV - 150: Events registered with (a) 9.9 mA/g cycling and (b) 30 mA/g cycling. CCCV 2.4-4.8V. Note the much larger number of cracking events with rapid charging mostly occurring at delithiation. (c) Detailed view of individual events during charging/discharging at high rate.

During the hold time at 4.6V, we detect a small number of crack events. Figure IV - 151 shows cumulative hits during the hold time. This study was performed without

additional cycling or aging. We will continue these studies in collaboration with ANL.

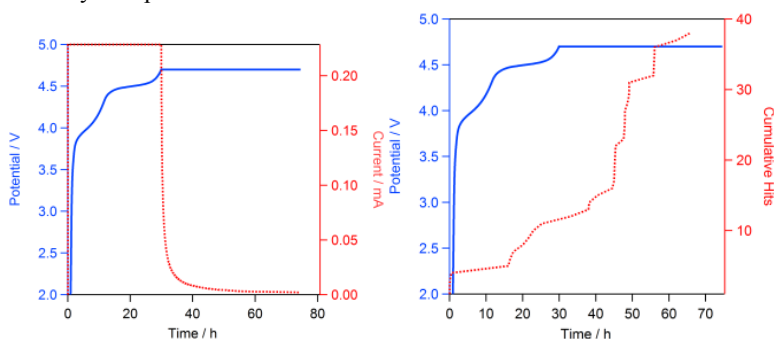


Figure IV - 151: Electrochemical hold and cracking events during the hold time.

**Sn thin film anodes:** Thin film electrodes for LIBs pose several attractive advantages over traditional composite electrodes including size and shape constraints, operating temperature range, and volumetric energy density. Tin is an attractive candidate for LIB anodes due to its exceptional specific capacity, cascading voltage profile, safety, wide availability, and low cost. Tin thin film electrodes were sputtered onto the Ti current collector of an *in situ* XRD cell and were monitored continuously by

XRD while cycling. A phase transformation from white tin, to Li<sub>2</sub>Sn<sub>5</sub>, to β-LiSn, to Li<sub>22</sub>Sn<sub>5</sub> was observed during lithiation with the same phases detected in reverse order during delithiation as shown in Figure IV - 152. This represents the successful attempt to apply this *in situ* XRD technique to thin film electrodes. This work sets the stage for future experiments to test the performance of thin films with different preferred orientations and surface coatings.

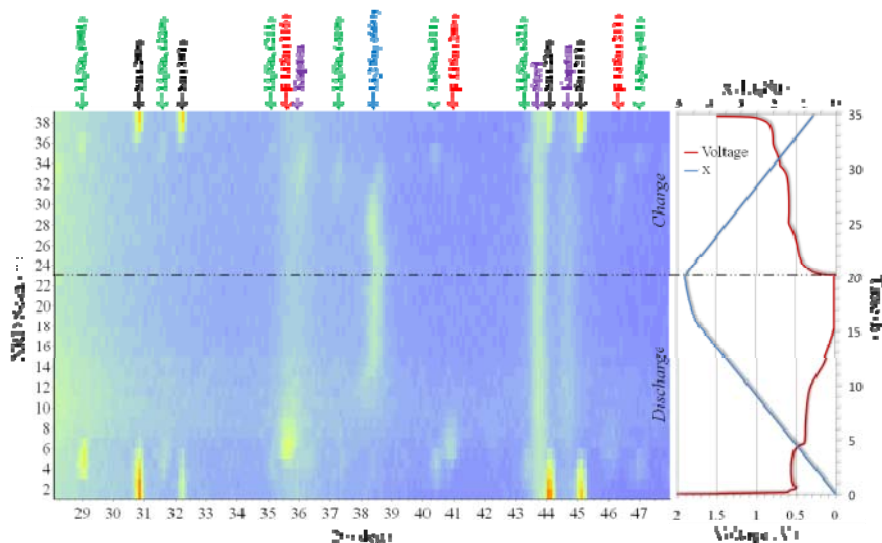


Figure IV - 152: An isoplot of in situ XRD data collected during the cycling of a tin thin film electrode. Clear transitions between the white tin,  $\text{Li}_2\text{Sn}_5$ ,  $\beta\text{-LiSn}$ , and  $\text{Li}_{22}\text{Sn}_5$  phases are seen.

## FY 2011 Publications/Presentations

### Publications

1. K. Rhodes, R. Meisner, Y. Kim, N. Dudney, C. Daniel, Evolution of Phase Transformation Behavior in  $\text{Li}(\text{Mn}_{1.5}\text{Ni}_{0.5})\text{O}_4$  Cathodes Studied by *In situ* XRD, *J. Electrochem. Soc.* 158 (2011) 8, A890-A897
2. K. Rhodes, M. Kirkham, R. Meisner, C. M. Parish, N. Dudney, C. Daniel, Novel cell design for combined *in situ* acoustic emission and x-ray diffraction study during electrochemical cycling of batteries, *Rev. Sci. Instr.* 82 (2011) 075107
3. K. J. Rhodes, R. Meisner, M. Kirkham, N. Dudney, C. Daniel, *In Situ* XRD of Thin Film Tin Electrodes for Lithium Ion Batteries, *J. Electrochem. Soc.* (in print)

### Presentations

1. Electrochemical energy storage and mechanical degradation of intercalation electrodes, Chapter 14, ESE511, University of Tennessee, Knoxville, TN, November 2, 2011
2. Materials and Processing for Electrochemical Energy Storage at ORNL, Dow Kokam Advanced Technology Exchange, Lee's Summit, MO, October 20, 2011
3. Mechanical Degradation and Materials Processing for Electrochemical Energy Storage Devices, 1st Annual Technology Summit, U.S. China Clean Energy Research Center, Clean Vehicle Consortium, Beijing, China, October 18, 2011
4. Mechanical Degradation in Intercalation Electrodes, Sandia National Laboratory, NM, July 6, 2011

5. Mechano-Electrochemical Behavior of Energy Storage Materials, Materials Science and Engineering Seminar, University of North Texas, TX, April 17, 2011
6. Mechanical Degradation of Insertion Electrodes, UMERC and College of Engineering Seminar, University of Maryland, College Park, MD, March 28, 2011
7. Diagnostics for energy storage materials, ABR Diagnostics Workshop, Department of Energy, Argonne National Laboratory, Chicago, IL, March 1, 2011
8. Keynote panel, Battery Projects and Developments in Government Laboratories Panel, Battery Power 2010, Dallas, TX, Oct. 19-20, 2010

### Acknowledgment

This research at Oak Ridge National Laboratory, managed by UT Battelle, LLC, for the U.S. Department of Energy under contract DE-AC05-00OR22725, was sponsored by the Vehicle Technologies Program for the Office of Energy Efficiency and Renewable Energy. Parts of this research were performed at the High Temperature Materials Laboratory, a National User Facility sponsored by the same office.

## IV.C.2 Cell Fabrication and Testing

### IV.C.2.1 Fabricate PHEV Cells for Testing & Diagnostics (ANL)

Andrew N. Jansen

Argonne National Laboratory  
9700 South Cass Avenue  
Argonne, IL 60439-4837  
Phone: (630) 252-4956; Fax: (630) 972-4461  
E-mail: jansen@anl.gov

#### Collaborators:

Bryant Polzin, Argonne  
Dennis Dees, Argonne  
Wenquan Lu, Argonne  
Sun-Ho Kang, formerly Argonne  
Paul Nelson, Argonne  
SAFT America  
EnerDel

Start Date: October, 2008

Projected End Date: September, 2014

#### Objectives

- The objective of this work is to speed the evaluation of novel battery materials from the ABR and BATT programs, as well as from universities and the battery industry. The main objective in FY11 is to develop the capability to fabricate in-house pouch and 18650 cells in Argonne's new dry room facility.

#### Technical Barriers

- Newly developed battery materials for PHEVs need to be tested in limited batch size before larger scale industrial commitment.
- Validation tests are needed in cell formats with at least 0.4 Ah in capacity.
- Electrode designs must be developed that are appropriate for PHEV batteries.

#### Technical Targets

- Produce electrodes and cells based on high energy negative and positive active materials and test performance.
- Use electrochemical performance data and battery design modeling to design PHEV battery.

- Distribute electrodes and cells to ABR/BATT members for testing and diagnostics.
- Design and install facility for making in-house electrodes, 18650 cells, and pouch cells at Argonne.

#### Accomplishments

- Completed installation of new dry room that is used to fabricate lithium-ion prototype cells.
- Installed 18650 and pouch cell making equipment in new dry room with necessary safety modifications and approvals.
- Installed customized electrode coating and hot roll press equipment with necessary safety modifications and approvals.
- Installed high shear planetary mixer from Ross.
- Completed setup of Cell Formation and Cycling Lab that will support prototype Cell Fabrication Facility.
- Designed and obtained baseline electrode sets to be used in high voltage electrolyte studies from contracted vendors.
- Determined optimum PHEV battery parameters using Battery Design Model (BatPac) with baseline electrode results as input.



#### Introduction

Several new battery chemistries are being proposed for PHEV batteries that must be evaluated in cell formats that are larger than a few mAh in capacity. Cell builds are generally based on materials recommended by the ABR Screening subtask, many of which are novel materials developed in the ABR and BATT programs, but also materials from industry and universities. The previous ATD program required cells designed for HEV applications, which used thin electrodes. The ABR Program has little experience with thicker electrodes that are now required for PHEV applications. The performance of these thicker electrodes must be determined and verified in cell builds using advanced battery materials. Once the influence of electrode thickness has been established, the many novel high-energy materials being developed world wide will be explored in new cell builds.

Historically, cell builds have been carried out through subcontracts with battery developers to produce flexible or rigid cells per the ATD and ABR Program directions. This approach can occasionally result in delays due to lack of sufficient material quantities for the larger coating equipment or due to the battery developer's internal priorities taking precedence. Thus, it was decided that Argonne should develop its own in-house cell making capability.

## Approach

Promising new exploratory materials are often developed in small coin cells, which may or may not scale up well in large PHEV battery designs. For this reason, pouch cells or rigid cells such as 18650's will be used for proofing of new materials in the capacity range of 0.4 to 2 Ah.

Pouch cells will be used for initial evaluations of long-term exploratory materials. Pouch cells are an efficient method of determining the stability of a cell system during calendar and cycle life aging. If the chemistry is not stable, it is likely that gassing will occur inside the cell. This will result in the pouch cell bulging or rupturing if the gassing is significant. More established materials and chemistries (or those that pass the pouch cell evaluation) will be used in rigid cells (e.g. 18650s).

## Results

**Cell Fabrication Facility.** A new dry room was installed by Scientific Climate Systems that will maintain <100 PPMv moisture (-42°C dew point) for an area of ~500 ft<sup>2</sup>, with 6 persons, and 750 SCFM exhaust

capability. The dry room became operational in August 2009.

Two vendors were located that deal with manufacturing of pilot scale lithium-ion cell making equipment. The decision was made to purchase the lithium-ion pouch cell making equipment from Media Tech, which will use the XX3450 cell format (34 mm wide by 50 mm high). This equipment includes: pouch stamper, electrode punch, winder/stacker, grid trimmer, ultrasonic welder, tab area sealer, side area sealer, and electrolyte-filling vacuum chamber.

Media Tech was also selected to make the lithium-ion 18650 cell making equipment. This equipment includes: electrode slitter, winder, groover, electrolyte filler, resistance welder, and crimper. Both sets of cell making equipment were received in the spring of 2010. Training was provided by Media Tech engineers soon after. Modifications were made to enhance the function and safety of all equipment during the installation process. A safety review process was conducted with approval to operate the pouch and 18650 cell making equipment granted in August of 2010.

The electrode coater and hot roll press equipment was contracted to A-Pro, and were received in September and October of 2010, respectively. Installation and training was provided by the vendor's engineers in December. Modifications were made to the coater and press to enhance their operation and safety in the dry room, with final approval to operate all equipment in the dry room granted in February, 2011. The final layout of the electrode and cell making equipment in the dry room is shown in Figure IV - 153. The coater and hot roll press are shown in Figure IV - 154 and Figure IV - 155, respectively.

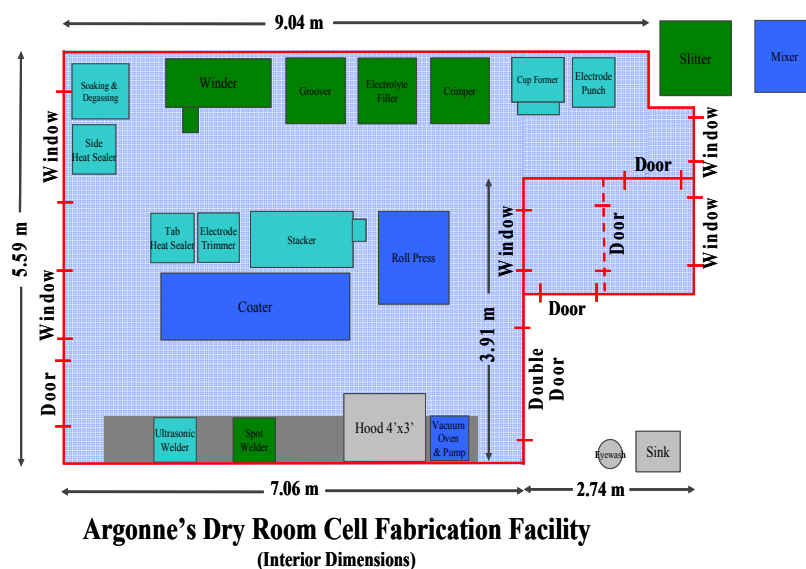


Figure IV - 153: Equipment layout in Cell Fabrication Facility.



Figure IV - 154: "Reverse comma" coater with dual drying zones and intermittent coating capabilities.



Figure IV - 155: Hot roll press capable of 1.5 tons/cm force and 120°C roll temperature.

The ability to make cells with long cycle life and good electrochemical performance is dependent on making high quality electrodes. Key to this is the ability to make homogeneously dispersed electrode slurries with intimate contact between active particles and conductive additives. To accomplish this step, a high energy/shear planetary mixer was purchased from Ross with a 2 liter chamber capacity (Figure IV - 156). This relatively small capacity size is ideal for the typical electrode builds made with the pilot scale coater, where supply of novel materials is often limited. Installation of this mixer was completed in October, 2011.



Figure IV - 156: High energy/shear planetary mixer from Ross with a 2 liter chamber capacity.

Cells made in the Cell Fabrication Facility need to be formed properly before undergoing electrochemical performance evaluation. A laboratory was renovated and equipped with electrical utilities needed to operate three 96 channel MACCOR cyclers with accompanying ovens and temperature chambers. Ventilation ducts with passive draw were provided to each oven and chamber to catch smoke or fumes from cells that go into thermal runaway. No thermal runaways were experienced so far. This Cell Formation and Cycling Lab is shown in Figure IV - 157.



Figure IV - 157: Cell Formation and Cycling Lab.

**First Cell Build.** Once the coater, press, and cell making equipment were approved for use (February, 2011), efforts were directed to making the first cell build. Today's high energy cathode material, HE5050 ( $\text{Li}_{1.2}\text{Ni}_{0.15}\text{Co}_{0.10}\text{Mn}_{0.55}\text{O}_2$ ), was selected for the first positive electrode build based on its screening results. ConocoPhillips' CGP-A12 high energy graphite was selected for the first negative electrode build based on its screening results. The selection of active materials to use was based chiefly on the criteria of high capacity and open availability.

Single-sided and double-sided electrodes were made with Toda’s HE5050 cathode, and with ConocoPhillips CGP-A12 graphite. Over a dozen pouch cell assemblies were made with these advanced electrodes (Figure IV - 158), seven of which were filled with electrolyte and then subjected to formation cycling and electrochemical performance characterization cycling. These cells performed well and were delivered to the EADL for independent verification and life testing. EADL completed testing of the first batch of Toda HE5050 cells at the end of June. A summary of these pouch cells is shown in Figure IV - 159, Figure IV - 160, and Table IV - 6 below.

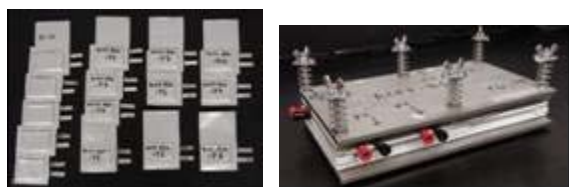


Figure IV - 158: First cell build and test fixture used.

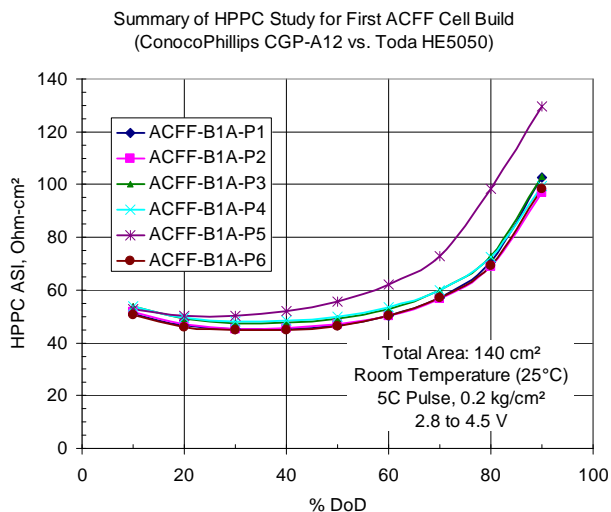


Figure IV - 160: HPPC impedance summary of first cell build made by the Cell Fabrication Facility.

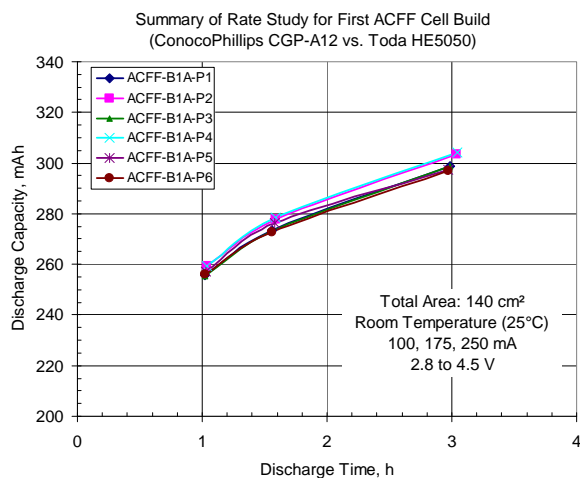


Figure IV - 159: Capacity summary of first cell build made by the Cell Fabrication Facility.

Table IV - 6: Rate capability of first cell build positive electrode material.

Rate	Capacity – mAh/g
C	146
C/2	163
C/3	172
C/5	183

**Second Cell Build.** Based on favorable results from the ABR Screening Task, one of Argonne’s advanced cathode materials under development was selected for the second cell build. This material is a high-energy layered-layered NMC cathode (Li<sub>1.2</sub>Ni<sub>0.3</sub>Mn<sub>0.6</sub>O<sub>2.1</sub>) made by staff at Argonne, referred to as ABR1 cathode. Several batches were made and then blended together to make a supply of nearly 2 kg of this high-energy NMC cathode. The ABR1 cathode was also selected to be the first material to be scaled up into kilogram quantities at Argonne’s Materials Engineering Facility (MEF) – expected delivery January of 2012. Single-sided and double-sided electrodes were made on the A-Pro coater and validated by the ABR Screening task. Over a dozen pouch cells were made in the Cell Fabrication Facility. These results are shown in Figure IV - 161 and Table IV - 7 below.

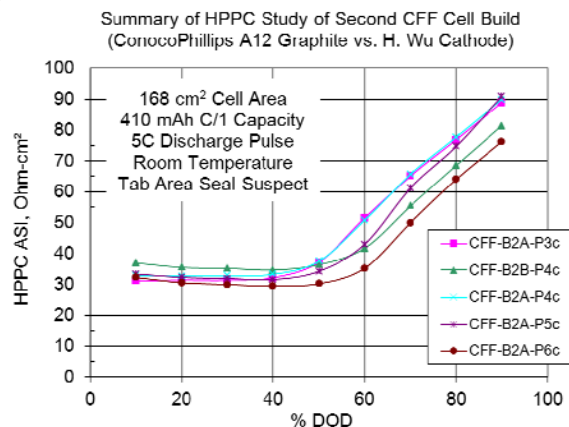


Figure IV - 161: HPPC impedance summary of second cell build made by the Cell Fabrication Facility.

Table IV - 7: Rate capability of second cell build positive electrode material.

Rate	Capacity – mAh/g
C	196
C/2	205
C/3	209
C/5	217.5

## Conclusions and Future Directions

The influence of electrode thickness on electrochemical performance is not expected to be a major concern for discharges less than a 1C rate, but problems in electrode fabrication and handling may arise for electrodes thicker than 100 microns each side. Adhesion of the electrode slurry to the current collecting foils is critical to a successful cell build.

Modifications were made to several pieces of equipment to enhance safety, with final approval to operate all equipment granted in February, 2011. Argonne now has the capability to coat and hot-roll press electrodes, and to make xx3450 pouch cells and 18650 cells in a dry room environment.

Cell Formation and Cycling Lab is operational with three 96 channel MACCOR cyclers and accompanying ovens and temperature chambers with safety ventilation.

Future work will include making xx3450 pouch cells using electrodes made with exploratory materials, such as the limited blended supply of ABR1 cathode (~1.2 kg left). Efforts will then switch to using the new scaled-up cathode materials from Argonne's Materials Engineering Facility (MEF) when they become available. The first MEF

material is expected in January 2012, which is based on the ABR1 cathode.

Effort will also be directed toward fabricating 18650 cells with commercially available materials and exploratory materials when they become available. It is anticipated that making 18650 cells will require significantly more material than pouch cell fabrication. For this reason, a commercial source is sought willing to supply openly at least 20 kg of advanced NMC material such as  $\text{Li}_{1.1}(\text{Ni}_{0.4}\text{Mn}_{0.4}\text{Co}_{0.2})_{0.9}\text{O}_2$ .

Variations in electrolyte additives and formation conditions will be explored, as well as methods to improve initial wetting before/during formation.

## FY 2011 Publications/Presentations

1. Poster presentation at the DOE Vehicles Technology Program 2009 Annual Merit Review Meeting.
2. Oral presentation at the DOE Vehicles Technology Program 2010 Annual Merit Review Meeting.
3. Poster presentation at the DOE Vehicles Technology Program 2011 Annual Merit Review Meeting.
4. "DOE's Lithium-ion Cell Fabrication Facility", Andrew N. Jansen, Bryant J. Polzin, Sun-Ho Kang, and Dennis W. Dees, poster presented at the *5th International Conference on Polymer Batteries and Fuel Cells (PBFC-5)*, Argonne National Laboratory, August 1-5, 2011.
5. "High-Energy Electrode Investigation for Plug-in Hybrid Electric Vehicles", Wenquan Lu, Andrew Jansen, Dennis Dees, Paul Nelson, Nicholas R. Veselka, and Gary Henriksen, *J. Power Sources*, 196, 2011, 1537-1540.

## IV.C.2.2 Baseline PHEV Cell Life Testing (ANL)

### Ira Bloom

Argonne National Laboratory (ANL)  
9700 South Cass Avenue  
Argonne, IL 60439-4837  
Phone: (630) 252-4516; Fax: (630) 972-4520  
E-mail : ira.bloom@anl.gov

### Co-Principal Investigators:

Kevin Gering/Jon Christophersen/  
Idaho National Laboratory (INL)  
P.O. Box 1625  
Idaho Falls, ID 83415  
Phone: (208) 526-4280; Fax: (208) 526-0690  
E-mail: kevin.gering@inl.gov

### Collaborators :

John K. Basco (ANL)  
Chinh D. Ho (INL)

Start Date: October 2008

Projected End Date: Open

- Calendar life testing completed



### Introduction

A battery testing manual for PHEVs has been released.<sup>22</sup> While the new manual contains procedures which are similar to those found in the old, more-established manual for HEV battery testing,<sup>23</sup> there are a number of significant changes and new test procedures. We recognize that the magnitude and type of aging mechanisms might differ between HEV and PHEV test conditions, and we are particularly interested in how these mechanisms impact execution of the PHEV duty cycles later in cell life. To determine the impact of these changes on battery aging characteristics, a well-understood and characterized cell chemistry is being used to test the procedures. The essential question to be answered is, what additional stresses are placed on the battery in the PHEV application? Additionally, the effects of electrode thickness and electrode coatings on cell performance and life will be determined. It is thought that there should be no difference in life when the electrodes in the cells are thicker and that the coatings should extend cell life.

### Approach

The approach for this work is to use cells made for the PHEV application and to test them using both sets of aging and characterization protocols in calendar and cycle life tests. A baseline for cell aging will be obtained by cell aging experiments at 45°C and 60% SOC using the HEV protocols and the changes in their performance will be characterized by reference performance tests (RPTs) at regular time intervals. After the baseline is obtained, the comparison of protocols will begin.

For this work, the distribution of cells to be tested is given in Table IV - 8.

### Objectives

- In support of the Applied Battery Research (ABR) Program, the objective of this work is to provide aged cells with well-documented histories for diagnostic studies.
- The effects of electrode thickness, electrode coatings, and electrolyte additives on cell performance and life will be determined.

### Technical Barriers

- The primary technical barrier is the development of a safe, cost-effective PHEV battery with a 40 mile all electric range that meets or exceeds all performance goals.
- Identification of cell degradation mechanisms.

### Technical Targets

- Establish the impact of PHEV-type cycles on aging relative to HEV-type cycles
- Establish a PHEV cell aging baseline for use in comparing advanced cell chemistries

### Accomplishments

- Test plan for protocol comparison developed

<sup>22</sup> Battery Test Manual for Plug-in Hybrid Electric Vehicles, ID/EXT 07-12536

<sup>23</sup> FreedomCAR Battery Test Manual For Power-Assist Hybrid Electric Vehicles, DOE/ID-11069, October 2003.

Table IV - 8 The cells were made by Leyden Energy (LE) and by EcoPro (EC). The cell chemistry consists of a  $\text{LiNi}_{0.8}\text{Co}_{0.15}\text{Al}_{0.05}\text{O}_2$  cathode, a MAG-10 anode and a mixed, organic carbonate electrolyte. The base ANL and LE electrolytes are compositionally equivalent, but came from different sources. The composition of both electrolytes is 1.2 M  $\text{LiPF}_6$  in EC/EMC (3:7 by wt).

The first round of testing repeats some of what was done with the Gen2 cells in the Advanced Technology

Development Program. Here, the cells labeled PH1C, PH1D, PH1E and PH1F will be subjected to HEV testing protocols. The initial characterization and subsequent RPTs will be performed at 25°C and after 28 days of testing. The RPTs will consist of C/1 and C/25 capacity measurements, the hybrid pulse-power characterization test at the low current value (HPPC-L) test and electrochemical impedance spectroscopy (EIS) characterization.

Table IV - 8: Cell distribution

ABRT label <sup>1</sup>	Cell designation	Calendar life at 45°C and 60%SOC <sup>2</sup>	PHEV combined cycling <sup>3</sup>			PHEV Deep CD cycling <sup>4</sup>	HEV cycle at 45°C and 60% SOC <sup>2</sup>
			30°C	45°C	55°C		
PH1A <sup>5</sup>	EC-B	5 cells	6	6	6	5	
PH1B <sup>5</sup>	EC-C	5	6	6	6	5	
PH1C	LE-360-A	3		3			3
PH1D	LE-360-B	4		4			4
PH1E	LE-362-A	3		3			3
PH1F	LE-362-B	2		2			2

**Notes:**

1. PH1A=bare cathode; PH1B=Alumina-coated cathode; PH1C=ANL electrolyte; PH1D=ANL electrolyte + VC; PH1E=LE electrolyte; PH1F=LE electrolyte + VC
2. Calendar life at 45°C and 60% SOC and the HEV cycling are being performed to compare to the earlier Gen2 results. The SOC will be defined by C/25 voltage at 40% DOD.
3. A PHEV combined cycle is defined as removing the scaled 3.4-kWh of energy using the charge-depleting profile, followed by 50 charge-sustaining profiles.
4. PHEV deep charge-depleting cycling is defined as discharging the battery using the CD profile until 15% SOC, as defined by initial C/1 discharge voltage measurements.
5. These cells will not be tested with the others. They will be held until after channels have opened up after the other cells are taken off test.

## Results

**Calendar Life.** The cells initially were characterized at 25°C using C/1 and C/25 capacity measurements, the HPPC-L test and EIS. The initial, average values of the capacities and the area-specific impedances are given in Table IV - 9. The average, initial value of the Gen2 baseline cells was about 27  $\Omega\text{cm}^2$ . The ASI values shown in Table IV - 9 are higher than those observed in the Gen2 baseline cells. The difference is due to thicker electrodes in the PHEV cells and slight differences in cell construction.

Table IV - 9: Initial values from cells used in the calendar life test.

ABR Label	C/1 capacity, Ah	C/25 capacity, Ah	ASI at 60% SOC, $\Omega\text{cm}^2$
PH1C	1.43	1.65	51.53
PH1D	1.46	1.65	52.50
PH1E	1.42	1.49	56.59
PH1F	1.45	1.66	52.65

Of key interest is how the performance of the cells changes with time at test temperature relative to the Gen 2 cells. Plots of the RPT data from 8 weeks of calendar testing are shown below. The least-squares fits to the Gen2 data for selected measurements are also included in the figures and are shown as solid curves. Since the initial data from the PHEV cells and those from the Gen2 cells were different, normalized data are used in the figures to facilitate the comparison.

As the cells age, their performance characteristics change with time. Figure IV - 162 shows that the ASI of the PHEV cells increases. After 24 weeks, the ASI values of the PH1C and PH1D cells has increased by more than 20% and that of the PH1E and PH1F cells has increased by 11-13% as compared to that from the Gen2 cells, 16%. Clearly, the addition of the VC additive decreased the change in the ASI of the cell.

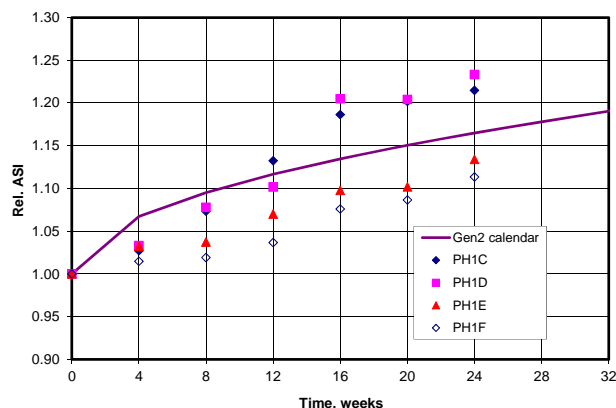


Figure IV - 162: Relative ASI vs. calendar time.

Figure IV - 163 and Figure IV - 164 show that the capacity of the cells tends to decrease, as expected with time. In both figures, the rate of capacity fade tends to be less than that displayed by the Gen2 curve. However, there is no clear difference in the relative capacity between the cells which contain VC and those which do not regarding capacity fade.

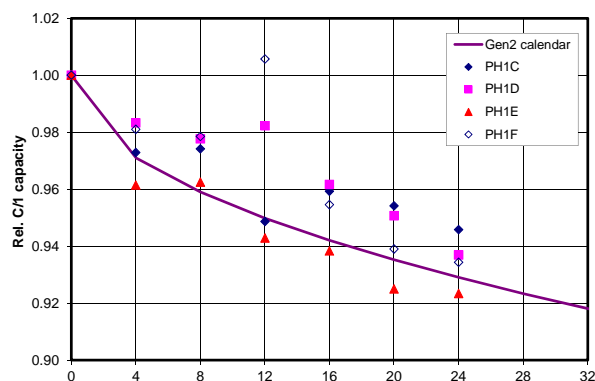


Figure IV - 163: Relative C/1 capacity vs. calendar time.

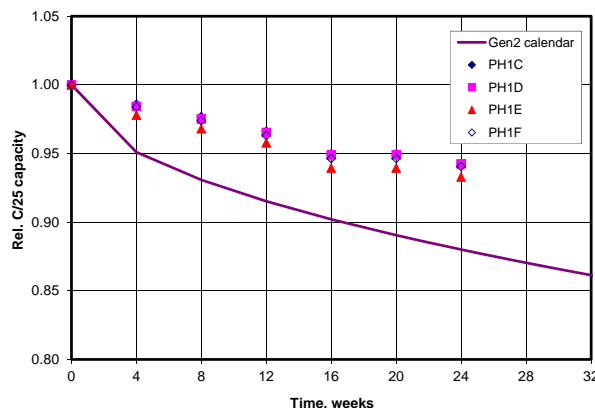


Figure IV - 164: Relative C/25 capacity vs. calendar time.

**Cycle Life.** The ABR program acquired lithium-ion cells of various chemistries having either a bare or coated NCA cathode. These cells are designed for HEV and

PHEV applications and were intended for performance testing at 25°C (HEV conditions) and 30°C (PHEV conditions) and accelerated calendar and cycle life evaluation. INL received 12 cells for HEV testing, and was slated to receive 12 more for PHEV-related testing. There were issues initially raised concerning the high impedance of these cells, which delayed the start of INL testing. These issues were resolved, and INL started cycle-life testing in early October 2010 under INL Test Plan EHV-TP-256-P290. However, on October 7, 2010 one cell experienced a catastrophic and sudden failure resulting in total destruction of the cell and slight damage to its closest neighbors. We await a root cause analysis from ANL prior to resumption of any INL Gen4 testing.

## Conclusions and Future Directions

The calendar life results indicate that the behavior of the PH1x (x=C and E) is very similar to that seen the baseline Gen 2. Addition of VC (PH1D and PH1F) retards impedance increase by about 5% as compared to Gen2 and about 5-7% as compared to PH1C and PH1E. The C/1 capacity data shows that there were no significant differences between the PH1-series of cells and the Gen2 cells. However, at slower discharge rates, there was a large difference in capacity loss, ~6% and ~12%, for the PH1-series and Gen2 cells, respectively.

## FY 2011 Publications/Presentations

- None.

## IV.D Abuse Tolerance Studies

### IV.D.1 Abuse Diagnostics

#### IV.D.1.1 Diagnostic Studies Supporting Improved Abuse Tolerance (BNL)

PIs: Kyung-Wan Nam and Xiao-Qing Yang

Hung-Sui Lee  
Xiaojian Wang  
Xiqian Yu

Brookhaven National Laboratory  
P.O. Box 5000  
Upton, NY 11973-5000  
Phone: (631) 344-3663; Fax: (631) 344-5815  
E-mail: [knam@bnl.gov](mailto:knam@bnl.gov)  
[xyang@bnl.gov](mailto:xyang@bnl.gov)

Projected Start Date: October, 2008  
Projected End Date: September, 2012

#### Objectives

- Develop new diagnostic techniques with the ability to distinguish bulk and surface processes, to monitor the degradation processes, to determine the effects of structural changes of electrode materials, the interfacial phenomena, and electrolyte decomposition on the cell capacity and power fading, as well as on the abuse tolerance related issues
- Using diagnostic techniques to evaluate and screen new materials, material processing and modification procedures which are aimed to improve the performance, calendar and cycling life, and the abuse tolerance of lithium batteries for HEV, PHEV, and EV

#### Technical Barriers

- Li-ion and Li-metal batteries with long calendar and cycle life
- Li-ion and Li-metal batteries with superior abuse tolerance
- To reduce the production cost of a PHEV batteries

#### Technical Targets

- To develop new *in situ* diagnostic techniques with surface and bulk sensitivity for studying the thermal stability of various cathode materials.
- To establish and investigate the thermal decomposition mechanisms of various cathode materials.
- To provide valuable information about how to design thermally stable cathode materials for HEV and PHEV applications.

#### Accomplishments

- Completed *in situ* hard and soft X-ray absorption spectroscopy (XAS) study on charged  $\text{Li}_x\text{Ni}_{0.8}\text{Co}_{0.15}\text{Al}_{0.05}\text{O}_2$  (Gen2) and  $\text{Li}_x\text{Ni}_{1/3}\text{Co}_{1/3}\text{Mn}_{1/3}\text{O}_2$  (Gen3) cathode materials during heating.
- Developed the combination of synchrotron-based *in situ* XRD with high resolution TEM (HR-TEM) to study the overcharged cathode materials for Li-ion battery during heating aimed at the improvement of the thermal stability.
- Initiated the new studies to apply atomic layer deposition (ALD) to improve the thermal stability of cathode materials.
- Working with GM, P&G (Duracell), and other collaborators, carried out diagnostic studies of new high energy density  $\text{Li}_2\text{MnO}_3$ - $\text{LiMO}_2$  (M=Ni, Co, Mn) and high voltage spinel ( $\text{LiNi}_{0.5}\text{Mn}_{1.5}\text{O}_4$ ) cathode materials.
- Initiated the synthesis and characterization of new electrolytes for high voltage Li-ion batteries.
- Developed new *in situ* diagnostic tool using high resolution TEM (HR-TEM) during heating to study overcharged cathode materials such as  $\text{Li}_x\text{Ni}_{0.8}\text{Co}_{0.15}\text{Al}_{0.05}\text{O}_2$  (Gen2) and  $\text{Li}_x\text{Ni}_{1/3}\text{Co}_{1/3}\text{Mn}_{1/3}\text{O}_2$  (Gen3). The formation and growth of rock-salt structure on the surface of Gen2 and the O1 type structure on the surface of Gen3 and their effects on thermal stability have been obtained.



## Introduction

Achieving DOE goals of batteries for HEVs, PHEVs, and EVs requires in-depth understanding of how to improve rate, capacity and long-term cycling performance. These understandings will provide the guidance on discovery of new materials and new mechanisms. This project has been working on these issues by developing new diagnostic tools to investigate battery materials both *in* and *ex situ*, and then applies these to understand relationships between structure and function for new material development.

## Approach

1. A combination of time resolved XRD, *in situ* soft and hard XAS, *in situ* transmission electron microscopy (TEM) techniques during heating to study the thermal stability of the electrode materials.
2. Apply the ALD technique for the surface modification of new cathode materials, using time resolved XRD to study the effects of surface modification on the thermal stability.
3. Perform *in situ* XRD, soft and hard XAS studies of new electrode materials during charge-discharge cycling to understand the power and energy fading mechanism for longer cycling life of Li-ion batteries.
4. Extended collaboration with other US and international academic institutions and US industrial partners and improving the model's capabilities.

## Results

Continued the *in situ* XAS and time-resolved XRD studies of  $\text{Li}_x\text{Ni}_{0.8}\text{Co}_{0.15}\text{Al}_{0.05}\text{O}_2$  (G2) and  $\text{Li}_{0.33}\text{Ni}_{1/3}\text{Co}_{1/3}\text{Mn}_{1/3}\text{O}_2$  (G3) cathode materials during heating:

As shown in Figure IV - 165 and Figure IV - 166, the time resolved XRD results of overcharged G2 and G3 cathode materials have different phase transition behavior during heating. Figure IV - 165 shows a series of time-resolved XRD patterns of the overcharged Gen2 particles ( $x < 0.15$ ) from room temperature to 450°C in the absence of the electrolyte. The XRD shows that the as-overcharged  $\text{Li}_x\text{Ni}_{0.8}\text{Co}_{0.15}\text{Al}_{0.05}\text{O}_2$  particles have a rhombohedral structure with the lattice parameter  $c=1.386$  nm. The phase transition from the rhombohedral to the spinel phase starts at about 171°C and is completed at about 207°C, both values being lower than those of the fully charged G2. The phase transition from spinel to the rock-salt phase starts at about 262 °C and finishes at about 335°C, as indicated by the decrease in intensity of the 311 and 511 (333) peaks of the spinel phase. The time-resolved XRD for the overcharged  $\text{Li}_x\text{Ni}_{1/3}\text{Co}_{1/3}\text{Mn}_{1/3}\text{O}_2$  (Figure IV - 166) also shows some different phase-transition behaviors compared to the fully charged  $\text{Li}_{0.33}\text{Ni}_{1/3}\text{Co}_{1/3}\text{Mn}_{1/3}\text{O}_2$ . Although rhombohedral is still the dominant phase up to 210 °C, a new phase appeared as indicated by the additional weak peaks that are indexed with a  $\text{CdI}_2$ -type structure (denoted as O1). The phase transition of the rhombohedral to the spinel phase of the overcharged  $\text{Li}_x\text{Ni}_{1/3}\text{Co}_{1/3}\text{Mn}_{1/3}\text{O}_2$  starts at about 210 °C and is completed at about 347 °C, which is significantly higher than those of the overcharged  $\text{Li}_x\text{Ni}_{0.8}\text{Co}_{0.15}\text{Al}_{0.05}\text{O}_2$ . Similar to the fully charged  $\text{Li}_{0.33}\text{Ni}_{1/3}\text{Co}_{1/3}\text{Mn}_{1/3}\text{O}_2$ , the spinel structure of the overcharged  $\text{Li}_x\text{Ni}_{1/3}\text{Co}_{1/3}\text{Mn}_{1/3}\text{O}_2$  undergoes another phase transition when heated above 298 °C, we refer this kind of structure as  $\text{M}_3\text{O}_4$  type spinel, in distinguish with  $\text{LiM}_2\text{O}_4$ -type spinel structure in which no transition metals occupy at Li site. This  $\text{M}_3\text{O}_4$  type spinel structure pushes the phase transition to rock-salt structure at a higher temperature.

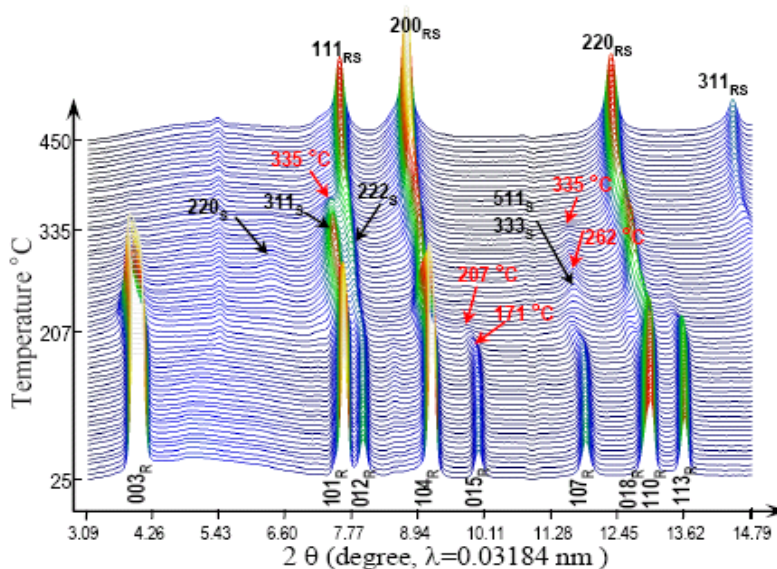


Figure IV - 165: TR-XRD of charged  $\text{Li}_{0.33}\text{Ni}_{0.8}\text{Co}_{0.15}\text{Al}_{0.05}\text{O}_2$  (G2) during heating

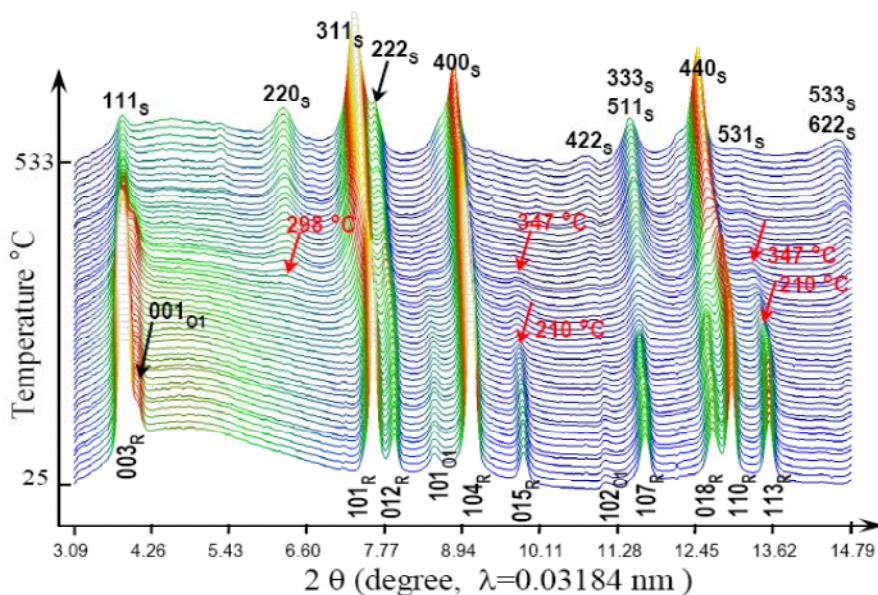


Figure IV - 166: TR-XRD of charged  $\text{Li}_{0.33}\text{Ni}_{1/3}\text{Co}_{1/3}\text{Mn}_{1/3}\text{O}_2$  (G3) during heating

Figure IV - 167a shows the SAEDP of the particle. We indexed the spots with strong intensity by the rhombohedral structure. One set of the weak spots marked by the green circles is indexed as the  $[111]_S$  pattern of the spinel structure  $\text{LiM}_2\text{O}_4$  ( $M=\text{Ni}_{1/3}\text{Co}_{1/3}\text{Mn}_{1/3}\text{O}_2$ ). Another set of the weak spots is marked by the red circles. By tilting the sample to the other orientations, we determined that this set of the spots correspond to the  $\text{CdI}_2$ -type structure  $\text{MO}_2$  (denoted as O1) which is formed by sliding two thirds of the  $\text{MO}_2$  layers after removal of the Li from the rhombohedral phase. This is consistent with the XRD

observation that shows weak O1 peaks. Figure IV - 167b illustrates the dark-field image formed by applying a small aperture to allow only the  $100_{\text{O}1}$  reflection to pass through the aperture. Undoubtedly, the O1 phase (bright area) is distributed at the surface of the particle. The dark-field image (Figure IV - 167c) formed by using the  $2-20_S$  reflection demonstrates that the distribution of the spinel phase is slightly off the surface. Figure IV - 167d is the HRTEM image from the edge of the particle. The diffractogram (right-middle inset) from the surface (red circle) has only the reflections of the O1 phase, while that from the area circled by a blue line (right-bottom inset) contains the

reflections of both the O1 and the spinel phases. Based on these observations, we conclude that most of the overcharged  $\text{LiNi}_{1/3}\text{Co}_{1/3}\text{Mn}_{1/3}\text{O}_2$  particles have a core-shell-surface structure with the O1 on the surface, the spinel phase in the shell, and the rhombohedral phase in the core. By comparison with the overcharged G2 at room temperature, the overcharged  $\text{Li}_x\text{Ni}_{1/3}\text{Co}_{1/3}\text{Mn}_{1/3}\text{O}_2$  forms an  $\text{CdI}_2$ -type  $\text{MO}_2$  structure at the surface, which protects the particle from losing oxygen. The differences in thermal decomposition mechanism of overcharged Gen 2 and Gen3 particles during heating are illustrated in Figure IV - 168 below.

As shown in Figure IV - 169 and Figure IV - 170, significant improvements of the thermal stability was obtained for the fully charged electrode with composition of  $\text{Li}_{1.2}\text{Ni}_{0.13}\text{Co}_{0.07}\text{Mn}_{0.6}\text{O}_2$  before charge with ALD coated  $\text{Al}_2\text{O}_3$  in comparison with the uncoated electrode. The phase transition temperature to Fm3m phase is increased by almost  $100^\circ\text{C}$ .

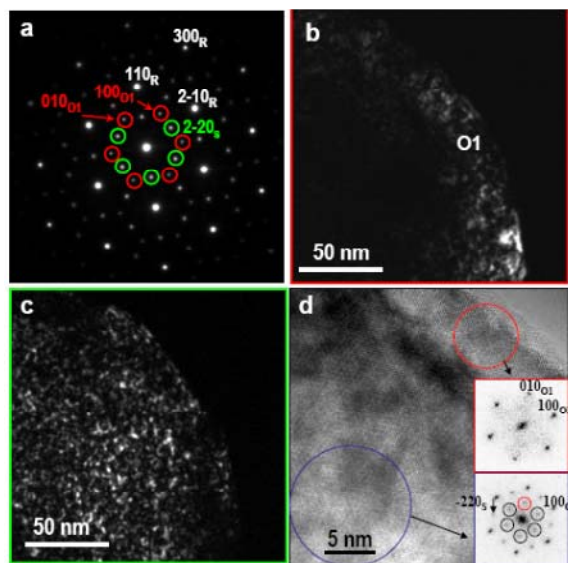


Figure IV - 167: SAEDP of an overcharged  $\text{Li}_x\text{Ni}_{1/3}\text{Co}_{1/3}\text{Mn}_{1/3}\text{O}_2$  particle. (b-c) Dark field images using reflections of (b)  $100_{\text{O}1}$  and (c)  $2-20_{\text{S}}$ . The dash lines indicate the same position in (b) and (c). (d) HRTEM image from the edge of the particle. The insets at the right-middle and the right-bottom are the diffractograms from the red and blue circled areas, respectively.

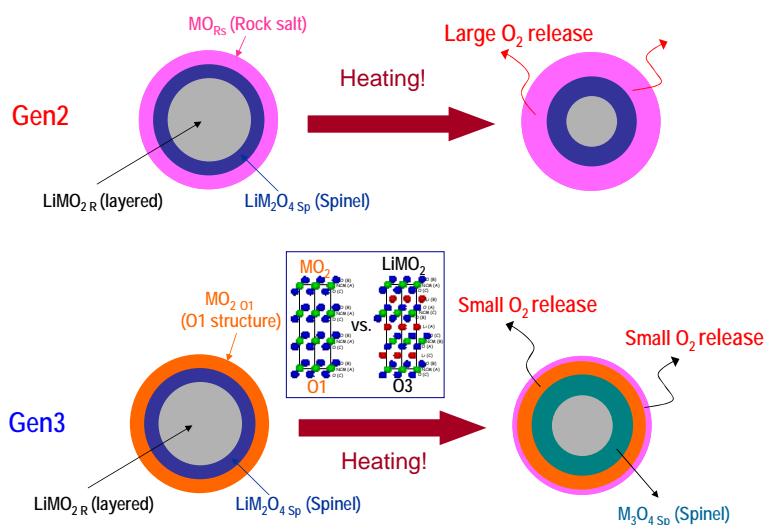


Figure IV - 168: Thermal decomposition mechanism of overcharged  $\text{Li}_x\text{Ni}_{0.8}\text{Co}_{0.15}\text{Al}_{0.05}\text{O}_2$  (Gen 2) and  $\text{Li}_x\text{Ni}_{1/3}\text{Co}_{1/3}\text{Mn}_{1/3}\text{O}_2$  (Gen3) particles during heating

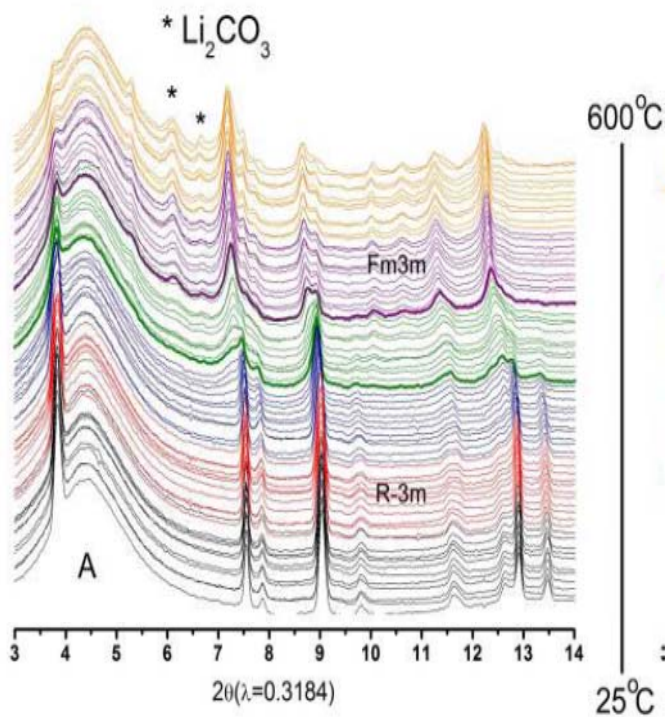


Figure IV - 169: Thermal stability study of fully charged  $Li_{1.2}Ni_{0.13}Co_{0.07}Mn_{0.6}O_2$  electrode without  $Al_2O_3$  surface coating using ALD

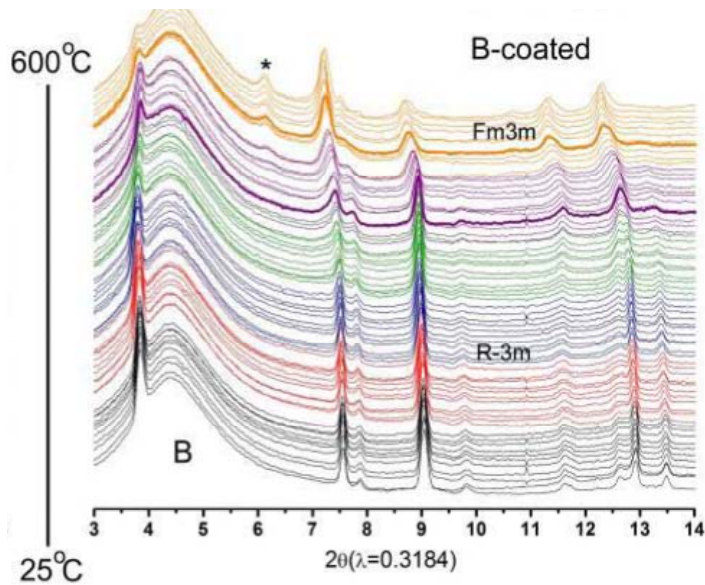


Figure IV - 170: Thermal stability study of fully charged  $Li_{1.2}Ni_{0.13}Co_{0.07}Mn_{0.6}O_2$  electrode with  $Al_2O_3$  surface coating using ALD. The phase transition temperature to Fm3m phase is increased by almost 100°C comparing to the uncoated electrode.

### Conclusions and Future Directions

1. In the Multi Year Program Plan (MYPP) of VTP, the goals for battery were described as: “Specifically,

lower-cost, abuse-tolerant batteries with higher energy density, higher power, better low-temperature operation, and longer lifetimes are needed for the development of the next-generation of HEVs, PHEVs, and EVs.” In this ES034 project, progress has been made to achieve these goals through diagnostic studies and collaborations with US industries and international research institutions.

2. New *in situ* diagnostic tools using high resolution TEM (HR-TEM) during heating have been developed and applied to study the overcharged cathode materials such as Gen2 and Gen3 in combination with time resolved XRD, soft and hard XAS. The formation and growth of rock-salt structure on the surface of Gen2 and the O1 type structure on the surface of Gen3 and their effects on thermal stability have been obtained.
3. The results provide valuable information about the role of each transition metal (Ni, Co, and Mn) on the thermal- and structural-instability of the materials during overcharging and heating and are applicable to the development of new cathode materials with a similar layered structure and high capacity and thermal stability.
4. New studies that apply the ALD of  $\text{Al}_2\text{O}_3$  on the surface of  $\text{Li}_2\text{MnO}_3\text{-LiMO}_2$  type cathode materials have been initiated and significant improvement for the thermal stability has been obtained. Other types of surface modifications and their effects on the capacity retention during cycling are underway.
5. In collaboration with GM R&D Center, diagnostic studies using *in situ* XAS for high energy density  $\text{Li}_2\text{MnO}_3\text{-LiMO}_2$  (M=Ni, Co, Mn) type new cathode materials have been carried out. More *in situ* XRD studies will be followed.
6. In collaboration with P&G (Duracell), diagnostic studies using *in situ* XRD for high voltage spinel ( $\text{LiNi}_{0.5}\text{Mn}_{1.5}\text{O}_4$ ) type of new cathode materials have been carried out. *In situ* XAS studies will be followed.

### Future Directions

1. Complete the *in situ* TEM studies on the thermal stability of layer structured Gen2 and Gen3 cathode materials.
2. Thermal stability study of surface modified high energy density  $\text{Li}_2\text{MnO}_3\text{-LiMO}_2$  composite cathode materials by ALD coating (e.g.,  $\text{TiO}_2$  and  $\text{SnO}_2$  coating): TR-XRD and *in situ* hard and soft XAS studies during heating.
3. Using *in situ* TEM to study the thermal stability improvement by surface modification via ALD on

high energy density  $\text{Li}_2\text{MnO}_3\text{-LiMO}_2$  composite cathode materials.

4. *In situ* XRD, TR-XRD, hard and soft XAS study of  $\text{LiNi}_x\text{Co}_y\text{Mn}_z\text{O}_2$  ( $x + y + z = 1$ ) cathode materials to identify the effect of Ni, Co, and Mn composition on the thermal stability, capacity and power fading during heating and/or charge-discharge cycling.
5. Expand the collaborative research with US and international academic research institutions and US industrial partners.

### FY 2011 Publications/Presentations

1. 2011 DOE Annual Peer Review Meeting Presentation, May 9<sup>th</sup>-13<sup>th</sup> 2011, Washington DC.
2. Lijun Wu, Kyung-Wan Nam, Xiaojian Wang, Yongning Zhou, Jin-Cheng Zheng, Xiao-Qing Yang and Yimei Zhu, “Structural Evolution and Related Thermal Instability of Overcharged  $\text{LiNi}_{0.8}\text{Co}_{0.15}\text{Al}_{0.05}\text{O}_2$  and  $\text{LiNi}_{1/3}\text{Co}_{1/3}\text{Mn}_{1/3}\text{O}_2$  Layered Cathodes for Li-ion Batteries”, *Chemistry Materials*, V23 (2011), 3953-3960, DOI: 10.1021/cm201452q.
3. Xiao-Jian Wang, Hai-Yan Chen, Xiqian Yu, Lijun Wu, Kyung-Wan Nam, Jianming Bai, Hong Li, Xuejie Huang, Xiao-Qing Yang, “New *in situ* synchrotron X-ray diffraction technique to study the chemical delithiation of  $\text{LiFePO}_4$ ”, *Chemical Communications*, V47 (2011), 7170-7172, DOI: 10.1039/C1CC10870K
4. Seong-Min Bak, Kyung-Wan Nam, Chang-Wook Lee, Sang-Bok Ma, Hyun-Chul Jung, Xiao-Qing Yang and Kwang-Bum Kim, “Spinel  $\text{LiMn}_2\text{O}_4$ /reduced graphite oxide hybrid as cathode material for high rate lithium ion batteries”, *Journal of Materials Chemistry* Accepted, (2011)
5. K. Karthikeyan, K.W. Nam, X.Q. Yang, and Y.S.Lee, A novel  $\text{Li}_{1.2}(\text{Fe}_{0.16}\text{Mn}_{0.32}\text{Ni}_{0.32})\text{O}_2$  layered material prepared by mixed hydroxide method for advanced lithium battery”, *Journal of Materials Chemistry*, submitted.
6. Jie Xiao, Xiaojian Wang, Xiao-Qing Yang, Shidi Xun, Gao Liu, Phillip K. Koech, Jun Liu, and John P. Lemmon, “Electrochemically Induced High Capacity Displacement Reaction of PEO/ $\text{MoS}_2$ /Graphene Nanocomposites with Lithium”, *Advanced Functional Materials*, V21 (2011), 2840-2846.
7. Kyung-Yoon-Chung, Won-Sub Yoon, Kwang-Bum Kim, Byung-Won Cho, and Xiao-Qing Yang, “Formation of an SEI on a  $\text{LiMn}_2\text{O}_4$  cathode during room temperature charge-discharge cycling studied by soft X-ray absorption spectroscopy at the Fluorine K-edge”, *Journal of applied Electrochemistry*, V (2011) DOI 10.1007/s10800-011-0344-6.

8. X. Q. Yang, K. W. Nam, H. S. Lee, X.J. Wang, Y. N. Zhou, X. Yu, L.J. Wu, Y. Zhu, L. F. Li, H. Li, and X. Huang, “The Development of New Electrolytes and *In situ* XRD XAS and TEM Studies of Cathode Materials for Lithium Batteries”, the 2010 (5th)International Forum on Li-ion Battery Technology & Industrial Development, November, 5-7, 2010, Beijing, China, **Invited**
9. I. T. Bae, J. Nelson, K-W. Nam, X-Q. Yang, J. Wang, “*In Situ* XAS and XRD Studies of High Voltage Spinel Oxides for Li-ion Batteries”, presented at the 218<sup>th</sup> Meeting of the Electrochemical Society, October 10-15, 2010, Las Vegas, Nevada, USA.
10. Kyung-Wan Nam, Xiao-Jian Wang, Xiqian Yu, Enyuan Hu, Seong Min Bak, Kyung-Yoon Chung, and Xiao-Qing Yang, “Thermal Stability Study of Surface Modified Ni-based Cathode Materials using *in situ*- XRD, hard and soft X-ray Absorption Spectroscopy during Heating”, presented at the 2011 MRS Spring Meeting, April, 25-30, 2011, San Francisco, California, USA.
11. Kyung-Wan Nam, Xiao-Qing Yang, Xiao-Jian Wang, Xiqian Yu, Enyuan Hu, Seong Min Bak, Kyung-Yoon Chung, Lijun Wu and Yimei Zhu “Thermal Stability Study of Ni-based Cathode Materials and the Effects of Surface Coating using *in situ*- XRD, X-ray Absorption and TEM during Heating”, presented at “the 5th International Conference on Polymer Batteries and Fuel Cells (PBFC-5)”, August 1-5, 2011, Argonne National Lab., USA., , **Invited**.
12. Xiao-Qing Yang, Kyung-Wan Nam, Xiqian Yu, Xiao-Jian Wang, Seong Min Bak, and Hung-Sui Lee, “The Structural Stability of  $\text{Li}_2\text{MnO}_3\text{-LiMO}_2$  (M = Ni, Co, Mn) Type Cathode Materials during Cycling and their Thermal Stability during Heating Studied by Synchrotron Based XRD and XAS”, presented at the “2011 (6th)International Forum on Li-ion Battery Technology & Industrial Development”, September 18-20, 2011, Beijing, China, , **Invited**.

---

## IV.D.2 Abuse Mitigation

### IV.D.2.1 Develop & Evaluate Materials & Additives that Enhance Thermal & Overcharge Abuse (ANL)

Zonghai Chen & Khalil Amine

Argonne National Laboratory  
9700 South Cass Avenue  
Argonne, IL 60439-4837  
Phone: (630) 252-6551  
E-mail: [Zonghai.chen@anl.gov](mailto:Zonghai.chen@anl.gov)

Collaborators:  
Yang ren, Argonne  
Yan Qin, Argonne  
Lu Zhang, Argonne  
John Zhang, Argonne  
Christopher J. Orendorff, Sandia  
Hitachi Chemical Inc.  
EnerDel

Start Date: October, 2008  
Projected End Date: September, 2011

#### Objectives

- Determine the role of cell materials/components in the abuse tolerance of lithium-ion cells.
- Identify and develop more stable materials that will lead to more inherently abuse-tolerant cell chemistries.
- Secure sufficient quantities of these advanced materials (and electrodes) to supply them to Sandia National Laboratories (SNL) for validation and quantification of the safety benefits in 18650-type cells.

#### Technical Barriers

- Determine role of the solid-electrolyte interface (SEI) layer on carbon anodes in cell safety.
- Determine role of cathode in cell safety.
- Provide overcharge protection of lithium-ion batteries.

#### Technical Targets

- Understand the response of the SEI layer to thermal abuses.

- Develop functional additives that enhance the stability of the SEI layer.
- Understand the response of cathode materials to thermal abuses.
- Develop functional protection strategies to enhance the thermal stability of batteries.
- Benchmark and develop advanced redox shuttles to improve the overcharge tolerance of lithium-ion batteries.

#### Accomplishments

- SEI formation on different carbon anodes
  - Material investigated: MCMB-1028, 3 types of surface modified graphite from Hitachi, and hard carbon
  - Multi-scale characterization techniques were deployed for correlation to the thermal stability of SEI layer. These techniques include *in situ* XRD, high resolution XRD and Raman spectroscopy.
  - The trace amount of residual functional groups on graphite surface was identified as critical to the thermal stability of SEI layer.
  - Synthesis effort to modify the surface functional groups is ongoing.
- Role of LiPF<sub>6</sub> for the thermal reactivity of cathodes
  - LiPF<sub>6</sub> was investigated against pure solvents, and the salts LiBF<sub>4</sub>, LiTFSI and Li<sub>2</sub>B<sub>12</sub>F<sub>12</sub>.
  - LiPF<sub>6</sub> has negative impact on safety of cathode by reducing the onset temperature from ~310°C to about ~230°C.
  - The negative impact of LiPF<sub>6</sub> on delithiated NMC will be further investigated using *in situ* high energy XRD.
- Enhancement of overcharge abuse
  - New aromatic redox shuttle with a redox at 4.2V vs. Li<sup>+</sup>/Li was synthesized at ANL.
  - Their overcharge protection functionality was confirmed with both half cells and full cells.
  - A large amount of heat is generated when the redox shuttle was activated. The possible impact

of the heat generation on cell performance will be further investigated in the coming year.



## Introduction

The safety of lithium-ion batteries is currently the major technical barrier for their application in hybrid electric vehicles and plug-in hybrid electric vehicles. Understanding the mechanism of thermal runaway reactions is a key to develop advanced technologies that improve the abuse tolerance and mitigate the safety hazard of lithium-ion batteries.

## Approach

The following approaches are being taken to tackle the safety issue of lithium-ion batteries:

- Understanding the impact of graphite surface functional groups on the safety of lithium-ion cell.
- Develop synthesis routes to modify the surface functional groups on resulted natural graphite.
- Explore new redox-shuttle materials to (a) improve the overcharge protection of lithium batteries and (b) achieve automatic capacity balancing of battery packs.
- Quantify the role of the additives and surface area of carbon on 18650-type cells in collaboration with SNL.

## Results

The following reports the progress on (1) understanding the bottleneck of the battery safety, and (2) improving the thermal abuse tolerance and overcharge protection of lithium-ion cells over the past year.

**Thermal Stability of Lithiated Graphite.** It is well known that lithium-ion cells are very sensitive to thermal abuse. A lithium-ion cell stored in a 160-180°C oven (UL hotbox test) will generally undergo thermal runaway. Figure IV - 171 shows the differential scanning calorimetry (DSC) profile of different cell components in a lithium-ion cell to identify the bottleneck chemical reaction that triggers the thermal runaway at such a low temperature (160-180°C), at which temperature the continuous decomposition/formation of SEI layer on graphite surface was triggered. This reaction is believed to heat the cell to higher temperature and trigger other major exothermal reactions; leading to thermal runaway. In order to confirm this speculation, five different carbons, whose physical parameters are listed in Table IV - 10, were investigated using DSC (Argonne) and ARC (Sandia). Both DSC and ARC data showed that SMG-N-20 had the highest thermal stability while MCMB was the least stable.

Table IV - 10: Physical and Chemical Properties of Carbon anodes investigated

	MCMB-1028	SMG-N-7b	SMG-N-20	SMG-Ns-15f
Description	MCMB	Surface modified	Nature graphite	Surface modified
D50 (μm)	11.8	11.1	19.5	21.6
BET (m <sup>2</sup> /g)	2.01	5.0	5.1	0.7
Ea (kJ/mol)	53.54	88.08	92.66	78.46

Figure IV - 171 shows the Raman spectra of the carbonaceous materials MCMB, SMG-N-20, SMG-Ns-15f, and SMG-N-7b. The strong and sharp peak at 1580 cm<sup>-1</sup>, the so-called G band, represents the resonant absorption of ordered sp<sup>2</sup> carbon atoms in graphite. It can be seen that the G band of different graphite samples shows similar shape, intensity, and peak position. However, a big difference was observed for the D band at ~1350 cm<sup>-1</sup> and D' band at ~1620 cm<sup>-1</sup>. Among the four materials investigated, MCMB shows the least signal from defective carbon atoms; it has the weakest D band intensity, and the D' band is barely visible. Figure IV - 171 shows that the intensity of the D band and D' band increases steadily in the order MCMB, SMG-N-20, SMG-N-7b, and SMG-Ns-15f. However, the kinetic data showed that the lithiated SMG-N-20 was the most thermally stable while the lithiated MCMB was the least (see Table IV - 10). Therefore, no positive correlation between the soft carbon coating and the thermal stability could be established.

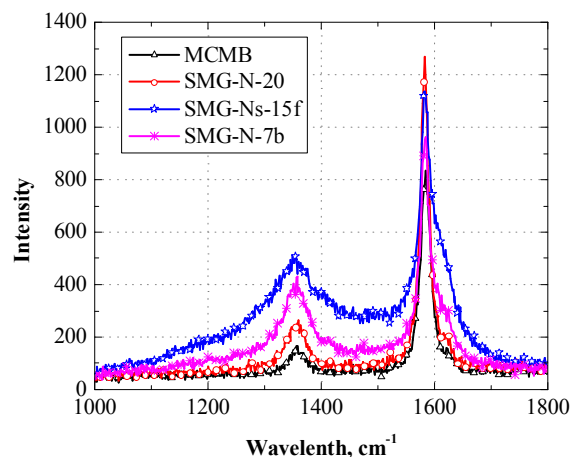
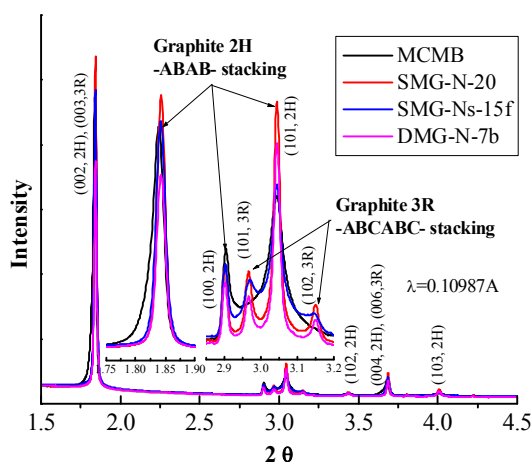


Figure IV - 171: Raman spectroscopy of four graphitic anode materials.

Figure IV - 172 shows the XRD patterns of the four graphitic materials, and the diffraction peaks were successfully indexed using 2H and 3R graphite. The diffraction peaks at 2.91° and 3.04° are characteristic (100)

and (101) peaks of 2H graphite, and the two at  $2.96^\circ$  and  $3.14^\circ$  are characteristic (101) and (102) peaks for 3R graphite. The peaks indicate that 2H graphite is the major component for all four samples, and their content of 3R graphite varied. The inset of Figure IV - 172 also shows that MCMB has no or very low content of 3R graphite, SMG-Ns-15f has a low concentration of 3R graphite with poor long-term ordering (broadened diffraction peaks for 3R graphite), and SMG-N-20 and SMG-N-7b have high 3R graphite content. Figure IV - 172 also shows broadened and weak signature diffraction peaks of 3R graphite for SMG-Ns-15f and strong and well-defined peaks for both SMG-N-20 and SMG-N-7b. The same trend can also be seen for the thermal stability of lithiated graphitic anodes, as shown in Table IV - 10. A possible explanation is that these anode materials were synthesized under different conditions, resulting in different surface functional groups at the graphite edge, which could affect the chemical composition of the SEI layer. The synthesis effort to vary the functional groups on graphite is ongoing and will be reported in the coming year.



**Figure IV - 172:** XRD patterns of four graphitic anode materials using high-energy X-ray beam ( $\lambda = 0.10978 \text{ \AA}$ ).

**Thermal Stability of Delithiated Cathode.** Figure IV - 173 shows the DSC profile of thermal decomposition of delithiated NMC in (a) EC/EMC; (b) EC; (c) EMC; (d) TBMPTFSI; (e) EC/EMC/LiPF<sub>6</sub>; (f) EC/LiPF<sub>6</sub>; (g) EMC/LiPF<sub>6</sub>; and (h) TBMPTFSI/LiPF<sub>6</sub>. Clearly, the thermal decomposition of delithiated NMC occurred at above  $300^\circ\text{C}$  when only solvent was presented, and the addition of LiPF<sub>6</sub> to the samples significantly reduced the onset temperature down to  $200^\circ\text{C}$ . In addition, the two lines (red dotted and black solid) in each panel show two independent runs for the sample to demonstrate the reproducibility of the experiment. It is clear that the reproducibility of sample with solvents was quite good, but it was significantly reduced with the presence of LiPF<sub>6</sub>.

When using DSC to investigate the thermal stability of delithiated  $\text{Li}_{1.1}(\text{Ni}_{1/3}\text{Mn}_{1/3}\text{Co}_{1/3})_{0.9}\text{O}_2$  (NMC), we encountered poor reproducibility due to the lack of chemical insight of investigated chemical reaction using DSC. Therefore, we have developed an advanced analytical technique, *in situ* high-energy X-ray diffraction, to help understand the chemical reactions between the electrode material and the electrolyte as shown in Figure IV - 174.

#### Overcharge Protection of Lithium-Ion cells.

Overcharge of lithium-ion batteries can lead to the failure of a battery pack or a fire hazard. A redox shuttle is an electrolyte additive that provides an intrinsic mechanism that enhances the overcharge tolerance of lithium-ion batteries. Moreover, the redox shuttle in lithium-ion batteries can also provide automatic capacity balancing for the battery pack.

Figure IV - 175 shows cyclic voltammograms of ANL-2 in 1.2 M LiPF<sub>6</sub> in EC/EMC (3:7). This voltammogram was obtained using Pt/Li/Li electrodes at various rates from 500 mV/s to 20 mV/s at room temperature. From the CV curves we can see that ANL-2 is perfectly electrochemically reversible, displaying nearly symmetric redox peaks.



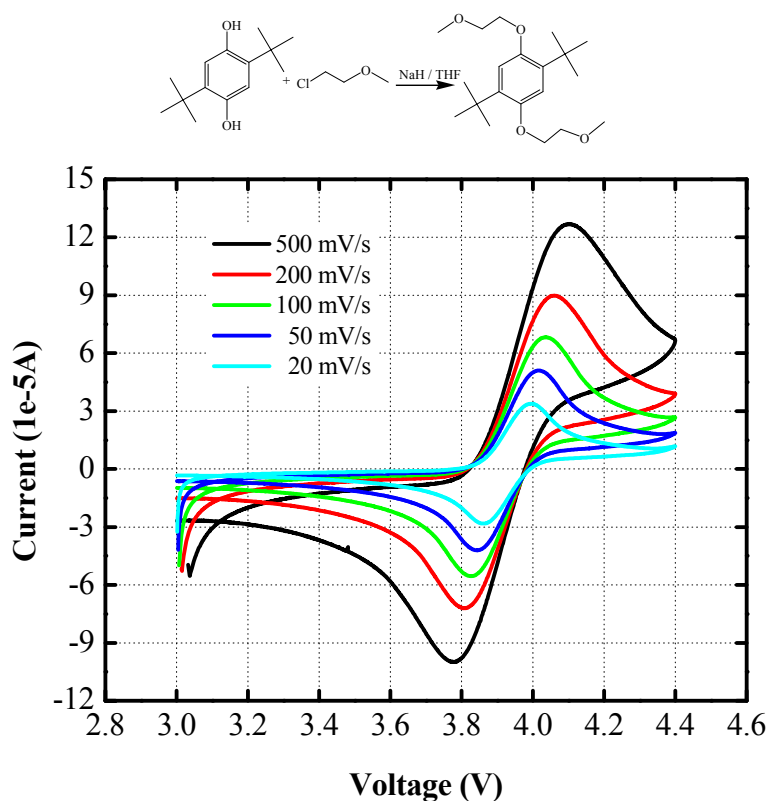


Figure IV - 175: Cyclic voltammogram of 0.01M ANL-2 in 1.2 M LiPF<sub>6</sub> in EC/EMC (3:7) at various rates using a Pt/Li/Li three-electrode system.

Figure IV - 176 shows the capacity retention profiles of an MCMB/LiFePO<sub>4</sub> cell containing 0.1 M ANL-2 in 1.2 M LiPF<sub>6</sub> in EC/EMC (3:7) during overcharge. The capacity differences between charge and discharge capacities represent the electricity shunted by ANL-2 redox shuttle.

For discharge capacities, it is clear that the discharge capacity of full cell dropped as the test proceeded but for the half cell the discharge capacity retention was kept stable with no drop.

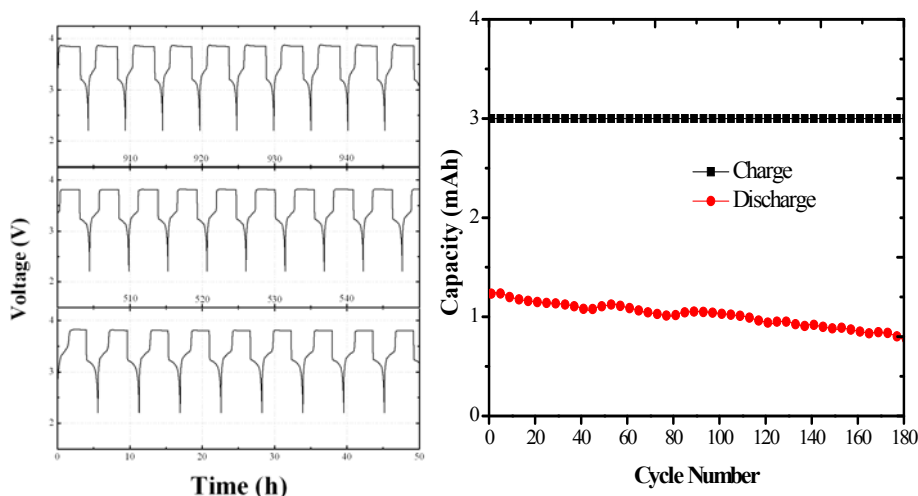


Figure IV - 176: Voltage and capacity profiles of MCMB/LiFePO<sub>4</sub> cells containing 0.4 M ANL-2 in Gen 2 electrolyte during the course of 0-960 h. Charging rate is C/2 and overcharge ratio is 100%.

Figure IV - 177 shows the generated heat flow of a Li<sub>4</sub>Ti<sub>5</sub>O<sub>12</sub>/LiFePO<sub>4</sub> lithium-ion cell during overcharge test

using isothermal microcalorimeter. It clearly shows huge amount of heat was generated when the redox shuttle was

activated. In the coming year, we will focus on the localized heat generation using *in situ* high energy X-ray

diffraction and quantify the impact of heat generation on the life of lithium-ion cells.

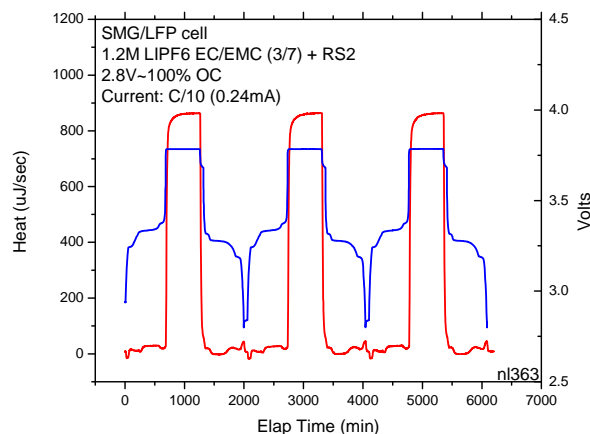


Figure IV - 177: Charge/discharge capacity of a  $\text{Li}_4\text{Ti}_5\text{O}_{12}/\text{LiFePO}_4$  lithium-ion cell during overcharge test.

### FY 2011 Publications/Presentations

- 2011 DOE Annual Peer Review Meeting Poster
- Z. H. Chen, Y.-K. Sun, and K. Amine, Material Perspectives for Safe and High Energy Density Lithium-Ion Batteries, submitted to *Angew. Chem. Int. Ed.*, (2011).
- Z. H. Chen, Y. Qin, Y. Ren, W. Q. Lu, C. Orendorff, and K. Amine, Multi-scale Study of Thermal Stability of Lithiated Graphite, *Energy Environ. Sci.*, 4(10): 4023-4030 (2011).
- Z. H. Chen, A. N. Jansen, and K. Amine, Novel Functionalized Electrolytes for  $\text{MCMB}/\text{Li}_{1.156}\text{Mn}_{1.844}\text{O}_4$  Lithium-Ion Cells, *Energy & Environmental Science* (in press), (2011).
- Z. H. Chen, J. Liu, A. N. Jansen, G. Girish Kumar, Bill Casteel and K. Amine, Lithium Borate Cluster Salts as Novel Redox Shuttles for Overcharge Protection of Lithium-Ion Cells, *Electrochem. Solid State Lett.*, 13(4): A39-A43 (2010).
- Z. C. Zhang, L. Zhang, J. A. Schlueter, and K. Amine, "3,5-Di-tert-butyl-1,2-dimethoxybenzene as a redox shuttle for overcharge protection of lithium-ion cells", *J. Power Source*, 195 (2010) 4957–4962.
- Zhang, Lu; Zhang, Zhengcheng; Amine, Khalil; "A Comparative Study of 3,5-di-tert-butyl-1,2-dimethoxybenzene and 2,5-di-tert-butyl-1,4-dimethoxybenzene for Overcharge Protection of Lithium-ion Batteries", *Proceedings of Power Source Conference 2010*.
- Y. Qin, Z. H. Chen, J. Liu and K. Amine, Lithium Tetrafluoro Oxalato Phosphate as Electrolyte Additive for Lithium-Ion Cells, *Electrochem. Solid State Lett.*, 13(2): A11-A14 (2010).
- Z. H. Chen, Y. Qin and K. Amine, Redox Shuttles for Safer Lithium-Ion Batteries, *Electrochimica Acta*, 54(24):5605-5613 (2009).
- Lu Zhang, Zhengcheng Zhang, Khalil Amine, "Redox shuttle additives for lithium-ion batteries", invention with internal # ANL-IN-10-076.
- IN-09-082, POLYETHER-FUNCTIONALIZED REDOX SHUTTLE ADITIVES FOR LITHIUM ION BATTERIES Zhengcheng Zhang, Lu Zhang, Khalil Amine
- IN-09-084, REDOX SHUTTLE ADDITIVES FOR HIGH VOLTAGE CATHODES Lu Zhang, Zhengcheng Zhang, Zonghai Chen, Khalil Amine
- IN-09-086, REDOX SHUTTLE FOR OVERCHARGE PROTECTION OF LITHIUM-ION BATTERIES Wei Weng, Zhengcheng Zhang, Khalil Amine.
- Lu Zhang, Zhengcheng Zhang, Khalil Amine, "Novel Redox Shuttle Additive for High Voltage Cathode Materials: Tetraethyl 2,5-di-tert-Butyl-1,4-Phenylene Diphosphate", submitted.
- Zonghai Chen, Yan Qin, Yang Ren and Khalil Amine, Advanced Electrolyte Additives to Enhance the Safety of Lithium-ion Batteries, Battery Safety 2010, Boston, November, (2010) (invited).
- Zonghai Chen, Yan Qin and Khalil Amine, Surface Chemistry in Lithium-Ion Batteries, Pacific Power Source Symposium, Big Island, Hawaii, January, (2011) (invited).
- Zonghai Chen, Yang Ren, and Khalil Amine, *In situ* High Energy X-ray Diffraction to Study Thermal Stability of Electrode Materials, 220<sup>th</sup> ECS Meeting, Boston, October (2011) (invited).

## IV.D.2.2 Impact of Materials on Abuse Response (SNL)

Christopher J. Orendorff

Sandia National Laboratories  
P. O. Box 5800, Mail Stop 0614  
Albuquerque, NM 87185-0614  
Phone: (505) 844-5879; Fax: (505) 844-6972  
E-mail: corendo@sandia.gov

### Collaborators:

Khalil Amine, Argonne National Laboratory  
Andrew Jansen, Argonne National Laboratory  
Zonghai Chen, Argonne National Laboratory  
Ram Nagubandi, Binrad Industries

Start Date: October, 2008

Projected End Date: September, 2012

### Objectives

- Elucidate degradation mechanisms in lithium-ion cells that lead to poor abuse tolerance (runaway thermodynamics, gas evolution, electrolyte combustion)
- Develop and evaluate advanced materials (or materials combinations) that will lead to more abuse tolerant lithium-ion cells and battery systems
- Build 18650 cells in the SNL fabrication facility for cell level evaluation of new materials in support of all ABR thrust areas

### Technical Barriers

There are several technical barriers to achieving the goals stated above including:

- Develop lithium-ion cells that are intrinsically abuse tolerant and do not lead to high order catastrophic failures
- Mitigate the gas evolution and decomposition of the electrolyte
- Passivation of cathode runaway reactions and interfacial reactions with electrolyte
- Limited quantities of advanced materials (and numbers of cells with new materials) to evaluate abuse response

### Technical Targets

- Quantify the thermal runaway response of materials at the cell level (18650)

- Determine the effect of electrolyte salts, solvents and additives on the abuse response of lithium-ion cells
- Evaluate the thermal response of candidate active materials
- Identify materials that could be used to reduce gas evolution and the heat and kinetics of runaway reactions

### Accomplishments

- Identification of electrolytes that can minimize the energetics of a thermal runaway
- Demonstrated dramatic improvements in the thermal stability of cathodes in LiF/ABA (anion binding agent) electrolytes and improvements in cell runaway response with LiF/ABA electrolytes
- Improved electrode designs for 1.3-1.4 Ah cells of commercial active materials as a baseline for evaluating ABR development materials



### Introduction

As lithium-ion battery technologies mature, the size and energy of these systems continues to increase (> 50 kWh for EVs); making safety and reliability of these high energy systems increasingly important. While most materials advances for lithium-ion chemistries are directed toward improving cell performance (capacity, energy, cycle life, etc.), there are a variety of materials advancements that can be made to improve lithium-ion battery safety. Issues including energetic thermal runaway, electrolyte decomposition and flammability, anode SEI stability, and cell-level abuse tolerance continue to be critical safety concerns. This report highlights work with our collaborators to develop advanced materials to improve lithium-ion battery safety and abuse tolerance and to perform cell-level characterization of new materials.

### Approach

The effect of materials (electrolytes, additives, anodes, and cathodes) on the thermal response of full cells is determined using several techniques. One of the most useful and quantitative techniques is accelerating rate calorimetry (ARC). The ARCs at SNL are fitted with uniquely designed high pressure fixtures to not only measure quantitative heat flow but also gas generation under ideal adiabatic conditions during full cell runaway. Cells were fabricated using a variety of active materials,

electrolytes, and additives in the SNL cell prototyping facility. The in-house prototyping capability gives us the versatility to target candidate materials, perform full cell evaluation, and correlate cell response to fundamental materials properties.

## Results

**Electrolyte Effects on Abuse Tolerance.** With the significant advances in the safety of anode and cathode materials and greater understanding of degradation mechanisms made in recent years, safety issues related to electrolytes are becoming increasingly important. A better understanding of the electrolyte degradation mechanisms and effects on abuse tolerance need to be developed to address electrolyte issues such as gas generation, flammability, combustion enthalpy, interfacial reactivity, and high voltage stability. Once these mechanisms are better understood, mitigation strategies can be effectively developed.

Lithium hexafluorophosphate ( $\text{LiPF}_6$ )/carbonate solvents are the most common liquid electrolyte systems because of their good conductivity (10 mS/cm at 25°C) and voltage stability (to 4.5V vs. Li). However,  $\text{LiPF}_6$  does have some shortcomings in terms of its thermal stability and decomposition products (e.g. HF,  $\text{PF}_5$ ,  $\text{POF}_3$ ) which can react to degrade other cell components (namely electrolyte solvent) and produce large volumes of decomposition gases (up to 2500 mL for a 1 Ah 18650 cell). Figure IV - 178 shows bomb calorimetry data for the rapid decomposition of EC in the presence of 1.2 M  $\text{LiPF}_6$ . There is a distinct difference in the measured ARC bomb gas pressure generated from the vapor pressure of boiling neat EC (blue trace), compared to the catalytic decomposition of EC by  $\text{PF}_6^-$  to produce primarily  $\text{CO}$ ,  $\text{CO}_2$ ,  $\text{CH}_4$ ,  $\text{C}_2\text{H}_6$ .

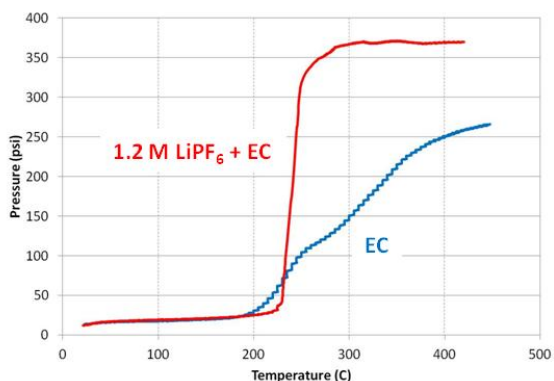


Figure IV - 178: Gas pressure as a function of temperature for neat EC (blue) and 1.2 M  $\text{LiPF}_6$  (red) samples in a bomb calorimetry experiment

In an effort to quantify the effect of  $\text{LiPF}_6$  on gas generation and contribution from carbonate solvent components (cyclic vs. linear), a series of bomb calorimetry

measurements was made for a series of solvents, solvent mixtures and electrolyte solutions. Figure IV - 179 shows total moles of gas product normalized to the moles of electrolyte as a function of temperature for this series of solvents, mixtures and electrolytes.

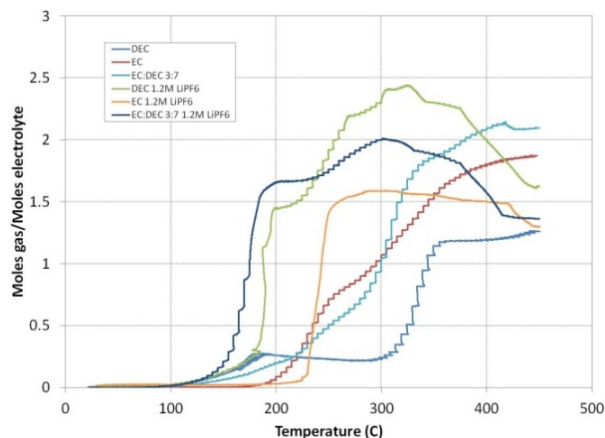


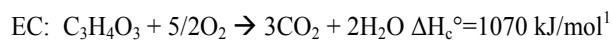
Figure IV - 179: Calorimetry measurements of moles of gas evolved per mole of electrolyte for neat carbonate solvents and  $\text{LiPF}_6$ -based electrolyte solutions.

For the neat EC and DEC samples, both boil at  $<200^\circ\text{C}$  and the gas evolved is solvent vapor from increasing vapor pressure with temperature. With the addition of  $\text{LiPF}_6$  there is a sharp transition at  $235^\circ\text{C}$  for EC +  $\text{LiPF}_6$  and  $195^\circ\text{C}$  for DEC +  $\text{LiPF}_6$  corresponding to the catalytic reaction to form a large mole fraction of decomposition gas products (primarily  $\text{CO}$  and  $\text{CO}_2$ ) and solvent vapor. It is interesting to note the onset temperature for the DEC +  $\text{LiPF}_6$  is  $\sim 40^\circ\text{C}$  lower than for EC +  $\text{LiPF}_6$  which suggests the reaction between  $\text{PF}_6^-$  and the linear carbonate is more thermodynamically favorable than the reaction with cyclic EC; while the total mole fractions of gas product are comparable ( $\sim 1.5$  moles of gas/mole of electrolyte). At temperatures  $> 300^\circ\text{C}$  the gas mole fraction from the DEC +  $\text{LiPF}_6$  reaction appears to decrease, however, this is an artifact from solvent condensation in the headspace above the heated volume of the calorimeter.

In the mixed EC:DEC +  $\text{LiPF}_6$  electrolyte the onset temperature for gas evolution is  $\sim 20^\circ\text{C}$  less than for DEC alone and the total moles of gas is greater than for DEC alone (up to 1.7 moles of gas/mole of electrolyte). This suggests that while the majority of the gas evolved comes from the linear carbonate, EC does contribute to gas generation in the mixed electrolyte system. Again, this is consistent with the observation that these reactions may be controlled thermodynamically by the DEC +  $\text{LiPF}_6$  component. In addition, qualitative and quantitative analysis of the gas products will be measured by GC-MS and FT-IR to identify the gas products and measure amounts of each component. Data will provide a better

understanding of the complex gas generating reactions that occur in lithium-ion cells under abuse conditions.

In addition to the electrolyte salt, the solvents and solvent mixtures used in for lithium-ion electrolytes can have a significant impact on the runaway reactivity and abuse tolerance. This is most readily observed in the combustion reaction of the electrolytes with either oxygen release from the cathode during a runaway or from ignition (either external or internal). For EC the combustion reaction follows:



18650 cells with  $\text{Li}_{1.1}(\text{Ni}_{1/3}\text{Mn}_{1/3}\text{Co}_{1/3})_{0.9}\text{O}_2$  (NMC 111) and graphite anodes were built with two different electrolytes: (1) 1.2 M  $\text{LiPF}_6$  in EC:EMC (3:7) and (2) 1.2 M  $\text{LiPF}_6$  in EC:PC:DMC (1:1:3) to study this effect in full cells. ARC runaway profiles for each cell type are shown in Figure IV - 180. The runaway reaction thermodynamics (kinetic and enthalpic components) are significantly diminished for the cells with EC:PC:DMC electrolyte compared to the EC:EMC electrolyte. This is the result of a combination of factors including the combustion enthalpy the solvent compositions (approx. 78 kJ/cell for EC:PC:DMC and 87 kJ/cell for EC:PC:DMC), possible co-intercalation of PC, interfacial reactivity of the electrolyte components, and reactivity with  $\text{PF}_6^-$ . It is clear from these data that electrolytes and solvents cannot be treated as inactive or passive materials when issues of abuse tolerance are considered.

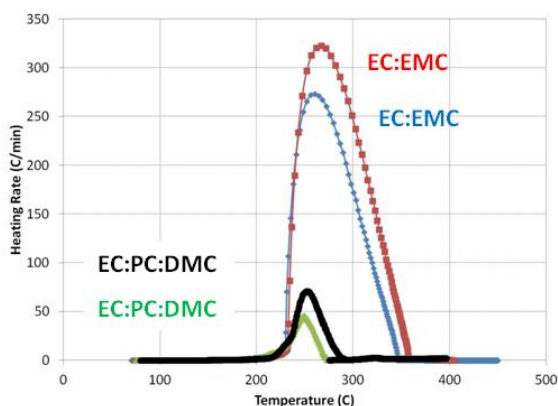


Figure IV - 180: ARC profiles of NMC111 cells with 1.2 M  $\text{LiPF}_6$  in EC:EMC (3:7) and EC:PC:DMC (1:1:3) electrolytes

**LiF/Anion Binding Agent (ABA) Electrolyte.** The use of lithium fluoride ( $\text{LiF}$ ) electrolyte salt has been considered as an alternative to  $\text{LiPF}_6$  because of its chemical and thermal stability, but early generation anion binding agents (ABAs, used to improve  $\text{LiF}$  solubility) were large molecules that were inapplicable to lithium-ion cell systems (large molecular weights, low rate capability, low conductivity, voltage instability, etc.). In collaboration with Binrad Industries we have developed  $\text{LiF}/\text{ABA}$  salts

for lithium-ion cells to show improved thermal stability and to eliminate some of the shortcomings of using  $\text{LiPF}_6$  salts.

The use of the ABA electrolytes in lithium-ion cells gives rise to some interesting behavior and interactions with cathode materials compared to conventional electrolytes. Figure IV - 181 shows heat flow as a function of temperature for two NMC cathode samples in ABA and  $\text{LiPF}_6$  electrolytes by DSC. While the onset temperatures of the ABA system are depressed relative to the  $\text{LiPF}_6$  samples, the specific heat measured for both the NMC111 and NMC 433 cathodes are considerably less than in  $\text{LiPF}_6$ . At this time, the mechanism for this apparent cathode runaway stabilization is unclear but work will continue in FY12 to better understand this phenomenon.

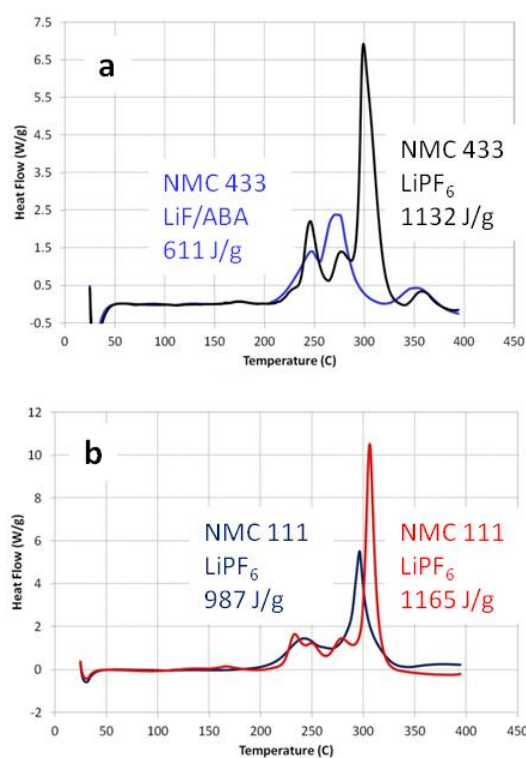


Figure IV - 181: DSC profiles of NMC433 and NMC111 at 4.3 V in 1.2 M  $\text{LiPF}_6$  in EC:EMC (3:7) and 1.0 M  $\text{LiF}/\text{ABA}$  in EC:EMC (3:7)

In cells, this same cathode runaway passivation is also observed. Figure IV - 182 shows cell ARC data for an NMC 433 cell with  $\text{LiPF}_6$  and ABA electrolytes. The ARC profile NMC 433 cell with 1.2 M  $\text{LiPF}_6$  in EC:EMC (3:7) (black trace) is characteristic of NMC chemistry in the EC:EMC electrolyte. The onset for the low rate exotherm is at  $\sim 70^\circ\text{C}$  (corresponding to anode SEI decomposition) and the high rate runaway onset is at  $\sim 240^\circ\text{C}$  and has a maximum peak heating rate of  $300^\circ\text{C}/\text{min}$ . However, the ARC profile for that same electrode couple in the 1.0 M  $\text{LiF}/\text{ABA}$  in EC:EMC (3:7) electrolyte shows no high rate

runaway. While this is consistent with the cathode passivation observed in the DSC measurements, the magnitude of cathode passivation in the full cell experiment is greater than expected. With the promise observed in these results, work is continuing with the ABA electrolytes to better understand their thermal stability and optimize their performance in lithium-ion cells.

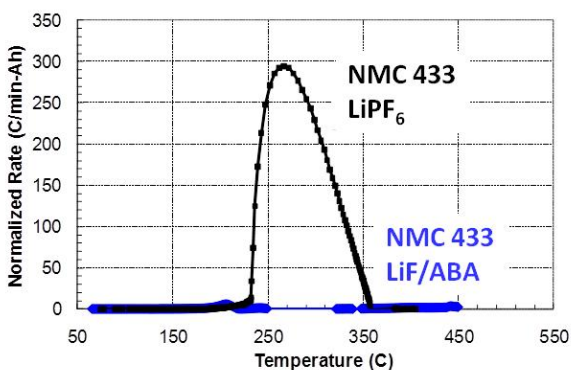


Figure IV - 182: ARC profiles for NMC433 18650 cells in 1.2 M LiPF<sub>6</sub> in EC:EMC (3:7) and 1.0 M LiF/ABA in EC:EMC (3:7) at 4.3 V

**Cell Fabrication Facility.** The SNL cell prototyping facility is fully equipped with three 18650 cell winders (in two separate dry rooms), two prototype-scale electrode coaters, electrode slitter, semi-automatic tabber, and an electrolyte filling station to support the ABR program cell thermal characterization and abuse tolerance of new materials in cells (Figure IV - 183). 18650 cell building at SNL has been critical to the success of this work as well as our internal short circuit test development effort (III.D.7) and our abuse testing work (III.D.4) within the ABR program. Looking forward, the SNL cell building facility will have a greater role in supporting electrolyte and materials development at ANL, INL and other Laboratory collaborators.



Figure IV - 183: Photograph of 18650 cells built at SNL

Figure IV - 184 shows charge and discharge capacity curves for a representative NMC 111 cell. NMC cells are designed as R&D cells with capacities ranging from 1.3-1.4 Ah. These cells also retain 95% of their initial capacity after 70 cycles (Figure IV - 185). In addition to designing

NMC cells, we also have comparable designs for LiCoO<sub>2</sub> and LiFePO<sub>4</sub> (LFP) chemistries. Future work will focus on designs for advanced materials developed within ABR including high capacity and high voltage cathodes and working with our collaborators at ANL and ORNL to standardize materials and cell designs for the ABR program.

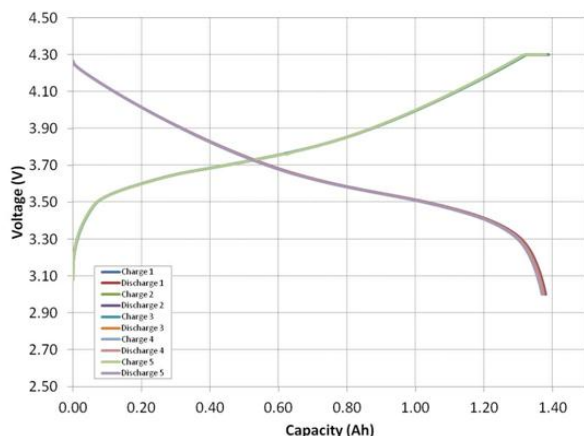


Figure IV - 184: Voltage as a function of capacity (Ah) showing charge and discharge capacity curves for NMC111 18650 cells

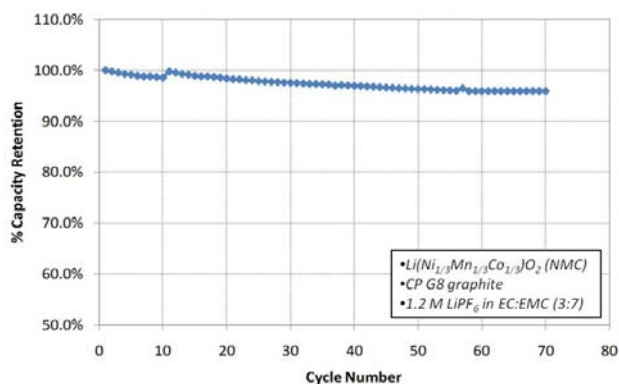


Figure IV - 185: Percent capacity retention as a functional of cycle number for an NMC111 18650 cell

## Conclusions and Future Directions

This work highlights our efforts to understand and improve abuse tolerance in lithium-ion cells. Specifically, this work focuses on electrolyte effects on abuse tolerance; where safety issues and instabilities of electrolytes are becoming increasingly important. Of those potential instabilities, we have shown that decomposition of carbonates in the presence of LiPF<sub>6</sub> produces 1.5-2 moles of gas product per mole of electrolyte and both the linear and cyclic carbonates participate in the decomposition reactions. We have also shown electrolyte solvent

properties (namely combustion enthalpy) have a significant impact on the abuse tolerance of lithium-ion cells. Non-LiPF<sub>6</sub> electrolyte salts like LiF and anion binding agents (ABAs) can be used to not only mitigate the reactivity of PF<sub>6</sub><sup>-</sup> that leads to gas generation, but can actually passivate the cathode runaway reaction. The prototyping capability at SNL facilitates the cell-level abuse tolerance work with R&D cells containing ABR relevant materials.

Future work in FY12 will focus on understanding electrolyte degradation mechanisms, the passivation mechanism of these and other ABA electrolytes, and determining the abuse response of a new class of ionic liquid electrolytes. In addition, SNL will continue to support materials development by our National Laboratory collaborators with cell prototyping and abuse tolerance evaluation of high energy cathodes, composite anodes, and advanced electrolytes.

## References

1. J. K. Cho et al. J. Chem. Eng. Data, 16, 87-90 (1971)

## FY 2011 Publications/Presentations

1. C. J. Orendorff, Lithium Mobile Power/Battery Safety, November 3<sup>rd</sup> 2011, Boston, MA
2. C. J. Orendorff, AABC, January 25<sup>th</sup> 2011, Pasadena, CA
3. C. J. Orendorff, Space Power Workshop, April 21<sup>st</sup> 2011, El Segudado, CA
4. 2011 DOE Annual Peer Review Meeting Presentation, May 9<sup>th</sup>-13<sup>th</sup> 2011, Washington DC.
5. C. J. Orendorff, ECS Detroit Chapter, May 25<sup>th</sup> 2011, Southfield, MI

## IV.D.2.3 Overcharge Protection for PHEV Cells (LBNL)

Guoying Chen  
Thomas Richardson

Lawrence Berkeley National Laboratory  
Environmental Energy Technologies Division  
Berkeley, CA 94720  
Phone: (510) 486-5843; Fax: (510) 486-5467  
E-mail: [GChen@lbl.gov](mailto:GChen@lbl.gov)  
[TJRichardson@lbl.gov](mailto:TJRichardson@lbl.gov)

Start Date: October 1, 2009  
Projected End Date: September 30, 2012

### Objectives

- Develop and implement an inexpensive, long-lasting mechanism that provides self-actuated, reversible and high-rate overcharge protection for high-energy lithium-ion batteries intended for PHEV applications.

### Technical Barriers

- Abuse tolerance
- Safety
- Poor cycle life

### Technical Targets

- Improved rate capability and cycle life of overcharge-protected Li-ion cells.

### Accomplishments

- Achieved ten-time increase in maximum sustainable current density on electroactive-polymer fiber incorporated composite membranes.
- Adapted electrospinning technique to prepare polymer fibers at low-cost and large-scale.
- Illustrated the redox process of polymer fibers through *in situ* studies.
- Identified a high-voltage polymer with improved stability at low voltage against Li anode.
- Demonstrated overcharge protection in large format pouch cells with both “sandwich-type” and parallel configurations.



### Introduction

The term “overcharge” is used to describe a variety of conditions, including simple charging at normal rates beyond rated capacity, overvoltage excursions for short or long periods, charging at a rate too high for one electrode (commonly the anode) without exceeding the maximum voltage, and other more complex scenarios. While overcharging is still a major safety issue for lithium batteries it is a serious lifetime issue as well. Even very slight overcharging reduces the discharge capacity of a cell, which can result in overdischarging, increased impedance, local heating, etc. Battery packs for consumer electronics are protected both by electronic controls and by internal shutdown mechanisms such as melting separators and disconnects acting in response to pressure or temperature excursions. In a multicell stack capable of delivering several hundred volts, permanently shutting down a cell reduces the usable capacity of the stack and puts added strain on the remaining cells in parallel with it. Complex re-routing of current around overcharged cells is impractical in these stacks. Internal protection mechanisms that maintain a cell’s potential and discharge capacity can provide protection without adding substantially to the size, weight or volume of the stack.

The electroactive polymer approach, developed at LBNL, protects cells by forming a reversible resistive shunt between the current collectors during overcharging. The process is self-activated by voltage, and it does not pose interference during normal cell charge and discharge. Unlike the commonly used redox shuttle method, it conducts overcharge current through an electronic rather than a diffusional path, and therefore is capable of high-rate and low-temperature protections. The placement of the polymer is also flexible, and the cells can be configured to best accommodate heat transfer in the event of overcharging. Overheating in internal redox shuttle protected cells, on the other hand, can only be avoided by restricting the cell to low-rate operation.

### Approach

The approach is to use electroactive polymers as self-actuating and reversible overcharge protection agents. The redox window and electronic conductivity of the polymer will be tuned to match the battery chemistry for non-interfering cell operation. Rate capability and cycle life of the protection will be maximized through the optimization of polymer composite morphology and cell configuration.

## Results

**Electroactive polymer-fibers.** In order to achieve improved rate capability and cycle life in protected Li-ion batteries, approaches were explored to prepare electroactive polymers in nanofibers that are capable of providing direct individual high-current paths between the electrodes. Poly(3-butylthiophene) (P3BT) was electrodeposited into the regular nanosized channels of a porous alumina membrane (AAO). By adjusting the deposition conditions, arrays of oriented polymer nanorods (Figure IV - 186a) and nanotubes (Figure IV - 185b) extending the full thickness of the AAO template were prepared.

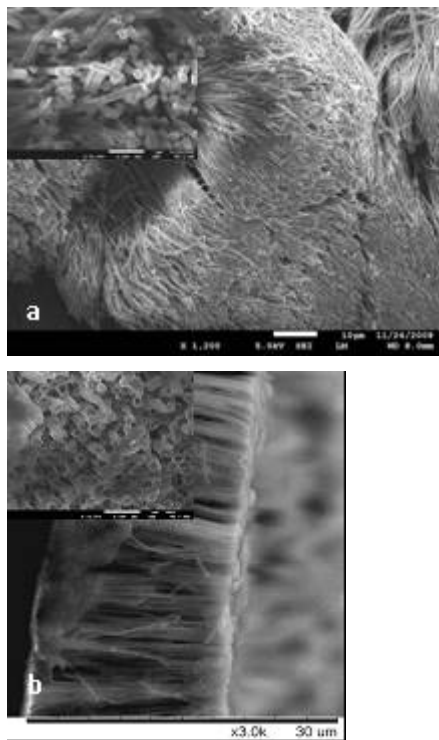


Figure IV - 186: (a) P3BT nanorods and (b) P3BT nanotubes prepared by electro-templating. Images were recorded after the removal of AAO templates.

Figure IV - 187a shows the performance of the P3BT nanotube/AAO composite at different current densities, evaluated in a “Swagelok - type” cell with the composite membrane as the cathode and Li foil as the anode and reference electrode. The cell was able to hold a constant potential by shorting through the conductive polymer for current densities up to  $5 \text{ mA/cm}^2$ , which was ten times higher compared to the maximum current density achieved on a solution-cast P3BT composite with a similar loading (Figure IV - 187b). The increased sustainable current densities on both nanorod and nanotube composites clearly suggest that the new morphologies improve polymer utilization.

Alternative methods were also explored to synthesize electroactive fibers at low-cost and large-scale. Electrospinning is a technology commonly used by industry to produce polymer fibers from aqueous solutions. During the process, a solution is pumped into the syringe, and a high potential is applied between the spinneret and a grounded collector. The fluid overcomes the surface tension under the external electric field and forms a fine charged jet, which is further elongated by electrostatic repulsion to form fibers.

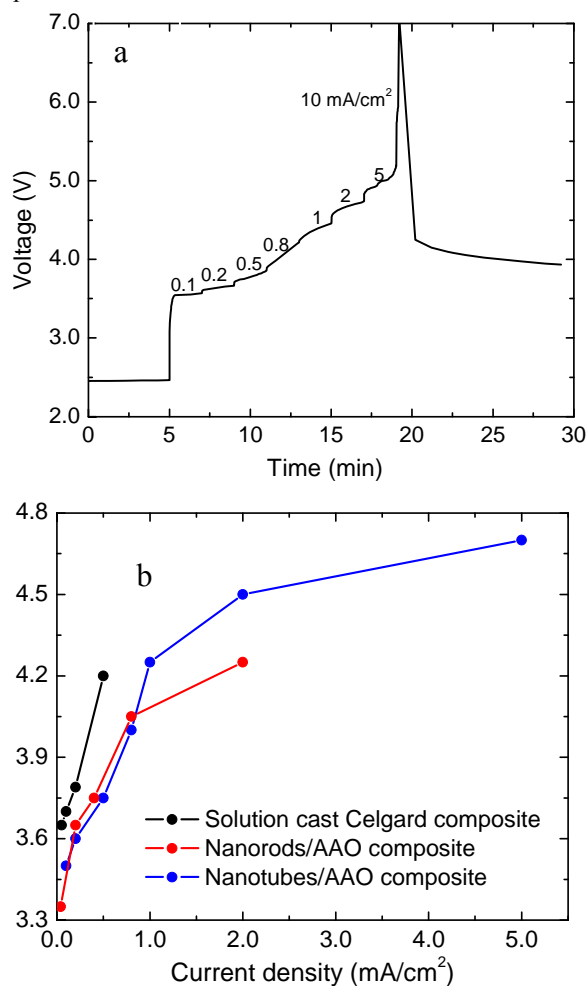


Figure IV - 187: (a) Voltage profile of the P3BT nanotube/AAO composite at the indicated current densities and (b) comparison of the sustainable current densities of the various P3BT composites.

This process was successfully adapted to the synthesis of electroactive polymer fibers from organic solvents. Figure IV - 188 shows poly[(9,9-dioctylfluorenyl-2,7-diyl)] (PFO) fibers collected on an Al substrate, obtained by electrospinning of a  $\text{CHCl}_3$  solution containing 3 wt% of the polymer. The fibers have an average diameter of  $1 \mu\text{m}$ , with  $100 \text{ nm}$  pores forming on the surface due to solvent evaporation. The presence of these relatively large-sized pores may improve electrolyte penetration, polymer utilization and rate capability during overcharge

protection. The aspect ratio of the fibers can be easily tuned through the adjustment of synthesis conditions, such as applied voltage, solvent, solution concentration and feeding speed.

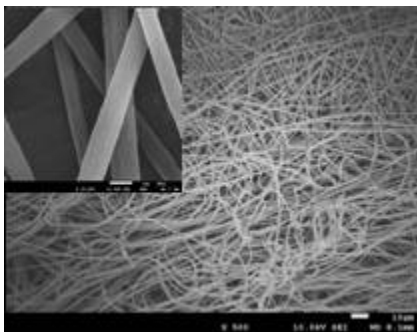


Figure IV - 188: SEM image of porous PFO polymer fibers prepared by an electrospinning method.

Electroactive fibers were studied as charge carriers in Li-ion batteries by visual examination of oxidation and reduction processes in an *in situ* optical cell with PFO fiber-film as working electrode and Li metal as counter and reference electrodes. Figure IV - 189 shows the cell configuration and a still image of the fibers during the passage of a steady state current of 40  $\mu$ A. Upon oxidation, the conduction front gradually moved from the positive electrode towards the end of the film. The color of the fibers changed from light yellow at neutral state to deep black upon oxidation, indicating an increase in electronic conductivity. A distinct boundary between the oxidized and the neutral PFO is clearly shown, suggesting that the inter-connection between fibers is sufficient to allow charge carriers to propagate across rather than only within individual fibers. Under current magnification, the volume change of the fibers was indiscernible.

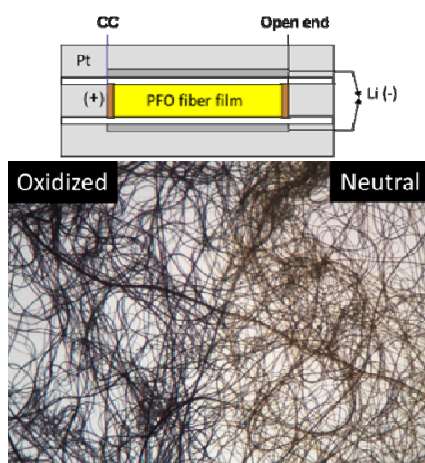


Figure IV - 189: Galvanostatic oxidation of the PFO fibers in 1M LiPF<sub>6</sub> in 1:1 EC: PC. The image was taken under an optical microscope at 100x magnification.

**Alternative electroactive polymer.** With a goal to achieve more efficient and stable protection for 4V and higher PHEV battery cells, alternative electroactive polymers were evaluated for their overcharge performance. Through cyclic voltammetry studies, poly[(9,9-dioctylfluorenyl-2,7-diyl)-co-(1,4-phenylene)] (PFOP) was found to have an onset oxidation potential of 4.25 V (Figure IV - 190a), one of the highest among electroactive polymers reported so far. Compared to PFO, the polymer also showed improved stability at low voltage, without the presence of significant redox peaks after initial 5 cycles (Figure IV - 190b).

Polymer composite separators were prepared by impregnating a CHCl<sub>3</sub> solution of PFOP into Celgard membranes. Figure IV - 191 compares the room-temperature rate performance of Li<sub>1.05</sub>Mn<sub>1.95</sub>O<sub>4</sub>-Li cells with and without the protection of a PFOP-impregnated separator. The “Swagelok-type” cells were charged and discharged at current densities of 0.13 (0.25C), 0.26 (0.5C), 0.51 (1C), and 1.0 mA/cm<sup>2</sup> (2C). For the protected cell, a steady-state potential was reached and maintained at each cycling rate, indicating that an electronic short was established and maintained by the conducting polymer. The potential at which the cell is shorted increases with the charging rate as the resistance across the polymer-impregnated separator varies with current density. Excellent capacity retention was observed even at the highest rate. Comparison with the unprotected cell clearly indicates that the protection mechanism improves cell discharge capacity, and that self-discharge due to the presence of the electroactive composite separator is negligible.

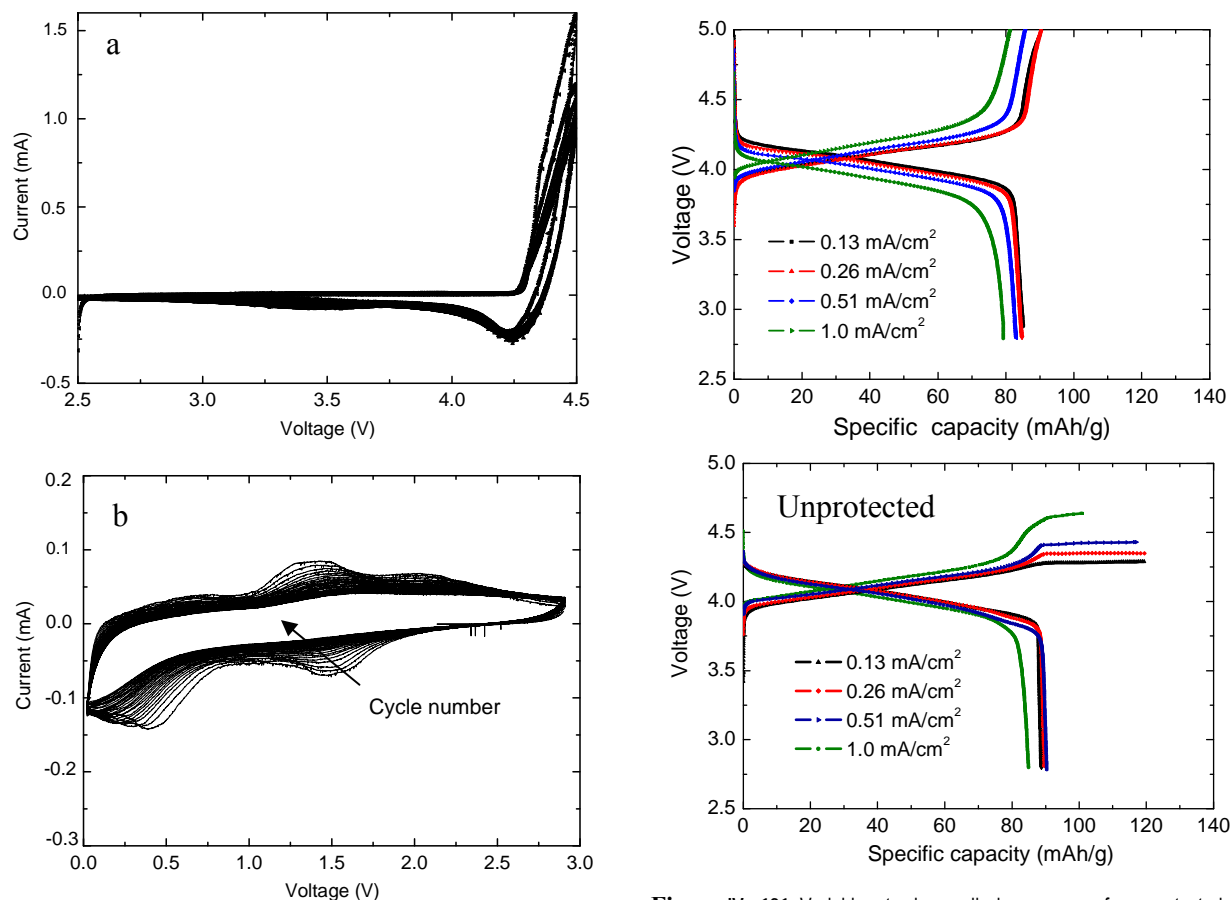


Figure IV - 190: Cyclic voltammetry of PFOP in 1M LiPF<sub>6</sub> in 1:1 EC: PC for 30 cycles: a) high voltage and b) low voltage region. Scan rate was 5 mV/s.

**Pouch cell protection.** In an effort to scale up the overcharge protection approach, the performance of the electroactive polymer composite was also studied in pouch cells that had an electrode area of 3cm x 4cm, ten times larger than that in the “Swagelok-type” cells. Both “sandwich-type” and parallel cell configurations were used, wherein a composite separator was placed between the electrodes and adjacent to the electrode assembly, respectively. Overcharge protection was achieved in both types of cells, although the steady-state voltage was significantly reduced in the latter case where the internal resistance was lower due to the absence of electroactive polymer between the electrodes (Figure IV - 192a). At a C/7 rate and 20% overcharging, the “sandwich-type” pouch cell was reversibly protected at 4.6 V (Figure IV - 192b).

Figure IV - 191: Variable rate charge-discharge curves for unprotected and protected Li/Li<sub>1.05</sub>Mn<sub>1.95</sub>O<sub>4</sub> “Swagelok-type” cells.

## Conclusions and Future Directions

Improved sustainable current density was achieved on polymer nanorods and nanotubes prepared by electrospinning. An easily scalable electrospinning process was developed to prepare electroactive fibers with various aspect ratios and porosities. An alternative electroactive polymer was found to have one of the highest reported oxidation voltages and improved stability at low voltages. Overcharge protection was successfully demonstrated in larger-sized pouch cells.

Future work will focus on preparing electroactive fiber composite membranes by electrospinning and evaluating their overcharge performance in lithium batteries. Cell design that improves the efficiencies for overcharge protection and heat transfer will be explored. Other high-voltage electroactive polymer candidates will be characterized and evaluated for their applicability in PHEV batteries. The approach will be further tested in pouch and other large-scale battery cells for its scalability.

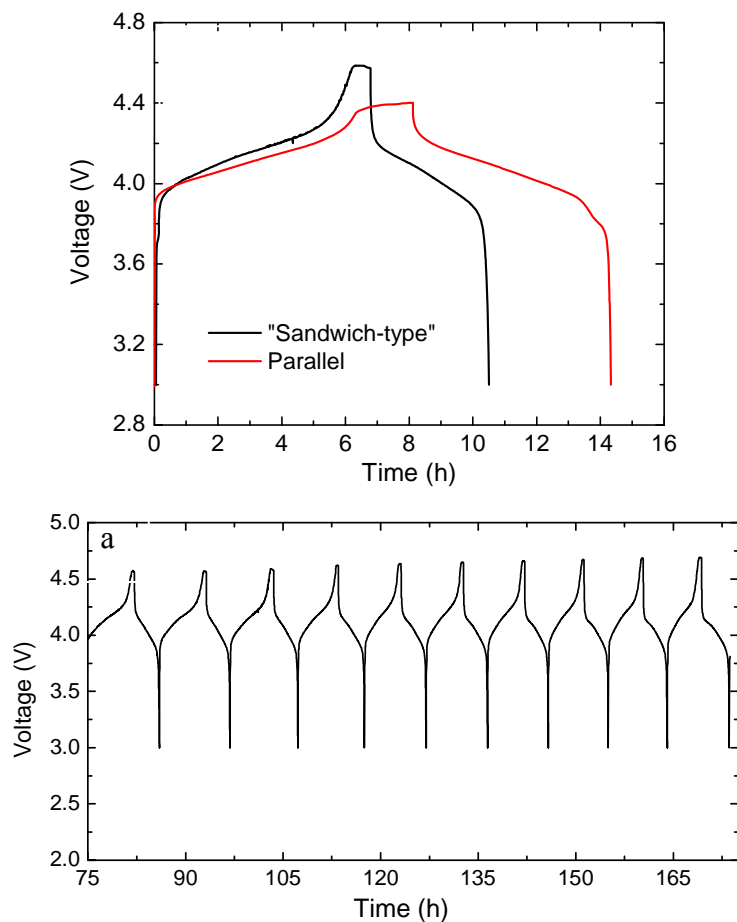


Figure IV - 192: Polymer-protected  $\text{Li}/\text{Li}_{1.05}\text{Mn}_{1.95}\text{O}_4$  pouch cells: a) voltage profile comparison between the two types of pouch cells and b) charge-discharge cycling of a "sandwich-type" pouch cell.

### FY 2011 Publications/Presentations

1. 2011 DOE Annual Peer Review Meeting Presentation.
2. G. Chen and T. J. Richardson, "Overcharge Protection for 4 V Lithium Batteries at High Rates and Low Temperatures," *Journal of the Electrochemical Society*, **157**, A735 (2010).

---

## IV.E Applied Research Facilities

### IV.E.1 Battery Materials Pilot Production Facility

#### IV.E.1.1 Process Development and Scale up of Advanced Cathode Materials (ANL)

Gregory K. Krumdick

Argonne National Laboratory  
9700 South Cass Avenue  
Argonne, IL 60439-4837  
Phone: (630) 252-3952; Fax: (630) 252-1342  
E-mail: [gkrumdick@anl.gov](mailto:gkrumdick@anl.gov)

##### Collaborators:

Young Ho Shin, Argonne National Laboratory  
Kaname Takeya, Argonne National Laboratory  
Sabine Gallagher, Argonne National Laboratory  
Ilias Belharouak, Argonne National Laboratory

Start Date: June, 2010

Projected End Date: September, 2012

### Objectives

The objective of this task is to conduct process engineering research for scale-up of Argonne's next generation high energy cathode materials. These materials will be based on NMC chemistries and may include lithium rich technology, layered-layered and possibly layered-spinel classes of cathode materials. The current multistep batch processes, capable of producing approximately 2 kg of material per week using a 4L reactor will be optimized and scaled up. Scaling up the process involves modification of the bench-scale process chemistry to allow for the semi-continuous production of material, development of a process engineering flow diagram, design of a mini-scale system layout, construction of the experimental system and experimental validation of the optimized process. A flexible processing system will be designed, built and operated to produce multiple batches for prototype testing. The design basis for scale-up will be based on a 20L reactor capable of producing a 10 kg batch of cathode materials per week.

### Technical Barriers

Processes for the production of next-generation high-energy cathode materials have been developed only at the bench scale. Sufficient quantity of material cannot be generated for prototype testing, which is required prior to scaling the process to the next level. Therefore, pilot-scale facilities are required for battery materials scale-up research and development.

### Technical Targets

- Install reactor system for the scale-up of cathode materials.
- Scale-up one cathode material in FY11.

### Accomplishments

- 4L synthesis system has been installed and tested.
- Reactor system was modified for better particle size, distribution & morphology
- Scale-up work has begun on the following cathode material:
- $\text{Li}_{1.14}\text{Mn}_{0.57}\text{Ni}_{0.29}\text{O}_2$
- Preliminary optimization has been completed for the following steps:
- Co-precipitation
- Washing & filtering
- Drying
- Sieving
- Mixing
- Calcination
- Classification
- Chemical analysis and coin cell testing on material has been completed.
- 20L synthesis system is in the process of being installed.



## Introduction

Researchers in the battery materials programs across the DOE complex are able to scale up as synthesis of battery materials in gram quantities, and with time consuming, multiple small-scale runs. There is a need to develop scale-up processes for battery materials (primarily lithium-ion based batteries) to the kilogram and tens-of-kilograms quantities at DOE labs to support the transition of these technologies to industry. Currently, there is no systematic engineering research capability or program across the DOE complex or in industry to identify and resolve constraints to the development of cost-effective process technology for the high-volume manufacture of these advanced materials.

## Approach

Next generation cathode materials have been developed at the bench scale by a number of researchers focusing on developing advanced lithium ion battery materials. Process engineers will work with these researchers to gain an understanding of the materials and bench-scale processes used to make these materials and then scale-up and optimize the processes. Standard chemical engineering unit operations will be utilized to develop flexible systems that will enable scaling of a wide range of next generation high energy cathode materials. Initial work will be based on NMC based processes, but may include lithium rich technologies and layered-layered and layered-spinel classes of cathode materials.

## Results

After a detailed assessment of the synthesis process used to produce  $\text{Li}_{1.14}\text{Mn}_{0.57}\text{Ni}_{0.29}\text{O}_2$  the following operational variables were identified and preliminary optimization completed using a 4L reactor system (see Figure IV - 193, Figure IV - 194, and Figure IV - 195).

### Co-precipitation.

- Reaction temperature
- Residence time
- Feed flow rate
- Feed concentration
- pH during co-precipitation
- Reactor geometry
- Baffle type
- Impeller shape

- Rotation speed
- **Washing & filtering.**
- Sedimentation time
- Agitation speed
- Agitation time
- Temperature of DIW
- Repetition number of cleaning
- **Drying.**
- Drying temperature
- Drying time
- **Sieving.**
- Crushing method for dried precursor cake before sieving
- Mesh size
- Sieving time
- Loading amount for each operation
- **Mixing.**
- Rotation speed
- Operation time
- Loading amount for each operation
- Particle size & distribution of  $\text{Li}_2\text{CO}_3$
- **Calcination.**
- Maximum temperature
- Residence time at maximum temperature
- Intermediate temperature
- Residence time at intermediate temperature
- Rate of temperature increment
- Flow rate of  $\text{O}_2$  &  $\text{N}_2$
- Pressure inside furnace
- Loading thickness
- Loading amount for each operation
- **Classification.**
- Mesh size
- Classification time
- Loading amount for each operation

Figure IV - 193 and Figure IV - 194 show preliminary capacity and coin cell testing data for one of the first production runs of  $\text{Li}_{1.14}\text{Mn}_{0.57}\text{Ni}_{0.29}\text{O}_2$  after process optimization.

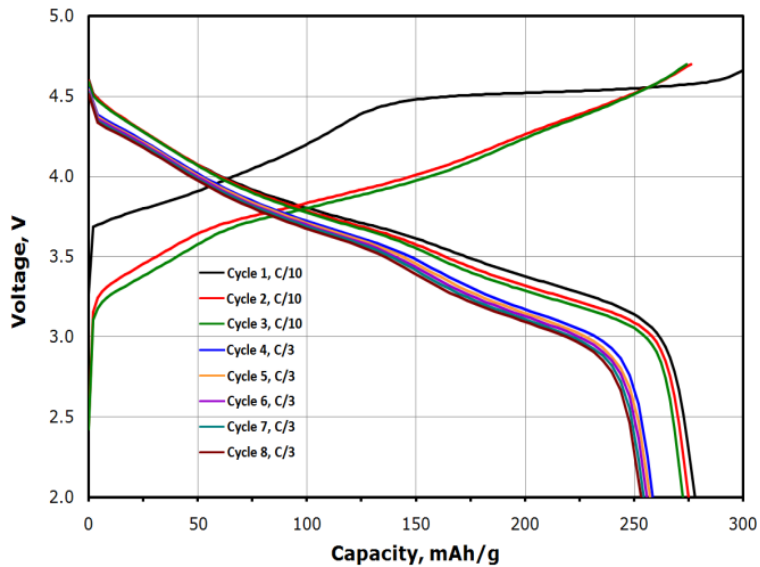


Figure IV - 193: Cathode capacity after preliminary process optimization.

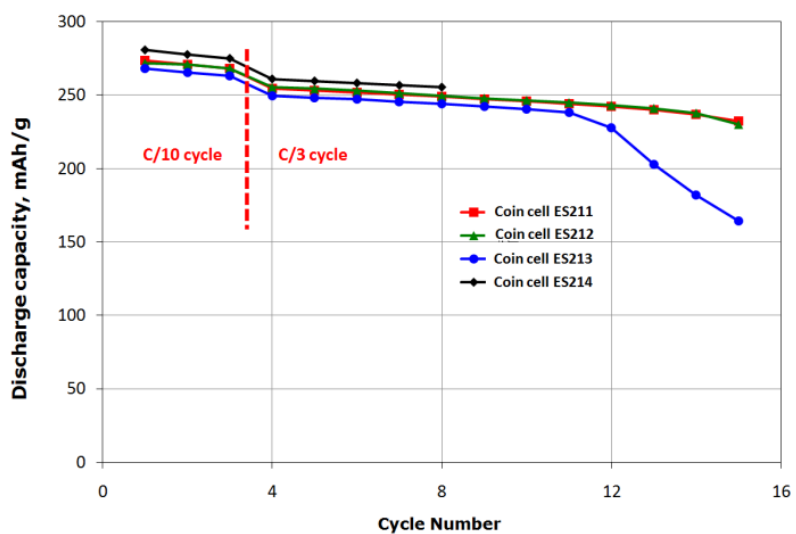


Figure IV - 194: Coin cell cycle performance.

One issue that was identified and must be resolved is the ability to control particle size and distribution for continuous processing.

## Particle Growth Issue

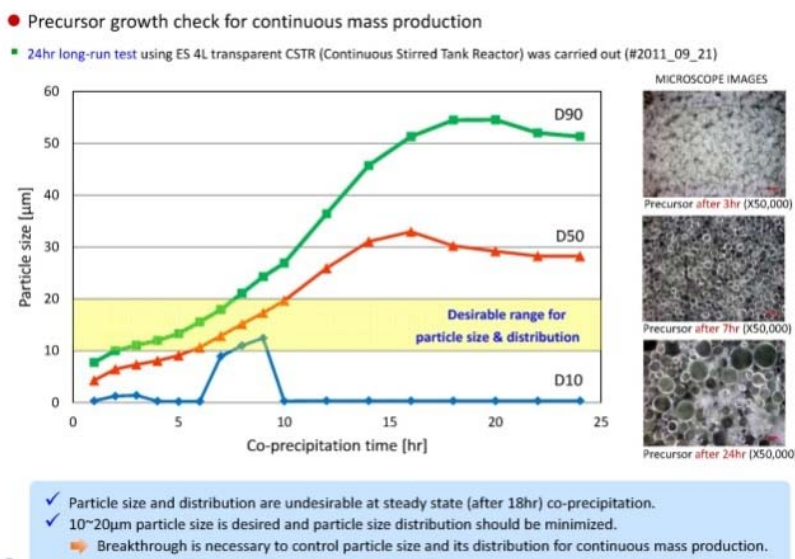


Figure IV - 195: Precursor particle growth issue

## Conclusions and Future Directions

Preliminary results of the scale-up of  $\text{Li}_{1.14}\text{Mn}_{0.57}\text{Ni}_{0.29}\text{O}_2$  indicate improved capacity over the initially discovered process using a 4L reactor system.

For FY12, scale-up work will continue on this material using a 20L reactor system, targeting multiple 10kg batches. Technique to resolve particle growth issue will be tested.

## FY 2011 Publications/Presentations

1. 2011 DOE Annual Peer Review Meeting, May 9<sup>th</sup>-13<sup>th</sup> 2011, Washington DC.

## IV.E.1.2 Process Development and Scale-up of Advanced Electrolyte Materials (ANL)

Gregory K. Krumdick

Argonne National Laboratory  
9700 South Cass Avenue  
Argonne, IL 60439-4837  
Phone: (630) 252-3952; Fax: (630) 252-1342  
E-mail: [gkrumdick@anl.gov](mailto:gkrumdick@anl.gov)

### Collaborators:

Krzysztof Papek, Argonne National Laboratory  
Trevor Dzwiniel, Argonne National Laboratory  
Zhengcheng Zhang, Argonne National Laboratory

Start Date: June, 2010

Projected End Date: September, 2012

### Accomplishments

- Scale-up work has been completed on the following electrolyte materials:
  - 1NM3
  - 2SM3
  - ANL-RS2
  - ANL-RS6
- Scale-up work has begun on the following electrolyte materials:
  - LiDFOB
  - 1S1M3
- The following material was found to be not feasible to scale-up:
  - LiTFOP



### Objectives

The objective of this task is to conduct process engineering research for scale-up of Argonne's new electrolytes and additive materials. Up to this point, these advanced electrolytes and additives has only been synthesized in small batches. Scaling up the process involves modification of the bench-scale process chemistry to allow for the semi-continuous production of materials, development of a process engineering flow diagram, design of a mini-scale system layout, construction of the experimental system and experimental validation of the optimized process. The mini system will be assembled utilizing an existing synthesis reactor system. Electrolyte materials produced will be analyzed to confirm material properties and for quality assurance.

### Technical Barriers

Advanced electrolytes and additives have been synthesized in small batches using 1-5L vessels, which produce approximately 200mL of material. The bench-scale processes are labor-intensive and time-consuming. Sufficient quantity of material cannot be generated for prototype testing, which is required prior to scaling the process to the next level. Therefore, pilot-scale facilities are required for battery materials scale-up research and development.

### Technical Targets

- Scale-up 4-6 electrolyte materials in FY11

### Introduction

Researchers in the battery materials programs across the DOE complex refer to scale up as synthesis of battery materials in gram quantities, and with time consuming, multiple small-scale runs. There is a need to develop scale-up processes for battery materials (primarily lithium-ion based batteries) to the kilogram and tens-of-kilograms quantities at DOE labs to support the transition of these technologies to industry. Currently, there is no systematic engineering research capability or program across the DOE complex or in industry to identify and resolve constraints to the development of cost-effective process technology for the high-volume manufacture of these advanced materials.

### Approach

Advanced electrolytes and additives have been developed at the bench scale by a number of researchers focusing on developing advanced lithium-ion battery materials. Process engineers will work with these researchers to gain an understanding of the materials and bench-scale processes used to make these materials, and then scale up and optimize the processes to produce larger quantities. Standard chemical engineering unit operations will be utilized to develop flexible systems that will be

enable scaling of a wide range of next generation electrolytes and additives.

## Results

Table IV - 11 below shows the status of the milestones associated with this task.

Table IV - 11: The Status of Milestones for Process Development and Scale-up of Advanced Electrolyte Materials

MILESTONE	DATE		
<b>ANL-RS2 – Scale up work completed</b>		process chemistry (10g bench scale)	
Select material to scale	10/1/2010	Second process scale-up (1000g pilot scale)	06/24/2011
Assess scalability of process	10/18/2010	<b>1,477 g produced in a single batch, purity &gt; 99.9%</b>	
WP&C documentation approved	11/1/2010	<b>ANL-RS6 – Scale up work completed</b>	
Develop and validate scalable process chemistry (10g bench scale)	12/1/2010	Select material to scale	01/07/2011
First process scale-up (100g bench scale)	12/23/2010	Assess scalability of process	01/14/2011
Second process scale-up (1000g pilot scale)	03/04/2011	WP&C documentation approved	03/14/2011
<b>1,576 g produced in a single batch, purity &gt; 99.9%</b>		Develop and validate scalable process chemistry (10g bench scale)	05/06/2011
<b>1NM3 – Scale up work completed</b>		First process scale-up (100g bench scale)	06/03/2011
Select material to scale	11/01/2010	Second process scale-up (1000g pilot scale)	07/25/2011
Assess scalability of process	11/15/2010	<b>1,815 g produced in a single batch, purity &gt; 99%</b>	
WP&C documentation approved	12/23/2010	<b>LiDFOB – Scale up work started</b>	
Develop and validate scalable process chemistry (10g bench scale)	02/18/2011	Select material to scale	01/07/2011
First process scale-up (100g bench scale)	03/11/2011	Assess scalability of process	08/12/2011
Second process scale-up (1000g pilot scale)	05/13/2011	WP&C documentation approved	
<b>3.36 kg, produced in a single batch, purity &gt;99.95%</b>		Develop and validate scalable process chemistry (10g bench scale)	08/26/2011
<b>2SM3 – Scale up work completed</b>		<b>LiTFOP – Scale up not feasible</b>	
Select material to scale	01/07/2011	Select material to scale	01/07/2011
Assess scalability of process	01/14/2011	Evaluate available literature and assess feasibility of large scale synthesis	05/31/2011
WP&C documentation approved	03/07/2011	<b>1S1M3 – Scale up work started</b>	
Develop and validate scalable process chemistry (10g bench scale)	04/28/2011	Select material to scale	01/04/2011
First process scale-up (100g bench scale)	05/20/2011	Assess scalability of process	08/03/2011
Initial attempt did not work.		WP&C documentation approved	2/22/2011
Develop and validate scalable	06/03/2011	Develop and validate scalable process chemistry (10g bench scale)	09/02/2011

## Conclusions and Future Directions

Initially, scale-up work will continue on LiDFOB and 1S1M3. Additional materials to scale will be added after discussions with the project sponsor. The scale-up of 4-6 electrolyte materials are targeted for FY12.

## FY 2011 Publications/Presentations

- 2011 DOE Annual Peer Review Meeting, May 9<sup>th</sup>-13<sup>th</sup> 2011, Washington DC.

---

## IV.E.2 Post-Test Diagnostics Facility

### IV.E.2.1 Post-Test Diagnostics Facility: Instrumentation and Protocol Development Activities (ANL)

Ira Bloom (Primary Contact), Nancy Dietz-Rago,  
Javier Bareño  
Argonne National Laboratory  
9700 South Cass Avenue  
Argonne, IL 60439  
Phone: 630 252 4516; Fax: 630 252 4176  
e-mail: [ira.bloom@anl.gov](mailto:ira.bloom@anl.gov)

Start Date: April 2010  
Projected End Date: Open

#### Objectives

- To accelerate the R&D cycle of DOE and industrial collaborators by developing and conducting standard procedures for post-test characterization of batteries in order to provide insight onto physicochemical causes of performance degradation.

#### Technical Barriers

This project addresses the following technical barriers as described in the USABC goals [1, 2, 3]:

- (A) Performance at ambient and sub-ambient temperatures
- (B) Calendar and cycle life

#### Technical Targets

- EV: 10-year calendar life; 1,000 80% DOD DST cycles
- HEV: 15-year calendar life, 300,00 charge-sustaining cycles; EOL performance (min): 25 kW and 300 Wh
- PHEV: 15-year calendar life, 300,00 charge-sustaining cycles, 5,000 charge-depleting cycles; EOL performance (min): 45 kW and 300 Wh
- LEES: 15-year calendar life, 300,00 charge-sustaining cycles; EOL performance (min): 20 kW and 56 Wh

#### Accomplishments

- A facility is being built for the post-test examination of batteries and battery materials. The design of the facility allows most of the examinations to be performed under inert-atmosphere conditions. It is about 95% complete: renovation and conditioning of the facility are complete; the analytical equipment has been purchased and installed; and final equipment calibration and training is almost complete. Safety reviews are being written and standard operating procedures are being developed. The facility is expected to be fully operational by December 31, 2011.



#### Introduction

Batteries are evaluated using standard tests and protocols which are transparent to technology [1, 2, 3]. The evaluation provides a lot of information about how battery performance changes with time under a given set of conditions. Post-test characterization of aged batteries can provide additional information regarding the cause of performance degradation, which, previously, could be only inferred.

#### Approach

Post-test analysis consists of physical, spectroscopic, metallographic, and electrochemical characterization of battery components that have been harvested from aged cells. The aged cells have undergone standardized testing. The cells can come either from exploratory DOE programs, such as ABR and BATT, or from pre-competitive R&D programs managed by USABC. The Post-Test Facility will use the experience and techniques developed in DOE's applied battery program in a standardized fashion.

## Results

An inert-atmosphere argon glove box (GB) has been installed. The GB (see Figure IV - 196) is divided in two sections GB-1 and GB-2. GB-1 is dedicated to cell disassembly and sample harvesting from cells that have

undergone performance and life testing. GB-2 is reserved for characterization of these harvested samples, and is kept free of organic solvents to preserve the integrity of the samples.

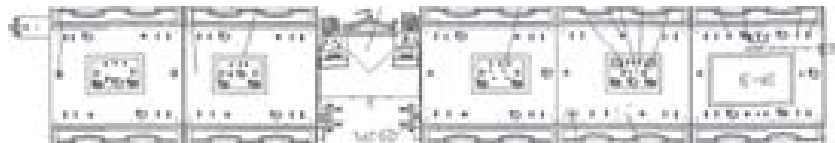


Figure IV - 196: Top view of the glove box. GB-1 is on the reader's left; GB-2, on the right.

GB-1 contains a diamond saw, a coin cell crimper/decrimper, and hand tools for cell disassembly and sample harvesting. Equipment for headspace gas and electrolyte sampling is currently under development. Additionally, GB-1 contains electrical connections to impedance and capacity testing equipment. Therefore, GB-1 provides capabilities for reassembly of aged cell components (cathode, anode, and/or separator) into half-cells or symmetric electrode cells for characterization.

GB-2 contains analytical equipment: an x-ray photoelectron spectrometer (XPS), a Raman spectrometer and microscope, and an integrated, thermogravimetric analyzer-gas chromatograph/mass spectrometer (TGA/GC-MS), allowing the thermal analysis of aged cell components and the analysis of the gases evolved. The GC-MS system can also accept gas and liquid samples through a manual injection port and an autosampler. Additionally, a Fourier-transform, infrared spectrometer (FT-IR) is available in a secondary glove box, allowing chemical analysis complementary to Raman spectroscopy without exposure to ambient air.

A high performance liquid chromatograph (HPLC) has been installed. Final setup is awaiting installation of high-pressure, high-flow N<sub>2</sub> service to the system, which is expected to be completed by November 2011.

For those samples which require it, the facility also contains standard metallography equipment, grinder, polisher and metallographic microscope. These are not in the glove box.

Samples can be transferred to the facility's environmental, scanning-electron microscope (SEM) without exposure to air. Samples are sealed in a jar in the glove box. The sample is then placed in the chamber of the SEM, which has been enclosed in an inert-atmosphere glove bag.

The SEM can operate either in standard high vacuum mode or in a low vacuum (environmental) mode, allowing samples which contain electrolyte to be readily examined. The SEM is equipped with an energy-dispersive x-ray (EDX) detector for composition analysis, and an electron backscatter diffraction (EBSD) detector, for crystal texture analysis.

The typical workflow is illustrated in Figure IV - 197. An aged cell –coin, cylindrical, or prismatic cell– is loaded onto GB-1 and punctured to recover the evolved gases and the electrolyte. These samples are examined by, respectively, GC-MS or a combination of HPLC and GC-MS. Then, the cell is disassembled into components, electrodes, separator, and packaging. Each of these components can be mounted and polished for metallographic examination, both in the optical and electron microscopes, as needed.

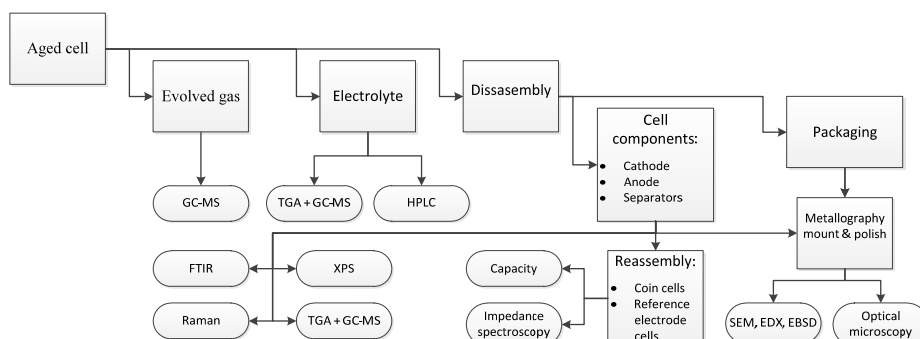


Figure IV - 197: Post-test analysis workflow diagram. Rectangular boxes indicate processes and samples. Ovals indicate analysis techniques.

Electrode and separator samples can be assembled into new coin cells and/or reference electrode cells for further electrochemical characterization, including capacity testing and impedance spectroscopy. Finally, electrode samples are examined by a combination of XPS, Raman, FT-IR, and TGA + GCMS.

### Conclusions and Future Directions

Post-test facility is being established at Argonne to support DOE and USABC projects. The facility is about 95% operational now. A few items remain which should be complete by December 2011. The next steps are as follows.

- Use commercial, 18650-sized cells to develop tear-down procedures and methods to sample head-space gas and electrolyte. Develop methods to cycle/electrochemically characterize aged cell materials.
- Examine initial cell builds from Cell Fabrication Facility to help elucidate possible issues that limit performance

- Examine old (~13 y) cells from the ATD program to characterize the long-term changes present in the cells
- Collaborate with ABR, BATT and USABC programs.

### FY 2011 Publications/Presentations

1. DOE Annual Merit Review Poster Presentation, May 2011.

### References

1. FreedomCAR Battery Test Manual for Power-Assist Hybrid Electric Vehicles, DOE/ID-11069, October 2003.
2. FreedomCAR Battery Test Manual for Plug-In Hybrid Electric Vehicles, June 2010.
3. Electric Vehicle Battery Test Procedures Manual, Revision 2, January 1996.

## IV.E.3 Battery Electrode and Cell Production Facility

### IV.E.3.1 Cell and Cell Component Manufacturing Equipment Modification and Process Development (ANL)

Bryant J. Polzin

Argonne National Laboratory  
9700 South Cass Avenue  
Argonne, IL 60439-4837  
Phone: (630) 252-6176; Fax: (630) 972-4952  
E-mail: polzinb@anl.gov

#### Collaborators:

Andrew Jansen, Argonne National Laboratory  
Wenquan Lu, Argonne National Laboratory  
Huming Wu, Argonne National Laboratory  
Nancy Dietz-Rago, Argonne National Laboratory

Start Date: October, 2011

Projected End Date: September, 2014

#### Objectives

- The objective of this work is to develop new material processes with custom tailored equipment for advanced battery materials. Additionally, the work will include fabricating prototype cells of various materials to establish the processes by which the systems need to be handled. This can be broken up into two main areas:
- Mixing, Coating and Calendering
- Prototype Assembly

#### Technical Barriers

The primary technical barrier is the development of a safe cost-effective PHEV battery with a 40 mile all electric range that meets or exceeds all performance goals.

- Optimization of battery formulation.
- Consistent prototype production.

#### Technical Targets

- Establish the prototype process and documentation.
- Validate prototype processes.
- Produce xx3450 prototype pouch cells for evaluation of various materials systems.

- Produce 18650 prototype can cells for evaluation of various materials systems.
- Support other research activities by utilizing the cell fabrication facility equipment (electrodes for development work, special cells for APS work, etc.)
- Identify any issues with materials systems and work with the developer to address the issues.

#### Accomplishments

- Established the system flow for the production of prototype cells.
- Established a Traveler for prototype production that captures information at every step of the process.
- Validated the slurry making, coating and calendering processes on several materials by comparing them to industrially made electrodes of the same electrode composition. (Physical and Electro-Chemical Analysis)
- Completed the first xx3450 pouch cell build containing Conoco Phillips A12 Graphite anode and Toda HE5050 NMC cathode.
- Completed the second xx3450 pouch cell build containing Conoco Phillips A12 Graphite anode and Argonne made material  $\text{Li}_{1.2}\text{Ni}_{0.3}\text{Mn}_{0.6}\text{O}_{2.1}$  cathode.
- Supported other development efforts in program.



#### Introduction

Transportation would benefit greatly from the development of a safe cost-effective battery for Plug-in Hybrid Electric Vehicles (PHEV) with a 40 mile all electric range that meets or exceeds performance goals. The U.S. Department of Energy has established several programs tasked with making this a reality. Many novel lithium-ion battery chemistries for PHEV batteries are being created in these programs. These promising new exploratory materials are often developed in small coin cells, which may or may not scale up well in large PHEV battery designs. These new battery chemistries must be evaluated in cell formats that are larger than a few mAh in capacity, preferably in the capacity range of 0.4 to 3 Ah.

To speed the evaluation of novel battery materials, the DOE tasked Argonne to develop the capability to fabricate in-house pouch and 18650 cells in a dry room environment.

Numerous discussions were held with state-of-the-art lithium-ion battery equipment vendors to design and produce electrode and cell making equipment capable of carrying out the DOE's mission. The ability to make high quality electrodes is crucial to the success of this facility. A high precision electrode coater with two drying ovens and a hot roll press were custom made to suit a pilot plant operation. Semi-automated equipment was installed to make industrial quality 18650 lithium-ion cells, which is the format commonly used in notebook computers. In addition, semi-automated equipment was installed to make industrial quality xx3450 lithium-ion "pouch" cells, which is the format commonly used in cell phones. A new dry room was also installed at Argonne that has an area of ~45m<sup>2</sup> and is capable of maintaining 100 PPMv (-42°C dew point) with 6 people working and a 750 SCFM exhaust for a hood and electrode drier. The Cell Fabrication Facility now has the capability to coat and hot-roll press electrodes, and to make xx3450 pouch cells and 18650 cells in a dry room environment.

### Approach

The first step for a material to be made into a prototype cell is for the material to be submitted to the ABR Materials Screening process. This testing provides the cell fabrication facility the necessary information to design an electrode and cell. This testing will also provide a baseline data set to be referenced back to. Once the cell design is completed a small batch of material is mixed, coated and calendered to the prototype cell specifications. This electrode is then submitted back to the ABR Materials Screening process so that it can be tested under the same conditions as the original material. If during the production of this electrode it is determined that the electrode formulation is not good (poor adhesion to the current collector, etc.) the electrode is re-formulated and re-made. The re-formulated electrode would then be submitted to the ABR Materials Screening process. Now having the initial Materials Screening data and the new Materials Screening data, it can be verified that process and electrode formulation that the cell fabrication facility used had no effect on performance of the material. Once this is done, the full prototype cells (xx3450 pouch or 18650s) are produced.

Additionally, samples of the starting materials as well as the electrodes are submitted for SEM analysis. By doing this, any changes in the particles during processing can be documented as well as the uniform distribution of the electrode components. The SEM data also provides the baseline date for any post-test analysis that may occur on the prototypes.

### Results

The first task of the cell fabrication facility was to validate the slurry making, coating and calendering process. This was done by making batches of electrodes with the exact same composition, one set done by industry and one set done by the cell fabrication facility. These electrodes were then physically and electro-chemically tested to determine if there were any variations between the two sets of electrodes. The sets of electrodes that were compared were one anode (Conoco Philips A12 Graphite) and one cathode (Toda HE5050 NMC). The images below (Figure IV - 198 and Figure IV - 199) are from the cell fabrication facility made electrodes.

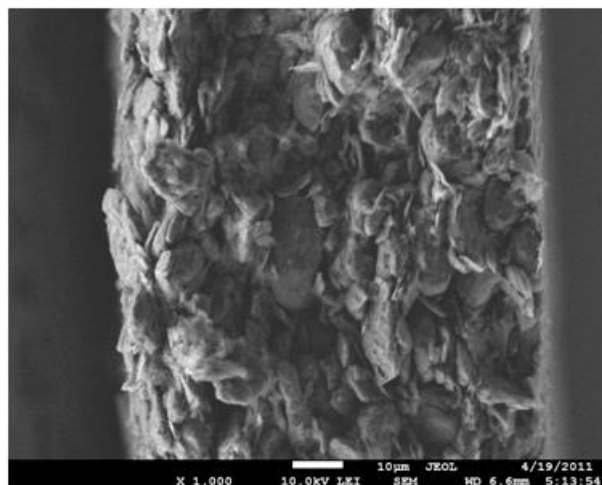


Figure IV - 198: Conoco Philips A12 Graphite Electrode made by the cell fabrication facility

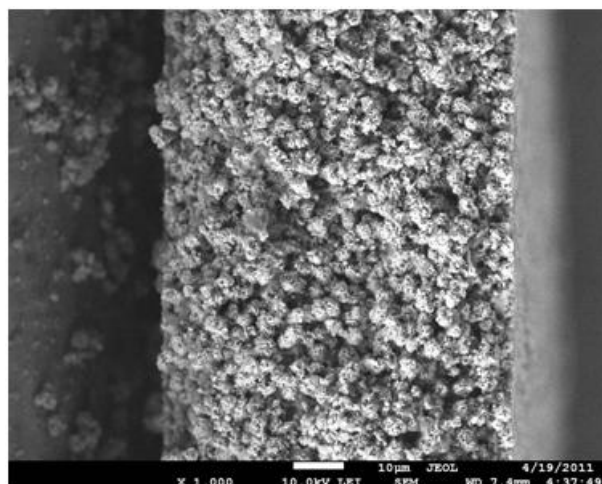


Figure IV - 199: Toda HE5050 NMC Electrode made by the cell fabrication facility

The electrodes that were made were assembled into a full cell and tested. The data on these cells are shown below (Figure IV - 200, Figure IV - 201).

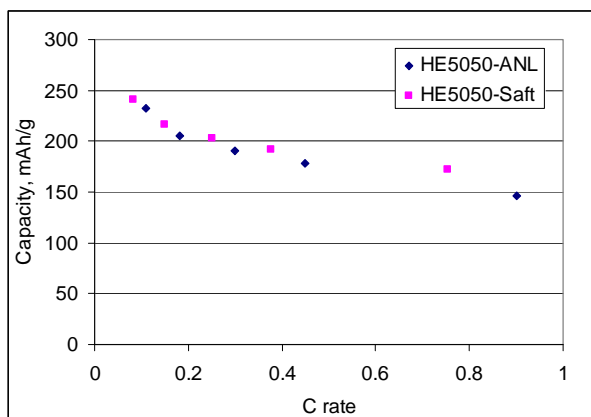


Figure IV - 200: Rate Capability Study of industrially made electrodes and cell fabrication facility made electrodes.

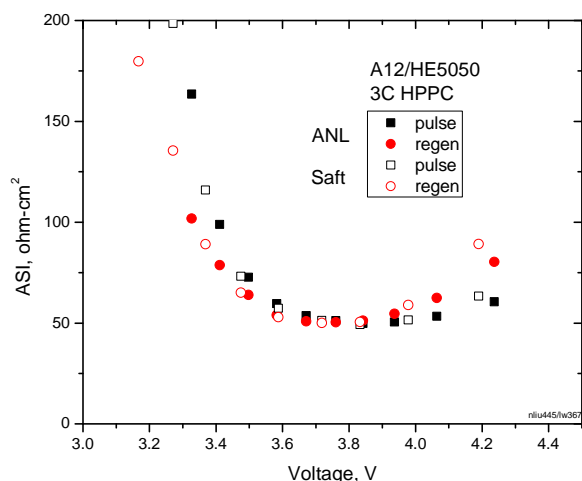


Figure IV - 201: HPPC testing of industrially made electrodes and cell fabrication facility made electrodes.

The above electrodes were used in the initial PHEV xx 3450 Pouch Cell Build 1.

The next material that was identified for a cell build was a  $Li_{1.2}Ni_{0.3}Mn_{0.6}O_{2.1}$  compound made by Argonne National Laboratory. This material was put through the ABR Materials Screening process and the data was collected. The capacity calculated for this material was ~230mAh/g from the materials screening data. Below is the image of the  $Li_{1.2}Ni_{0.3}Mn_{0.6}O_{2.1}$  powder (Figure IV - 202).

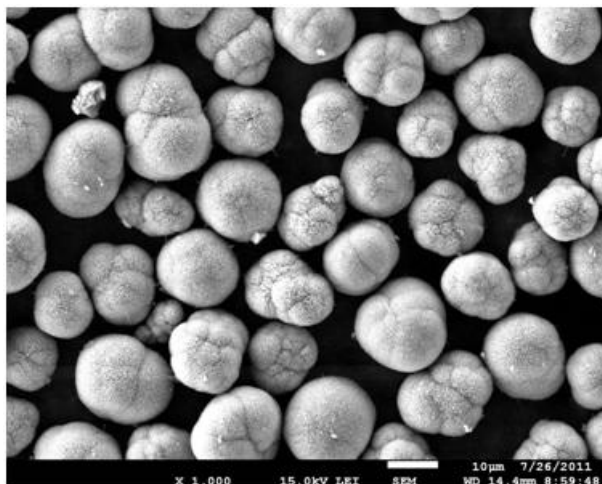


Figure IV - 202:  $Li_{1.2}Ni_{0.3}Mn_{0.6}O_{2.1}$  Powder

An electrode was made with this material and examined with an SEM. Below are the surface and cross section of the as coated electrode (Figure IV - 203, Figure IV - 204).

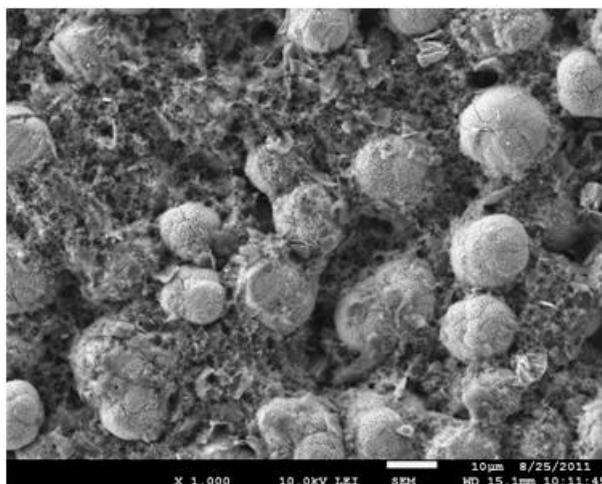


Figure IV - 203:  $Li_{1.2}Ni_{0.3}Mn_{0.6}O_{2.1}$  As-Coated Electrode Surface

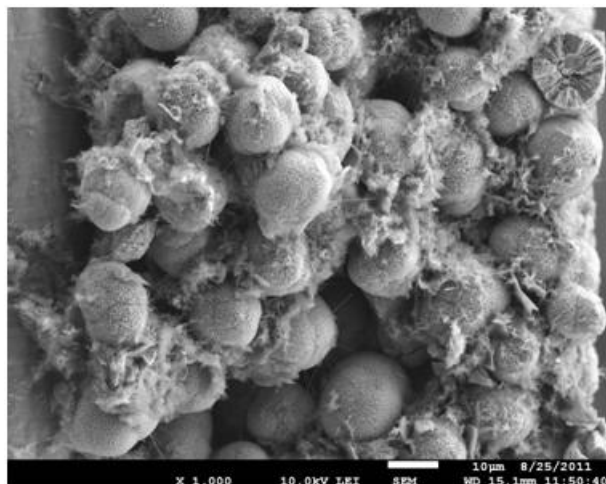


Figure IV - 204:  $\text{Li}_{1.2}\text{Ni}_{0.3}\text{Mn}_{0.6}\text{O}_{2.1}$  As-Coated Electrode Cross Section

Once the electrodes were fabricated on the coater, they were then hot roll pressed at  $80^\circ\text{C}$  down to  $\sim 33\%$  porosity. Surface and cross-sectional images of the final electrode are shown below (Figure IV - 205, Figure IV - 206).

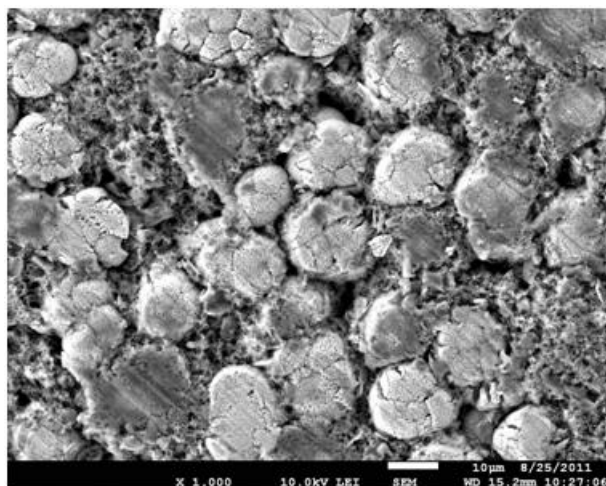


Figure IV - 205:  $\text{Li}_{1.2}\text{Ni}_{0.3}\text{Mn}_{0.6}\text{O}_{2.1}$  Final Electrode Surface

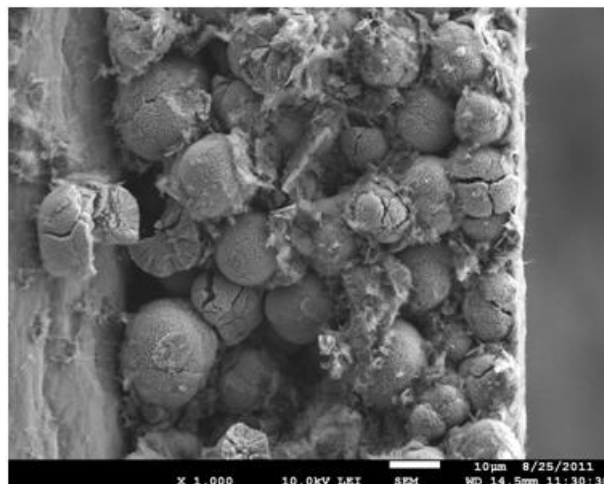
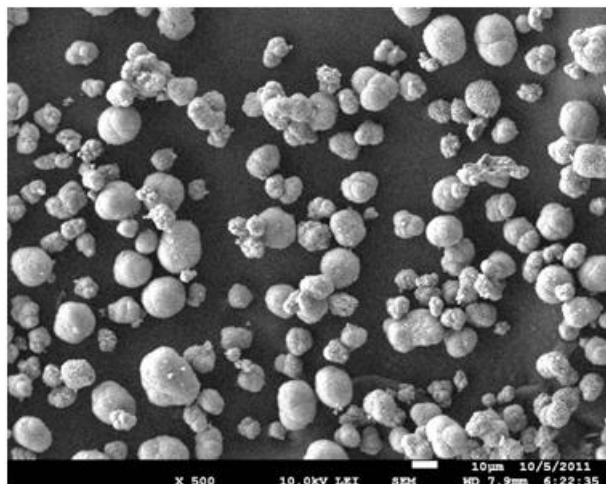


Figure IV - 206:  $\text{Li}_{1.2}\text{Ni}_{0.3}\text{Mn}_{0.6}\text{O}_{2.1}$  Final Electrode Cross Section

As shown in the images, this material exhibits a large amount of particle fracturing during the calendaring process. Not only does the fracturing occur at the surface of the electrode but it propagates through the thickness of the electrode. Seeing this breakdown in the particles, several different levels of calendaring were performed and both the surface and the cross section of the electrode was examined. From this analysis, the conclusion was drawn that the surface of the electrode immediately sustains damage no matter what the calendaring level. However, the depth of particle fracture in the electrode was dictated by the calendaring level.

Even with these results, it was decided to move forward with a cell build on this material. This material was used in the PHEV xx3450 Pouch Cell Build Number 2.

After looking at the above results, the conclusion was that due to the large particle size and morphology, it created a particle that was not strong enough to withstand the calendaring process. It was decided that a smaller particle of the  $\text{Li}_{1.2}\text{Ni}_{0.3}\text{Mn}_{0.6}\text{O}_{2.1}$  composition was to be made and fabricated and tested under the same condition as the electrode showing particle fracturing. An image of the smaller particle powder is shown below (Figure IV - 207).



**Figure IV - 207:**  $\text{Li}_{1.2}\text{Ni}_{0.3}\text{Mn}_{0.6}\text{O}_{2.1}$  Smaller sized powder.

The idea is that the smaller particles will be stronger and be able to move more during the calendaring process. There is no definitive data that shows what the effects are of the particles fracturing on the performance of a cell.

### Conclusions and Future Directions

The cell fabrication facility is a functioning facility that completed two PHEV cell builds as well as a number of individual cells and electrodes to help push research along in different areas.

From the data that was collected from the industry made electrode and the cell fabrication facility made electrodes, it can be said that they are comparable in quality and performance.

On the second PHEV cell build a process issue was encountered with the  $\text{Li}_{1.2}\text{Ni}_{0.3}\text{Mn}_{0.6}\text{O}_{2.1}$  powder that was supplied for the cell build. The powder supplied was not strong enough to hold up to the pressure generated in the calendaring process. Based upon this result, the effect of particle size and morphology on particle fracture strength is being examined. To further study this issue, an electrode of the same composition material with a smaller particle size was made and is going to be examined to determine if that size particle is strong enough to hold up in the calendaring process.

Additionally, methods for measuring single particle strength are being explored. The hope is that not only will the understanding of what particle strength is required for a particle not to break during calendaring be gained, but also how the morphology and production affects the strength (carbonate, hydroxide, acetate, etc. starting materials).

As more and more materials are processed through the cell fabrication facility, more process related issues will come to light. As these issues arise, they will be examined and addressed in the required fashion.

### FY 2011 Publications/Presentations

1. 2011 DOE Annual Peer Review Meeting Presentation, May 9<sup>th</sup>-13<sup>th</sup> 2011, Washington DC.